

**Investigation of Cardiac Myosin Binding  
protein C (cMyBPC) Domains and their  
Interactions.**

Thesis submitted for the Degree of  
Doctor of Philosophy  
at the University of Leicester

by

Joyce Ratti, MSc  
Department of Biochemistry  
University of Liecester

March 2009

**Joyce Ratti**

**Title:** Investigation of cardiac Myosin Binding Protein C (cMyBPC) domains and their interactions.

**Abstract**

Myosin binding protein C (MyBPC) is a multidomain protein present in the thick filament of striated muscles involved in both sarcomere formation and contraction. It appears that the C-terminus of the protein is involved in sarcomere formation, through interaction with Light Meromyosin (LMM), while the N-terminus seems to play a role in muscle contraction, being localized close to the motor domain of myosin that interacts with the thin filament protein actin, causing muscles to contract. It exists in three different isoforms, one for each type of muscle, the cardiac isoform being linked to hypertrophic cardiomyopathy (HCM), a genetic disorder associated with cardiac dysfunction that can manifest itself through arrhythmias, heart failure and sudden cardiac death, especially in the young. The present work has focused on two aspects of the cardiac isoform (cMyBPC) investigating both the function and the role in sarcomere assembly played by cMyBPC. The first part of the research presented in this thesis consisted in the determination of the three dimensional structure of the cardiac specific N-terminal domain cC0 using NMR spectroscopy, and the investigation of the interaction with its probable binding partner, the regulatory light chain of myosin, through  $^1\text{H}/^{15}\text{N}$  HSQC NMR spectroscopy titrations. The knowledge of the three dimensional structure has proven a vital tool to map the interacting surface on cC0, giving the possibility to make hypothesis on the way cMyBPC might interact with the S1 domain of myosin, thus influencing muscle contraction. The second part of this research is based on the hypothesis that the central domain cC5 could interact with domain cC8 of another molecule of the same protein, suggesting that the way cMyBPC could incorporate in the sarcomere would be through a trimeric collar wrapped around the myosin filament. This aspect has been studied using  $^1\text{H}/^{15}\text{N}$  HSQC NMR spectroscopy titrations but no conclusive results were obtained, suggesting that this interaction might not take place and indicating an axial arrangement, with cMyBPC running parallel to the thick filament, as the most likely.

## Acknowledgments

Firstly, I would like offer my thanks to my supervisor Dr. Mark Pfuhl for providing me with the opportunity to conduct this research and for all his guidance. I would also like to thank the members of my committee, Prof. Clive Bagshaw and Prof. Mark Carr, and Prof. Mathias Gautel for their advise and input throughout the course of my research. I would also like to offer my gratitude to the British Heart Foundation for funding this studentship.

I would like to thank all those who have directly and indirectly contributed to the work described in this thesis, inparticular Dr Fred Muskett for his invaluable help in performing both NMR experiments and structure calculation and Dr Phil Renshaw for his advise and expertise in the lab work.

All my thanks also go to the members of Dr Mark Pfuhl's group, Dr Sam Schroder, Dr Didier Philippe and especially Claudia Fogl, who, together with Dr Mohammed El-Mezgueldi, has helped me perform the actin binding assay, and to everyone at the Henry Wellcome Laboratories for Structural Biology.

My sincerest thanks go to my parents for their love and for always believing in me and to Cosimo for all his love and dedication.

Finally, to all my friends and family who I have not been able to mention above, thank you for your support, understanding and friendship.

Joyce Ratti, Leicester, March 2009

## Contents

<b>Abstract</b>	1
<b>Acknowledgements</b>	2
<b>Contents</b>	3
<b>Figures</b>	7
<b>Tables</b>	12
<b>Abbreviations</b>	14
<b>Chapter 1, General Introduction</b>	
<i>1.1 Myosin Binding Protein C (MyBPC)</i>	15
<i>1.1.1 Muscle structure and function</i>	15
<i>1.1.2 Striated muscles and sarcomere organization</i>	16
<i>1.1.2.1 The thick filament</i>	20
<i>1.1.2.2 The thin filament</i>	25
<i>1.1.2.3 The titin filament</i>	29
<i>1.1.3 Myosin Binding Protein C (MyBPC)</i>	30
<i>1.1.4 Hypertrophic Cardiomyopathy (HCM)</i>	42
<i>1.1.5 Main HCM related mutations found in cMyBPC role in Hypertrophic cardiomyopathy</i>	50
<i>1.1.6 How does MyBPC assemble into the sarcomere?</i>	57
<i>1.1.6.1 Trimeric collar model</i>	59
<i>1.1.6.2 Axial model</i>	61
<i>1.1.7 Aims of the project</i>	62
<i>1.2 Structure determination</i>	63

1.2.1	<i>NMR spectroscopy</i>	63
1.2.2	<i>Three dimensional structure determination with the program CYANA</i>	68
1.2.2.1	<i>TALOS</i>	70
1.2.2.2	<i>Automated NOE assignment using the CANDID algorithm</i>	72
1.2.2.3	<i>Structure calculation</i>	76
1.2.2.4	<i>Structure validation</i>	78
1.2.3	<i>Protein dynamics</i>	81
1.2.3.1	<i>Relaxation</i>	81
1.2.3.2	<i>Model free analysis</i>	83

## **Chapter 2, Materials and Methods**

2.1	<i>DNA Methods</i>	87
2.1.1	<i>PCR</i>	87
2.1.2	<i>Ligation</i>	89
2.1.3	<i>Competent cells transformation</i>	89
2.1.4	<i>PCR Screening</i>	90
2.2	<i>Protein expression and purification</i>	91
2.2.1	<i>Competent cells transformation for protein expression</i>	91
2.2.2	<i>Expression in Luria- Bertani (LB) medium</i>	91
2.2.3	<i>Expression in minimal medium (M9)</i>	92
2.2.4	<i>Protein purification</i>	92
2.2.5	<i>Refolding of insoluble proteins</i>	95
2.3	<i>Actin Binding assay</i>	96
2.4	<i>NMR spectroscopy</i>	97

## **Chapter 3, Solution structure of domain cC0 of cardiac Myosin Binding Protein C (cMyBPC) and characterisation of its interaction with the Regulatory Light Chain (RLC) of myosin.**

3.1	<i>Results</i>	98
3.1.1	<i>Protein expression and purification</i>	98
3.1.1.1	<i>cC0</i>	98

3.1.1.2	<i>RLC</i>	100
3.1.2	<i>NMR spectroscopy</i>	101
3.1.3	<i>Sequence specific assignment of domain cC0</i>	106
3.1.4	<i>Structure calculation of domain cC0</i>	106
3.1.5	<i>Structure validation</i>	113
3.1.6	<i>Protein dynamics</i>	116
3.1.7	<i>Studies of the interaction between cC0 and RLC</i>	120
3.1.7.1	<i><sup>1</sup>H/<sup>15</sup>N NMR spectroscopy titration between cC0 and miniHMM</i>	123
3.1.7.2	<i><sup>1</sup>H/<sup>15</sup>N NMR spectroscopy titration between cC0 and RLC</i>	125
3.1.8	<i>Mutogenesis studies</i>	130
3.1.9	<i>Actin binding assay</i>	135
3.2	<i>Discussion</i>	138
3.2.1	<i>Structural features of domain cC0</i>	138
3.2.2	<i>Characterisation of the interaction between cC0 and the Regulatory Light Chain</i>	144
3.2.3	<i>Hypertrophic Cardiomyopathy (HCM) missense mutations in domain cC0 of cMyBPC</i>	149
3.2.4	<i>Model of the incorporation of the cMyBPC N-terminus in the sarcomere</i>	150
3.2.5	<i>Conclusions</i>	155

## **Chapter 4, Study of the interaction between domains cC5 and cC8 of cMyBPC**

4.1	<i>Results</i>	156
4.1.1	<i>cC5 protein expression and purification</i>	156
4.1.2	<i>Expression of domain cC8</i>	158
4.1.3	<i>Is domain cC8 properly folded?</i>	158
4.1.3.1	<i>Urea denaturation</i>	160
4.1.3.2	<i>1D <sup>1</sup>H NMR melting curve</i>	164
4.1.4	<i>cC8 expressed as a fusion protein</i>	166
4.1.4.1	<i>Cloning of cC8 in pETM-20 and expression of TrxA_cC8</i>	167
4.1.4.2	<i>Cloning of cC8 in pETM-60 and expression of NusA_cC8</i>	173

4.1.5	<i>Expression of t-RNA supplemented hosts cells</i>	175
4.1.5.1	<i>Expression of cC8 in BL21 Codon Plus (DE3) RP competent cells</i>	175
4.1.5.2	<i>Expression of cC8 in Arctic Express RP competent cells</i>	178
4.1.6	<i>Study of the interaction between domains cC5 and cC8</i>	180
4.1.7	<i>Cloning and protein expression of groups of domains cC5-7 and cC8-10</i>	181
4.1.7.1	<i>Group of domains cC8-10</i>	185
4.1.7.2	<i>Group of domains cC5-7</i>	186
4.2	<i>Discussion</i>	192
4.2.1	<i>Problem of the solubility of domain cC8</i>	192
4.2.2	<i>Stability of domain cC8</i>	194
4.2.2.1	<i>Thermodynamic stability of domain cC8</i>	194
4.2.2.2	<i>Stability of the hydrophobic core of the domain</i>	196
4.2.3	<i>Interaction between cC5 and cC8 of cMyBPC</i>	198
4.2.4	<i>Conclusion</i>	200
<b>Chapter 5, Conclusions</b>		202
<b>Appendices</b>		205
A.1	Culture Media	205
A.2	Sequence specific assignment for domain cC0	208
A.3	Sequence alignment of cMyBPC	219
<b>References</b>		222

## Figures

Figure 1.1	<i>Types of muscles as seen under the light microscope</i>	16
Figure 1.2	<i>Muscle structure</i>	17
Figure 1.3	<i>Striated muscles appearance under the electron microscope</i>	18
Figure 1.4	<i>Sarcomere structure</i>	19
Figure 1.5	<i>Myosin head disposition in the thick filament</i>	21
Figure 1.6	<i>Sarcomere cross section</i>	22
Figure 1.7	<i>Myosin</i>	23
Figure 1.8	<i>Myosin S1 domain</i>	24
Figure 1.9	<i>Actin filament</i>	27
Figure 1.10	<i>Molecular structure of the thin filament</i>	28
Figure 1.11	<i>Isoforms of MyBPC</i>	31
Figure 1.12	<i>IgI and FnIII folds</i>	32
Figure 1.13	<i>Sequence alignment of C1-linker-C2 for the three human isoforms</i>	38
Figure 1.14	<i>Cardiac remodelling</i>	44
Figure 1.15	<i>Model of cC1-cC2 interaction with S2A</i>	58
Figure 1.16	<i>Trimeric collar model</i>	60
Figure 1.17	<i>Axial model</i>	61
Figure 1.18	<i>Heteronuclear coupling constants <math>J</math> between nuclei of a protein backbone</i>	64
Figure 1.19	<i>Phase coherence transfer between nuclei in triple resonance NMR experiments</i>	66
Figure 1.20	<i>Iterative process followed by the program CYANA</i>	69

Figure 1.21	<i><math>\varphi</math>, <math>\psi</math> and <math>\omega</math> torsion angles</i>	70
Figure 1.22	<i>Graphic interface of the TALOS output</i>	71
Figure 1.23	<i>Conditions that must be fulfilled by a valid assignment</i>	73
Figure 1.24	<i>Constraints combination</i>	76
Figure 1.25	<i>Relaxation processes</i>	82
Figure 3.1	<i>Purification of domain cC0</i>	99
Figure 3.2	<i>Ht<sub>7</sub>RLC after TEV digestion and purification with IMAC on Ni<sup>2+</sup> columns</i>	100
Figure 3.3	<i><sup>1</sup>H/<sup>15</sup>N HSQC spectrum for domain cC0</i>	102
Figure 3.4	<i><sup>15</sup>N strips for HNCaCb and HN(CO)CaCb spectra of domain cC0</i>	103
Figure 3.5	<i><sup>1</sup>H/<sup>1</sup>H/<sup>15</sup>N TOCSY and NOESY spectra of domain cC0</i>	104
Figure 3.6	<i>HCCH-TOCSY and <sup>1</sup>H/<sup>1</sup>H/<sup>13</sup>C NOESY spectra of residue Gln75 of domain cC0</i>	105
Figure 3.7	<i>Longrange NOEs obtained for domain cC0</i>	109
Figure 3.8	<i>Structure of domain cC0 of cMyBPC</i>	110
Figure 3.9	<i>Ribbon view of domain cC0 structure</i>	111
Figure 3.10	<i>Number of constraints per residue</i>	112
Figure 3.11	<i>Ramachandran plot obtained for the structure of domain cC0</i>	113
Figure 3.12	<i>Procheck NMR residue by residue results for the calculated structure of domain cC0</i>	115
Figure 3.13	<i>Correlation time values</i>	118
Figure 3.14	<i>Rigidity of the molecule versus number of constraints</i>	119
Figure 3.15	<i>Sequence alignment of the regulatory Light Chain (RLC) of</i>	

	<i>myosin</i>	121
Figure 3.16	<i>Structure of myosin and how it could interact with domain cC0</i>	122
Figure 3.17	<i><math>^1\text{H}/^{15}\text{N}</math> HSQC spectrum for the cC0+miniHMM titration</i>	124
Figure 3.18	<i>Chemical shift changes for the amide groups of domain cC0 following the titration with miniHMM</i>	125
Figure 3.19	<i><math>^1\text{H}/^{15}\text{N}</math> HSQC spectrum for the cC0+RLC titration. Panel 1</i>	127
Figure 3.20	<i><math>^1\text{H}/^{15}\text{N}</math> HSQC spectrum for the cC0+RLC titration. Panel 2</i>	127
Figure 3.21	<i>Residue Lys14 during the cC0+RLC titration</i>	128
Figure 3.22	<i>Residue Arg16 during the cC0+RLC titration</i>	128
Figure 3.23	<i>Chemical shift changes for amide groups of domain cC0 following the titration with RLC</i>	129
Figure 3.24	<i>Results of the cC0+RLC titration</i>	130
Figure 3.25	<i>pLEICS-3 vector map</i>	131
Figure 3.26	<i>Chemical shift changes for amide groups of domain cC0_G4R following the titration with RLC</i>	133
Figure 3.27	<i>Chemical shift changes for amide groups of domain cC0_R34W following the titration with RLC</i>	134
Figure 3.28	<i>Chemical shift changes for amide groups of domain cC0_K89E following the titration with RLC</i>	135
Figure 3.29	<i>Actin binding assay</i>	137
Figure 3.30	<i>Sequence alignment for domain cC0</i>	139
Figure 3.31	<i><math>\beta</math>-bulge</i>	140
Figure 3.32	<i>Aromatic residues at the core of domain cC0</i>	141
Figure 3.33	<i>Electrostatic surface of domain cC0</i>	142

Figure 3.34	<i>Sequence alignment of the top five structures identified by the DALI server</i>	144
Figure 3.35	<i>Sequence alignment of human cardiac and <i>Aequipecten Irradians</i> (bay scallop) isoforms of RLC</i>	145
Figure 3.36	<i>Model of human cardiac RLC</i>	146
Figure 3.37	<i>Electrostatic surface of RLC</i>	148
Figure 3.38	<i>HCM missense mutations of domain cC0</i>	150
Figure 3.39	<i>Model of the interaction between the N-terminus of cMyBPC and myosin</i>	152
Figure 3.40	<i>Model of a possible interaction between cMyBPC and myosin</i>	153
Figure 3.41	<i>Model of a possible interaction between cMyBPC and myosin</i>	154
Figure 4.1	<i>Purification of cC5</i>	157
Figure 4.2	<i>1D <sup>1</sup>H NMR spectrum of domain cC8</i>	159
Figure 4.3	<i>Urea denaturation of domain cC8</i>	161
Figure 4.4	<i>Urea denaturation curve and Gibbs free energy for domain cC8</i>	162
Figure 4.5	<i>Melting curve for domain cC8</i>	165
Figure 4.6	<i>pETM-20 vector map</i>	168
Figure 4.7	<i>Cloning of cC8 in pETM-20</i>	168
Figure 4.8	<i>SDS-PAGE gel of cC8_TrxA expressed in different competent cells</i>	169
Figure 4.9	<i>SDS-PAGE gel of cC8_TrxA expressed in Rosetta (DE3) PLysS at 15°C after IMAC purification on Ni<sup>2+</sup> columns</i>	170

Figure 4.10	<i>Size exclusion chromatography purification step of TrxA_cC8</i>	171
Figure 4.11	<i><math>^1\text{H}/^{15}\text{N}</math> HSQC spectrum of cC5 after different additions of TrxA_cC8</i>	172
Figure 4.12	<i>pETM-20</i>	173
Figure 4.13	<i>Purification of cC8_NusA</i>	174
Figure 4.14	<i>SDS-PAGE gel and size exclusion chromatogram of domain cC8 in pET-8c expressed in Codon Plus (DE3) RP cells</i>	177
Figure 4.15	<i>Purification of cC8 expressed in Arctic Express RP cells</i>	179
Figure 4.16	<i>SDS-PAGE gel of the samples used to study the C5+cC8 interaction</i>	180
Figure 4.17	<i><math>^1\text{H}/^{15}\text{N}</math> HSQC spectrum for the cC5+cC8 titration. Panel 1</i>	181
Figure 4.18	<i>pETM-11 vector map</i>	182
Figure 4.19	<i>Cloning of cC5-7 in vector pETM-11</i>	184
Figure 4.20	<i>Cloning of cC8-10 in vector pETM-11</i>	185
Figure 4.21	<i>SDS-PAGE gel of group of domains cC8-10 expressed in BL21 Star (DE3) cells after IMAC purification on <math>\text{Ni}^{2+}</math> columns</i>	186
Figure 4.22	<i>SDS-PAGE gel and size exclusion chromatogram of group of domains cC5-7 expressed in BL21 Star (DE3) cells</i>	187
Figure 4.23	<i>1D <math>^1\text{H}</math> NMR spectrum of cC5-7</i>	188
Figure 4.24	<i><math>^1\text{H}/^{15}\text{N}</math> HSQC spectrum of group of domains cC5-7</i>	190
Figure 4.25	<i><math>^1\text{H}/^{15}\text{N}</math> TROSY spectrum of group of domains cC5-7</i>	191
Figure 4.26	<i>Effect of the ring current generated by the aromatic systems.</i>	197

## Tables

Table 1.1	<i>HCM related mutations identified in sarcomeric proteins</i>	46
Table 1.2	<i>cMyBPC point mutations causing HCM</i>	48
Table 1.3	<i>NMR experiments necessary for a structure calculation</i>	64
Table 1.4	<i>Spectral density function used in the numerical fit to the experimental <math>T_1</math>, <math>T_2</math> and NOE values.</i>	85
Table 2.1	<i>PCR conditions</i>	88
Table 2.2	<i>PCR cycles</i>	88
Table 2.3	<i>Restriction digestion reaction</i>	88
Table 2.4	<i>Ligation reaction conditions</i>	89
Table 2.5	<i>PCR screening reaction</i>	90
Table 2.6	<i>PCR screening cycles</i>	90
Table 2.7	<i>Sample composition of the solutions used in the actin binding cosedimentation assay</i>	97
Table 3.1	<i>NMR constraints and structural statistics for domain cC0</i>	107
Table 3.2	<i>Delay used for the relaxation experiments</i>	116
Table 3.3	<i>Ratios and final concentrations of cC0 and miniHMM fragment used in the titration performed to study their interaction</i>	123
Table 3.4	<i>Ratios and final concentrations of cC0 and RLC used in the titration performed to study their interaction</i>	126
Table 3.5	<i>Primers used to clone wildtype cC0 and the four mutants</i>	131
Table 3.6	<i>DALI results. Proteins with the most similar structure to domain cC0 within the Protein Data Bank</i>	143
Table 4.1	<i>Urea denaturation of domain cC8</i>	160

Table 4.2	<i>ID NMR melting curve of domain cC8</i>	164
Table 4.3	<i>Primers used to clone cC8 in both vectors pETM-20 and pETM-60</i>	167
Table 4.4	<i>Ratios of cC5 and cC8_TrxA used in the titration performed to study their interaction</i>	172
Table 4.5	<i>Ratios of cC5 and cC8_NusA used in the titration performed to study their interaction</i>	174
Table 4.6	<i>Ratios of cC5 and cC8 used in the titration performed to study their interaction</i>	180
Table 4.7	<i>Primers used to clone cC5-7 and cC8-10 in pETM-11</i>	182

## Abbreviations

CANDID	Combined automated NOE assignment and structure
CYANA	Combine assignment and dynamic algorithm for NMR applications
DSC	Differential scanning calorimetry
DTT	1,4- dithiothreitol
HCM	Hypertrophic cardiomyopathy
HSQC	Heteronuclear Single Quantum Coherence
IMAC	Immobilised metal affinity chromatography
IPTG	Isopropyl- 1- thio- $\beta$ - D- galactopyranoside
LB	Luria- Bertani
MyBPC	Myosin Binding Protein C
NMR	Nuclear Magnetic Resonance
NOE	Nuclear Overhauser Effect
NOESY	Nuclear Overhauser Effect Spectroscopy
PCR	Polymerase Chain Reaction
PDB	Protein Data Bank
RLC	Regulatory Light Chain
TOCSY	TOTal Correlation Spectroscopy
TROSY	Transverse Relaxation Optimized Correlation Spectroscopy
$\beta$ ME	2-Mercaptoethanol
$\phi$	Phi, the dihedral angle between amide nitrogen and alpha carbon
$\psi$	Psi, dihedral angle between alpha and carboxyl carbons
$\omega$	Omega, dihedral angle between amide nitrogen and carboxyl carbon
Ht	Six Histidine tag
Ht <sub>r</sub>	Six Histidine tag with TEV protease digestion site

# Chapter 1

## Introduction

### 1.1 *Myosin Binding protein C (MyBPC)*

#### 1.1.1 Muscle structure and function

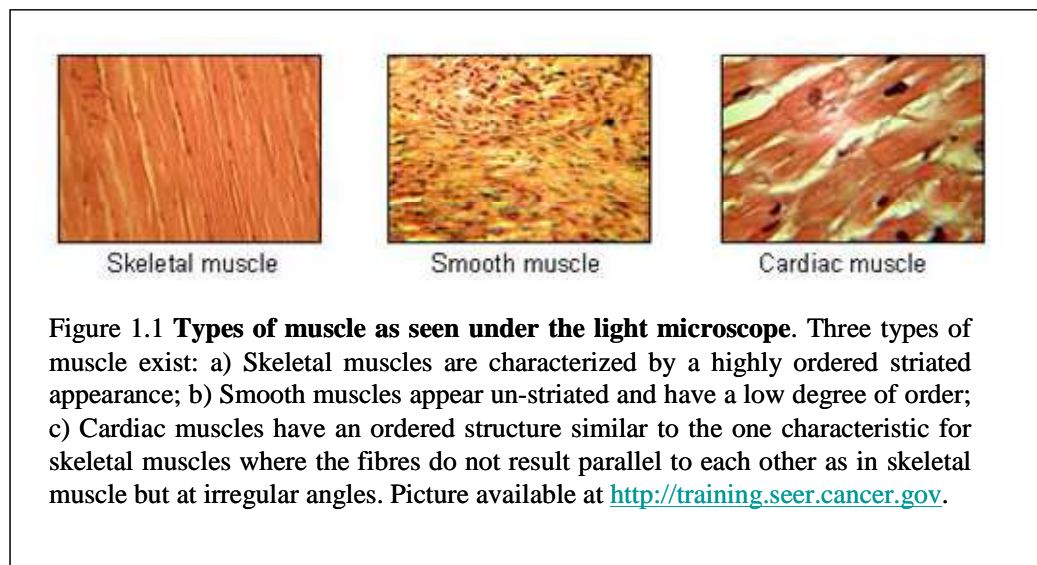
The capacity to move is one of the most important characteristics of higher organisms and the way this is achieved may vary. The basic machinery involved in movement is formed by muscles and different types of muscle exist to meet the need of different species or of different parts of an organism.

In mammals different kind of muscles can be identified, some voluntary some involuntary.

Three type of muscle exist: skeletal, smooth and cardiac muscles.

- Skeletal muscles have a characteristic striated appearance under the light microscope due to the alignments of their myofibrils, they are responsible for voluntary movements and are under nervous regulation. They can be divided in two main categories, according to the function they have, which is mirrored at the molecular level. We can distinguish between red and white skeletal muscles, the red, also called slow skeletal muscles, being responsible to keep the posture and perambulate, their colour is due to the presence of myoglobin that stores the oxygen needed for the sustained contraction necessary to maintain the posture and walk; white muscles, also known as fast skeletal, on the other hand, are more rarely used and rely on glycogen as fuel and can give rise to short burst of contraction for a limited period of time.

- The cardiac muscle is an involuntary muscle whose contraction is regular and continuous throughout the organism's life. Its appearance under the light microscope is similar to that of skeletal muscles but instead of having parallel fibres, as in skeletal muscles, they appear forming irregular angles between one another (Figure 1.1).

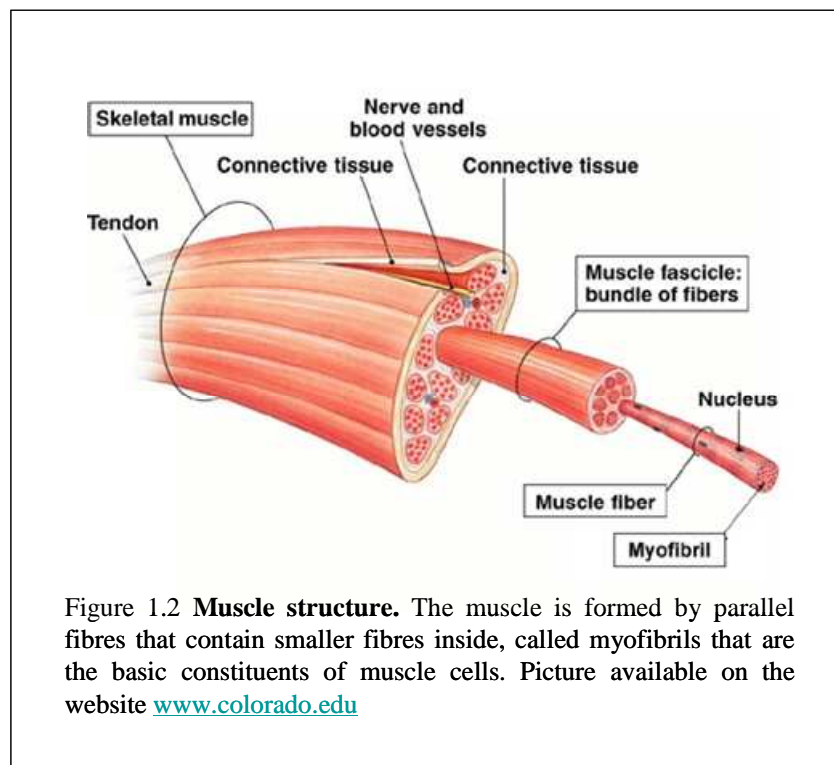


- Smooth muscles are involuntary, they appear un-striated at the light microscope. They are not under nervous regulation and are responsible for a variety of function in the body, from contraction of blood vessels to skin response to cold temperatures. Theirs structure is less ordered than that of striated muscles.

### 1.1.2 Striated muscles and sarcomere organization

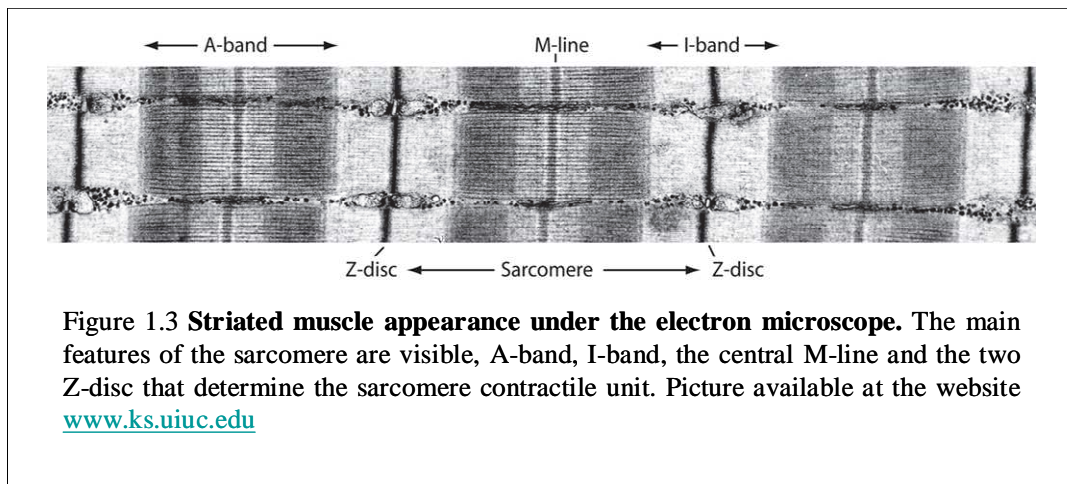
Morphologically striated muscles are formed by a belly that is surrounded by the epimysium, a membrane that enclose the fibres, and contains a connective tissue, the

endomysium, between adjacent fibres and the perimysium around the bundle of fibres. The muscle is formed by primary fibres, called fasciculus, that are divided in secondary (sarcolemma) and tertiary (myofibril) fibres (Guyton, 2005). Each fibre is a giant multinucleated cell formed by thousands myofibrils that form 80% of the total volume of a muscle (Figure 1.2).



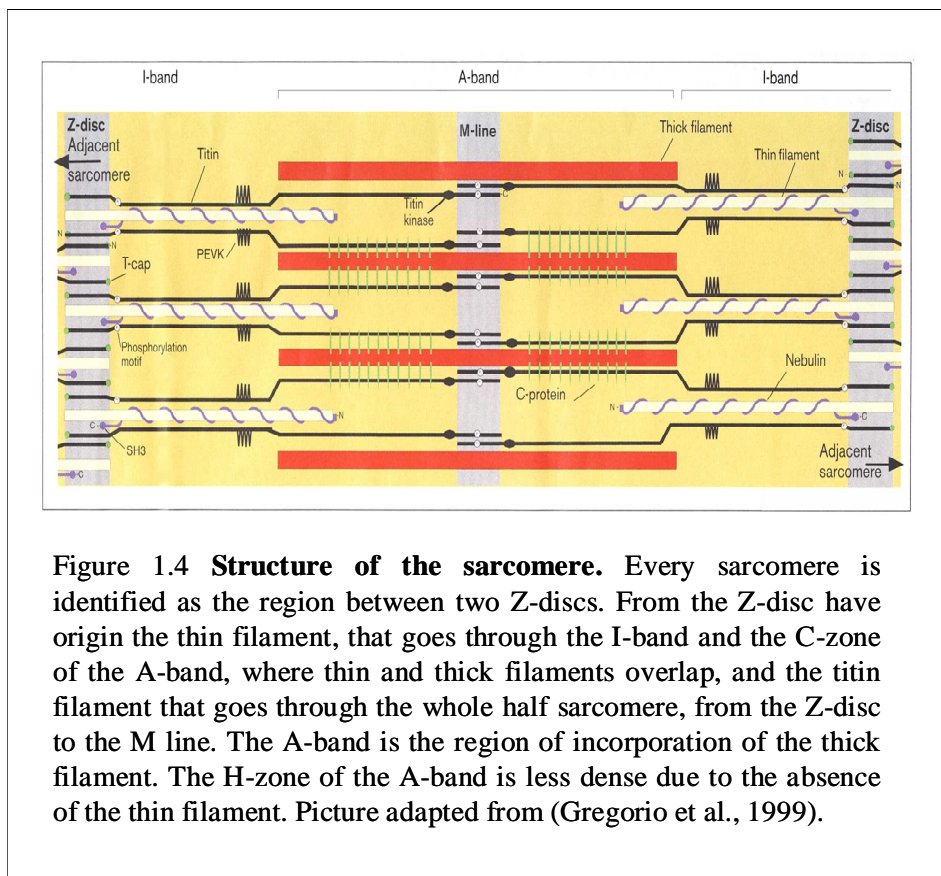
In striated muscles it is possible to individuate cross bands arising from aligned striation on each myofibril. The contractile unit of striated muscles is the sarcomere, which possesses three properties that are fundamental for its function: the ability to shorten rapidly and efficiently, the ability to switch on an off in milliseconds and its structural regularity. The sarcomere is bordered at each end by the Z- disc, a dark narrow line that appear in stained muscle fibres, which bisects the I band that is shared by adjoining sarcomeres. At the centre of each sarcomere is a darker A band bisected by a less dense

H band; inside the H band is located a still less dense region named the pseudo H band at the centre of which is the M line, that is also at the centre of the whole sarcomere (Figure 1.3).



The A band is formed by an array of thick filaments in longitudinal register and running parallel to the fibre axis, while each half I band contains an array of thin filaments also in longitudinal register. The thin filaments starts at the Z line and run through the I band to the A band where they overlap with the thick filaments. The H band is less dense than the st of the A band due to the absence of thin filaments. Simplifying the structure of the sarcomere, we could say that it comprises three different type of proteins: contractile, regulatory and structural. Actin and myosin are the main contractile constituents, they organise in polymers called thin and thick filaments respectively, that interact with one another to give rise to muscle contraction. Their interaction is mediated by the presence of regulatory proteins, such as tropomyosin and the troponin complex that regulate actin- myosin interaction and hence contraction in response to  $\text{Ca}^{2+}$  concentration. A large number of structural proteins play a role during development to achieve the final structure of the sarcomere. Myosin binding proteins

help the assembly of the myosin thick filament and play a role also in contraction in the cardiac muscle. Capping proteins, localised at the end of the filaments, prevent polymerisation or depolymerisation, thus helping to maintain precise filament length. Cross-linking proteins in the Z and M line link the thin and thick filaments respectively into ordered longitudinally registered three dimensional lattice. Finally, the giant proteins titin and nebulin specify the assembly of the thick and thin filaments in the sarcomere and titin also plays a critical mechanical role in contraction (Figure 1.4).



The sarcomere contains at least 28 different proteins of which actin and myosin account for more than 70% of the total (actin 20%, myosin 54%) (Hanson and Huxley, 1957; Huxley and Hanson, 1957). The actin- myosin complex hydrolyzes ATP, the source of energy for contraction.

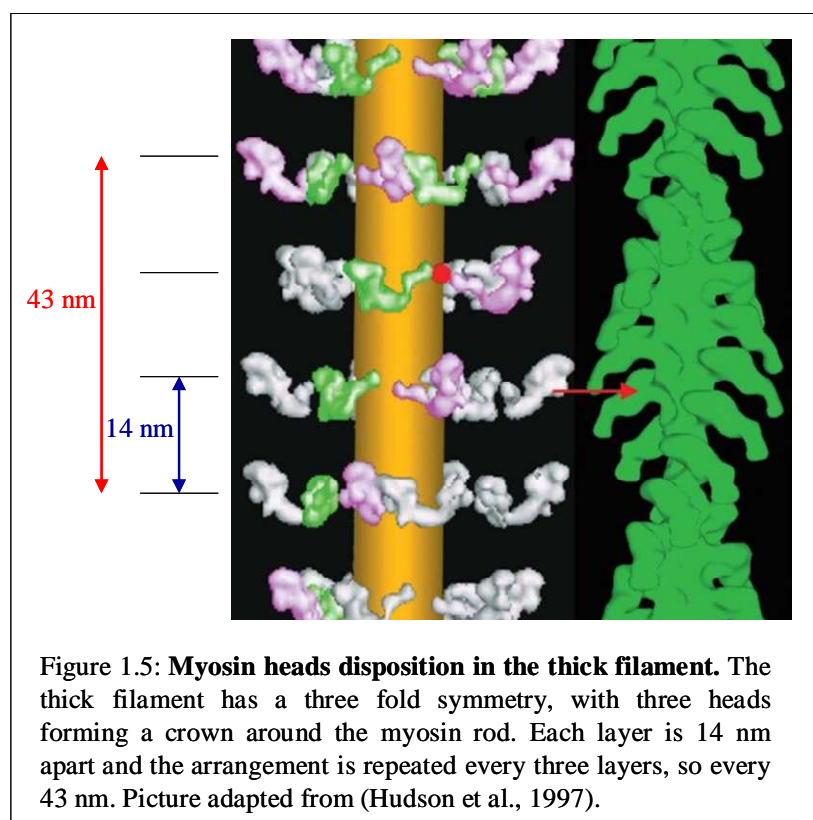
It was long believed that the myofibrils were formed by a single sets of filaments and that contraction resulted from some form of internal unfolding, until works in the early 1950s show quite a different situation. In 1954 it was suggested (Huxley and Niedergerke, 1954; Huxley and Hanson, 1954) that muscle contraction was the result of sliding of filaments over one another, without changes in their lengths. The sliding filament model was based on the observation at the light microscope that the A band did not change its length during contraction, while the I band and the H band shortened.

It was noted (Huxley, 1957) that the thick filaments had projections (cross-bridges) on their surfaces that bound to the thin filaments in the region where the thick and thin filaments overlap. This suggested the idea that cross-bridge formation could provide the link between the filaments to enable them to slide.

#### *1.1.2.1 The thick filament*

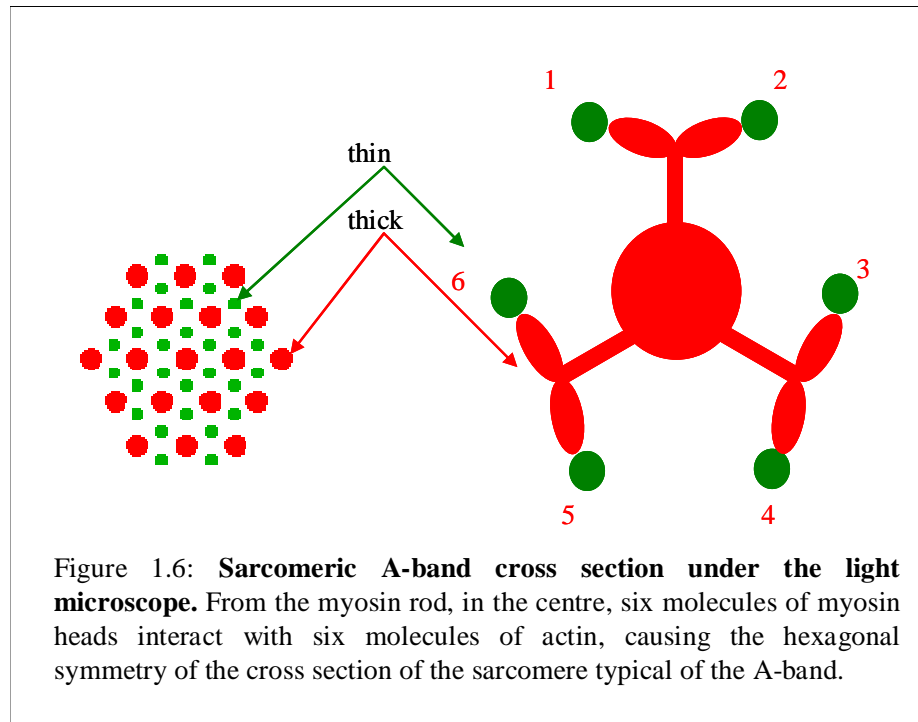
The thick filament of vertebrate skeletal muscles is 1.6  $\mu\text{m}$  long and 15 nm in diameter (Huxley, 1969), with a rough appearance along most of its length due to the presence of cross-bridges formed with the thin filament. The only region without cross-bridges is the central H band. The thick filament is a polymer formed by 300 molecules of the protein myosin II (Huxley, 1963), a hexamer consisting of two heavy chains (223 kDa) and two pairs of light chains (15- 22 kDa). Myosin is both an enzyme and a structural protein and its structure reflects it, having an enzymatic domain (head) physically separated from the tail of the protein that has a structural function. The  $\alpha$ -helices twist around each other to form a stable  $\alpha$ -helical coiled- coil tail 155 nm long (Lowey et al., 1969). Sequence analysis of the myosin tails show the presence of a heptad repeat where hydrophobic residues are packed against each other causing the packing of the

two helices in a stable coiled- coil in a structure that is repeated every seven residues. Another longer repeating structural unit of 28 amino acids has been identified in which a region of positive charged residues is separated from a region of negatively charged amino acids by 14 residues (McLachlan and Karn, 1982). At the N-terminus, each heavy chain folds into a globular head 19 nm long and 5 nm wide at its maximum (Rayment et al., 1993). The myosin heads stretch out from the  $\alpha$ -helical coiled-coil to interact with actin, forming the cross- bridges. In all vertebrate striated muscles the axial distance between adjacent levels of myosin heads is 14.3 nm and the repeat distance of the helix is three times this, so 43 nm (Huxley and Brown, 1967; Matsubara, 1974; Matsubara and Millman, 1974) (Figure 1.5).



Looking at myofibril in cross section, it is easy to identify the myosin rod and three molecule of myosin head, each of them formed by two heads respectively, that reach

out to interact with actin, as shown in figure 1.6. This causes the appearance of the sarcomeric A-band when seen under the light microscope.

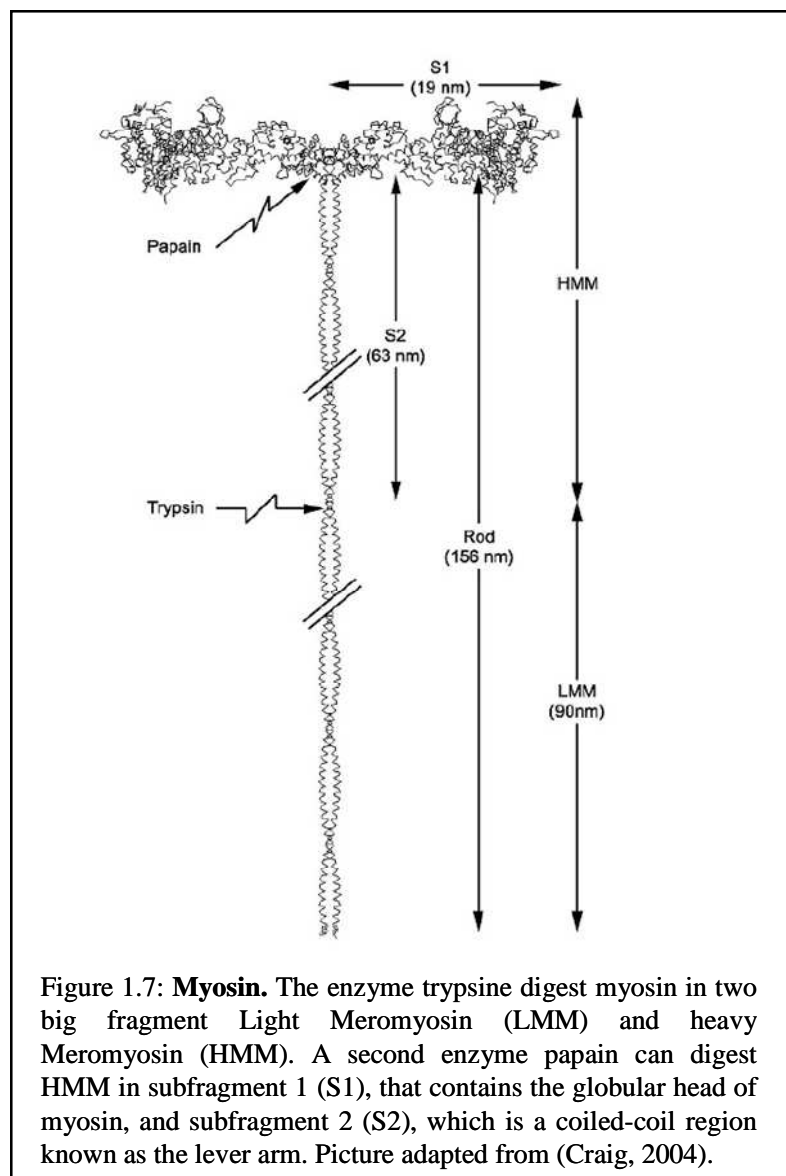


Different myosin fragments have been identified through proteolysis (figure 1.7). Two big fragments named heavy and light meromyosin, HMM and LMM respectively, have been obtained after digestion with the enzyme trypsin. LMM corresponds to the coiled-coil region. HMM can be divided in two parts through digestion with papain: subfragment 1 (S1) comprises the heads of myosin, the domains that interact with actin and have a ATPase activity and the two light chains, and subfragment 2 (S2), the coiled-coil region of myosin.

LMM is insoluble at physiological ionic strength, indicating a strong propensity to self associate; the other coiled-coil fragment, S2, is more soluble than LMM, indicating a weaker tendency to self-associate and this is very important as it allows the myosin

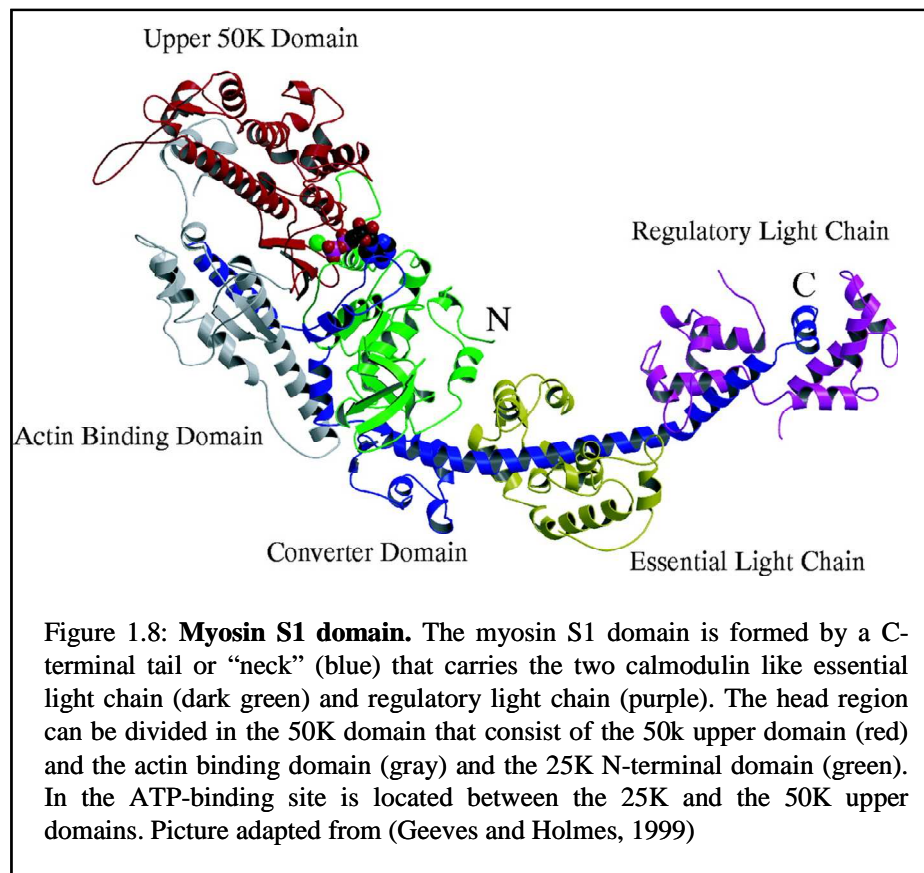
heads the freedom of movement they need to interact with actin during muscle contraction.

Each myosin head (S1), which is soluble at physiological condition, has a molecular mass of 130 kDa (Vibert and Cohen, 1988) and comprises the first 843 residues of the heavy chain, together with the two light chains.



Three different domains have been identified proteolytically (Mornet et al., 1981) in S1, named after their molecular masses: 25K (N-terminus), 50K (middle) and 20K (C-

terminus) (Mornet et al., 1979). All the three fragments contribute to a 7-stranded  $\beta$ -sheet with numerous  $\alpha$ -helices surrounding it to form a cleft that extends from the ATP to the actin binding sites.



The 50K domain can be divided in two subdomains, named 50K upper and 50K lower, or actin binding, domains respectively (Rayment et al., 1993). The N-terminus (25K domain) is in proximity to the neck region where the two light chains are and, together with the 50K upper domain, forms the bulk of the protein that contains the ATP binding site, which is located at the boundary between the two domains. The 50K lower domain forms the actin binding site, followed by a large, positively charged loop also involved in the interaction with actin. This 75 kDa (50+25 kDa) region of myosin is known as the motor domain, while the remaining 20K domain and the two light chains, forms the

regulatory domain or lever arm because of its function during contraction (Dominguez et al., 1998; Rayment et al., 1993). The ATPase site is 5nm from the tip of the head and 4 nm opposite the actin binding site.

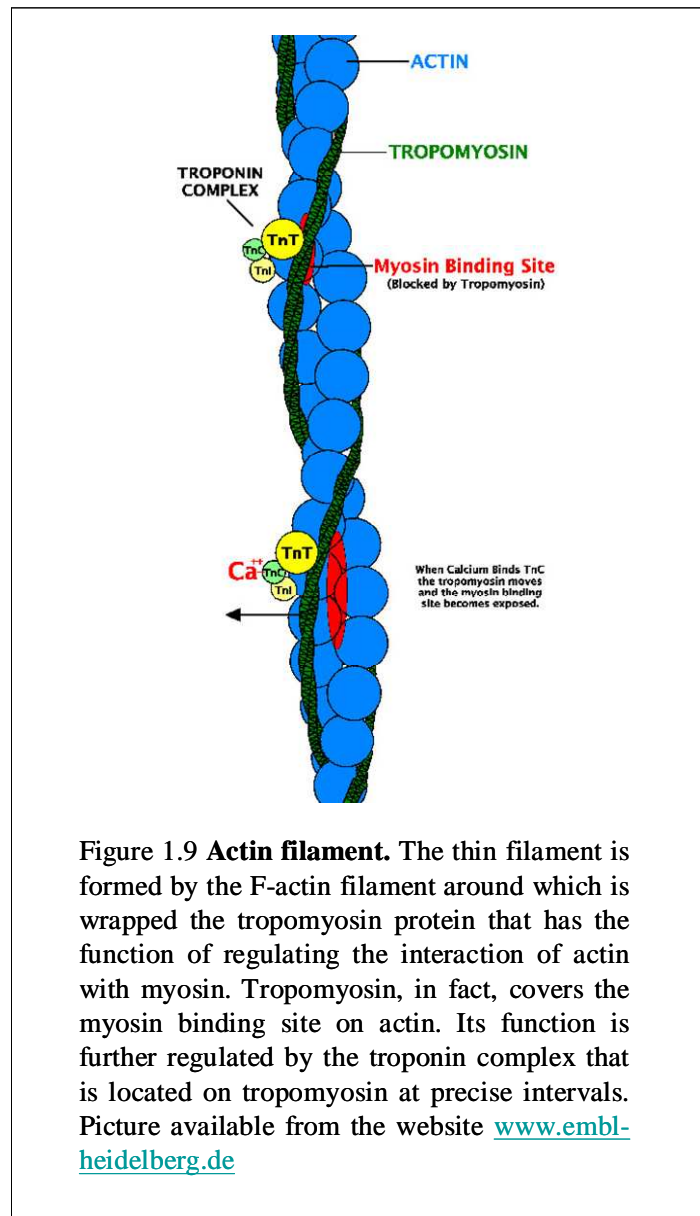
### **1.1.2.2 Thin filament**

The thin filament in the sarcomere runs from the Z disc to the edge of the H band, is about 1 $\mu$ m long and 10 nm in diameter (Huxley, 1969). The major component of the thin filament is actin (Pollard, 1990; Sheterline et al., 1995) a globular protein (G actin) with a molecular mass of 42 kDa, that self-associate to form a helical polymer known as F actin formed by 360 molecules of G actin. Attached to actin are regulatory proteins, such as tropomyosin and troponin (Gordon et al., 2000; Solaro and Rarick, 1998; Zot and Potter, 1987), that regulate the actin-myosin interaction, and the giant protein nebulin (Gregorio et al., 1999; Horowitz et al., 1996; Wang and Wright, 1988) that runs for the entire length of the thin filament and is thought to be involved in determining the filament length.

At low ionic strength in vitro, actin exists in its monomeric form G-actin; when the ionic strength is increased to its physiological value then actin tends to polymerize to form F-actin. The filament is formed by two helices of F-actin twisted around each other to form an double helix. G-actin is a globular protein formed by a single polypeptide chain containing 375 amino acids, its secondary structure is partially formed by  $\alpha$ -helices, part by  $\beta$ -sheets and about two quarters random coil (Kabsch and Vandekerckhove, 1992). The sequence of actin is widely conserved between isomers (skeletal, cardiac, non-muscular actins) and species, this is probably due to the fact that actin interacts with a great variety of proteins and needs to conserve a large number of binding sites.

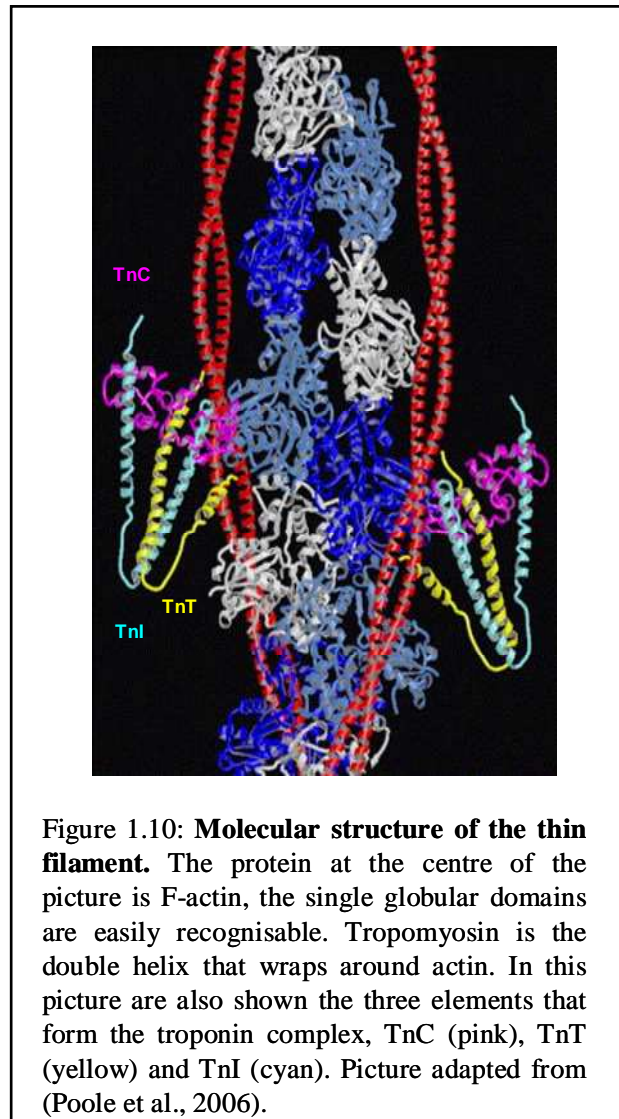
Muscle contraction is regulated by the concentration of  $\text{Ca}^{2+}$ : at low level of  $\text{Ca}^{2+}$  ( $10^{-8}$  M) the muscle is relaxed, at high concentration of  $\text{Ca}^{2+}$  ( $10^{-5}$  M) the muscle contracts. In vertebrate muscles the contraction is regulated primarily by the thin filament proteins tropomyosin and troponin, which respond to changes in the concentration of  $\text{Ca}^{2+}$  in the sarcoplasmic reticulum. Tropomyosin (Perry, 2001) is an elongated protein that associate with seven actin monomers, while troponin is a complex of three subunits which attach every 38.5 nm to a specific site of tropomyosin. Troponin is the  $\text{Ca}^{2+}$  binding protein that regulates contraction inhibiting actin-myosin interaction at low  $\text{Ca}^{2+}$  concentration; when the concentration increases troponin binds to  $\text{Ca}^{2+}$ , releasing the inhibitory effect of the troponin- tropomyosin complex, allowing actin and myosin to interact causing the sarcomere to contract.

Tropomyosin is a two-stranded  $\alpha$ -helical coiled-coil of molecular mass 65kDa. Its chains run parallel to each other, wrapping around the F-actin molecule, 41 nm long and 2 nm in diameter (Perry, 2001).



Troponin is a 80 kDa complex formed by three subunits, TnI, TnT and TnC. Troponin I is the inhibitory component and when bound to actin is able to inhibit the actin-myosin interaction on its own, without the presence of any other component . When Ca<sup>2+</sup> binds to TnC, the bond between TnI and TnC becomes stronger and the link between TnI and actin weakens, making it possible for actin and myosin to interact. TnC is the Ca<sup>2+</sup> binding component of the troponin complex, it belongs to the family of EF-hand proteins, all of which are able to coordinate metal ions. Fast skeletal isoforms of TnC

have four metal binding site of the helix-loop-helix kind, two high affinity sites occupied by  $Mg^{2+}$  in the cell, and two low affinity sites where  $Ca^{2+}$  binds, bringing on muscle contraction (Gordon et al., 2000).



TnT (Perry, 1998) is the component of troponin that binds to tropomyosin. It binds to the other two subunits of troponin, to tropomyosin and to actin, working as a glue to keep the three proteins in contact. TnT is responsible for the positioning of the troponin complex on tropomyosin at its characteristic 38.5 nm intervals along the thin filament.

### 1.1.2.3 Titin filament

The idea that a third set of filaments might exist was suggested by the integrity of sarcomeres stretched beyond actin-myosin overlap and from which actin and myosin have been extracted. A giant protein named titin, (Gregorio et al., 1999; Maruyama, 1999; Trinick, 1996) is responsible for this behaviour. Titin is a single polypeptide chain with molecular mass of 3 MDa, formed by 27000 amino acids (Labeit et al., 1997). It is the largest protein known and constitutes 10 percent of the myofibrillar mass, being the third most abundant sarcomeric protein. A single molecule of titin is extraordinarily long (1 $\mu$ m) and thin (4 nm in diameter). In the muscle a molecule of titin extends for half the sarcomere, from the Z disc to the M line. The molecule originates at the Z disc, then follows an elastic region which runs parallel to the thin filament through the I band, while the C-terminus of the proteins forms part of the thick filament, binding to myosin and ending in the M line (Gregorio et al., 1998). At the Z disc and M line titin from neighbouring sarcomeres overlap creating a continuous system of filaments.

Like other myosin binding proteins, titin has a modular structure and is formed by immunoglobulin (Ig) and fibronectin (Fn) like domains. Fn like domain are present only in the A band and are arranged in superrepeat, together with the Ig-domains. The I-band region of titin contains just Ig-like domains, organised in two blocks of repeats separated by a region rich in proline (P), glutamate (E), valine (V) and lysine (K), the so called PEVK domain (Labeit et al., 1997).

Titin is one of the first proteins to assemble in the sarcomere during its development and is the only one that extends for half sarcomere, interacting with various other proteins at precise interval, suggesting a structural role as a molecular template during sarcomere assembly, coordinating thin and thick filament incorporation.

In a mature sarcomere titin seems to have the important mechanical role of elastic element; titin elasticity is found in the I band where the two block of Ig domains are separated by the PEVK region (Horowitz, 1999). Passive tension and slack length of a muscle are determined primarily by titin, when a muscle is stretched beyond its slack length the Ig region straightens with a little increase in tension, and if stretched even more, the PEVK domains unravels, with exponentially increasing tension.

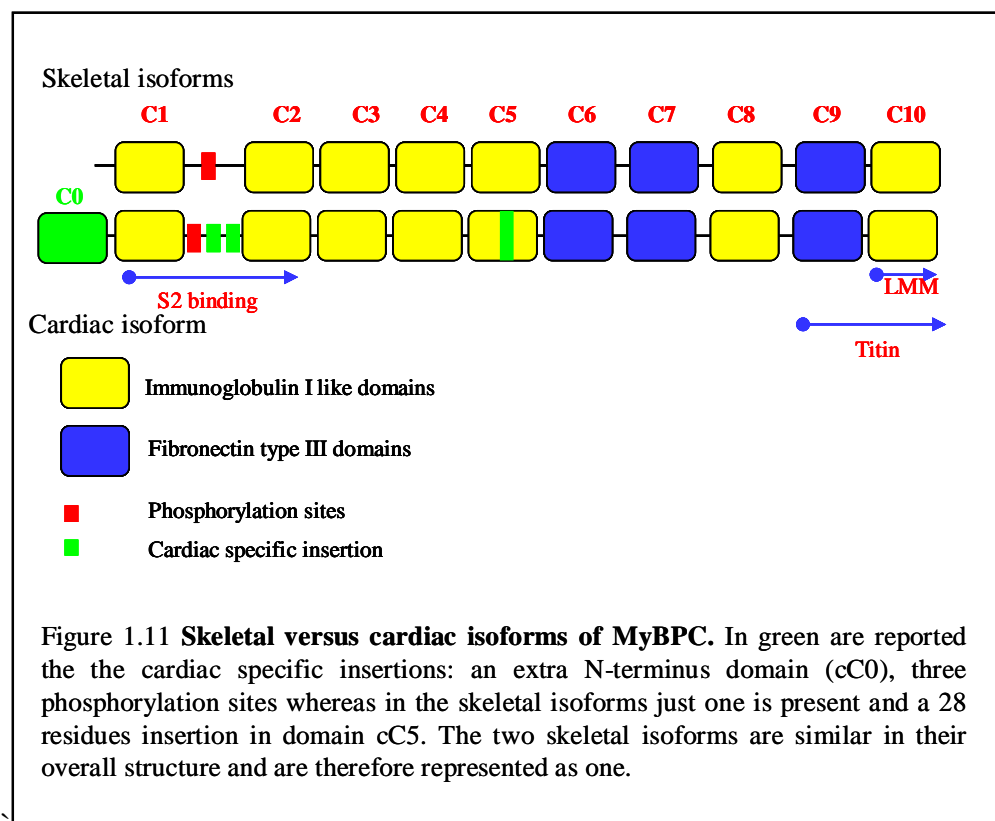
### **1.1.3 Myosin binding protein C**

A set of proteins that bind to myosin at regular intervals is found in all vertebrates striated muscles, both skeletal and cardiac, and being totally absent from smooth, invertebrate and nonmuscle cells it can be considered a feature of the highly specialised A band of striated muscles (Bennett et al., 1999). Myosin binding protein C (MyBPC) (Offer et al., 1973), the most abundant of this set of proteins, is a multidomain protein located in a region of the A-band where thick and thin filaments overlap, known as C-zone (Figure 1.4). In mammalian muscles MyBPC usually forms seven to nine of the eleven structurally regular transverse C- zone stripes, however, the distribution of this and other myosin binding protein tends to be species and fibre specific. The distance between stripes corresponds with the myosin helical repeat, that is one every third myosin molecule, so 43 nm apart. The position of MyBPC seems to be dictated by the presence of binding sites on titin (Bennett et al., 1999). MyBPC is present only in this specific region of the A- band and is absent from any other region of the sarcomere, representing about 2% of the myofibril mass. All this, limits the interaction between myosin and MyBPC to one every three myosin heads.

MyBPC exists in three isoforms, fast skeletal, slow skeletal and cardiac (Yamamoto and

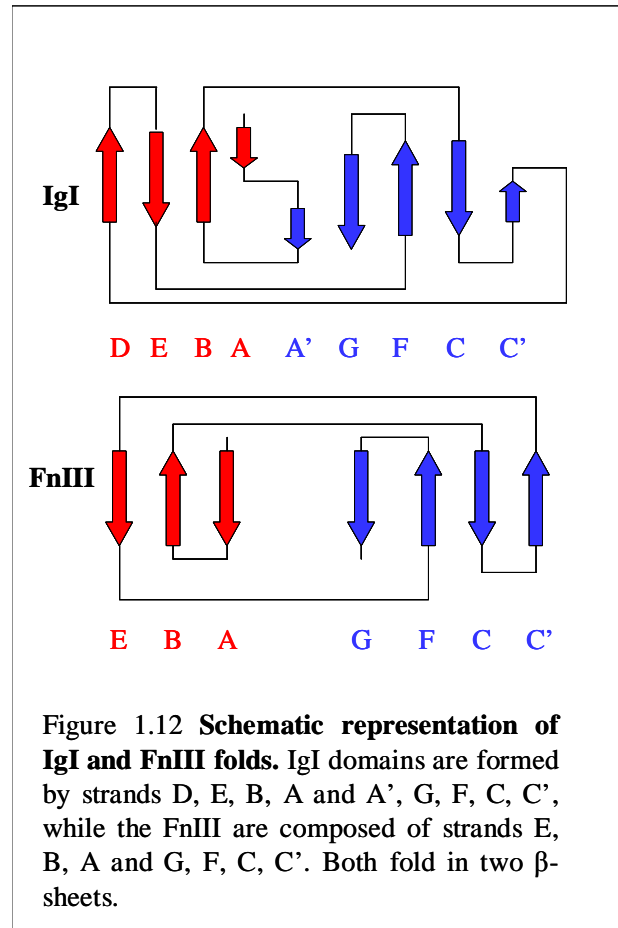
Moos, 1983). In human, the three isoforms map to different chromosomes: fast skeletal to chromosome 19q13.33, slow skeletal to chromosome 12q23.3 and cardiac to chromosome 11p11.2, showing that the three isoforms are not products of alternative splicing. The isoforms tent to be fibre specific, with the cardiac form present only in the heart; however, fast and slow skeletal isoforms seem to co-exist in some form of muscle (Flashman et al., 2004).

Each skeletal MyBPC contains ten domains, seven I-class immunoglobulin (Ig-I) domains and three fibronectin type III (FnIII) domains arranged in the same order (Ig-Ig-Ig-Ig-Fn-Fn-Ig-Fn-Ig), identified as domains C1 to C10 (Okagaki et al., 1993).



The immunoglobulin fold is composed of two  $\beta$ -sheets comprising five anti parallel  $\beta$ -strands in each sheet. In an Ig-I domain one of the  $\beta$ -sheet is composed of strands A, B,

E and D and the other of strands A', G, F, C and C' (Harpaz and Chothia, 1994). The other class of protein modules found in MyBPC is, as already mentioned, the FnIII that are also composed of two  $\beta$ -sheets, one containing strands A, B and E and the other G, F, C and C', that fold into a  $\beta$ -sandwich (Goll et al., 1998; Main et al., 1992).



The alignment of different forms of this protein shows that the sequence identity across human isoforms (domains C1-C10) is 39.6% (Thompson et al., 1997), regions of low identity were found outside the Ig and Fn domains, especially the sequence that precedes domain C1, the linker between domains C1 and C2 and, in the cardiac isoform, in the insert of domain C5. The identity between cardiac isoforms from different species is 46.8% (see appendix A3 p. 210).

The cardiac isoform differs from the two skeletal isoforms in four ways:

1. it contains an additional amino terminal Ig-I domain (C0) (Gautel et al., 1995);
2. there is a 9- residue insertion in the linker between domain C1 and C2, the so called MyBPC motif, in the cardiac variant, which is the key substrate site for the phosphorylation (Gautel et al., 1995). In this region in the cardiac isoform are present three phosphorylation sites, while just one is present in both types of skeletal muscle cells. The number of phosphorylation sites seems to vary between species but the cardiac isoform always present more sites, usually three.
3. it contains a prolin/charged residue-rich insertion into the domain C5 (Gautel et al., 1995).
4. it shows a ten residues insertion between C4 and C5 that contribute to the formation of the enlarged  $\beta$ - bulge present in domain cC5 (Idowu et al., 2003).

The skeletal isoforms are 3 nm in diameter and 40 nm long (Hartzell and Sale, 1985; Swan and Fischman, 1986) and have a molecular mass of 128 kDa, whereas the cardiac isoform is longer, with a length of ~44 nm with an approximately 137 kDa molecular mass (Bennett et al., 1999).

MyBPC seems to have diverse functions in the sarcomere physiology, it might be involved in sarcomere formation and stability as well as show a regulatory function, specially via phosphorylation/ de-phosphorylation of the MyBPC motif.

Because of the inability of myosin to form normal thick filaments in the absence of MyBPC (Koretz, 1979a; Rhee, 1994; Schultheiss, 1990), this protein is assumed to play an important role in the formation of a normal thick filaments; however, a research using cMyBPC knockout mice suggests that the role of MyBPC could be more modulatory rather than essential, as all the knockouts were viable and possessed well developed sarcomeres even though showed a significant cardiac hypertrophy, fibrosis

and myocytes disarray (Harris et al., 2002). It has also been shown that myosin forms disordered filaments in vitro at low concentration of MyBPC (Moos et al., 1975) and addition of physiological ratios of the protein results in increased filament compactness and length (Davis, 1988; Koretz, 1979b). Moreover, in presence of cMyBPC, synthetic myosin filaments display a decrease in diameter and an increase in length and uniformity (Flashman et al., 2004). The MyBPC role in sarcomere assembly seems to be mediated by the C-terminal part of the protein. The last four domains of the protein (C7-C10) interact with LMM (Okagaki et al., 1993), the presence of the final domain C10 is essential for binding to myosin (Alyonycheva et al., 1997; Okagaki et al., 1993), in fact it binds to four molecules of LMM via positively charged residues that are found on its surface (Miyamoto et al., 1999). To reach the maximal binding to myosin is necessary also the presence of the other three C-terminal domains, C7, C8 and C9, so the presence of this C-terminal fragment C7-C10, seems to be essential for sarcomere incorporation of MyBPC (Welikson and Fischman, 2002).

An interaction with titin also occurs (Furst et al., 1992; Koretz et al., 1993; Labeit et al., 1997; Soteriou et al., 1993), via the C-terminal region. The fragment containing domains C8-C10 has been shown to bind to titin, while domains C5-C8 do not, this leads to the conclusion that the interaction with titin occurs via domains C9 and/ or C10 of MyBPC (Freiburg and Gautel, 1996). As said previously, MyBPC is found only in the C-zone of the sarcomere, region where is also present the 11 superrepeat of titin, also made up of IgI and FnIII domains (Labeit et al., 1992; Labeit and Kolmerer, 1995), each repeat has a 43 nm periodicity (Furst et al., 1989) and MyBPC binds only to this specific part of titin, always at the first domain of the 11 superrepeat (Freiburg and Gautel, 1996). However MyBPC is not present in every C-zone stripe, being absent in the first two, therefore an additional localisation mechanism must be present that

localises MyBPC only in those strips.

It is by the interaction with the thick and titin filaments that MyBPC contribute to the sarcomere structure and stabilisation. When these interactions are prevented by the missing of the myosin and titin binding sites, a defective sarcomere is formed.

Experiments on mutant cardiac MyBPC (cMyBPC) have shown that truncated forms of this protein missing all C-terminal domains following cC1, cC3 or cC4, incorporate in the sarcomere in 10% of the expressing myocytes, even without the C-terminal titin/myosin binding domains, while wild type and forms of the protein containing missense mutations, like E542Q, incorporate in the A band in 76% of the expressing myocytes (Flavigny et al., 1999). In their study Flavigny et al. showed that even MyBPC truncated after domain C1, and therefore not possessing the MyBPC motif, could incorporate in the sarcomere. This evidence lead to the hypothesis that an additional myosin binding site must be present at the N-terminus of the protein, possibly in the cardiac specific domain C0 or in the linker between C0 and C1. Recent studies on the N-terminal domains of cMyBPC have shown that they bind to the S2 $\Delta$  fragment of myosin, formed by the first 125 residues of the S2 fragment of myosin, domain cC1 close to the hinge between the myosin rod and the lever arm (Ababou et al., 2008), cC2 a bit more towards the C-terminus (Ababou et al., 2007), confirming an interaction between MyBPC and myosin other than through the C-terminal domains.

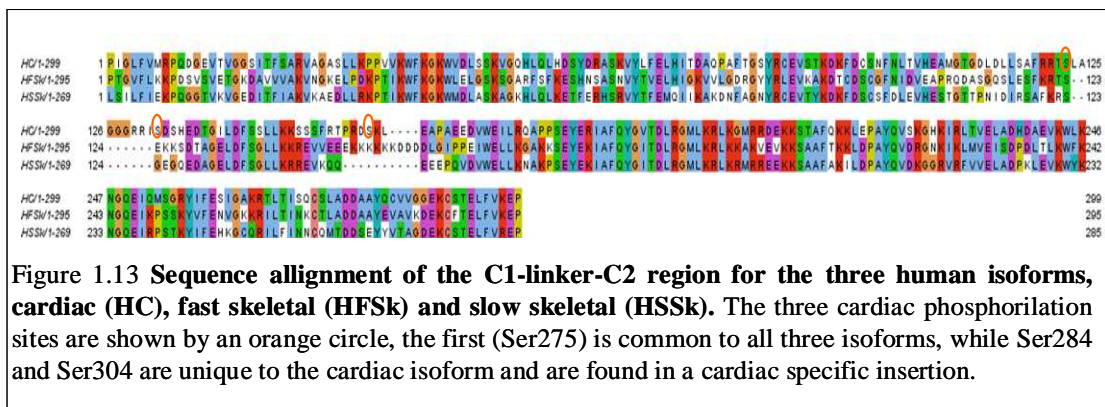
A second role proposed for cMyBPC is localised at the N-terminus of the protein and consists in the regulation of muscle contraction via phosphorylation/ dephosphorylation. Regulation of protein- protein interaction by phosphorylation is a common mechanism to control cell function and in cMyBPC it seems to be achieved via the three phosphorylation sites present in the so called MyBPC motif, a 100 residue long linker between domains cC1 and cC2. This linker has recently been suggested to be an IgI

domain on the basis of small angle X-ray scattering studies (Jeffries et al., 2008), however, this was not confirmed by NMR data registered for the group of domains C1-C2, including the MyBPC motif that links them; in a  $^1\text{H}/^{15}\text{N}$  HSQC spectrum it was shown how all the linker residues are localised in the random coil region of the spectrum and additional dynamic studies on this region showed that it is highly mobile and with a low degree of order (Ababou et al., 2008), as expected for an unstructured peptide. It is therefore possible that the linker is unfolded in solution but that it can adopt a compact shape, as seen for other unstructured peptides, such as  $\alpha$ -synuclein (Eliezer et al., 2001). The N-terminus of cMyBPC is the part of the protein most dissimilar from the skeletal isoforms, due to the presence of the extra domain cC0 and an insertion in the MyBPC motif that comprises two of the three phosphorylation sites, named from A to C, in contrast with the only site present in the skeletal isoforms which corresponds to site A in cMyBPC. This fact could be indicating that cMyBPC might play an important role in regulating cardiac contraction in response to  $\beta$ -adrenergic stimulation due to the presence of the two extra phosphorylation sites. In fact, cMyBPC is rapidly phosphorylated when the myocardium is stimulated by  $\beta$ -adrenergic agonists, such as adrenalin (Garvey et al., 1988), resulting in an increase in contraction force and speed. Dephosphorylation occurs in response to cholinergic agonists, such as acetylcholine (Hartzell and Titus, 1982); in vitro studies have shown that this occurs by action of a protein phosphatase 2A (Schlender et al., 1987) that co-purifies with cMyBPC (Schlender and Bean, 1991). Heart disease and cardiac failure are often associated with diminished  $\beta$ -adrenergic sensitivity, impaired cardiac contractility, abnormalities in  $\text{Ca}^{2+}$  flux (Houser et al., 2000; Port and Bristow, 2001) and altered sarcomeric protein phosphorylation (Decker et al., 2005; van der Velden et al., 2003). cMyBPC is extensively phosphorylated in basal conditions, but it undergoes partial

dephosphorylation during heart disease or pathological hypertrophy, with the three-phosphorylated form largely absent in case of advanced heart failure as demonstrated by Sadayappan by works on transgenic animal models: this seems to be independent of the type of cardiac stress, as pressure overload and genetic alteration in the cardiac machinery both resulted in significantly reduced phosphorylation (Sadayappan et al., 2005). The phosphorylation sensitive region of cMyBPC is found in the linker between domains C1 and C2; when de-phosphorylated, the C1-C2 region interacts with the S2 fragment of myosin but, upon phosphorylation of the MyBPC motif, this binding is inhibited (Kunst et al., 2000; Levine et al., 2001).

Three different kinases have been identified that can phosphorylate the three sites Ser275, Ser284 and Ser304, the cyclic adenosine monophosphate (cAMP)- dependant kinase (PKA), protein kinase C (PKC) and a  $Ca^{2+}$ / calmodulin dependent kinase (CaM-II). PKA has the capacity to phosphorylated all the three sites, while PKC can act on Ser275 and Ser304 and CaM-II is active only on the central phosphorylation site B (Gautel et al., 1995). It has been proven that phosphorylation of cMyBPC has an effect on filament orientation and contractile mechanisms (Gautel et al., 1995; Kunst et al., 2000; Winegrad, 2000). In vitro studies have shown that PKA mediated phosphorylation of cMyBPC extends the myosin-actin crossbridges from the backbone of the thick filament, increases their degree of order, changes their orientation and decreases crossbridge flexibility (Weisberg and Winegrad, 1996). The alignment of cardiac and fast skeletal isoforms shows an insertion in cMyBPC of the residues LAGGRRIS, that is probably preceded by a flexible sequence and is the region where phosphorylation site B is located (Figure 1.13). This site seems to be very important for cardiac contraction regulation since, when made inactive by substitution of the serine residue with an alanine, the other two phosphorylation sites are inactivated as well

(Gautel et al., 1995). This could mean that, upon phosphorylation of site B, the MyBPC motif undergoes conformational changes that make the further sites accessible. This has been confirmed by the fact that mutating this serine to an acid residue, such as aspartate, thus mimicking the phosphorylated state, can restore the accessibility of A and C phosphorylation sites, probably by inducing a conformational change in the flexible loop surrounding site B.



A further evidence of the importance of Ser284 is the result of deletion of the LAGGRRIS insertion from cMyBPC, resulting in a region more similar to that present in the skeletal isoforms; in this mutated form of the protein the phosphorylation of sites A and C was unregulated, with decreased phosphorylation by both PKA and CaM-II like kinases (Gautel et al., 1995). All this suggests that this cardiac specific insertion has a strong regulatory function. Moreover, it seems that the thick filament would change its structure upon phosphorylation of cMyBPC (Levine et al., 2001; Weisberg and Winegrad, 1998); in the fully phosphorylated state, in fact, the myosin heads appear to extend from the thick filament backbone in a more ordered fashion, thus the packing of myosin filaments and their heads seem to be closely linked to the state of cMyBPC phosphorylation: the more cMyBPC is phosphorylated the easier it is for myosin to

interact with the thin filament. MyBPC motif phosphorylation appear also to have an effect on the ATPase activity of myosin S1, with dephosphorylation of cMyBPC decreasing ATPase activity the most (Winegrad, 1999). It has been suggested by Weisberg and Winegrad that regulation of myosin ATPase activity may be mediated by changes in myosin S1 position and flexibility upon cMyBPC phosphorylation (Weisberg and Winegrad, 1998). As the level of cMyBPC phosphorylation increases, contractility is increased, generating a higher maximum  $\text{Ca}^{2+}$ - activated force ( $F_{\text{max}}$ ), together with a higher  $\text{Ca}^{2+}$  sensitivity, that is, a lower concentration of  $\text{Ca}^{2+}$  is necessary to initiate muscle contraction (McClellan et al., 2001). This has been confirmed by a mouse model, where the three serines have been replaced by alanine, mimicking the dephosphorylated state of cMyBPC, that had impaired contractility function (Sadayappan et al., 2005).

It is well established that, in absence of phosphorylation, the C1-C2 region, that comprises also the phosphorylation sites, interacts with the S2 region of myosin (Kunst et al., 2000; Levine et al., 2001), as confirmed on more recent studies (Ababou et al., 2007; Ababou et al., 2008), and that upon phosphorylation this interaction is abolished (Gruen et al., 1999). This would allow the myosin heads to become free of any steric constraint that could be imposed on them by cMyBPC.

Interestingly, the N-terminal fragments C0-C2 and C0-C1, can affect force production and crossbridge activity in skinned myocytes (Herron et al., 2006). At concentration higher than 10  $\mu\text{M}$  of C0-C2 and C0-C1 on skinned myocytes, both fragments induced a  $\text{Ca}^{2+}$  independent activation of crossbridge cycling and force development. It is well established that  $\text{Ca}^{2+}$  is required to switch on crossbridge cycling and produce force development, however Herron et al. found that at concentration above 10  $\mu\text{M}$  the two N-terminal fragments of cMyBPC, C0-C2 and C0-C1, had an activating effect similar to

that of  $\text{Ca}^{2+}$ . On the other hand, the activation by cMyBPC fragments achieved a smaller maximum force but a higher rate of crossbridge cycling. Moreover, this activating effect was present also in myocytes where TnC has been extracted, in which  $\text{Ca}^{2+}$  activation was therefore abolished. These effects suggest that cMyBPC fragments are activating the thin filament via a mechanism different from the one that relies on  $\text{Ca}^{2+}$ .

It was shown by Herron and co-workers that the fragment C0-C1 binds weakly to S2 but has the same effect of the fragment C0-C2 on crossbridge activation, while fragment C1-C2, that binds to myosin S2, does not have any effect on force generation or crossbridge cycling; this brings to the conclusion that the MyBPC motif, present in both fragments, does not have an influence in these regulatory functions, and that the Pro/Ala rich linker between domains C0 and C1, present only in fragment C0-C2, could play this important role. This  $\text{Ca}^{2+}$  independent crossbridge cycling could be achieved by the N-terminus of cMyBPC by either binding to the thin filament directly, as suggested by two independent studies (Kulikovskaya et al., 2003; Squire et al., 2003), or by binding to the thick filament to promote the attachment of myosin S1 to actin in a sufficient number to activate the thin filament. Labelling studies (Herron et al., 2006) have also demonstrated that the C0-C2 and C0-C1 fragments bind to the thick filament crossbridge region; this A-band localization of exogenous C0-C1 fragment, that do not contain the whole S2 binding site, suggests the presence of a region, possibly the Pro/Ala rich region between C0 and C1, that could bind to a thick filament protein. It has been hypothesised (Flavigny et al., 1999) that domain cC0 could bind to the myomesin binding site on myosin; however, cC0 alone did not show any effect on crossbridge activation and was localized diffusely in the ventricular cells used for the studies carried out by Herron et al. It was also found that the fragment C0-C2 increased the  $\text{Ca}^{2+}$  sensitivity at sarcomere length (SL) 1.9  $\mu\text{m}$ ; this is probably achieved by binding to

myosin and increasing the freedom and flexibility of the myosin heads, allowing them to interact more readily with actin. Surprisingly, this effect was absent at SL=2.3  $\mu\text{m}$  and this could be due to the fact that at this sarcomere length, the spacing between thick and thin filaments is small enough for this interaction to be favoured. All this leads to the conclusion that the N-terminus of cMyBPC may function to modulate the  $\text{Ca}^{2+}$  activation of crossbridge cycling in cardiac myofibrils.

It has been suggested by different groups (Flavigny et al., 1999; Kulikovskaya et al., 2003; Squire et al., 2003; Witt et al., 2001) that the N-terminus of MyBPC could interact with actin and the fact that all isoforms have shown a low affinity for the F-actin in co-sedimentation assays (Moos et al., 1978; Yamamoto and Moos, 1983) makes it improbable that this interaction might take place via a cardiac specific insertion, such as domain cC0. The Pro/ Ala rich region between domain cC0 and cC1 is also thought to be capable of interacting with the F-actin filament (Kulikovskaya et al., 2003; Squire et al., 2003). This hypothesis is based on the fact that the essential light chain (ELC) has at its N-terminal end a region of similar composition that is thought to form an extended rod-shaped structure, stable under a variety of conditions, that binds to actin (Timson and Trayer, 1997). An interesting possible function of this extension might be that the binding to actin may affect the actomyosin ATPase properties of myosin. It is conceivable, in conclusion, to think that also the Pro/ Ala rich region of MyBPC might have a similar function. That an interaction between this region of cMyBPC and actin takes place has been shown by Kulikovskaya (Kulikovskaya et al., 2003) and is reported as unpublished data by Govada et al (Govada et al., 2008), in both cases as results of co-sedimentation assays. The first report of an interaction between MyBPC and actin dates back to 1978 (Moos et al., 1978) but the exact location of this interaction has not yet being conclusively determined. There have been reports of increased actomyosin

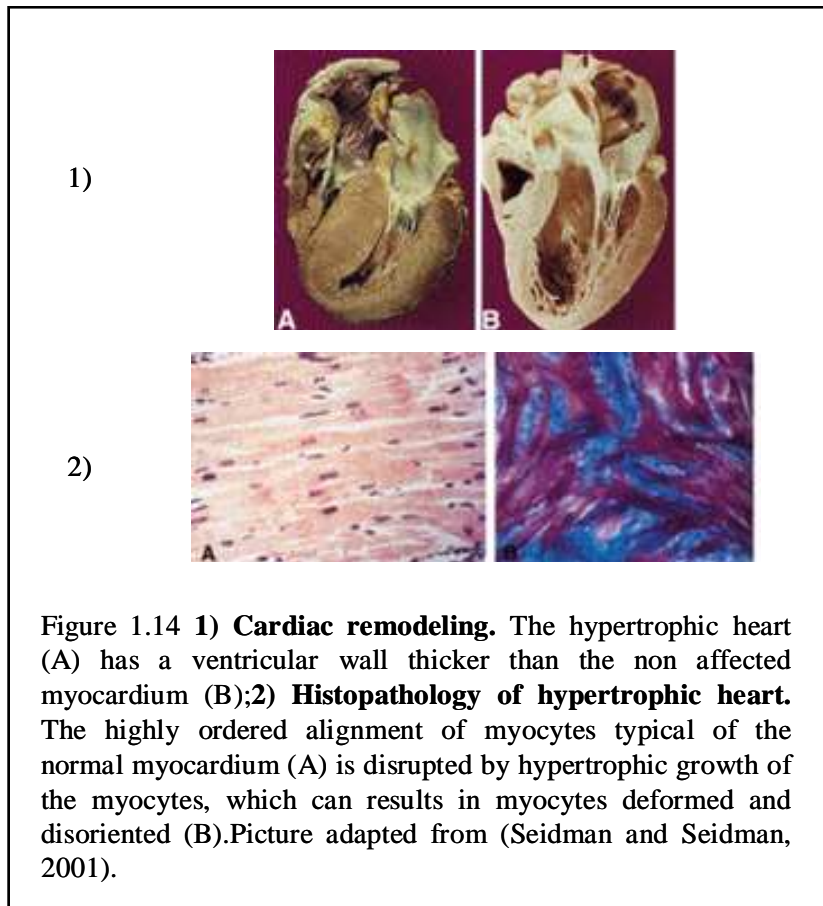
ATPase activity upon MyBPC binding to actin, presumably by producing links between actin and myosin, to form aggregates of the two contractile proteins (Moos et al., 1978). It has been demonstrated that binding of MyBPC to actin is  $\text{Ca}^{2+}$  sensitive and that binding of this protein to F-actin causes side-by-side association of thin filaments (Yamamoto, 1986). A more recent study has shown that cMyBPC, and more precisely the C1-C2 fragment, binds to F-actin, even in the presence of tropomyosin, troponin and  $\text{Ca}^{2+}$ , with both motility assays and co-sedimentation experiments (Razumova et al., 2006); even though increasing ionic strength was found to reduce the interaction, binding was still evident at physiological ionic strength (0.2 M KCl), indicating a persistent interaction between the C1-C2 fragment and actin at physiological conditions. Using a variety of fragments, C0-C1, C0-C2, C1-C2 and C2-C4, Razumova et al have demonstrated that the presence of the MyBPC motif affected both the sliding motility of F-actin on myosin filaments and reduced the myosin ATPase rates in solution. They found that the C1-C2 region, that has already been shown to bind to the S2 fragment of myosin, binds to actin, and confirmed it, finding that fragments missing C1 and the MyBPC motif, like C2-C4, fail to show any effect on actin binding (Razumova et al., 2006).

#### **1.1.4 Hypertrophic cardiomyopathy (HCM)**

The reason of the growing interest in cMyBPC is its connection with the disease Hypertrophic Cardiomyopathy (HCM). Cardiomyopathies are diseases of the myocardium associated to cardiac dysfunction that can be complicated by heart failure, arrhythmias and sudden death (Richardson et al., 1996) and are a major cause of cardiovascular morbidity and mortality, being a frequent reason of cardiac

transplantation. HCM, as well as other forms of cardiomyopathy, is a genetic disorder associated with mutated forms of sarcomeric proteins. The first HCM-related mutation was discovered in a large French-Canadian family in 1990 and affects the  $\beta$ -myosin heavy chain (Geisterfer-Lowrance et al., 1990). Since then many other mutations have been identified in genes coding for sarcomeric proteins, including *MYBPC3*.

HMC is defined by an unexplained left ventricular hypertrophy (LVH), usually involving the inter-ventricular septum, in cases where other detectable causes of heart remodelling, such as hypertension or amyloidosis, must be excluded. A consequence of hypertrophy is that the left ventricular volume is diminished. Histopathology of the hypertrophic heart can be noticeably abnormal with the highly registered alignment of myocytes, typical of the healthy myocardium, distorted by hypertrophic growth of the myocyte that can produce enlarged and deformed myocytes and disorientation of adjacent cells (Figure 1.14). These features are collectively known as myocyte disarray and can be found mixed with normal myocyte or widespread throughout the left ventricle (Maron, 2002; Seidman and Seidman, 2001) . In HCM, systolic function is increased or at least preserved, while most affected individual develop dyspnea and angina due to impaired diastolic relaxation of the hypertrophied heart (Spirito et al., 1997).



Despite the fact that in the hypertrophic left ventricle the internal cavity is a lot smaller than in a normal heart, usually the heart muscle is able to pump properly and thus most people do not have limiting symptoms. However in some cases the thickened heart muscle is abnormally stiff and so when the left ventricle fills with blood, the stiffness of the muscle increases the pressure inside the right ventricle and this is reflected into the lungs, causing shortness of breath. In some cases the increase in the thickness of the ventricular septum occurs just below the aortic valve and may block the normal flow out of the heart into the large blood vessel that supply the whole body, the aorta, this phenomenon is better described as hypertrophic obstructive cardiomyopathy. This kind of HCM can also affect the second cardiac valve, the mitral valve, which prevents backwards flow from the left ventricle to the left atrium; when there is distortion of the

mitral valve motion, the blood can flow backwards causing shortness of breath. Individuals with HCM can experience two major types of arrhythmia, atrial fibrillation, which is an abnormal heart rhythm where the top part of the heart, the atrium, undergoes disorganized electrical activation and sends multiple, fast, irregular impulses to the left ventricle, resulting in the heart beating rapidly and irregularly leading to palpitations, shortness of breath and decreased exercise capacity, and the more serious ventricular tachycardia, also called ventricular fibrillation, that can lead to cardiac death. The incidence of HCM is of 1 person every 500 people with an annual mortality of 1% and being the first cause of death in athletes (Maron, 1996). HCM is inherited as a mendelian autosomal dominant trait caused by mutations in genes encoding 13 proteins of the cardiac sarcomere, making it primarily a sarcomeric disorder.

The proteins that carry the HCM-related mutations are reported in table 1.1: three myofilament proteins,  $\beta$ -myosin heavy chain ( $\beta$ -MyHC), the essential light chain (MLC-3) and the regulatory light chain (MLC-2); three thin-filament proteins, cardiac troponin T (cTnT), cardiac troponin I (cTnI), and  $\alpha$ -tropomyosin ( $\alpha$ -TM) and, finally, in the cardiac isoform of myosin binding protein C (cMyBPC). The gene *MYBPC3* that encodes cMyBPC is located in the chromosome 11p11.2 and comprises 24000 bp divided in 35 exons.

In all clinical studies the two genes *MYH7* and *MYBPC3* were the most common genes responsible for the disease, each of them being involved in 30% to 40% of cases.

Sarcomeric Protein	Gene	Locus	n° HCM point mutations
$\beta$ - Myosin heavy chain	<i>MYH7</i>	14q12	194
<b>Myosin Binding Protein C</b>	<b><i>MYBPC3</i></b>	<b>11q11.2</b>	<b>149</b>
Cardiac troponin T	<i>TNNT2</i>	1q32	31
Cardiac troponin I	<i>TNNI3</i>	19p13.2	27
$\alpha$ -tropomyosin	<i>TPM1</i>	15q22.1	11
Regulatory light chain	<i>MYL2</i>	12q23- q24.3	10
Cardiac $\alpha$ actin	<i>ACTC</i>	11q	7
Essential light chain	<i>MYL3</i>	3p21.3- p21.2	5

**Table 1.1: HCM related mutations identified in sarcomeric protein. Data obtained from from databases <http://genepath.med.harvard.edu/~seidman/cg3/> and <http://beta.uniprot.org/uniprot/Q14896>**

70% of the *MYH7* mutations are located in the region coding for the globular head and neck domain, while 30% affect the rod of myosin. Almost all of these (96%) are missense mutations. In *MYBPC3*, on the other hand, half of the ~150 mutations are non-sense mutations leading to termination codons, splice site mutations, small deletion or insertion disrupting the reading frame that bring to the formation of truncated forms of the protein. Truncation mutations are thought to cause haploinsufficiency since the mutated cMyBPC without the C-terminus seems not to incorporate in the sarcomere (Rottbauer et al., 1997). 75 missense mutations have been found in *MYBPC3* (table 1.2) so far. Investigations of the consequence of some of these point mutations have been particularly informative in defining structure and function of the domains in which they have been found. Nevertheless, the mechanism by which many of these mutations cause HCM remains unsolved and is still very difficult to predict the exact functional consequences of mutations only from their nature and position.

In recent years, the generation of engineered animal models of human mutations has allowed a more accurate evaluation of the process leading from gene defect to HCM phenotype (Geisterfer-Lowrance et al., 1996; Marian et al., 1999; Tardiff et al., 1998; Yang et al., 1998), however the results of studies performed either in vitro or on animal

models have been contradictory. In some cases  $\text{Ca}^{2+}$  sensitivity and ATPase activity were reduced, resulting in decrease of actin-myosin interactions and diminished myocyte contractility (Crilley et al., 2003; Lankford et al., 1995). The impaired contractility is supposed to activate the release of stress-related signalling kinases and trophic factors which stimulate myocyte hypertrophy. Contrasting results have shown, on the other hand, an enhancement of ATPase activity in myosin, with a consequently increase in actin-myosin interaction leading to enhanced force generation and cardiomyocyte contractility (Olsson et al., 2004) with a consequent increase in work and energy consumption. Moreover, the presence of both wild-type and mutant protein within the sarcomere may result in uncoordinated contraction. There is also a high probability of energy depletion, myocyte death and fibrosis. (Seidman and Seidman, 2001). All these results reveal the complexity of this condition and the probable involvement of multiple mechanisms implicating multiprotein complexes in the pathophysiology of HCM. Most of the patients are heterozygous for the mutation that is transmitted by one of the parents. The symptoms tend to be more severe the earlier the disease presents in life, so elderly patients are very unlikely to be severely affected, with just a minority of over 75 to show heart failure.

Domain	Mutation	Domain	Mutation	Domain	Mutation
cC0	Gly5Arg	cC3	Arg470Gln	cC5	Asp770Asn
cC0	Arg35Trp	cC3	Gly490Arg	cC6	Val771Met
cC0	Thr59Ala	cC3	Arg495Gln	cC6	Trp792Arg
cC1	Pro161Ser	cC3	Arg502Trp	cC6	Arg810His
cC1	Arg177Cys	cC3	Arg502Gln	cC6	Lys811Arg
cC1	Gln208His	cC3	Gly507Arg	cC6	Arg820Gln
cC1	Val219Leu	cC3	Gly523Trp	cC6	Ala833Thr
cC1	Asp228Asn	cC3	Gly531Arg	cC6	Ala833Val
cC1	Tyr237Ser	cC3	Glu542Gln	cC6	Arg834Thr
cC1	Val256Ile	cC4	Leu545Met	cC6	Arg834Trp
MyBPC motif	His257Pro	cC4	Cys566Arg	cC7	Pro873His
MyBPC motif	Glu258Lys	cC4	Asp604Val	cC7	Val896Met
MyBPC motif	Gly263Arg	cC4	Asp605Asn	cC7	Asn948Thr
MyBPC motif	Arg273His	cC4	Pro608Leu	cC7	Thr958Ile
MyBPC motif	Gly278Glu	cC4	Glu619Lys	cC8	Gln998Arg
MyBPC motif	Gly279Ala	cC4	Ala627Val	cC8	Arg1002Gln
MyBPC motif	Arg282Trp	cC5	Arg654His	cC8	Pro1003Gln
MyBPC motif	Arg326Gln	cC5	Arg668His	cC8	Glu1017Lys
MyBPC motif	Cal342Asp	cC5	Arg668Pro	cC9	Phe1113Ile
MyBPC motif	Leu352Pro	cC5	Pro677Leu	cC9	Val1115Ile
cC2	Gly415Ser	cC5	Arg733Cys	cC9	Val1125Met
cC2	Ala416Ser	cC5	Asn755Lys	cC9	Ile1131Thr
cC2	Glu441Lys	cC5	Val757Met	cC10	Ala1194Thr
cC2	Glu451Gln	cC5	Gly758Asp	cC10	Gly1206A sp
cC3	Arg458His	cC5	Glu759Asp	cC10	Ala1255Thr

**Table 1.2: cMyBPC point mutation causing HCM obtained from from databases**

**<http://genepath.med.harvard.edu/~seidman/cg3/> and <http://beta.uniprot.org/uniprot/Q14896>.**

The degree of hypertrophy, the age of onset and the prognosis seem to be dependent directly from the precise gene mutation, for example mutations in the gene *TNNT2*, that code for troponin T, are usually associated with a severe phenotype and high risk of sudden death, specially in young patients, despite the mild degree of hypertrophy (Watkins et al., 1995b). In *MYH7* mutations the phenotype varies considerably according to the mutations, some being associated with a benign phenotype, like V606M, while others, like R403Q, are associated with severe hypertrophy and reduced survival expectancies (Charron et al., 1998; Watkins et al., 1992). Mutations in the *MYBPC3* gene are usually associated with late onset and milder phenotype and delayed penetrance until the fifth decade of life, while mutations in other genes are almost completely penetrant by the second or third decade. However, recent data report of cardiac death in extremely young patients with a mutated *MYBPC3* gene (Lekanne Deprez et al., 2006). Survival of patients with cMyBPC mutations have shown to be better than that observed with mutations in cardiac troponin T or in malignant cardiac  $\beta$ -myosin heavy chain. Many young and middle-age persons presenting a mutation in the *MYBPC3* gene show no symptoms of HCM and it is possible that some of these mutations will remain nonpenetrant throughout life. HCM penetrance seems to decrease with age in people with cMyBPC mutations (Niimura et al., 1998). For this reason, it has been suggested that *MYBPC3* is the most commonly involved in HCM but, given its benign phenotypes and low penetrance, the prevalence of the mutations found in these gene has been underestimated (Richard, 2003a). However, contrasting results were obtained by VanDriest and co-workers (Van Driest et al., 2004) that fail to identify a difference in age of diagnosis in patients with mutations in the *MYH7* and *MYBPC3* genes. Patients with multiple sarcomeric mutations had the most severe phenotype, which means youngest at diagnosis and higher degree of hypertrophy.

### **1.1.5 Main HCM related missense mutations found in cMyBPC role in Hypertrophic cardiomyopathy**

Given the strong association of cMyBPC with HCM, mutagenesis studies are an extremely important tool to try and elucidate the function of the domains that contain a specific mutation. This kind of analysis has been carried out on domain cC1 (Ababou et al., 2008), cC2 (Ababou et al., 2007) and cC5 (Idowu et al., 2003), and have given important insight on both the domains structure and function. Despite being unique to the cardiac isoform of MyBPC, domain cC0 presents a small number of HCM related mutations. The function of this domain is still unclear as well as its presence in the heart muscle. An interaction between domain C0 and myosin has been thought to occur on the basis of a mutant MyBPC mouse model (Okagaki et al., 1993), as MyBPC missing the C-terminal domains was still incorporated in the sarcomere (around 10%), an additional myosin binding site must be present toward the N-terminus. Sequence comparison between C0 and myomesin suggests that C0 contains a novel LMM binding site (Flavigny et al., 1999). Whether this interaction occurs and what is its function is still unclear. An actin binding site has been proposed but it has been shown that all the isoforms of MyBPC have a low affinity for actin (Moos et al., 1978; Yamamoto and Moos, 1983) indicating that any interaction with actin via a cardiac- specific region, such as cC0, is very unlikely to occur. The linker between C0 and C1, that in the skeletal isoforms represent the N-terminus of the whole protein, is thought to be a more likely candidate for binding actin (Squire et al., 2003) but no HCM related mutations have been found in this region to confirm this hypothesis. More recently it has been shown that fragments of MyBPC containing C0 are able to bind to actin and has been suggested that it may contribute to the weak binding state by shifting the binding of the

N-terminus of the C-protein between actin and myosin (Kulikovskaya et al., 2003). However, C0 and the cC0-cC1 linker are very unlikely to be able to bind to the myosin crossbridge, the myosin backbone and actin at the same time but it is possible that MyBPC cycles through different binding partners. Further research is required to clarify this point.

As discussed diffusely in a previous section, domains C1 and C2 and the linker between them interact with the S2 $\Delta$  fragment of myosin (Gruen and Gautel, 1999) that comprises the first 18 heptad repeats of myosin S2 formed by the first 125 residues, from residue 838 to residue 963; this region contains the R870H mutation linked to HCM. This interaction between the N-terminus of cMyBPC and S2 $\Delta$  is regulated by phosphorylation of the three phosphorylation sites (S275, S284 and S304) present in the C1-C2 linker. Detailed studies on this interaction carried out using NMR spectroscopy have recently been published elucidating the role of domains cC1 and cC2 and their interaction with S2 $\Delta$  (Ababou et al., 2007; Ababou et al., 2008). Monitoring the binding of the two domains with S2 $\Delta$  by NMR spectroscopy had the advantage of allowing, once the structure was known, to map the residues more affected by the interaction on the domain surface. Several HCM related missense mutations have been identified in domain cC1, all of them seem to be found around the C-terminus surface of the protein. Some of them, like Y237S and V256I, involve mutation of very conserved residues found in the hydrophobic core of the protein, fundamental for the overall folding of the domain and, as a consequence, are thought to cause strong destabilization of the domain; others, like D288N involve residues exposed on the surface that have a role in the interaction with the myosin S2 $\Delta$  fragment. At the centre of the interaction between cC1 and S2 $\Delta$  there is residue W196 which is located in CD-loop and, with A232, forms a little hydrophobic patch that interacts with residues F856 and M852 on S2 $\Delta$ ; all the

other residues involved in the interaction are of a polar nature. Of the HCM related mutations, two have been incorporated in recombinant cC1, D228N and Y237S (Ababou et al., 2008). The latter involves an hydrophobic residue highly conserved through isoforms and species which has a strong influence on the domain stability; as a consequence, it was impossible to produce soluble protein, confirming the hypothesis that the protein was not able to assume a proper fold. Interestingly, Y237S results in a mild HCM phenotype but shows a strong disease association (Morner et al., 2003). The second mutation D228N, on the other hand, involves a polar residue positioned on the interaction surface with S2 $\Delta$  and causes a weakening of this interaction without affecting the stability of the domain. Two other HCM related mutations, R177C and V219L, are distant from the S2 $\Delta$  binding surface and, affecting residues whose side chain is exposed on the surface, are unlikely to affect the structural stability of the protein; on the other hand they might affect the interaction of domain cC1 with a sarcomeric protein other than S2. also domain cC2 was shown to interact with S2 $\Delta$ , precisely at the regions between residues 220 and 230 and residues 280 and 300. All the residues involved in the interaction with S2 $\Delta$  are grouped on the F, G and A' strands and the A'B loop of cC2, all in the vicinity of the C-terminus of the domain. The chemical shift changes were small but significant, as expected for an interaction happening via polar residues. The surface involved in the interaction with S2 $\Delta$  is completely free from positively charged residues, in a domain where charges are otherwise evenly distributed; this pattern is well established for the C2 domain in different isoforms and species. To confirm these results, the same experiments were repeated with a mutant of fragment S2 $\Delta$ , that contained the missense mutation R870H, which has been reported to cause HMC (Gruen and Gautel, 1999); the results obtained indicated that residues in the same region were affected but the binding was

significantly reduced (Ababou et al., 2007) by a factor between 3 and 4, in agreement with the results obtained previously by ITC (Gruen and Gautel, 1999). The reason of this reduction seems to be due to the difference in shape between the side chains of arginine and histidine; R870 is forming a salt bridge or hydrogen bond with the cC2 residue Glu445 that cannot be formed if an histidine replaces an arginine. Interestingly, using the mutant S2 $\Delta$ -R870H, some residues that were not involved in the interaction using the wildtype myosin fragment, showed a perturbed chemical shift; this could be explained by a rearrangement occurring so that Glu445 could interact with either Arg869 or Arg871 which are available and very near. It is worth noting that residue R869, when mutated to cysteine, glycine or histidine, has been reported to cause HCM (Anan et al., 2000).

Domains C3 and C4 are thought to play a role in the flexibility of the N- terminal region and in its interaction with either the S2 region of myosin or the actin filament. Three of the HCM mutations found in C3 (R495Q, R502Q and R502W) involve highly conserved residues but they seem to be not essential for defining the IgI fold and the three mutations result in a favourable disease prognosis (Maron et al., 2001; Niimura et al., 1998; Richard, 2003b). C5 domain has two cardiac-specific insertion. It shows a ten residues long segment at the N-terminus that previously was assumed to be part of a linker between the domains C4 and C5 but that has been shown to be part of the enlarged  $\beta$ -bulge of domain C5 (Idowu et al., 2003). The second peculiarity of the domain cC5 is the 28 amino acids insertion between the strands C and D, known as the CD-loop. This region is completely unstructured and highly dynamic. It presents a proline/ charge rich insert that points away from the domain's surface. This insertion is always present in the cardiac isoforms but varies greatly in sequence and length between different species. Domain C5 has been studied by different groups because of

its unique cardiac insertion and the identification of several HCM related mutations. A study has shown that domain C5 bind to domain C8 of a different molecule of the same protein using a yeast two-hybrid assay, with domain C5 as a “bait” (Moolman-Smook et al., 2002). The same kind of experiment has shown that domain C7 interacts with domain C10 and an interaction between C6 and C9 has been proposed too. As a consequence of these results, a model of the myosin filament was developed, where three MyBP-C molecules form a collar around the thick filament of myosin, stabilized by intermolecular interaction between domains cC5-7 of each molecule and the domains cC8-10 of the next molecule. Only three of the ten HCM related mutations identified so in domain cC5 have been studied in detail so far: N755K, R654H and R668H. The first point mutation exhibits a severe phenotype, as Asn755 is located in the highly conserved position 1 of the  $\beta$ -turn connecting the F and G strands, the mutation makes the protein unstable and unfolded compared to the wild-type cC5, due to the loss of several key interactions (Idowu et al., 2003); phenotype corresponding with this mutation is extremely severe, associated with marked hypertrophy even in children and sudden cardiac death in one of eight affected patients (Okagaki et al., 1993), suggesting a complete or partial loss of structure and thus of function. Mutation R654H is characterised by a milder phenotype with low penetrance and moderate hypertrophy even in adults (Moolman-Smook et al., 1998). Being residue R654 localised on the domain surface it does not affect the stability of the domain (Daehmlow, 2002). The surface where residue Arg654 is found has a high percentage of negatively charged amino acids and it has been proposed to be the binding site of domain cC8, as a consequence the R654H mutation could affect the proposed interaction with domain cC8. A third mutations, R668H, has been found in this domain (Morner et al., 2003) but, since the polar positive histidine substitutes the polar positive arginine, it does not seem

to cause significant structural instability of the fold of domain C5. R668H could have an impact on the ability to bind a ligand, however, this residue is not located on the surface proposed to be a target for domain C8 and is unlikely to interfere with C8 binding.

Domain C6 is the first of the three FnIII domains in the protein, together with domains C7 and domain C9, that is thought to be its binding partner; this interaction has not been tested yet and is postulated based on the interactions between domains 5 and 8 and domains 7 and 10 that have been shown to occur. Usually two interacting FnIII domains interact via electrostatic charges: the EF loop at the end of the first domain (C6) is supposed to form a salt bridge and hydrogen bonds with the BC loop of the following domain (C7). Residue A833 is a highly conserved amino acid located in the strand E of C6 and is probably involved in the bond between domains C6 and C7; when mutated it may disrupt bonds between the two residues and cause an incorrect packing and assembly of the protein (Morner et al., 2003; Richard, 2003b). Two mutations occur in strand C at the conserved residues R810 and K811 (Nanni et al., 2003; Richard, 2003b). The reported mutation, R810H and K811R, do not alter the charge of the residue and are not likely to affect the stability of the domain. These mutations result in a mild phenotype. Another mutation found in domain cC6 is R820Q but it is not clear whether this is an HCM related mutation or a neutral polymorphism, since the phenotype appears to be mild, usually with first presentation late in life (de Pereda, 1999; Sharma et al., 1999).

The C-terminal region is where the binding sites for myosin thick filament (Moos et al., 1975; Starr and Offer, 1978) are situated. The primary myosin and titin binding regions of MyBP-C are localised to domain 10 and domains 8-10, respectively (Freiburg and Gautel, 1996; Okagaki et al., 1993). These three domains C8-C10 are the minimal requirement for incorporation into the A-band of the sarcomere (Gautel et al., 1995),

while domain C7 improves the targeting of MyBP-C to the C-zone (Gilbert et al., 1999). The C-terminus of MyBPC plays an important role in the formation of a normal sarcomere, so C-terminal truncated forms of the protein cause severe changes in hearts ultrastructure both in transgenic mouse models (McConnell et al., 1999; Yang et al., 1998; Yang et al., 1999) and in HCM affected individuals (Bonne et al., 1998; Niimura et al., 1998).

A large number of HCM mutations result in premature termination of translation of the C-terminus of MyBP-C, resulting in loss of the titin and/ or myosin binding sites (Bonne et al., 1995; Niimura et al., 1998; Rottbauer et al., 1997; Watkins et al., 1995a; Yu et al., 1998). As a consequence these truncated mutant protein do not incorporate in the sarcomere and can cause extremely severe cases of HCM (Lekanne Deprez et al., 2006). Several missense mutations are located in domain cC7. P873H (Hartzell and Sale, 1985) is a very rare mutation found in just one patient with a mild phenotype. It occurs in a residue that is highly conserved across species and isoforms and is thought to affect the formation of strand A or the stability of the linker between cC6 and cC7. It is not clear whether mutation V896M is disease causing, disease modifying or a neutral polymorphism (Jaaskelainen et al., 2002; Richard, 2003b). Usually patients with this mutations also show other HCM related mutations in the myosin heavy chain (Morner et al., 2003; Richard, 2003b), thus this mutations may not cause disease but it may increase the severity of the disease in presence of other HCM mutations. Residue V896 is conserved and is predicted to point into the core of the FnIII domain; when a methionine replaces a valine, the domain stability may be affected but this mutation is unlikely to lead to incorrect folding of the domain given the non-polar nature of the residues involved. N948T occurs in a conserved position but was found in only one patient resulting in a severe disease phenotype (Daehmlow, 2002). Residue Asn948 is

expected to be located in the  $\beta$ -type turn connecting strand F and strand G (Goll et al., 1998), in a position similar to the residue Asn755 in cC5, where an important mutation has been found. Therefore, Asn948 is probably of crucial importance for the domain folding and its loss could result in a poorly folded domain unable to target MyBP-C to the A band of the sarcomere and that may disrupt the interaction between domain C7 and its possible binding partner C10.

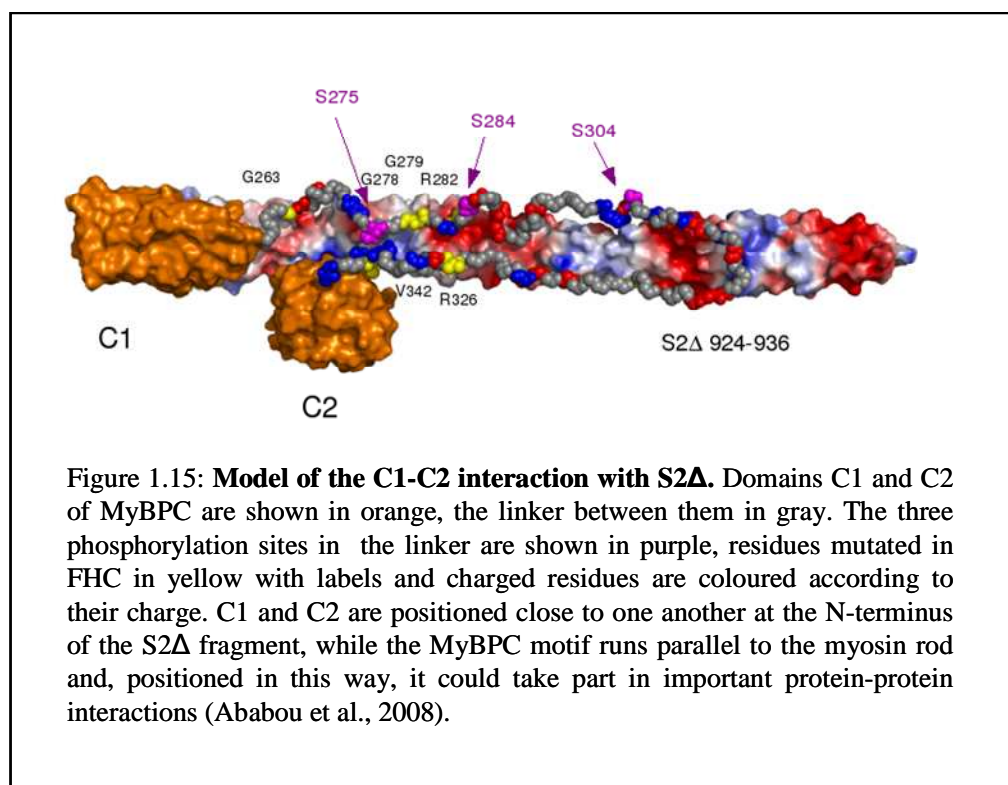
Domain C10 is of great importance due to its binding to myosin with nine key residues involved in binding to this filament been identified (Gilbert et al., 1996; Miyamoto et al., 1999; Okagaki et al., 1993). The myosin binding faces are thought to be located on two surfaces, the first formed by strands B and E, the other by strand C of the IgI fold. Of the mutations found in this domain, an insertion-mutation of residues 1248-1253 (Watkins et al., 1995a) and a missense mutation, A1255T (Richard, 2003b), are very unlikely to interfere with myosin binding since the mutated residues are not found on the surface involved in the interaction with this sarcomeric protein (Maron et al., 2001; Richard, 2003b). These result suggests that they both may affect some other function of domain C10, possibly its binding to titin (Moolman-Smook et al., 1998) or an alteration in the interaction that may occur with C7 or the adjacent C9.

Mutation A1194T (Richard, 2003b) could interfere with myosin binding as residue Arg1194 is found close to two identified key myosin-binding residues (Miyamoto et al., 1999) and therefore may disrupt binding of MyBP-C to the myosin filament.

### **1.1.6 How does the cMyBPC assemble in the sarcomere?**

Following the detailed mutagenesis studies Ababou and coworkers were able to build a model of the interaction between the cC1-cC2 fragment of cMyBPC and the S2 $\Delta$  part of myosin (Ababou et al., 2008). The position of C1 and C2 is such that the MyBPC motif

runs parallel to S2 $\Delta$  to reach the area around residue 930, where is found a group of HCM mutations, one of which, E924K makes the interaction between the two proteins undetectable by ITC (Gruen and Gautel, 1999). Domain cC1 is positioned close to the hinge region between fragments S2 and S1 of myosin, probably playing an important role in regulation of muscle contraction, while cC2 is positioned on the S2 fragment in the proximity of domain cC1. In fact, despite the presence of the long linker between them, the two domains resulted being quite close in space, with the linker running parallel to the myosin filament in a sort of U shape; the linker has been shown to be unstructured and highly mobile (Ababou et al., 2008) but it can probably adopt a compact structure upon binding to myosin.



It is on the basis of these results that an interaction between domain cC0 and the Regulatory Light Chain (RLC) of myosin has been hypothesised, aspect that will be

dealt with in this thesis. All these results give an insight in the manner the N-terminus of the protein can assemble into the sarcomere, while on the overall way of incorporation of MyBPC in the sarcomere two different models have been proposed.

#### **1.1.6.1 Trimeric collar model**

In the trimeric collar model, proposed by Moolman- Smook co-workers (Moolman-Smook et al., 2002), three cMyBPC molecules form a ring around the thick filament, interactions between domains C5-C7 and domain C8-C10 of another molecule of MyBPC are needed to stabilize this model, while domains C0-C4 are thought to reach out from the thick filament and interact with the myosin crossbridge and/or the actin filament (Squire et al., 2003; Witt et al., 2001). Although this model is able to explain some aspects, it is not satisfactory on others, firstly the diameter of the myosin thick filament is 13-15 nm (Squire et al., 1998), resulting in a circumference of approximately 41-44 nm but according to this trimeric collar model, the ring around the thick filament is formed by nine IgI domains, which have a diameter of maximum 3.4-3.9 nm, resulting in the largest ring possible being 35-36 nm, so 5-12 nm shorter than the measured circumference of the myosin thick filament (47 nm). Furthermore, there is no evidence that the C-terminal region of MyBP-C is subjected to high degree of stretch. It is possible that some of the linkers may provide additional length to form a collar around the myosin filament, however, the only linker of significant length in this region is the one between domains C9 and C10, but stretching it may result in mismatch between interacting domains in the trimeric collar model. A second unsolved problem is how the titin molecule fits in this model; titin is the molecular ruler of the sarcomere (Whiting et al., 1989). The C-terminal domains C7- C10 of MyBPC bind to both titin

and the LMM of the myosin thick filament but this model does not clarify how cMyBPC interacts with titin, since in the model the titin molecule would be perpendicular to the trimeric collar (Freiburg and Gautel, 1996). Recent data (Flashman et al., 2008) have given support to this model, confirming the presence of the C5-C8 interaction also in fast skeletal muscle but interestingly not in slow skeletal muscles.

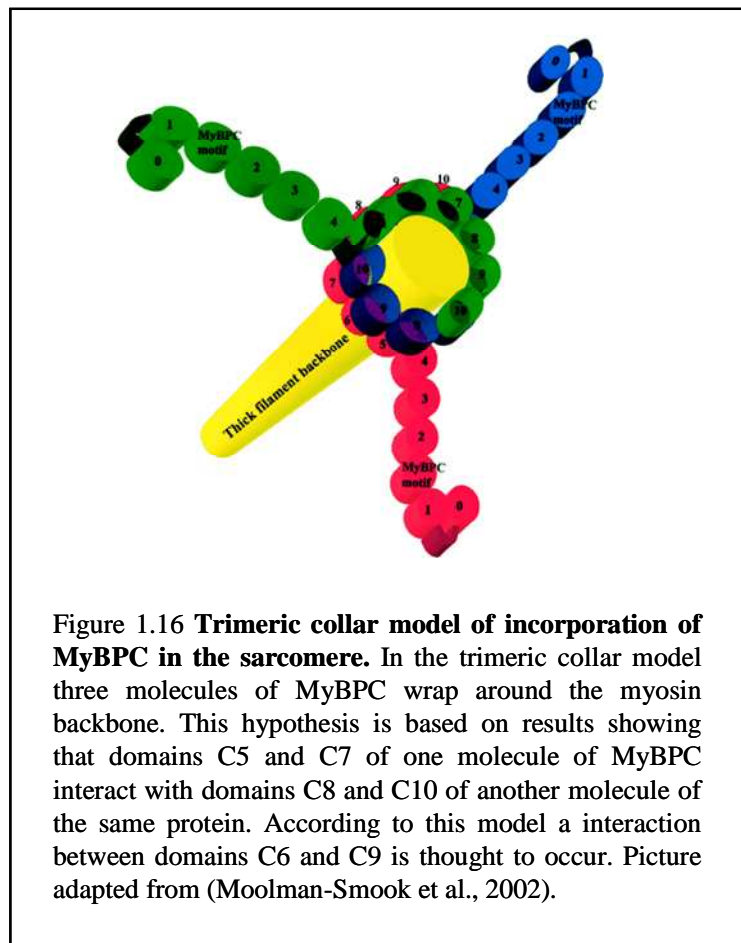
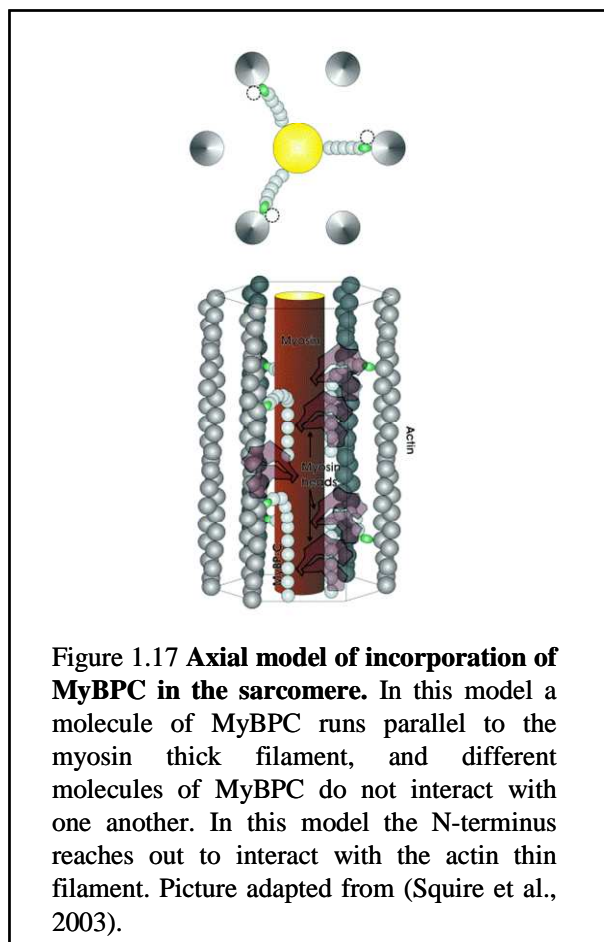


**Figure 1.16 Trimeric collar model of incorporation of MyBPC in the sarcomere.** In the trimeric collar model three molecules of MyBPC wrap around the myosin backbone. This hypothesis is based on results showing that domains C5 and C7 of one molecule of MyBPC interact with domains C8 and C10 of another molecule of the same protein. According to this model a interaction between domains C6 and C9 is thought to occur. Picture adapted from (Moolman-Smook et al., 2002).

### 1.1.6.2. Axial model

In a second model, proposed by Squire and co-workers (Squire et al., 2003), cMyBPC is arranged axially along the myosin backbone and is able to interact with titin and LMM with its C-terminus while the N-terminus reaches out to interact with the myosin crossbridge and/or actin.



In this model two MyBPC molecules are separated by 43 nm on the myosin filament. The N-terminal region is allowed to interact with the myosin head or actin, while the C-terminal zone is involved in binding the C-protein to the myosin thick filament. Figure 1.17 shows how MyBP-C would assemble in the sarcomere: according to this model

domains C7-C10 run axially along the myosin filament backbone not allowing different molecules of the same protein to interact with one another; this model does not take into consideration the observed cC5-cC8 and cC7-cC10 interaction.

### **1.1.7 Aim of the project**

To have a better understanding of the function of cMyBPC, it is important to characterize the interactions between this protein and other sarcomeric polypeptides. To do so, many techniques have been used, but a particular potent method to study protein-protein interactions on a molecular level, is to follow the changes in an NMR spectrum of a protein of known structure. The structures of three domains of cMyBPC have been determined so far, domain C1 (PDB ID: 2avg) (Ababou et al., 2008), C2 (PDB ID: 1pd6) (Ababou et al., 2007) and the central domain C5 (Idowu et al., 2003) have been solved by NMR spectroscopy and the X-ray structure of domain C1 has been very recently deposited and published (PDB ID: 2v6h) (Govada et al., 2008). It is in this context that the present study has been developed.

The aims of the project are:

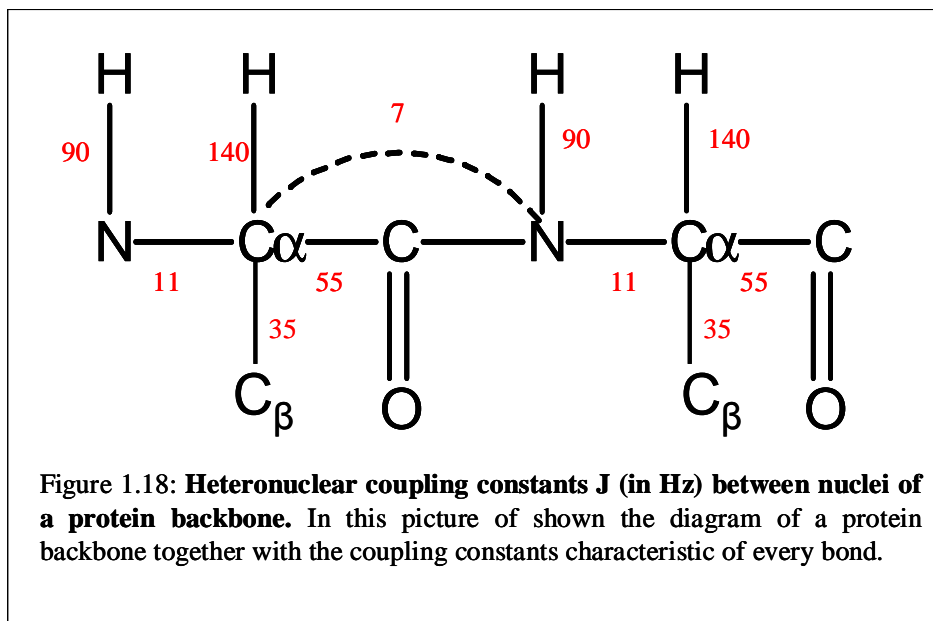
- To determine the structure of domain cC0 and to study its interaction with the Regulatory Light Chain (RLC) of myosin.
- To study the interaction that is thought to happen between domains C5 and C8 of cMyBPC (Moolman-Smook et al., 2002).

## 1.2 *Structur determination*

### 1.2.1 **NMR spectroscopy**

The following section describes the mains steps followed to obtain all the NMR data needed to determine the three dimensional structure of domain cC0. First is given a description of the triple- resonance experiments used for the backbone assignment of the proteins, then the NOE effect and its use in structure determination is described.

NMR spectra contain all the information needed to determine the three-dimensional structure of a protein in solution. However, none of these information can be used without a sequence specific resonance assignment that associates NMR signals with specific atoms in the protein. The experiments that are necessary to record to carry out a sequence specific assignment need to contain information about all hydrogen, nitrogen and carbon atoms but, since the naturally abundant isotopes of the latter two nuclei are either not NMR-active ( $^{12}\text{C}$ ) or have a quadrupole moment that dominates its relaxation behaviour and prevents its use in most structural work on biological macromolecules ( $^{14}\text{N}$ ), it is necessary to produce protein samples labelled with  $^{13}\text{C}$  and  $^{15}\text{N}$ . In such samples, it is possible to transfer phase coherence between  $^1\text{H}$ ,  $^{15}\text{N}$  and  $^{13}\text{C}$  by using one-bond connectivities which are strong and make it possible to overcome the sensitivity problems caused by the small magnetogyric ratios of  $^{13}\text{C}$  and  $^{15}\text{N}$  that lead to low sensitivity detection.



In these experiments, phase coherence that is generated on protons is transferred to nitrogen or carbon atoms and then transferred back to protons, as shown in Figure 2.2

The experiments that are necessary to record for a protein sample to be able to solve the three-dimensional structure are reported in table 2.7; in some of these experiments the magnetization is transferred through the bonds, while in other experiments, based on the Nuclear Overhauser Effect (NOE), it is transferred through space.

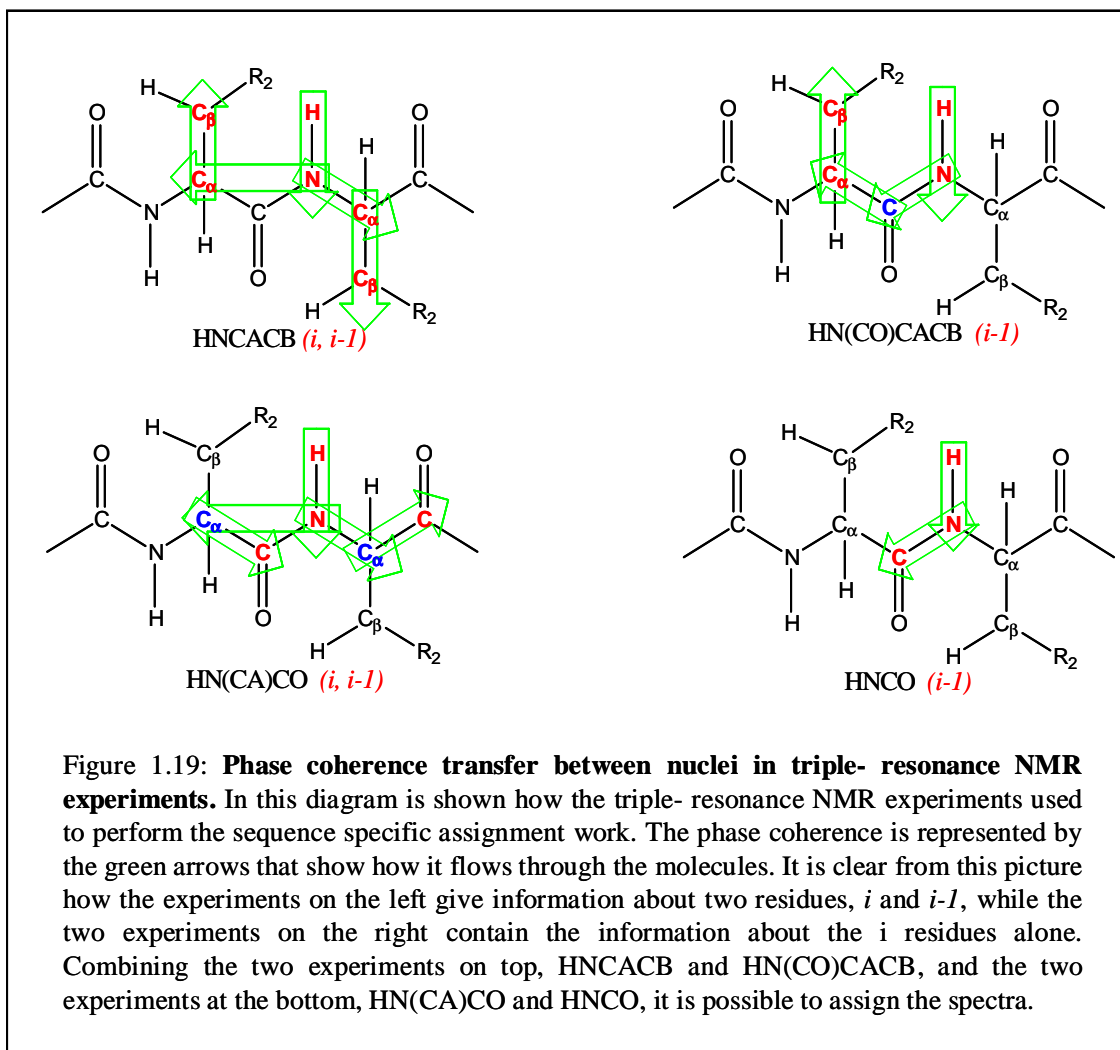
n° exp	Type of exp	Assignment	Through
1	$^1\text{H}/^{15}\text{N}$ HSQC	Backbone	Bond
2	$^1\text{H}/^{13}\text{C}$ HSQC	Backbone	Bond
3	HNCaCb	Backbone	Bond
4	HN(CO)CaCb	Backbone	Bond
5	HN(Ca)CO	Backbone	Bond
6	HNCO	Backbone	Bond
7	HN(CaCb)HaHb	Backbone	Bond
8	HN(CaCbCO)HaHb	Backbone	Bond
9	$^1\text{H}/^{15}\text{N}$ TOCSY-HSQC	Sidechain	Bond
10	$^1\text{H}/^{13}\text{C}$ HCCH TOCSY	Sidechain	Bond
11	TROSY	Sidechain	Bond
12	$^1\text{H}/^{15}\text{N}$ NOESY-HSQC	Sidechain	Space
13	$^1\text{H}/^{13}\text{C}$ NOESY-HSQC	Sidechain	Space
14	$^1\text{H}/^1\text{H}$ NOESY	Sidechain	Space
15	$^1\text{H}/^1\text{H}$ TOCSY	Sidechain	Bond

**Table 1.3: NMR experiments needed for the structure calculation.**

The first experiment to be recorded for any new protein is the  $^1\text{H}/^{15}\text{N}$ - HSQC spectrum (Bodenhausen, 1980). This 2D experiment consists of an H,N chemical shift correlation map and the number of correlation signals should roughly correspond to the number of residues present in the protein. Prolines, however, do not give a signal, due the absence of a free N-H group, while additional signals could be present caused by side-chain NH groups.

The same kind of experiment can be performed for  $^1\text{H}$  and  $^{13}\text{C}$  correlation ( $^1\text{H}/^{13}\text{C}$ -HSQC). In this case the spectrum will present more peaks as every C-H group present in the macromolecule will give a signal.

Four triple- resonance experiments have been performed to carry out the sequence-specific assignment: HNCACB (Wittekind, 1993), HN(CO)CACB (Grzesiek and Bax, 1993; Grzesiek et al., 1992), HNCO (Ikura et al., 1990) and HN(CA)CO. Figure 2.2 shows the magnetization transfers that takes place in these experiments. In HNCACB the magnetization is transferred through the bonds, from the amide proton, to the  $\text{C}\alpha$  and  $\text{C}\beta$  atoms of the same and previous residues, while in HN(CO)CACB the magnetization is forced through the carbonyl and so in the spectrum just two peaks will be present, the  $\text{C}\alpha$  and  $\text{C}\beta$  of the preceding amino acid. Combining these two experiments it is therefore possible to identify uniquely the  $\text{C}\alpha$  and  $\text{C}\beta$  nuclei for the sequential residues.



Experiments HNCO and HN(CA)CO work in the same way and give information about the carbonyls, these are also the only experiments that give us information about the C=O groups. In HN(CA)CO, magnetization is transferred from the amide proton to the  $^{13}\text{C}$  of the carbon alpha, thus involving two coupling constants,  $^1\text{J}(\text{N},\text{H})$  which is 90Hz, and  $^1\text{J}(\text{N},\text{CA})$ , which is 11Hz, and give rise to two peaks, one for the same and one for the preceding residue. On the other hand, NHCO gives rise to one peak corresponding to the *i-1* residue. Again, combining the two experiments it is possible to identify the signal of each amino acid and, as a consequence, carry out a sequence specific assignment.

To identify the proton chemical shifts, other experiments, like  $^1\text{H}/^{15}\text{N}$  TOCSY-HSQC (Marion et al., 1989 a; Marion, 1989 b) have been recorded. This experiment yields a  $^1\text{H}/^1\text{H}$  TOCSY plane for each  $^{15}\text{N}$  chemical shift. An analogue experiment could be done taking advantage of the Nuclear Overhauser Effect, that is the  $^1\text{H}/^{15}\text{N}$  NOESY-HSQC (Marion, 1989 b); similarly to the TOCSY corresponding experiment, in this case a  $^1\text{H}/^1\text{H}$  NOESY plane is obtained for each  $^{15}\text{N}$  chemical shift, in which the selected NH proton gives NOE cross-peaks with protons of the same amino acid as well as protons of residues close in space. Combining  $^1\text{H}/^{15}\text{N}$  TOCSY-HSQC and  $^1\text{H}/^{15}\text{N}$  NOESY-HSQC it is possible to distinguish between cross-peaks generated by protons in the same residue, that are present in both experiments, and the protons that are close in space but not in the sequence, that are present only in the  $^1\text{H}/^{15}\text{N}$  NOESY-HSQC spectrum. The latter experiment is very important as it contains vital information to determine the structure of the protein.

All the experiments described so far give information about the backbone nuclei; to perform a side-chain assignment it is necessary to record specific experiments, such as  $^1\text{H}/^{13}\text{C}$  HCCH-TOCSY (Bax, 1990); in this experiment the magnetization of the aliphatic protons is transferred to their  $^{13}\text{C}$  nuclei through the whole aliphatic side-chain. After a back-transfer, the chemical shift of the aliphatic protons are recorded. The spectra resulting from this experiment are  $^1\text{H}/^1\text{H}$  TOCSY planes edited by the  $^{13}\text{C}$  chemical shift and generated by a TOCSY transfer through the carbon chain.

Once the  $^1\text{H}/^{13}\text{C}$  HCCH TOCSY spectrum has been fully assigned, it is possible to assign also the  $^1\text{H}/^{13}\text{C}$  NOESY-HSQC which is the spectrum that, together with the  $^1\text{H}/^{15}\text{N}$  NOESY-HSQC, contains all the information for the three-dimensional structure determination. Ideally it should be possible to obtain one  $^1\text{H}/^1\text{H}$  NOESY plane for each  $^{13}\text{C}$  chemical shift and, being the experiment based on the Nuclear Overhauser Effect, it

shows peaks that are both from sequential amino acid and residues that are close in space but not necessarily in the sequence. The assignment of the  $^1\text{H}/^{13}\text{C}$  NOESY-HSQC is now done automatically using software that also carry out the structure calculation.

Additional experiments, such as  $^1\text{H}/^1\text{H}$  TOCSY and  $^1\text{H}/^1\text{H}$  NOESY have been recorded in the aromatic region to do the assignment of the aromatic side-chains.

### **1.2.2 Three dimensional Structure determination with the program**

#### **CYANA**

This is an iterative process that consists in assignment of all NOEs peaks and subsequent calculation of a three dimensional structure that will be used in the following cycle to carry out the new NOE assignment. A CYANA calculation comprises normally of seven cycles of automatic NOE assignment and subsequent structure calculation, to obtain a final optimized structure .

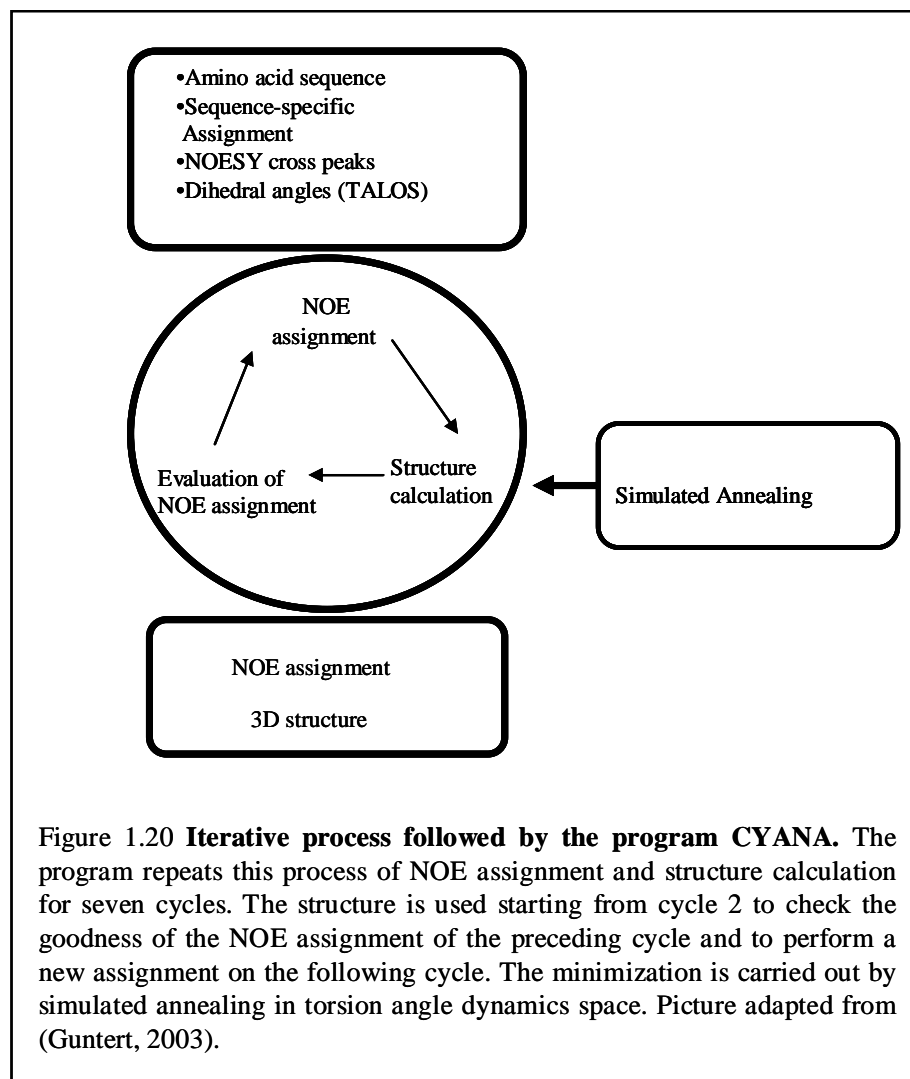
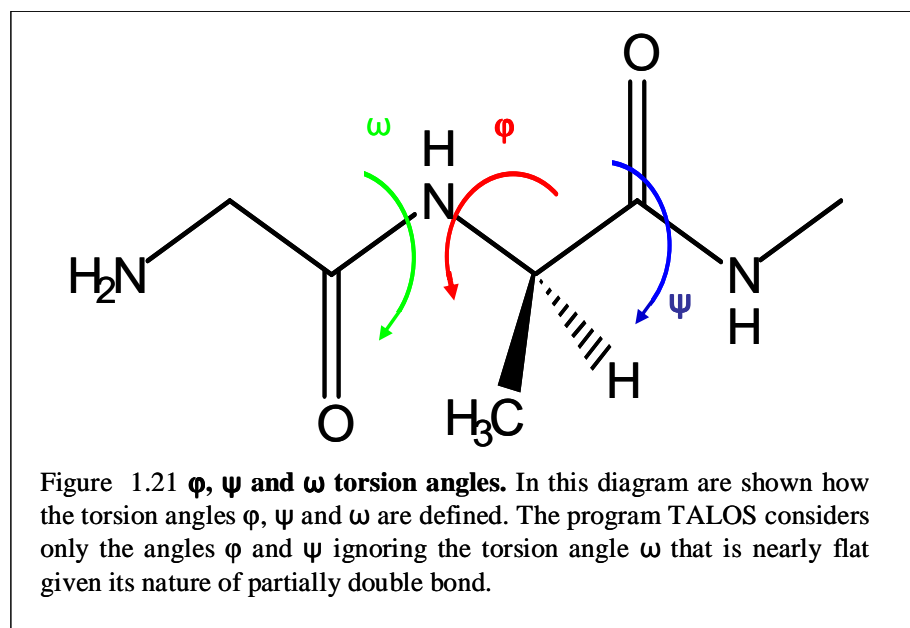


Figure 1.20 **Iterative process followed by the program CYANA.** The program repeats this process of NOE assignment and structure calculation for seven cycles. The structure is used starting from cycle 2 to check the goodness of the NOE assignment of the preceding cycle and to perform a new assignment on the following cycle. The minimization is carried out by simulated annealing in torsion angle dynamics space. Picture adapted from (Guntert, 2003).

In the 3D structure determination of proteins in solution by NMR spectroscopy, the data containing the conformational information are upper distance constraints derived from the NOE spectra. It is therefore necessary to assign each cross peak, to identify the pairs of interacting hydrogen atoms. The NOESY assignment is based on previously determined chemical shift values that result from the assignment of different spectra, as discussed in the previous section. Nowadays the assignment of the NOEs is done automatically by a software, in this work the program CYANA (Guntert et al., 1997) was used, which contains the CANDID algorithm for automated NOE assignment (Herrmann et al., 2002).

The input data for CANDID comprise amino acid sequence, chemical shift lists from sequence specific resonance assignment, list of NOESY cross peaks positions and volumes and, optionally, additional information such as dihedral angles constraints derived from the program TALOS (Cornilescu et al., 1999).

### 1.2.2.1 TALOS



TALOS compares the similarity in amino acid sequence and secondary shifts of the protein in exam with twenty proteins of known structure. TALOS database, in fact, contains  $^{13}\text{C}\alpha$ ,  $^{13}\text{C}\beta$ ,  $^{13}\text{C}'$ ,  $^1\text{H}\alpha$  and  $^{15}\text{N}$  chemical shifts assignments of these twenty proteins, together with the backbone torsion angles  $\phi$  and  $\psi$  derived from the crystal structures. When analysing a new protein, TALOS reads the experimental chemical shifts of the protein and converts them in secondary chemical shifts before entering them into the database. A graphical interface makes very easy and intuitive the use of the program, three windows display the output obtained from the comparison of the

experimental secondary chemical shift with the database data: in the sequence display the amino acid sequence of the examined protein is shown with all residues colour-coded corresponding to a good (green), bad (red) or ambiguous (yellow), standard deviation bigger than  $45^\circ$ , prediction.

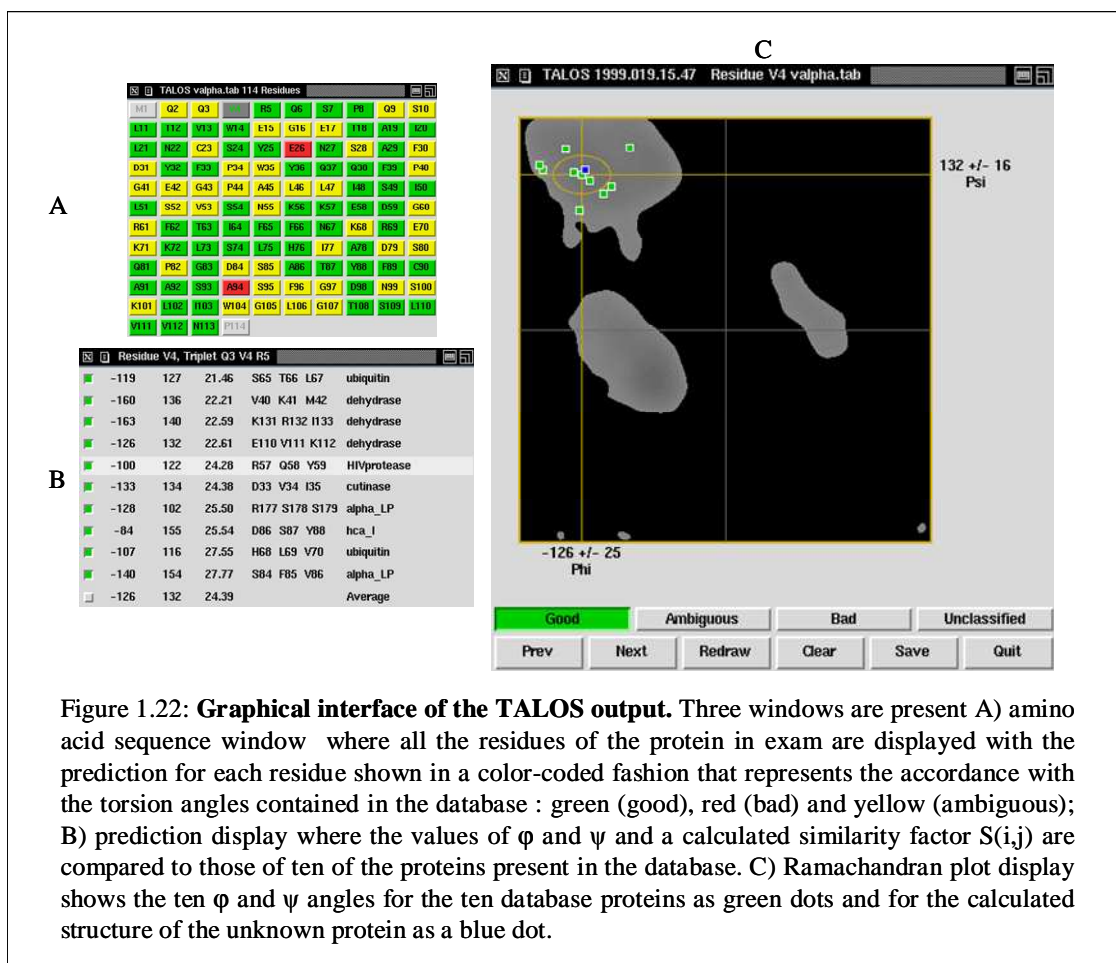


Figure 1.22: **Graphical interface of the TALOS output.** Three windows are present A) amino acid sequence window where all the residues of the protein in exam are displayed with the prediction for each residue shown in a color-coded fashion that represents the accordance with the torsion angles contained in the database : green (good), red (bad) and yellow (ambiguous); B) prediction display where the values of  $\phi$  and  $\psi$  and a calculated similarity factor  $S(i,j)$  are compared to those of ten of the proteins present in the database. C) Ramachandran plot display shows the ten  $\phi$  and  $\psi$  angles for the ten database proteins as green dots and for the calculated structure of the unknown protein as a blue dot.

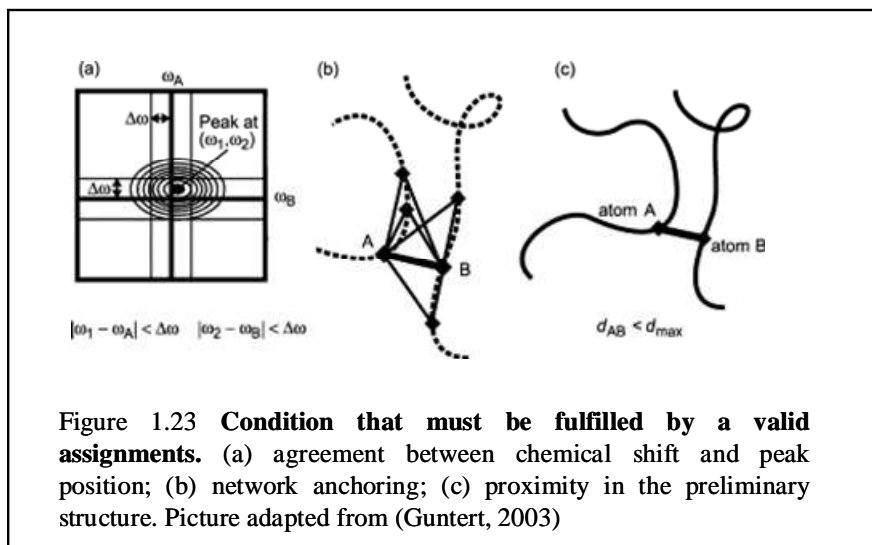
The TALOS output for the  $\phi$  and  $\psi$  dihedral angles of the centre residue in each three residue string taken into consideration, consists in the average of the corresponding angles in the ten strings in the database with the highest degree of similarity. In the first run, the program classifies only those prediction for which at least 9 out of 10 fall in the same region of the Ramachandran plot and none of the central residues has a positive value of  $\phi$ . If a residue has  $\phi$  and  $\psi$  that fall outside the region in the Ramachandran plot

where all the other nine residues are located, this residue will be excluded from the calculation of the average and rmsd. In the prediction display of the program are shown the ten proteins with the most similar torsion angles to the three residue string taken in exam. At the bottom is shown the calculated average value and the similarity factor. These results are also shown in the third window, the Ramachandran plot display, where the ten green dots shown represent the ten protein listed in the prediction window, with the average values for  $\phi$  and  $\psi$  in evidence on the  $\phi$  and  $\psi$  axis of the map, respectively, and the standard deviation is shown as a circle around the point with coordinates  $\phi$  and  $\psi$ . When available, a blue dot shows the structure calculated for the protein under investigation, this is present only after the first cycle of structure calculation when TALOS can be revised to improve the final result by checking the accordance between the experimental values of  $\phi$  and  $\psi$  and the same values for the ten proteins in the database that give the best result. This step is done on the ambiguous residues so that the amino acids that were depicted in yellow in the first output program window, can be set manually by the operator as in good accordance with the  $\phi$  and  $\psi$  values contained in the database or discard if in bad accordance.

### **1.2.2.2 Automated NOE assignment using the CANDID algorithm**

A CANDID cycle starts by generating an assignment list that contains the hydrogen atoms that could contribute to a peak. For each cross peak, these initial assignments are weighted against filtering criteria, such as agreement between values of chemical shifts and peak position, self consistency within the entire network of NOEs (network anchoring) and, if available, the compatibility with the 3D structure calculated in the preceding cycle. In the first cycle, where a 3D structure is not available, network

anchoring has a predominant effect. Initial assignments with low overall score are discarded.



For each cross peak, the retained assignments are interpreted as upper distance limits derived from the cross peak volume; upper distance constraints can be obtained from a single assigned cross peak or can be ambiguous distance constraints if more than one assignment is retained by the cross peak. The introduction of ambiguous constraints revolutionised the automated NOE assignment as, before, just unambiguously assigned NOEs could be used as distance constraints for the structure calculation. The majority of NOEs, however, cannot be assigned unambiguously from chemical shift information alone and this severely limited the application of automated NOE assignment in the past. When including the ambiguous distance constraints, each NOESY cross peak with  $n > 1$  possible assignments can be seen as the superimposition of  $n$  degenerate signals.

- *Network anchoring*

Any network of distance constraints that is dense enough for the determination of a protein 3D structure, forms a self-consistent subset of correctly assigned constraints. Network anchoring evaluates this self-consistency of NOE assignments independently from the knowledge of the three dimensional structure of the protein in question and can thus be used in the first cycles of NOE assignments when a 3D structure is not available to evaluate the goodness of the assignment. The fact that each NOE assignment must be embedded in the network of all other assignments makes this approach very powerful in detecting erroneous constraints that are not reinforced by the presence of consistent NOEs around it.

Network anchoring for two atoms  $\alpha$  and  $\beta$  consists in looking for all atoms  $\gamma$  present either in the same or in the neighbouring residues, that are connected simultaneously to  $\alpha$  and  $\beta$ . The connection might be an assignment or the fact that the structure implies that the corresponding distance must be short enough to give rise to an observable NOE. Interestingly, all peaks from the peak list contribute simultaneously to the network anchored assignment.

- *Constraints combination*

The presence of artifacts and the misinterpretation of noise signals, could lead to erroneous structure calculations. This is particularly true at the first cycles of NOE assignments as a 3D structure based filtering of constraints is not available. Constraints combination is applied in the first two cycles of CANDID to minimize the impact of the experimental imperfection of the spectra on the resulting structure at the expense of a temporarily loss of information.

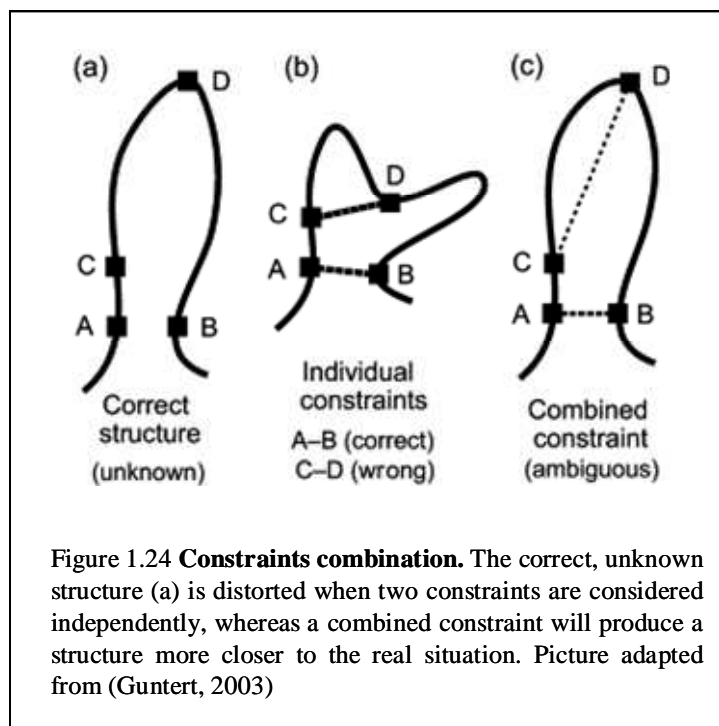
Constraints combination consists in generating distance constraints with combined assignments from different, unrelated cross peaks. The basic property for ambiguous constraints is that a constraint will be fulfilled by a correct structure as long as at least one of its assignments is correct, even if additional, erroneous assignments are associated with the constraint. This implies that the combined constraints have a lower probability of being wrong than the corresponding original constraints, provided that less than half of the original constraints are erroneous.

CANDID provides two methods of constraints combination:

- 2→1 in which two assignments  $A$  and  $B$  are replaced by a single ambiguous constraint with assignment  $A \cup B$
- 4→4 is a pairwise combination that replaces four assignments  $A$ ,  $B$ ,  $C$  and  $D$  with four distance constraints  $A \cup B$ ,  $A \cup C$ ,  $A \cup D$  and  $B \cup C$ .

Since in case of error the effect on the global fold is more pronounced with long range NOEs, the constraints combination is applied only on these signals and not on short or medium range NOEs.

In the 2→1 case, the number of long-range constraints is halved, whereas in the 4→4 combination more of the original information are conserved. The latter combination, moreover, takes into account that some peaks have assignments more reliable than others, as the four peaks  $A$ ,  $B$ ,  $C$  and  $D$  are used 3, 2, 2 and 1 times respectively, to form the final combined constraints.



### 1.2.2.3 Structure calculation

In the program CYANA, the calculation of the three dimensional structure of a protein is a minimization of a target function that measures the agreement between a structure and its set of constraints. The CYANA target function (Guntert et al., 1997) is defined such as it is zero if all experimental distance and torsion angle constraints are fulfilled and all non bounded atom pairs satisfy a check for the absence of steric overlap, a conformation that satisfies these criteria more closely than another, will lead to a lower value of the target function.

- *Torsion angles dynamics*

The minimization algorithm in CYANA is based on simulated annealing (Kirkpatrick et al., 1983) by molecular dynamic simulation in torsion angle space. Torsion angle dynamics consists in molecular dynamic simulation using torsion angles instead of Cartesian coordinates as degree of freedom. Compared to the minimization of a target function, the molecular dynamics simulation comprises also the kinetic energy that allows overcoming barriers of potential, reducing the probability of encountering a local minimum.

The only degree of freedom in torsion angle dynamics is the rotation about the covalent bonds, so that the conformation of the protein is defined by the values of all torsion angles.

- *Simulated Annealing*

In solving a protein structure, the potential energy profile is complex and studded with local minima, it is therefore important to adopt a calculation method that will minimize the probability of being stuck in one of these local minima. The method of choice is simulated annealing, a combinatorial optimization method. The concept of simulated annealing is taken from the crystallisation procedures applied to metals, where a metal is melted at high temperature (high kinetic energy phase) and then slowly cooled down in order to minimize the structural defects.

The standard simulated annealing protocol in CYANA starts from a conformation with all torsion angles treated as independent and consists of five steps. An initial minimization step, including only constraints between atoms up to three residues apart along the sequence, is performed to reduce high- energy interaction that could disrupt the torsion angle dynamics algorithm, and is then followed by the high- temperature

phase, a torsion angle dynamics calculation carried out at constant high temperature, so to ensure of not falling in any local minima. The third step consists in the slow cooling close to a zero temperature. Up to this point the hydrogen atoms have not been included in the calculation and are included at this stage of low temperature phase with individual hydrogen atoms, then a final minimization is carried out, consisting of 1000 conjugate gradient steps.

With torsion angle dynamics it is possible to calculate protein structure on the basis of NMR data efficiently.

#### **1.2.2.4 Structure validation**

Once the structure has been determined, it has to be evaluated to understand how reliable the result obtained is. Cyana implements six criteria (Guntert, 2003) that allow to evaluate the goodness of a structure; these criteria are as follow:

1. average target function for cycle 1 below 250 Å
2. average target function for cycle 7 below 10 Å
3. less than 20% unassigned NOEs
4. less than 20% discarded long- range NOEs
5. RMSD for cycle 1 below 3Å
6. RMSD between cycles 1 and 7 below 3Å

Thanks to these criteria it is possible to evaluate a newly determined three dimensional structure, however this can be done also with the help of different software. An important one and also the one used in this work is PROCHECK in its version PROCHECK NMR (Laskowski et al., 1996), that carries out validation of the geometric quality of the structure determined. Since the information contained in NMR data alone

is not enough to determine a molecular structure, it is particularly important to check NMR structures for geometric abnormalities and errors.

Most of the checks use reference values of the considered geometric parameter to judge if a structure is normal or not. The validation criteria used to evaluate the goodness of a structure could be concerning the local geometry, like bond lengths and angles, chirality, tetrahedral geometry and side chain planarity, or overall quality, evaluated by the Ramachandran plot, rotameric states, backbone conformation and packing of the side-chains in the hydrophobic core of the protein, plus additional criteria like inter-atomic bumps, hydrogen bonds and electrostatics.

The most relevant of the local geometry criteria to be considered are the  $\chi_1$  and  $\chi_2$  angles that define the states of the rotamers. Side-chain rotamers have a preferred staggered conformation with dihedral angles of  $-60$ ,  $60$  and  $180^\circ$ ; this preference is due to the difference in energy between the eclipsed conformation, that is characterised by a more relevant steric interaction and as a consequence has a higher energy, and the staggered conformation, that is energetically favoured; both states can occur in a protein, as transitions are possible between the two states. The relative population between these two states vary with amino acid type, secondary structure elements and environment. In PROCHECK the  $\chi_1$ -  $\chi_2$  side chain rotamer distribution is considered for each amino acid in the sequence and displayed on a graphic where allowed and disallowed regions are depicted.

A similar kind of evaluation could be done for the backbone dihedral angles  $\phi$  and  $\psi$ . Based on steric consideration, it was shown (Ramachandran et al., 1963) that the combination of the two angles in a polypeptide chain are restricted to certain ranges, which can be visualised in the so-called Ramachandran plot. Apart from steric restrictions,  $\phi$  and  $\psi$  show different preferences that depends on residue type and

secondary structure elements. The Ramachandran plot is a renowned method to evaluate the quality of a structure (Hoofst et al., 1997) and the most widely used method to do so is to divide the plot in four regions: favoured, additionally allowed, generously allowed and disallowed. This is also the method used in the program PROCHECK.

Another important angle to be considered is the torsion angle  $\omega$  about the peptide bond. Given its partially double-bond nature, its free rotation is impaired and the peptide bond is always close to planarity. The angle  $\omega$  is mostly found in the *trans* conformation ( $180^\circ$ ) but can be found also in the less favoured *cis* conformation ( $0^\circ$ ). Most of the *cis* peptide bonds involve a proline (Xaa-Pro) but rare cases of *cis* conformations without the presence of a proline residue are also known.

Particularly interesting are the non-bonded interactions such as inter-atomic bumps. These occur when the distance between the centres of two atoms is less than physically realistic; PROCHECK identifies atoms as being involved in a bad contact if they are closer in space than 2.6 Å. This is done considering only the non-hydrogen atoms and those pairs that do not form hydrogen bonds. Hydrogen bonding in fact, plays a very important role in the stability and overall folding of a polypeptide. The difference in energy between the folded and unfolded state of a protein is between 5 and 15 kcal mol<sup>-1</sup>, while the energy for the formation of a single hydrogen bond is in the order of 2-5 kcal mol<sup>-1</sup> (Branden, 1999) so the absence or presence of as little as 1 to 3 hydrogen bonds can have a profound effect on the protein stability. The packing of the side chains in the hydrophobic core is another important parameters that can give an idea of the goodness of a calculated structure, as different type of amino acids display a different preference for their neighbouring residues and these preference have a strong impact in determining the global fold of the protein. This is particularly true for aromatic and hydrophobic residues that should pack against one another in the core of the protein

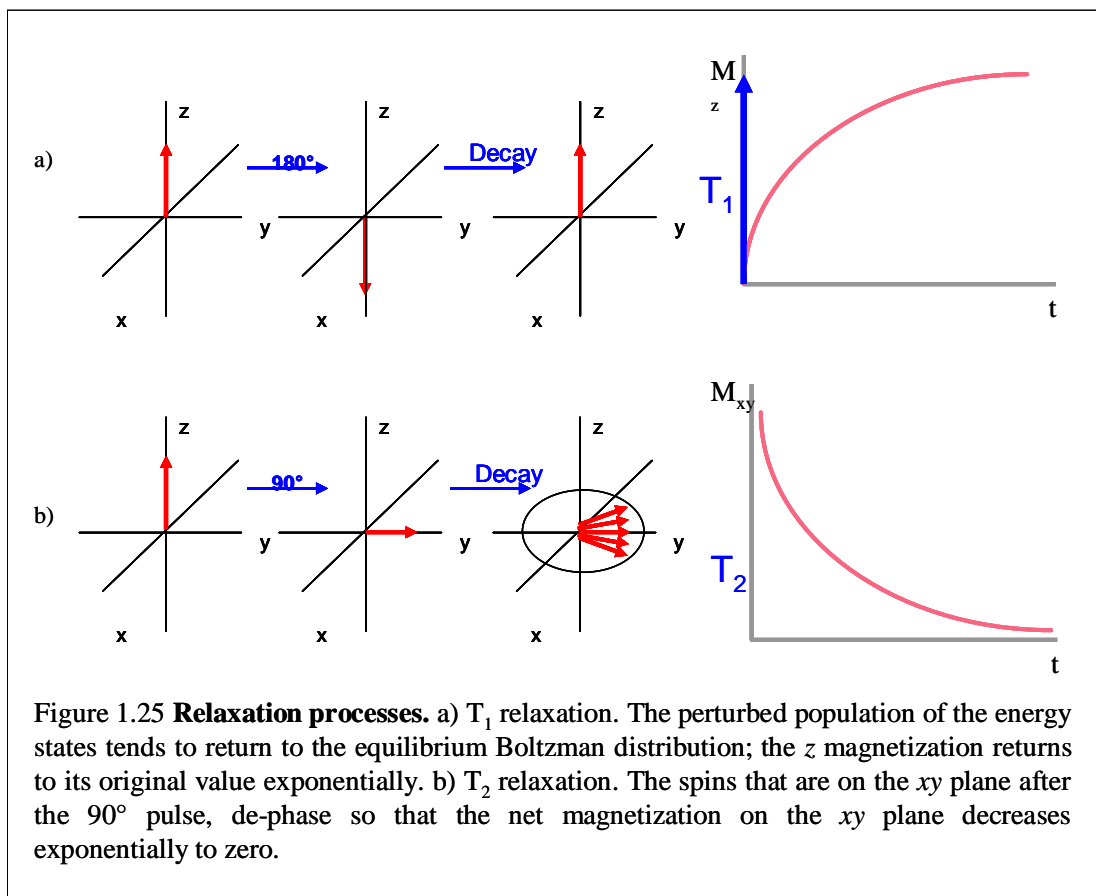
structure. All these aspect together give an idea of how good and reliable a structure calculated based on NMR data is. The PROCHECK results are all displayed in graphic form so they are very direct and intuitive (see figures 3.11 and 3.12 p 111- 112).

### **1.2.3 Protein dynamics**

Dynamics play an important role in protein function (Brooks et al., 1988; Jardezyk, 1996; McCammon and Harvey, 1987) and NMR sensitivity to motion makes it a powerful tool for the study of macromolecular dynamics through the phenomenon of nuclear spin relaxation (Palmer, 1997; Wagner et al., 1993). Some spectral properties, in fact, can be correlated to intra-molecular motion, so once the NMR peaks of a spectrum, usually a  $^1\text{H}/^{15}\text{N}$  HSQC spectrum, are assigned it is possible to investigate the properties of the corresponding nuclei based on their relaxation behaviour.

#### **1.2.3.1 Relaxation**

Once a spin has been perturbed, it tends to relax back to its equilibrium state over a period of time. Every spin has two different kind of relaxation:



- *Longitudinal relaxation* ( $T_1$ ) is the time necessary for the population of the energy states to return to the original Boltzman distribution and corresponds to the time taken by the net  $z$  magnetization ( $M_z$ ) to return exponentially to its starting value  $+z$ .
- *Transversal relaxation* ( $T_2$ ) is the time necessary for the coherence in the  $xy$  plane ( $M_{xy}$ ) generated by the  $90^\circ$  pulse, to de-phase decaying exponentially to zero.

Dynamic information is derived by both longitudinal and transverse relaxation rates  $R_1$  ( $1/T_1$ ) and  $R_2$  ( $1/T_2$ ) and also from the cross-relaxation  $^1\text{H}/^{15}\text{N}$  rates (NOE). For the evaluation of the dipole cross-relaxation two separate experiments are run, a reference experiment, corresponding to a  $^1\text{H}/^{15}\text{N}$  HSQC without the initial INEPT step, so the initial magnetization is localized on  $^{15}\text{N}$  nuclei instead of  $^1\text{H}$  as in the  $^1\text{H}/^{15}\text{N}$  HSQC experiment. Nevertheless the peaks obtained correspond to the one of the  $^1\text{H}/^{15}\text{N}$  HSQC

experiment so the assignment can be transferred between the two. This will have the function of reference spectrum, while the second experiment is registered with  $^1\text{H}$  saturation so to generate a Nuclear Overhauser Effect (heteronuclear NOE). Comparing the two spectra it is then possible to recognize which residues are more affected by the NOE and so take part in dynamic phenomena. From these experimental data it is possible to extract information on the dynamic processes specific for the molecule in exam.

### 1.2.3.2 Model free analysis

The dynamic information on fast internal motion that can be extracted from the NMR experiments are contained in two parameters:

- *General order parameter ( $S$ ):* is a measure of the degree of spatial restriction of the motion; it can assume values between 0 and 1.
- *Effective correlation time ( $\tau_e$ ):* is a measure of the rate of the motion.

These two parameters can be defined in a model independent way and are at the core of the Lipari-Szabo analysis (Lipari and Szabo, 1982a; Lipari and Szabo, 1982b) to obtain dynamic information from relaxation experiments. The idea of using a model-free analysis is to avoid the danger of over-interpretation of a limited set of data.

The first step of this analysis is to determine the nature of the overall motion by determining the *correlation time* ( $\tau_c$ ) which corresponds to the average time taken by a molecule to achieve an orientation of one radian from its starting position due to

random motion. The correlation time is linked to the *correlation function*  $G(\tau)$  that is a way of characterizing the time dependence of the random internal motion; performing a Fourier transformation on  $G(\tau)$  that is a function of time, a function of frequency is obtained, exactly in the same way the time dependent FID is transformed in a frequency dependent spectrum. This frequency dependent quantity is the *spectral density*  $J(\omega)$  and tells us how much motion is present at a particular Larmor frequency.

Assuming the molecule subject to an isotropic motion,  $\tau_c$  can be extracted directly from the relaxation data for nuclei rigidly attached to the macromolecule. Once this is fixed, it is possible to extract the information on the internal motion, determining the spectral density  $J(\omega)$  that is linked to the three observable NMR relaxation parameter:

$$R_1 = \left( \frac{d^2}{4} \right) [3J(\omega_N) + 7J(\beta_1\omega_H) + c^2 J(\omega_N)]$$

$$R_2 = \left( \frac{d^2}{8} \right) [4J(0) + 3J(\omega_N) + 13J(\beta_2\omega_H)] + \frac{c^2}{6} [4J(0) + 3J(\omega_N)]$$

$$NOE = \left( \frac{d^2}{4} \right) 5J(\beta_3\omega_H)$$

where  $d = \frac{\hbar^2 \gamma_N^2 \gamma_H^2}{r_{NH}^6}$  is the dipolar relaxation contribution and  $\beta_1 = 0.921$   $\beta_2 = 0.955$   $\beta_3 = 0.87$  for  $^{15}N$ .

The spectral density  $J(\omega)$  can be described in terms of  $S^2$  and  $\tau_e$  without considering a specific model for internal motion; these two quantities, in fact, are treated in the Lipari-Szabo approach, as adjustable parameters;  $S^2$  and  $\tau_e$ , in fact, uniquely determine  $T_1$ ,  $T_2$  and NOE via the spectral density, so  $S^2$  and  $\tau_e$  are varied in such a way to minimize the

sum of the squared differences between the theoretical and experimental values. Five models have been used in this work to describe the molecular motion:

Model	Spectral density function	Parameters
1	$J(\omega) = \frac{2}{5} \left[ \frac{S^2 \tau_c}{1 + (\omega \tau_c)^2} \right]$	$S^2$
2	$J(\omega) = \frac{2}{5} \left[ \frac{S^2 \tau_c}{1 + (\omega \tau_c)^2} \right]$ $R_{2,ex} = R_2 + R_{ex}$	$S^2, R_{2,ex}$
3	$J(\omega) = \frac{2}{5} \left[ \frac{S^2 \tau_c}{1 + (\omega \tau_c)^2} + \frac{(1 - S^2) \tau}{1 + (\omega \tau)^2} \right]$	$S^2, \tau_e$ $\frac{1}{\tau} = \frac{1}{\tau_c} + \frac{1}{\tau_e}$
4	$J(\omega) = \frac{2}{5} \left[ \frac{S^2 \tau_c}{1 + (\omega \tau_c)^2} + \frac{(1 - S^2) \tau}{1 + (\omega \tau)^2} \right]$ $R_{2,ex} = R_2 + R_{ex}$	$S^2, \tau_e, R_{2,ex}$ $\frac{1}{\tau} = \frac{1}{\tau_c} + \frac{1}{\tau_e}$
5	$J(\omega) = \frac{2}{5} S_f^2 \left[ \frac{S_s^2 \tau_c}{1 + (\omega \tau_c)^2} + \frac{(1 - S_s^2) \tau}{1 + (\omega \tau)^2} \right]$	$S^2, S_s^2, \tau_e,$ $\frac{1}{\tau} = \frac{1}{\tau_c} + \frac{1}{\tau_e}$

**Table.1.4: spectral density function used in the numerical fit to the experimental T1, T2 and NOE values.**  $S^2$  is the generalised order parameter,  $S_s^2$  is the order parameter for slow internal motions;  $R_{ex}$  is the function of the chemical shift evaluated as an exchange term;  $\tau_c$  is the rotational correlation time of the molecule;  $\tau_e$  is the effective correlation time of the internal motion.  $S_f^2$  is the order parameter for fast internal motion. Note that  $S^2 = S_f^2 S_s^2$ ,  $R_{ex}$  is given as an additional term in the transverse relaxation time.

Model 1 is the simplified Lipari- Szabo model which assumes that only very fast internal motions take place, such as thermal vibrations. Model 2 takes into account also relaxation phenomena that might happen in the molecule, with the result of a relaxation faster than expected; in this case  $R_{2,ex}$  is the experimental result and  $R_2$  the calculated transverse relaxation rate, from these it is possible to obtain  $R_{ex}$  that gives an estimation of the exchange rate that the molecule undergoes. Model 3 and 4 correspond to the complete Lipari- Szabo model, with model 4 taking into account exchange phenomena, similarly to what happens in model 2, and model 5 is the extended form of the Lipari- Szabo equation (Clare et al., 1990) used when fast ( $\tau_f$ ) and slow ( $\tau_s$ ) correlation times

differ by at least one order of magnitude and it is then necessary to consider the two motions separately and, as a consequence, two values for  $S_s$  and  $S_f$  should be taken into account on calculating the spectral density.

For every residue present in the analyzed protein, the spectral density is calculated by the five models shown above; for each residue is then chosen the model that gives the best fit between calculated and experimental values. The way a model is chosen over another is by evaluating the error using F-test and P values; if increasing the number of parameters used, that is using a more complex model, the error does not diminish significantly, it is not worth using such a model; for this reason the most used model is normally model number 1.

## Chapter 2

### Materials and Methods

#### 2.1 DNA Methods

##### 2.1.1 PCR

The Polymerase Chain Reaction (PCR) was used to clone the DNA fragments coding for different domains of cMyBPC in vectors of the pET family. The majority of the cloning has been carried out in collaboration with Dr Elena Rostkova (King's College, London); the fragments coding for the domains of cMyBPC have been cloned in a modified version of vector pET-8C.

For certain domains it was necessary to repeat the procedure to clone the DNA coding fragments in different vectors, essentially to increase the protein solubility by producing a fusion protein with either Thioredoxin (pETM-20) (LaVallie et al., 1993) or NusA (pETM-60) (De Marco et al., 2004).

To do this, primers have been designed to be compatible with the chosen vector and to contain appropriate restriction sites in order to be able to digest the amplified DNA fragments with NcoI and BamHI restriction enzymes and, subsequently, to ligate the fragments in the desired vector.

For the PCR the *PfX* DNA Polymerase (from Invitrogen) was used with the reaction conditions are reported in table 2.1.

	Volume	Final concentration
10X Amplification Buffer	5 $\mu$ l	1X
PCRx Enhancer Solution	5 $\mu$ l	1X
10mM dNTP mix	1.5 $\mu$ l	0.3 mM each
50 mM MgSO <sub>4</sub>	1 $\mu$ l	1 mM
Primers mix (10 $\mu$ M each)	2 $\mu$ l	0.3 $\mu$ M each
Template DNA	2 $\mu$ l	100ng
<i>Pfx</i> DNA Polymerase	1 $\mu$ l	2.5 units
H <sub>2</sub> O	32.5 $\mu$ l	

**Table 2.1: PCR conditions**

The general cycle used for the PCR are reported in table 2.2

Temperature	Time	Cycles
94°C	2 min	1
94°C	15 sec	30
50-60 °C	30 sec	
68°C	30 sec	
72°C	12 minutes	1
4°C	Until the end	1

**Table.2.2: PCR cycles**

For best results, the PCR products were purified using QIAGEN QIAquick PCR purification kit before proceeding with the restriction digestion with BamH1 and NcoI (both from Roche).

The restriction reaction was carried out using the following quantities:

Plasmid	1 ng
10x Buffer B	5 $\mu$ l
BamH1	1 $\mu$ l (10 units)
Nco1	1 $\mu$ l (10 units)
dH <sub>2</sub> O	3 $\mu$ l

**Table 2.3: restriction digestion reaction**

The reaction has been incubated for 2 h 30 min at 37°C. Buffer B was chosen as it gave the maximum activity (100%) to BamH1 and high activity (50-75%) to Nco1, while buffer H would have given a maximum activity (100%) to Nco1 but a low activity (25-50%) to BamH1, so the choice was the best compromise to be able to carry out a double digestion using the two enzymes together.

The products were then purified by gel extraction using the QUIAGEN QIAquick gel extraction kit.

### 2.1.2 Ligation

The restriction endonuclease digested fragments were gel purified from a 1% agarose gel using QIAgen Gel Extraction Kit. The resultant vector and fragment were ligated using T4 DNA ligase (from Roche):

	Control ( $\mu$ l)	Ratio 1:1 ( $\mu$ l)	Ratio 1:3 ( $\mu$ l)
Plasmid	2	2	2
DNA fragment	-	2	6
1x DNA dilution buffer	1	6	2
T4 DNA ligation buffer	10	10	10
Ligase 1 U/ $\mu$ l	1	1	1

**Table 2.4: Ligation reaction conditions**

The reaction has been incubated at room temperature for 30 minutes and the product transformed into competent DH5 $\alpha$  cells.

### 2.1.3 Competent cells transformation

The competent cells were thawed for 1 hour on ice before inoculating with 2  $\mu$ l of the vector containing the desired cDNA fragment.

After leaving the cells on ice for 30 minutes, they were heated at 42°C for 30-45 seconds, and then 250  $\mu$ l of SOC medium (from Invitrogen) were added. After incubation at 37°C for 60 minutes, a 50  $\mu$ l aliquot of transformed cells was plated out on LB- Agar plates containing appropriate antibiotic, while the remaining 200  $\mu$ l of

cells were spun down at 13000 rpm for 1 minute, the pellet resuspend in 50  $\mu$ l of autoclaved water and plated out on LB- Agar plates containing appropriate antibiotic.

#### 2.1.4 PCR screening

After incubating overnight, a PCR screen was performed on the colonies grown on the plate. Each colony was resuspended in 50  $\mu$ l of H<sub>2</sub>O and then a PCR reaction was performed.

DNA template	10 $\mu$ l
Primers mix	1 $\mu$ l
dH <sub>2</sub> O	1.5 $\mu$ l
Red taq (from Sigma)	12.5 $\mu$ l

**Table 2.5: PCR screening reaction**

The PCR reaction was performed as follows:

Temperature	Time	Cycles
94°C	5 min	1
94°C	30 sec	30
60 °C	30 sec	
72°C	30 sec	
72°C	8 minutes	1
4°C	Until the end	1

**Table 2.6: PCR screening cycles**

Of the colonies that resulted positive at the PCR screening was performed either a mini prep (High Pure Plasmid Isolation Kit from Roche) form a 50  $\mu$ l culture or a midi prep (S.N.A.P. midi from Invitrogen) for a 50 ml culture, to produce enough DNA to be checked by DNA sequencing and to be used in the following procedures. All DNA samples were sequenced by the Protein Nucleic Acid Chemistry Laboratory (PNAACL) at the University of Leicester.

## 2.2. *Protein Expression and Purification*

### 2.2.1. *Competent cells Transformation for protein expression*

The competent cells were thawed for 1 hour on ice before inoculating with 2  $\mu$ l of the vector containing the desired cDNA fragment.

After leaving the cells on ice for 30 minutes, they were heated at 42°C for 30-45 seconds, and then 250  $\mu$ l of SOC medium (from Invitrogen) were added. After incubation at 37°C for 60 minutes, the transformed cells were plated out in 20 and 50  $\mu$ l aliquots of culture, on LB- Agar plates containing appropriate antibiotic.

### **2.2.2 Expression in Luria- Bertani (LB) medium**

The transformed *E. Coli* cells were grown in 5 ml LB cultures containing appropriate antibiotic during the day (8 hours) and then grown in 200 ml LB cultures overnight. In the morning, 4L of LB medium with antibiotic, were inoculated with 20 ml culture each. All the cultures were grown at 37°C while shaking (200 rpm), if not specified otherwise. Protein expression has been induced in the late- log phase,  $A_{600nm}$  between 0.7 and 1, with 0.75 mM IPTG (Isopropyl  $\beta$ -D-1.thiogalactopyranoside) (form Sigma). Four hours after induction, the cultures have been harvested spinning down for 15 minutes at 6000 rpm (9782 g) in Sorvall rotor SLC-6000 at 4°C. the pellets were kept at -20°C until needed for purification.

### **2.2.3 Expression in Minimal medium M9**

Minimal medium has been used to obtain  $^{15}\text{N}$  or  $^{15}\text{N}/^{13}\text{C}$  labelled protein. The same procedure for protein expression in LB was repeated as described in the section above, until reaching an OD of 0.8, then the culture has been spun down at 5000 rpm (9782 x g) for 8 minutes in a Sorvall rotor SLC-6000. After centrifugation the pellet has been re-suspended in 1X M9 salts and then spun down again for 8 minutes at 5000 rpm. The pellet has been re-suspended in 50 ml minimal medium (M9), containing  $^{15}\text{NH}_4\text{Cl}$  to  $^{15}\text{N}$  labelled protein or  $^{15}\text{NH}_4\text{Cl}$  and  $^{13}\text{C}$  glucose to doubly label the protein, and then transferred in the M9 medium and left in the shaker at  $37^\circ\text{C}$  for 1 hour before inducing protein expression with 1 ml IPTG 0.75M (Isopropyl  $\beta$ -D-1-thiogalactopyranoside) (form Melford). After 4 hours induction the cells have been harvested spinning down for 15 minutes at 6000 rpm and kept at  $-20^\circ\text{C}$  until needed for the purification.

### **2.2.4 Protein Purification**

The pellet obtained from 4L of LB culture has been re-suspended in 10 ml FF6 wash buffer, sonicated for 2 minutes (20 sec on, 20 sec off, 10 amplitude) and spun down again for 90 minutes at 18000 rpm (59768 x g).

Running a SDS PAGE ( Sodium DodecylSulphate PolyAcrylamide Gel Electrophoresis) it was possible to determine if the protein expressed in the conditions reported above is soluble, being present in the supernatant.

In case of soluble protein, the supernatant has been kept and purified by Immobilized Metal ion Affinity Chromatography (IMAC) using Ni Sepharose 6 Fast Flow columns

(form Amersham), due to the presence of the hexa- histidine tag. The resin contained in each column consists of 90  $\mu\text{m}$  beads of agarose with a coupled chelating group, which has been charged with  $\text{Ni}^{2+}$  ions. The columns were packed using 4 ml of re-suspended resin, corresponding to 2 ml of resin in each column. The protein, once loaded on the columns, was washed with 40 ml of FF6 buffer and finally eluted with 8 ml of FF6 elution buffer, containing 500 mM Imidazole (form buffer composition see appendix A.1 p. 198).

Further purification was achieved using Size Exclusion Chromatography on a Superdex 75 HiLoad 16/60 pre-packed column, or by Immobilized Metal ion Affinity Chromatography (IMAC) following digestion with Tev protease.

Size Exclusion Chromatography is based on the fact that the stationary phase is formed by a surface, that can be made of silica or a polymer, that presents pores of different size. The sample that has to be purified is injected in the column and the different components will travel through the column at different rates, according to their size: bigger molecules, that cannot permeate the resin entering the small diameter pores, will travel through the column faster than the small components that are able to enter the pores and then following a longer route through the column before being eluted. Molecules with dimensions bigger than the average pore size will not be retained and will be excluded; on the other hand, molecules that are sensibly smaller than the pores can be retained for a long time and they will be the last to be eluted. Between the two extremes there are the molecules with an intermediate size that travel through the column according to their molecular weight. Another factor that can influence the retention time of a molecule is its shape, as molecules with a bigger steric hindrance will travel faster through the column at equal molecular weight. An important aspect of this technique is the absence of physical- chemical interaction between the sample

components and the stationary phase, as happens in all other liquid chromatography techniques. Two types of size exclusion chromatography exist, one, called gel-filtration, uses hydrophilic substrates in the columns, the other, known as gel permeation, based on hydrophobic substrates. In this work only gel filtration was used as all the samples were present in aqueous solution.

All the plasmid used in this research, except pET-8C, have a TEV protease recognition site that allow to cut away the hexa- histidine tag at the N-terminus of the expressed protein. In some cases the chromatography step showed difficult and it was preferred to repeat the IMAC purification after digestion with TEV protease. In this second step of Metal Ion Affinity Chromatography the protein of interest will not be retained by the column and will flow through, while the hexa- histidine tag will be chelated by the resin and will not pass through the column. At the end of this step the protein is obtained in its pure form.

To run the NMR experiments, all the proteins were dialysed against NMR buffer using either dialysis membranes (Spectra/ Pro Dialysis membranes MWCO: 3500) or cassettes (PIERCE Slide-A-Lyzer Dialysis Cassettes MWCO: 3500, 3-12 ml) . Usually three steps of dialysis were performed using 1L of NMR buffer each (see appendix A.1 for buffer composition). Finally, the proteins were concentrated by centrifugation (concentrators: Viva Spin MWCO:3000, 20 ml or Amicon Centriprep MWCO: 3000, 15 ml). the protein concentration was checked measuring the absorbance of the protein solution at 280 nm and then calculating the concentration according to the Beer-Lambert law.

### 2.2.5 Refolding of insoluble proteins

Some of the proteins studied in the course of this research were expressed as insoluble aggregated folding intermediates known as inclusion bodies. In order to recover an active protein, the insoluble proteins had to be solubilised with denaturants such as 8M urea to dissolve the inclusion bodies, that afterward needed to be removed to allow the protein to fold in its native state.

Two protocols have been used:

#### Long refolding protocol

Step1: TBS pH7.5, Urea 2M, 0.01% Brij58	48h
Step2: TBS pH7.5, Urea 1M, 0.01% Brij58	48h
Step3: TBS pH7.5, Urea 0M, 0.01% Brij58	24h
Step4: TBS pH7.5, Urea 0M, 0.01% Brij58	24h
Step5: TBS pH7.5, Urea 0M, 0% Brij58	24h
Step6: TBS pH7.5, Urea 0M, 0% Brij58	24h

#### Short refolding protocol

Step1: TBS pH7.5, Urea 2M, 0.01% Brij58	48h
Step2: TBS pH7.5, Urea 0M, 0.01% Brij58	24h
Step3: TBS pH7.5, Urea 0M, 0.01% Brij58	24h

Every one of these steps was performed using 1L of each buffer and in a cold room at 4°C, using dialysis membranes (Spectra/ Pro Dialysis membranes MWCO: 3500).

The problem arising from this procedure is the fact that many conditions, such as buffer composition, protein concentration, temperature, just to mention the most common, have to be optimized for each specific protein. And even for optimized refolding processes, the yield of re-natured protein may be limited.

### 2.3 *Actin binding assay by cosedimentation*

All proteins studied in the course of this research being muscle proteins, it was necessary to perform on some of them an actin binding assay to determine whether or not they interacted with the second main constituent of muscle fibres. The purified actin for the assay was donated by Dr El-Mezgueldi's group.

To perform the assay, 50 µl aliquots of the two proteins at a concentration of 50 µM were used. The assay consists in mixing the two proteins together at room temperature incubating for 10 minutes and then spinning down the samples at 8500 rpm (436159 x g) for 30 minutes at 4°C in a Beckman Optima TLX centrifuge. The supernatant was then freeze dried and re-suspended in SDS-PAGE buffer, while the pellet was washed with actin binding assay buffer and then re-suspended in SDS-PAGE buffer. Different samples were used, some containing the mixture of actin and protein of interests, and some controls. The result of the assay consists in establishing, through SDS-PAGE analysis, whether the protein precipitates together with actin as a consequence of the ultracentrifugation or stays in the supernatant. An essential condition for this assay to work is that the protein should not precipitate in the pellet during ultracentrifugation in absence of actin.

	1	2	3	4	5
Actin	-	-	159 $\mu$ l	159 $\mu$ l	159 $\mu$ l
cC0	333 $\mu$ l	-	-	333 $\mu$ l	-
MS1	-	134 $\mu$ l	-	-	134 $\mu$ l
Buffer	667 $\mu$ l	866 $\mu$ l	841 $\mu$ l	508 $\mu$ l	707 $\mu$ l

**Table 2.7 Sample composition of the solutions used in the Actin Binding cosedimentation assay**

## *2.2 NMR spectroscopy*

All NMR spectra were obtained running the corresponding experiments on 600 MHz, with or without cryoprobe, or 800 MHz with cryoprobe Bruker spectrometers. All experiments were carried out at 30°C for domain cC0 and 25°C for domain cC8. The pulse sequences used were the ones implemented by NMR centre manager.

## Chapter 3

# **Solution structure of domain C0 of cardiac Myosin Binding Protein C (cMyBPC) and characterisation of its interaction with the Regulatory Light Chain (RLC) of Myosin**

### *3.1 Results*

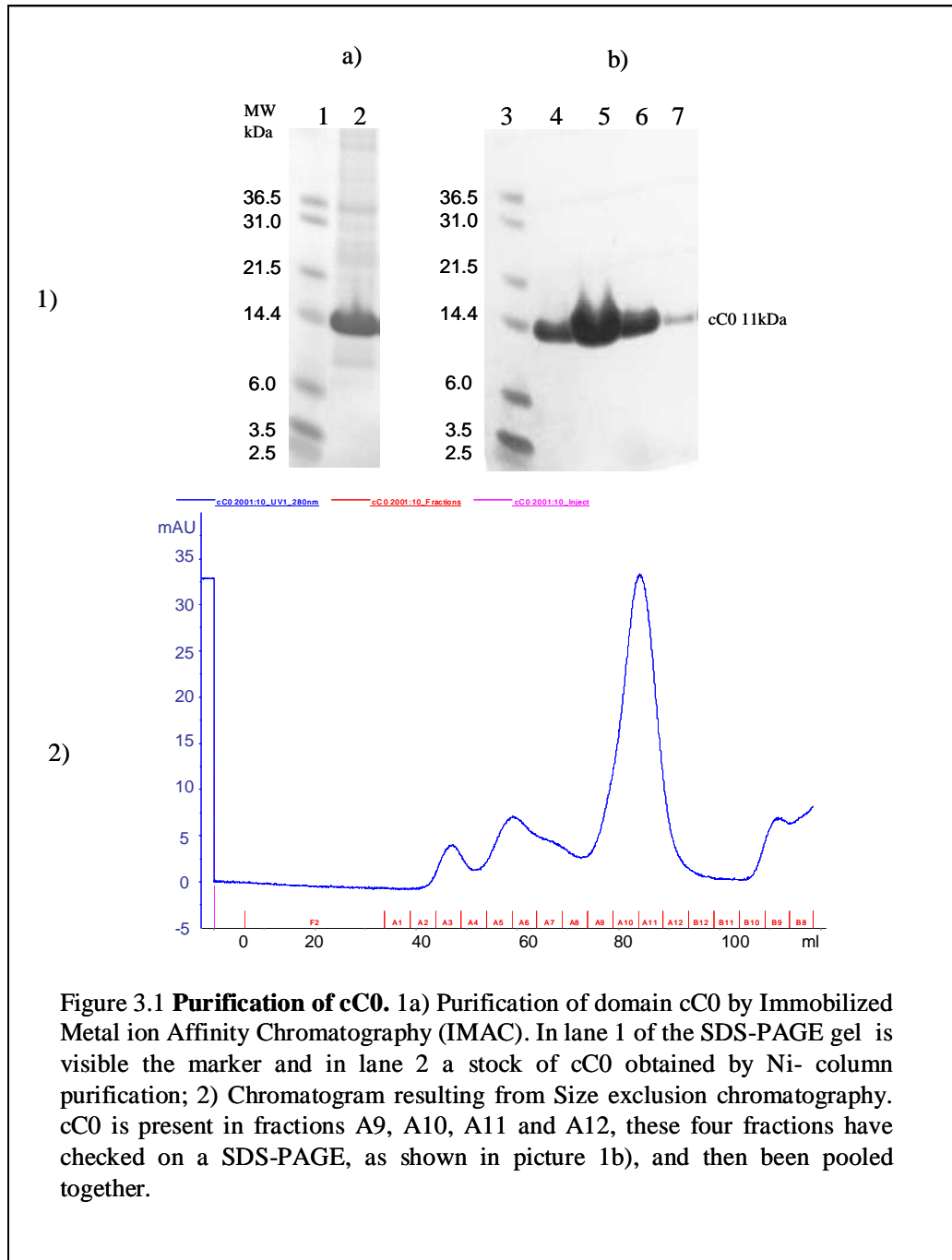
In order to understand the function of domain cC0, the only unique domain of the cardiac isoform of MyBPC, its structure was determined and a study of the interaction between cC0 and its probable binding partner, the Regulatory Light chain of Myosin, was performed. The results obtained are reported in this chapter.

### **3.1.1 Protein Expression and Purification**

#### **3.1.1.1 cC0**

DNA sequences coding for human cardiac cC0 and RLC have been cloned in vectors pET-8C and pLEICS-1 respectively. Both vectors were inoculated in *E. Coli* host cells: in BL21(DE3) STAR (from Invitrogen) were used for both proteins, while RLC was also expressed in Arctic Express (from Stratagene) with comparable results. The regulatory light chain was expressed in LB to produce unlabelled samples, while cC0 was expressed in M9 medium, enriched with either  $^{15}\text{N}$  to produce singly labelled samples or  $^{15}\text{N}$  and  $^{13}\text{C}$  to produce the doubly labelled samples, necessary for triple resonance experiments, and in LB to produce the unlabelled sample used for the assignment of the aromatic side chains. Due to the presence of a hexa- histidine tag at

the N-terminus, both proteins were purified by Immobilized Metal ion affinity chromatography (IMAC) and then either by gel filtration (cC0) or by cleavage using TEV protease and repeating the metal affinity chromatography step (RLC).



cC0 was expressed in both LB and M9 media giving good yields, 23 mg/l and 19 mg/l respectively.

### 3.1.1.2 Regulatory Light Chain

The original construct intended for the study of the interaction with domain cC0 was that of a complex formed by the Regulatory Light Chain (RLC) and its binding site on myosin (MyBS) that is located between residues 808 and 842. Expression and purification of this complex proved very difficult and so, after various failed attempt to produce enough protein to perform a titration, it was decided to use the RLC alone, despite the fact that its stability in absence of the MyBS seems to be limited. In fact the  $\alpha$ - helical content of the protein when not bound to myosin is as low as 18% as shown by the result obtained by CD spectroscopy (Szczesna et al., 2001).

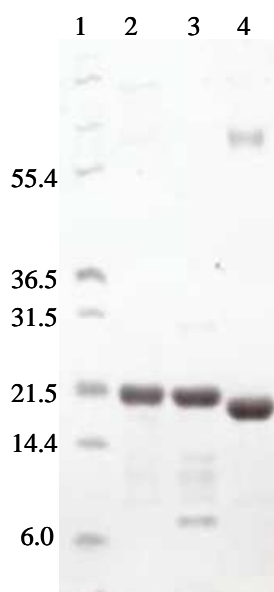


Figure 3.2 **Ht<sub>1</sub>RLC after TEV digestion and purification with IMAC on Ni<sup>2+</sup> columns.** In lane 1 is shown the marker. In lanes 2 and 3 the Ht<sub>1</sub>RLC before digestion and in lane 4 the Ht<sub>1</sub>RLC after digestion with TEV protease and IMAC purification. This sample was used to perform the studies on the interaction between this protein and domain cC0.

The expression of the Regulatory Light Chain (RLC) in pET-8C in BL21Star (DE3) competent cells was not satisfactory, so the gene coding for this protein was re-cloned in vector pLEICS1 and expressed in both BL21Star (DE3) (from Invitrogen) and Arctic Express RIL (from Stratagene) giving good results. The RLC was purified by Immobilized Metal Affinity Chromatography after digestion with standard uncalibrated stock of TEV protease obtained from the PROTEX laboratory at the University of Leicester, as described in the Material and Methods section. The protein was expressed giving a yield of 7mg/l.

### 3.1.2 NMR spectroscopy

Different samples were made to perform the NMR experiments:

- $[^{13}\text{C}/^{15}\text{N cC0}] = 1.4 \text{ mM}$
- $[^{15}\text{N cC0}] = 670 \mu\text{M}$
- $[\text{cC0}_{\text{Ar}}] = 1.7 \text{ mM}$

The first, doubly labelled sample was used to record the triple resonance experiments, HNCaCb, HN(CO)CaCb, HN(Ca)CO, HNCO, HN(CaCb)HaHb, HN(CaCbCO)HaHb and the  $^{13}\text{C}$  specific experiments such as  $^1\text{H}/^{13}\text{C}$  HSQC,  $^1\text{H}/^{13}\text{C}$  HCCH TOCSY and  $^1\text{H}/^{13}\text{C}$  NOESY-HSQC; while from the  $^{15}\text{N}$  enriched sample were obtained  $^1\text{H}/^{15}\text{N}$  HSQC,  $^1\text{H}/^{15}\text{N}$  TOCSY-HSQC and  $^1\text{H}/^{15}\text{N}$  NOESY-HSQC. An unlabelled sample was used to record the spectra relative to the aromatic side chains  $^1\text{H}/^1\text{H}$  TOCSY,  $^1\text{H}/^1\text{H}$  NOESY. The NMR samples were concentrated down and transferred to a clean NMR tube. The  $^{13}\text{C}/^{15}\text{N}$  cC0 and cC0<sub>Ar</sub> samples were frozen and lyophilized overnight to eliminate the water and then re-suspended in high purity D<sub>2</sub>O (from Sigma). All the  $^{15}\text{N}$  spectra, recorded using the  $^{15}\text{N}$  cC0 sample, were, on the other hand, recorded in H<sub>2</sub>O with addition of 5% of D<sub>2</sub>O to allow locking the machine and water suppression.



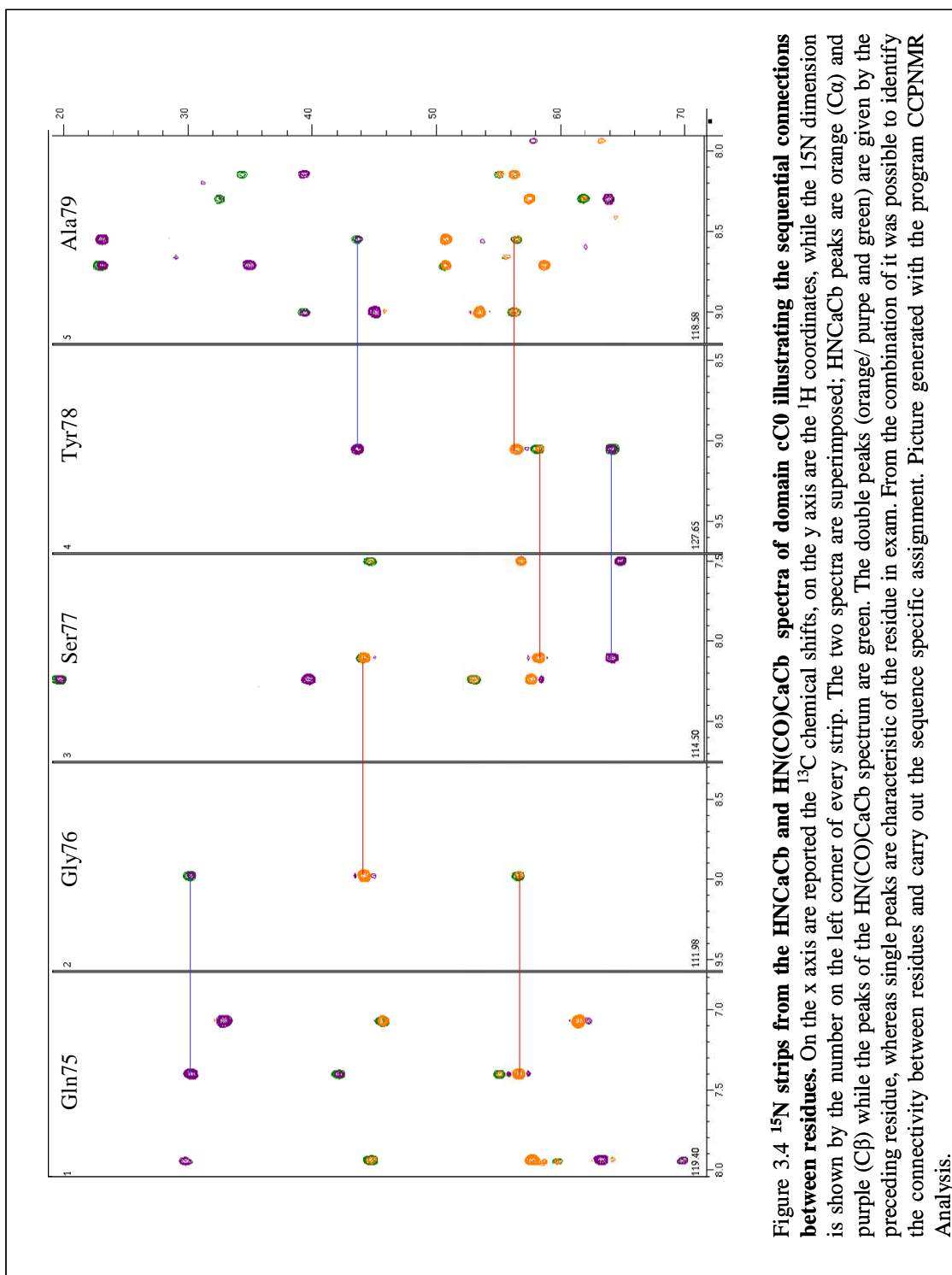


**Figure 3.4  $^{15}\text{N}$  strips from the HNCaCb and HN(CO)CaCb spectra of domain cC0 illustrating the sequential connections between residues.** On the x axis are reported the  $^1\text{H}$  chemical shifts, on the y axis are the  $^{15}\text{N}$  coordinates, while the  $^{13}\text{C}$  coordinates are reported on the left corner of every strip. The two spectra are superimposed; HNCaCb peaks are orange (C $\alpha$ ) and purple (C $\beta$ ) while the peaks of the HN(CO)CaCb spectrum are green. The double peaks (orange/ purple and green) are given by the preceding residue, whereas single peaks are characteristic of the residue in exam. From the combination of it was possible to identify the connectivity between residues and carry out the sequence specific assignment. Picture generated with the program CCPNMR Analysis.

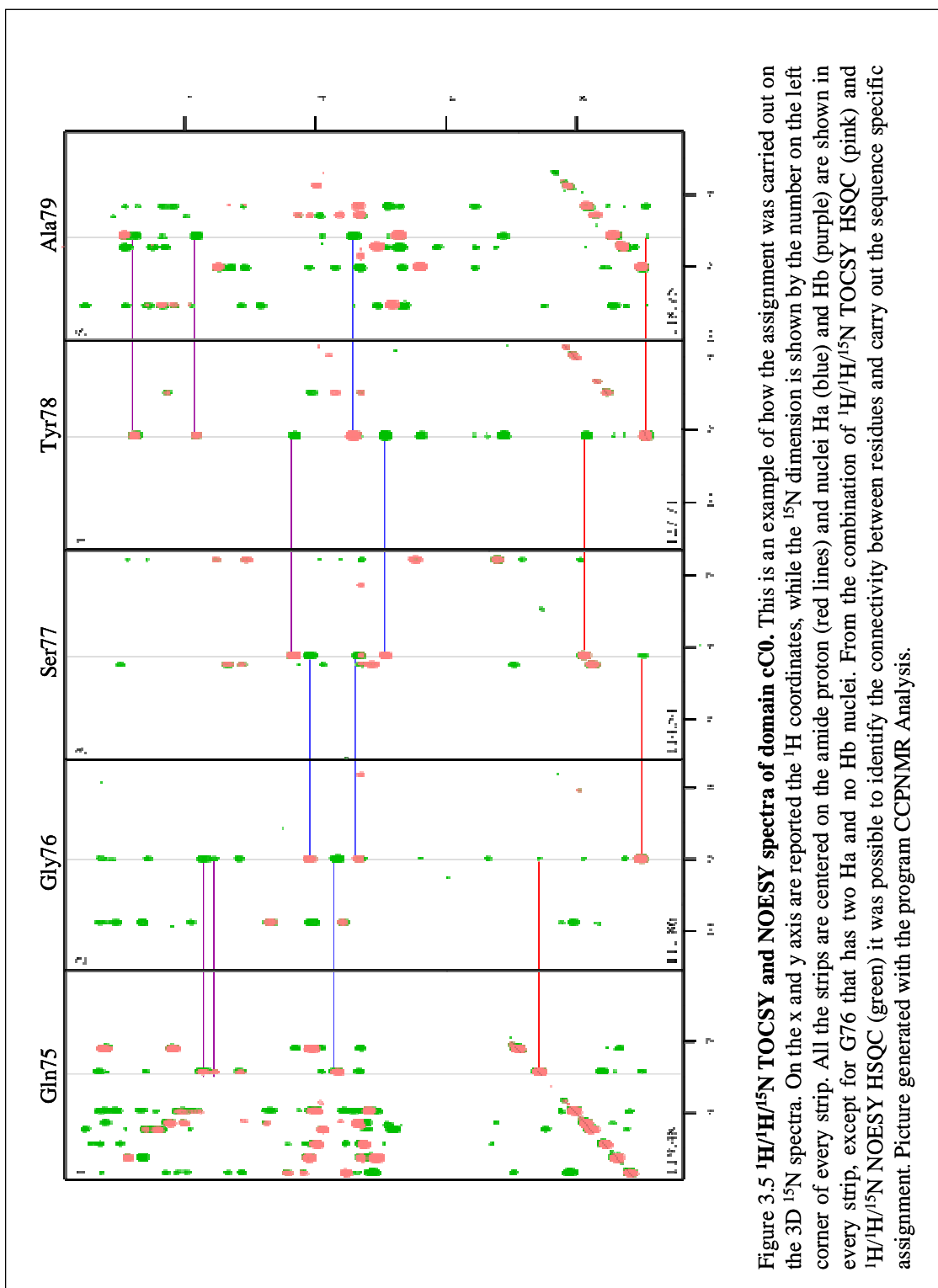


Figure 3.5  $^1\text{H}/^{15}\text{N}$  TOCSY and NOESY spectra of domain cC0. This is an example of how the assignment was carried out on the 3D  $^{15}\text{N}$  spectra. On the x and y axis are reported the  $^1\text{H}$  coordinates, while the  $^{15}\text{N}$  dimension is shown by the number on the left corner of every strip. All the strips are centered on the amide proton (red lines) and nuclei Ha (blue) and Hb (purple) are shown in every strip, except for G76 that has two Ha and no Hb nuclei. From the combination of  $^1\text{H}/^{15}\text{N}$  TOCSY HSQC (pink) and  $^1\text{H}/^{15}\text{N}$  NOESY HSQC (green) it was possible to identify the connectivity between residues and carry out the sequence specific assignment. Picture generated with the program CCPNMR Analysis.

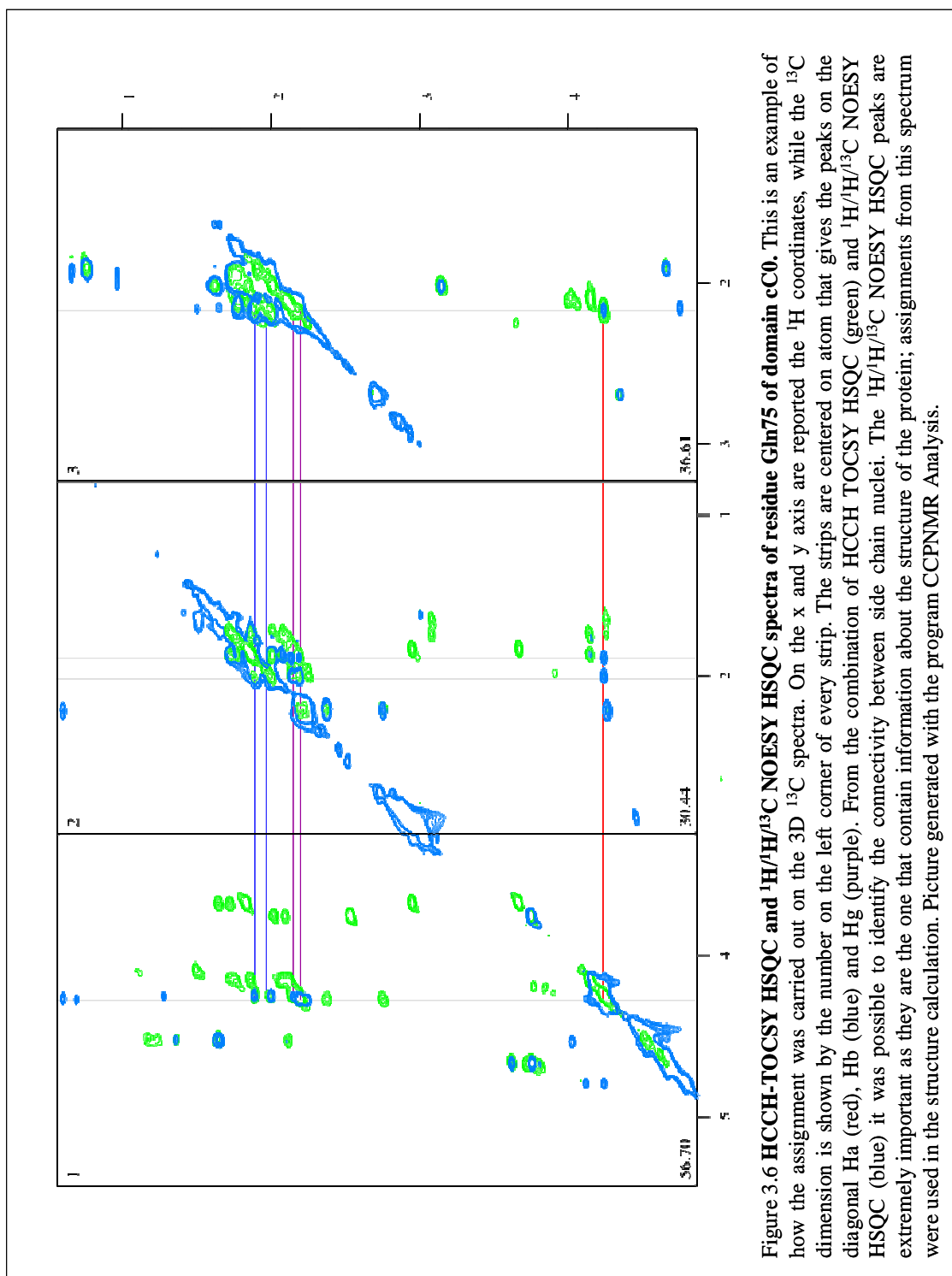


Figure 3.6 HCCH-TOCSY HSQC and  $^1\text{H}/^1\text{H}/^{13}\text{C}$  NOESY HSQC spectra of residue Gln75 of domain cC0. This is an example of how the assignment was carried out on the 3D  $^{13}\text{C}$  spectra. On the x and y axis are reported the  $^1\text{H}$  coordinates, while the  $^{13}\text{C}$  dimension is shown by the number on the left corner of every strip. The strips are centered on atom that gives the peaks on the diagonal Ha (red), Hb (blue) and Hc (purple). From the combination of HCCH TOCSY HSQC (green) and  $^1\text{H}/^1\text{H}/^{13}\text{C}$  NOESY HSQC (blue) it was possible to identify the connectivity between side chain nuclei. The  $^1\text{H}/^1\text{H}/^{13}\text{C}$  NOESY HSQC peaks are extremely important as they are the one that contain information about the structure of the protein; assignments from this spectrum were used in the structure calculation. Picture generated with the program CCPNMR Analysis.

### 3.1.3 Sequence specific Assignments for domain cC0

Very comprehensive sequence specific assignments were carried out for domain cC0, with all non-proline backbone amides identified in the  $^1\text{H}/^{15}\text{N}$  HSQC spectrum except for residues Glu2, Gly44, Gly45, Asn52 and Ser85 (95%). Backbone nuclei  $\text{C}_\alpha$  and  $\text{C}_\beta$  were assigned in the triple resonance experiments with a very high percentage of completion, being missing the assignments for only the first two residues at the N-terminus of the domain; the aliphatic side chains were assigned in the  $^1\text{H}/^{13}\text{C}$  HCCH TOCSY experiment.

Aromatics  $^1\text{H}$  signals were assigned in the two dimensional  $^1\text{H}/^1\text{H}$  TOCSY experiment, while the  $^{13}\text{C}$  signals were identified in the TROSY experiment.

### 3.1.4 Structure Calculation of domain cC0

The automatic assignment of the peaks picked manually in the three-dimensional  $^1\text{H}/^{13}\text{C}$  NOESY-HSQC experiment was carried out using the CANDID protocol, as part of the software CYANA 2.1. Out of the total 2460 peaks, 88% were assigned (2170) while just 292 (12%) were left unassigned at the end of the procedure; all these unassigned peaks were the product of artefacts in the NMR experiments and were all checked manually at the end of the automatic assignment procedure. The uniquely assigned NOE peaks produced 1154 upper distance limits that were used as constraints on which to base the structure determination.

The final family of structures for domain cC0 was obtained using 1360 structural constraints derived from experimental NMR data, including 441 sequential ( $i, i+1$ ), 85 medium range ( $i, i\leq 4$ ) and 628 long range ( $i, i\geq 5$ ) upper distance limits, 180 backbone

torsion angles constraints ( $90\ \phi$  and  $90\ \psi$ ) and 26 hydrogen bond constraints found in region with defined secondary structure.

Following the final round of CYANA calculation, 81 converged structures were obtained from 100 random starting structures. The converged structures contain no distance or van der Waals violation greater than  $0.5\text{\AA}$  and no dihedral angle violations greater than  $5^\circ$ , with an average value of the CYANA target function of  $1.08\pm 0.0637\text{\AA}^2$ . The rmsds of the violations for upper distance limit, lower distance limit and torsion angles are  $0.0109\pm 0.0006\text{\AA}$ ,  $0.0007\pm 0.0009\text{\AA}$  and  $0.3582\pm 0.0579^\circ$  respectively, while the sum of the van der Waals violations is  $4.1\pm 0.3\text{\AA}$ . Similarly, the maximum violations for the converged structures were  $0.28\pm 0.02\text{\AA}$ ,  $0.01\pm 0.01\text{\AA}$ ,  $2.8\pm 0.63^\circ$  and  $0.27\pm 0.01\text{\AA}$ .

Number of constraints used in the final structure calculation		
Total number NOEs	1154	
Sequential NOEs ( $i, i+1$ )	441	
Medium- range NOEs ( $i, i\leq 4$ )	85	
Long range NOEs ( $i, i\geq 5$ )	628	
Torsion angles	180	( $90\ \phi$ and $90\ \psi$ )
Hydrogen bonds	26	
Maximum and total constraints violations in the converged structures (RMSD)		
Upper distance limits ( $\text{\AA}$ )	$0.28\pm 0.02$	$0.0109\pm 0.0006$
Lower distance limits ( $\text{\AA}$ )	$0.01\pm 0.01$	$0.0007\pm 0.0009$
Van der Waals contacts ( $\text{\AA}$ )	$0.27\pm 0.01$	$4.1\pm 0.3$
Torsion angle ranges ( $^\circ$ )	$2.8\pm 0.63$	$0.3582\pm 0.0579$
Average CYANA target function ( $\text{\AA}^2$ )	$1.08\pm 0.0637$	
Structural statistics for the family of converged structures for domain cC0		
Residues within the allowed region of the Ramachandran plot (%)		98.7
Average Backbone atom r.m.s.d.		$0.40\pm 0.07$
Average Heavy atoms r.m.s.d.		$0.92\pm 0.07$

**Table 3.1: NMR constraints and structural statistics for domain cC0.**

The solution structure of domain cC0 of cMyBPC has been deposited in the Protein Data Bank (accession code 2K1M).

The structure is determined to a good quality, which is evident from the superimposition of the protein backbone shown for the family of converged structures in figure 3.8 and is also reflected in low root mean square deviation (r.m.s.d) values to the mean structure for both the backbone and all heavy atoms,  $0.40 \pm 0.07$  Å and  $0.92 \pm 0.07$  Å respectively.

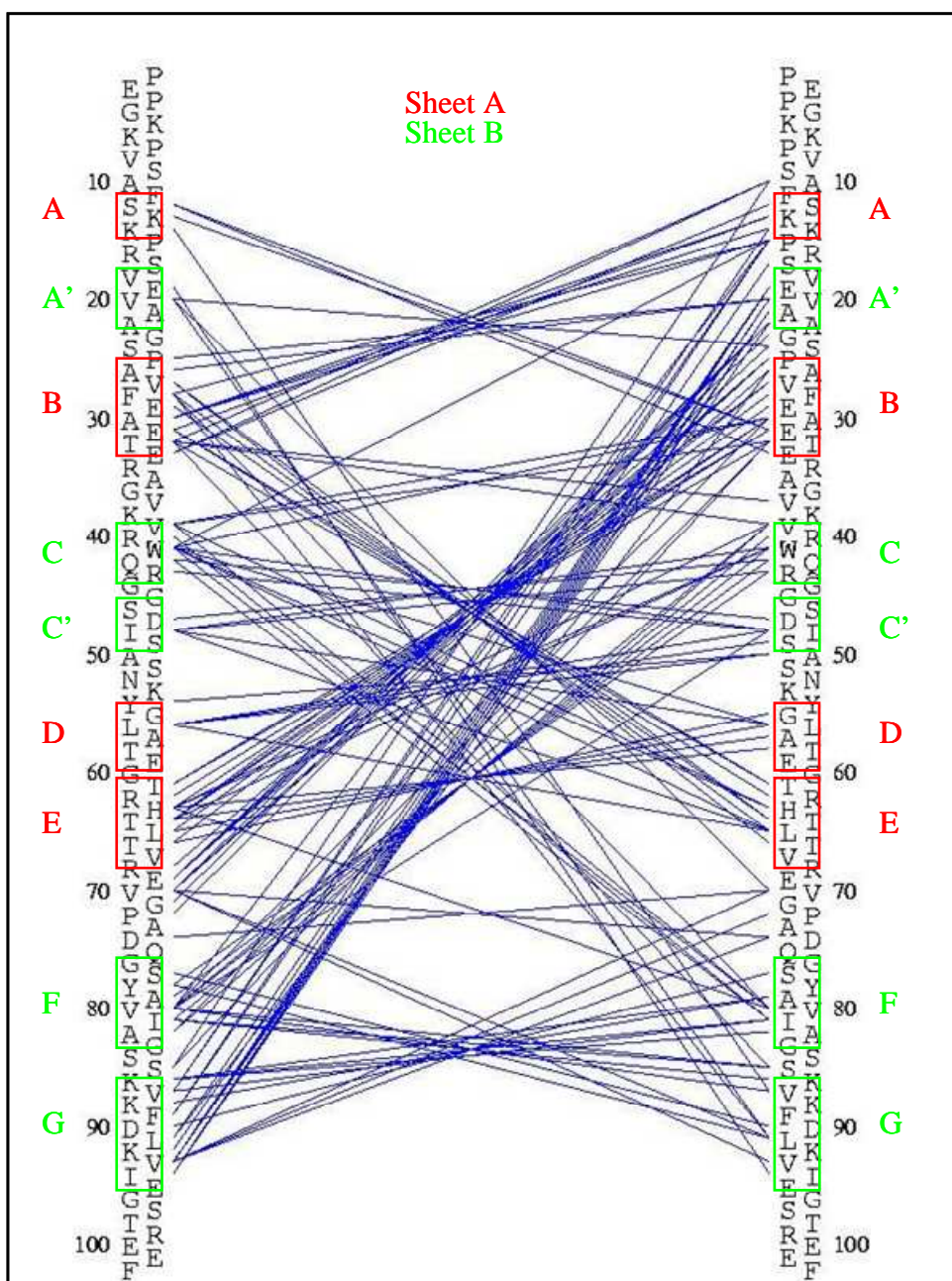


Figure 3.7 **Long range NOEs obtained for domain c0.** Long range NOEs between atoms five or more residues apart recorded for domain c0 of cMyBPC and used to solve its structure. Lines that goes from lines that goes from upper left to lower right represent restraints between side chain atoms, lines that go from upper right to lower left represent backbone atoms. It is evident from the picture that the residues of c0 give NOEs to each other even if they are far from each other in the sequence. In green and red are shown the different  $\beta$ -strands that form the two  $\beta$ -sheets in the domain. It is evident how different  $\beta$ -strands give NOEs to one another. This determine the secondary structure of the protein. Picture generated by the program Cyana 2.1.

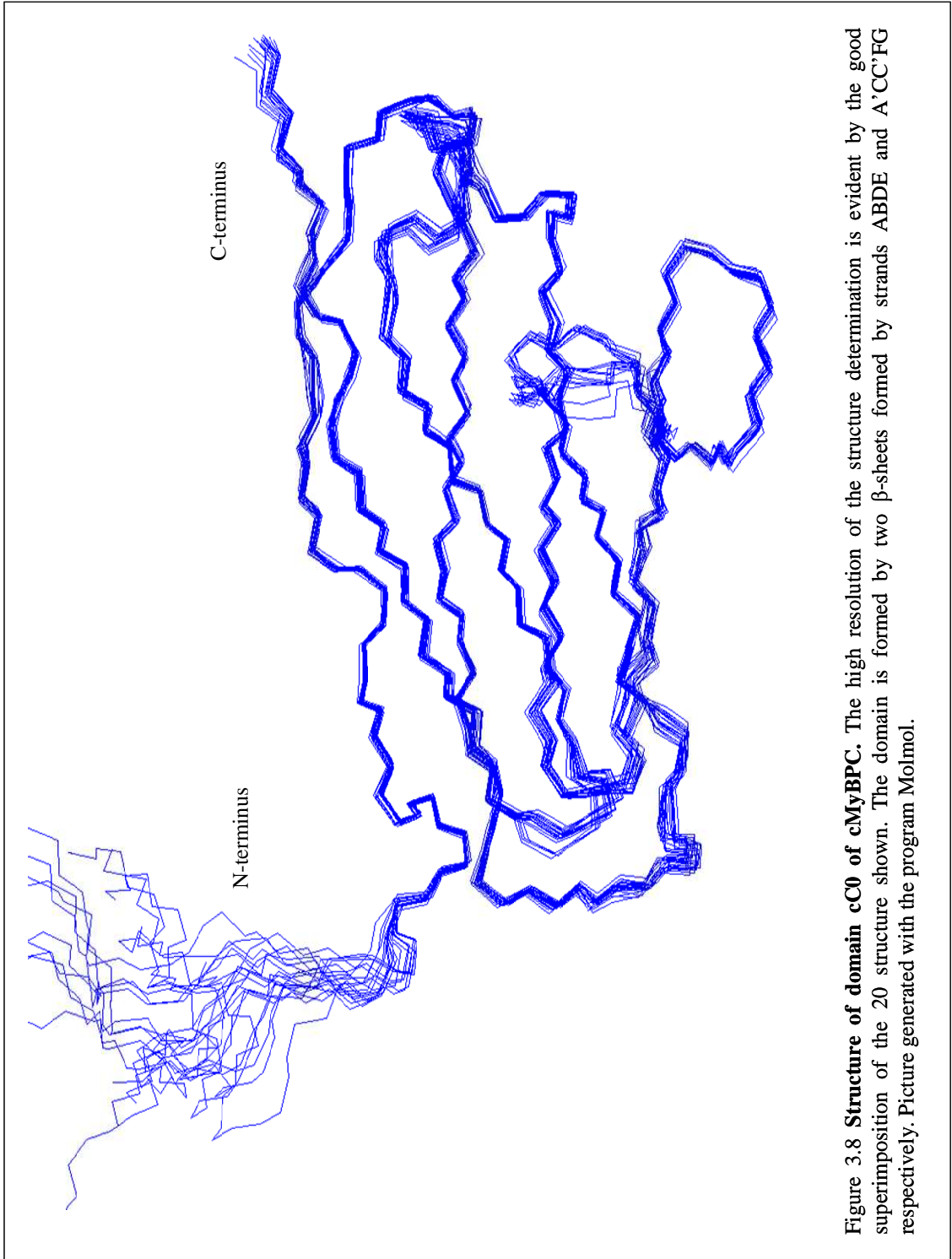


Figure 3.8 **Structure of domain cC0 of cMyBPC.** The high resolution of the structure determination is evident by the good superimposition of the 20 structure shown. The domain is formed by two  $\beta$ -sheets formed by strands ABDE and A'CC'FG respectively. Picture generated with the program Molmol.

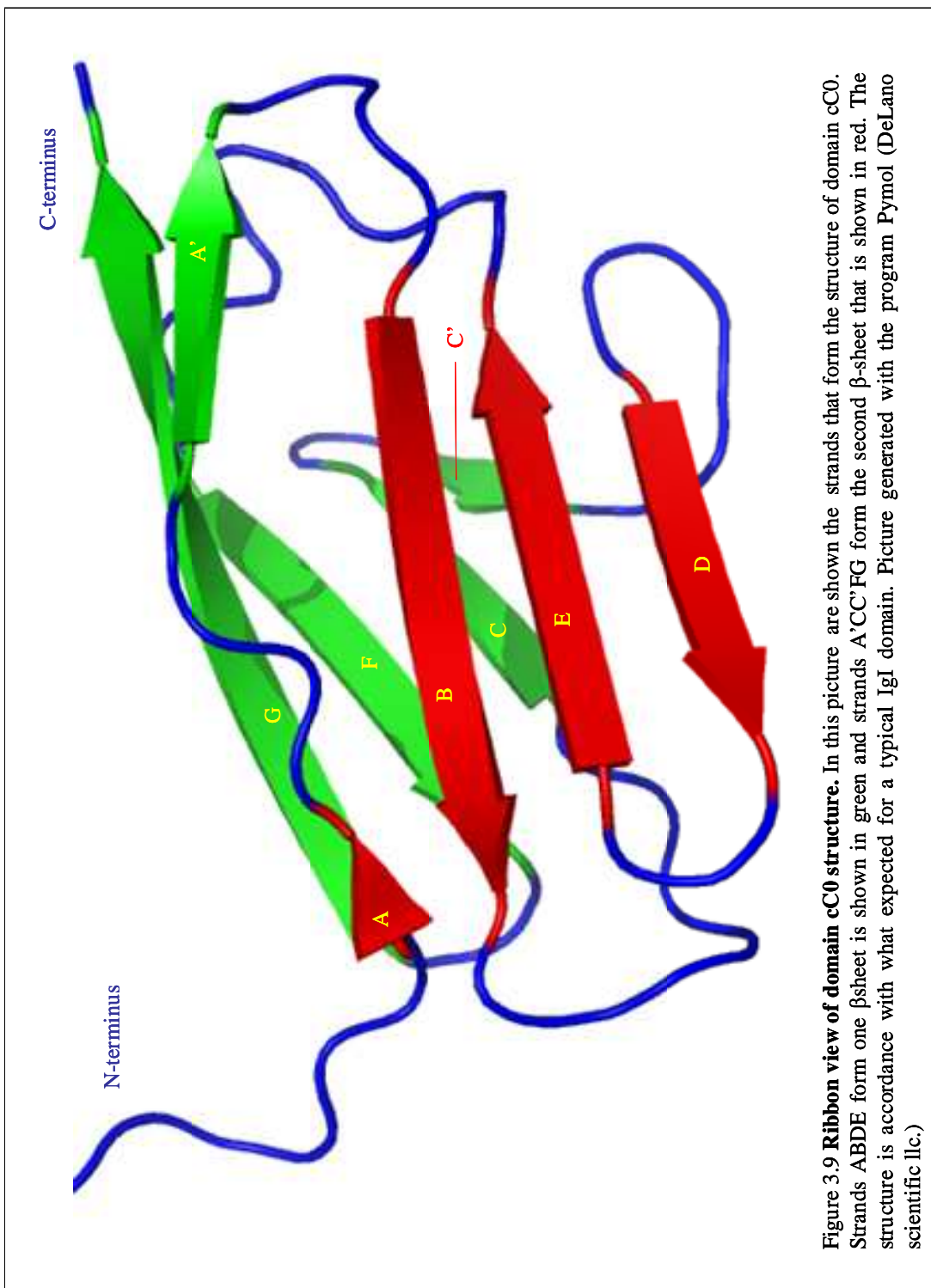
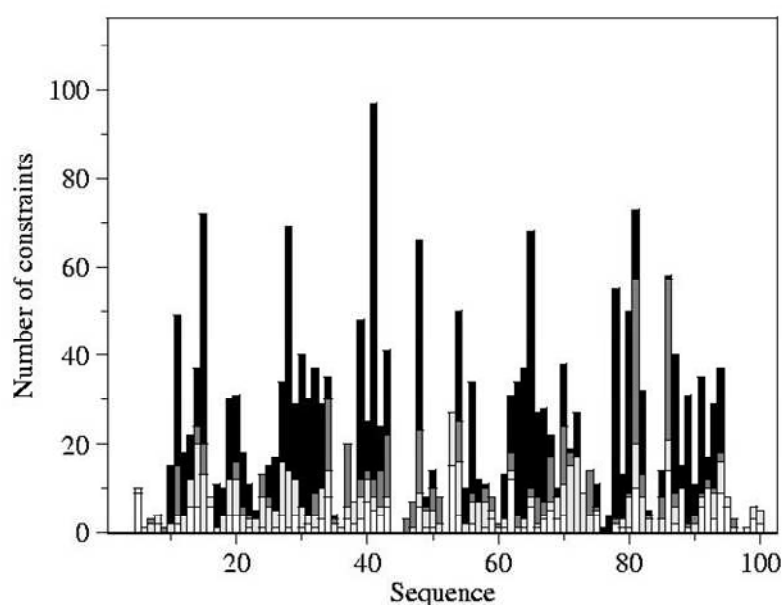


Figure 3.9 **Ribbon view of domain cC0 structure.** In this picture are shown the strands that form the structure of domain cC0. Strands ABDE form one  $\beta$ sheet is shown in green and strands A'CC'FG form the second  $\beta$ -sheet that is shown in red. The structure is accordance with what expected for a typical IgI domain. Picture generated with the program Pymol (DeLano scientific llc.)

The domain is formed by two  $\beta$ -sheets, formed by strands ABDE and A'CC'FG respectively. In picture 3.9 the two sheets are shown in different colours, sheet A in red and sheet B in green, using the same colour coding seen in picture 3.7 where the NOEs between amino acids localised in different strands are shown.

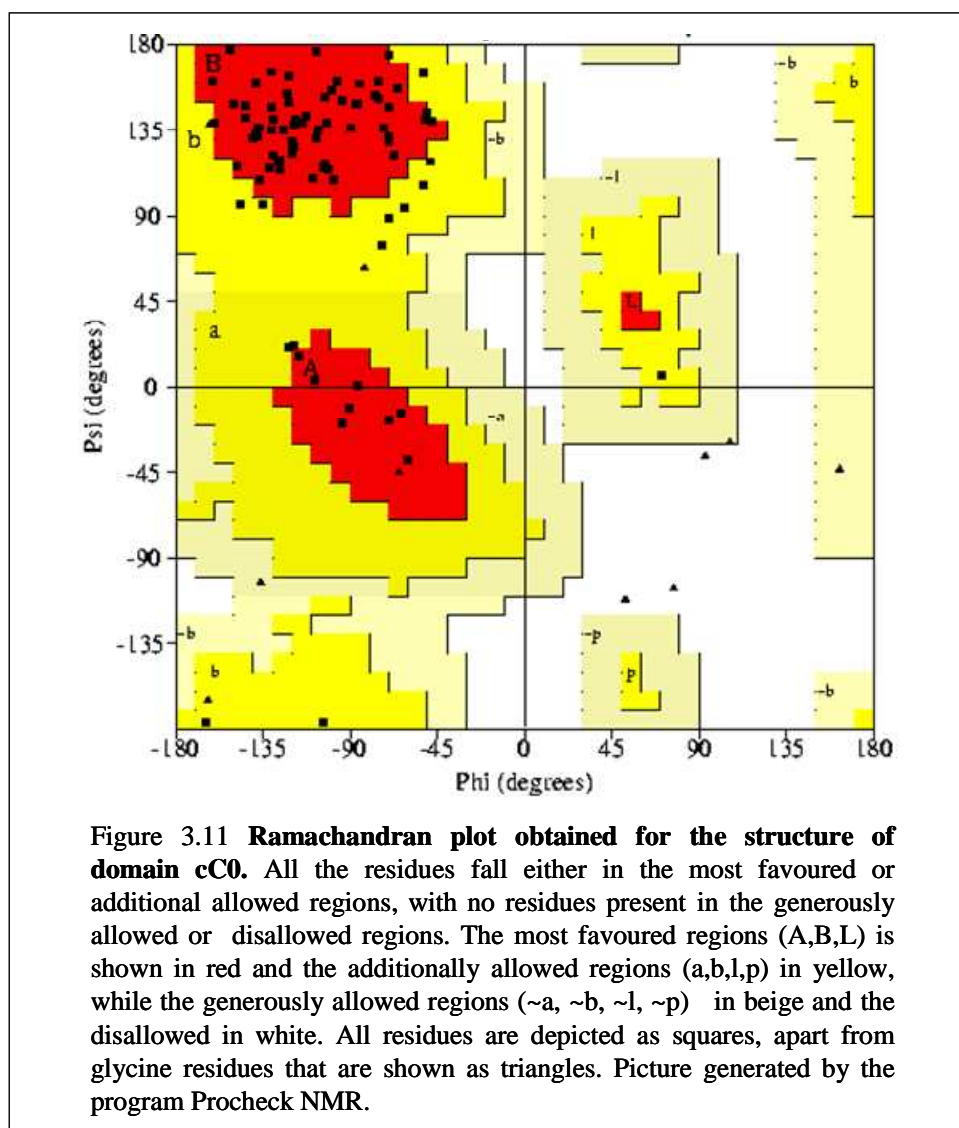
The long range NOEs, shown in black in the following graph, correspond to amino acids positioned in the  $\beta$ -strands, while regions with low number of NOEs or short distance NOEs are given by residues found in unstructured regions, such as loops or the termini of the domain.



**Figure 3.10 Number of constraints per residue.** This picture shows the number of NOEs per residue used for the structure calculation. The long range NOEs are shown in black, medium range NOEs are depicted in gray and short range NOEs in white. It is obvious that short range NOEs are common to all residues while long range NOEs are present just for those residues that are part of a region with a precise secondary structure. The regions with the highest number of long range NOEs in fact, correspond to the  $\beta$ -strands that form the two  $\beta$ -sheets of the domain. Picture generated by the program Cyana 2.1.

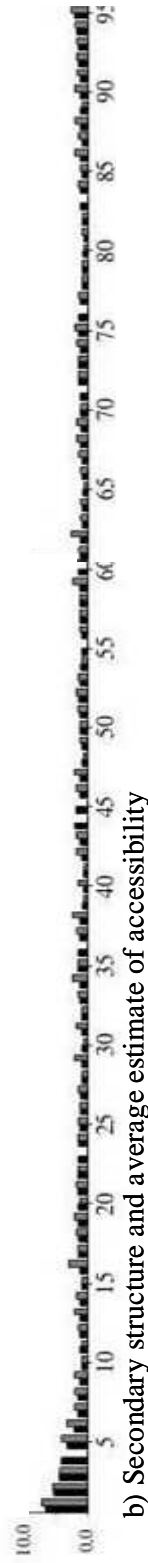
### 3.1.5 Structure validation

The protein structure was validated using the program Procheck NMR (Laskowski et al., 1996) as described in the material and methods section 2.5.3. The Ramachandran plot produced by the Procheck contains all the 95 residues either in the most favoured or in the allowed region of the graph, no residue is found in the generously allowed or disallowed regions, meaning that the  $\phi$  and  $\psi$  angles are in accordance with the average values detected in the majority of structures.

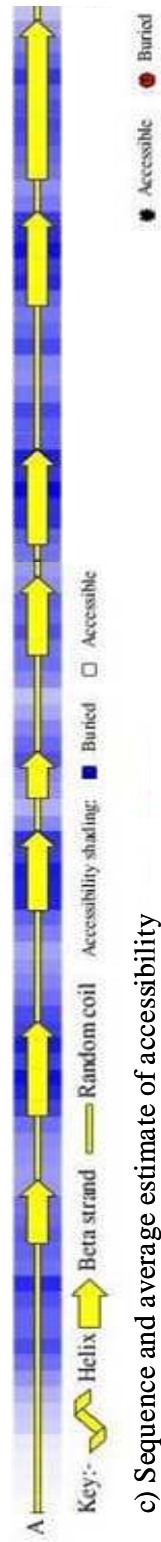


Procheck also displays the RMSD calculated for each residue, its accessibility, defining whether or not an amino acid is positioned on the surface or buried in the hydrophobic core and the secondary structure. All these parameters are shown in picture 3.12. From the Procheck results it is obvious that the structure obtained for domain cC0 is a good quality structure, with low RMSD, apart from the poorly structured N-terminus and a secondary structure corresponding to the one expected for an IgI domain, with very well defined secondary structure elements, also confirmed by the accessibility analysis carried out on each residue, as shown in picture 3.12 c).

a) RMSD from mean coordinates: main chain (black) and side chain (gray)



b) Secondary structure and average estimate of accessibility



c) Sequence and average estimate of accessibility



Figure 3.12 Procheck NMR residue by residue results for the calculated structure of domain cC0. a) RMSD from the coordinates of both backbone and sidechains. It is evident how the RMSD values are higher at the N-terminus of the protein, as expected for an unstructured part of the protein, while the decrease in the regions characterized by a specific secondary structure; b) secondary structure of domain cC0; c) in this section of the picture is shown the sequence of the domain together with an estimate of how a residue is accessible or buried in the hydrophobic core. It is easy to spot that the buried residues tend to correspond to the  $\beta$ -sheet regions of the domains.

### 3.1.6 Protein Dynamics

The relaxation experiments were performed on a  $^{15}\text{N}$  labelled sample of domain cC0 using the standard sequences implemented by the NMR centre manager. Twelve point were recorded for  $T_1$  and  $T_2$  interleaving the  $^1\text{H}/^{15}\text{N}$  HSQC spectra and using a Carr-Purcell- Meiboom- Gill (CPMG) pulse train for  $T_2$  experiments, while the heteronuclear NOE was measured from a pair of spectra recorded with and without proton saturation (Barbato et al., 1992) as described in the introduction (section 1.2.3). All experiments were performed using a 600MHz spectrometer.

# spectrum	$T_1$ [ms]	$T_2$ [ms]
1	16	5.125
2	48	10.250
3	96	15.374
4	192	20.499
5	288	30.749
6	384	40.998
7	512	61.498
8	704	81.997
9	880	102.496
10	1120	133.245
11	1440	153.744
12	288	40.998

**Table 3.2:** delays used to perform the relaxation experiments.

The NMR spectra obtained were analysed with the program CcpNmr Analysis and the peak intensities were determined from the peak heights. The NOE values were calculated by taking the ratio of the  $^{15}\text{N}$  intensities for experiments performed with and without proton saturation. Relaxation rates were determined by fitting the delay

dependent peak intensities to an exponential function using the program MATHEMATICA (Wolfram research).

An estimation of the overall correlation time ( $\tau_c$ ) was obtained from  $R_2/R_1$  ratios using MATHEMATICA with a filter applied to ensure that only residues that do not suffer from large amplitude fast motions and chemical exchange are included in the determination; a standard deviation cut-off of 1.5 and a NOE cut-off of 0.65 were applied to all data. Residues with an NOE effect larger than 0.65 are considered rigid, while if the NOE effect is below this value the residue involved is in a flexible region. It is important to note that the Lipari-Szabo analysis used in this research considers the protein as a spherical object, not taking into account any anisotropy that might be present in the molecule.

The initial data consisted of 75 residues, out of which seven were eliminated because of the NOE cut-off and four were removed due to the  $R_2/R_1$  standard deviation cut-off that resulted more than the set 1.5. As a consequence the fit was performed on 64 residues.

The average values obtained were:

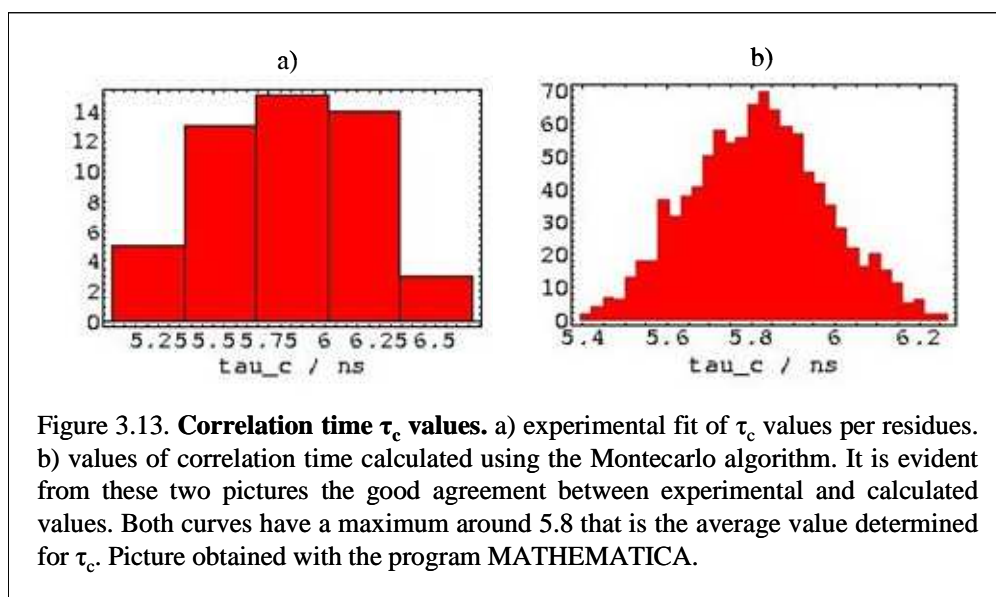
$$R_1 = 1.44 \pm 0.10 \text{ s}^{-1}$$

$$R_2 = 10.68 \pm 2.02 \text{ s}^{-1}$$

$$\text{NOE} = 0.78 \pm 0.04$$

The value of  $\tau_c$  was fitted from the experimental data and calculated with the Monte Carlo simulation algorithm, which provides an estimate of the expected value of a random variable,  $\tau_c$  in this case, and predicts the estimation error which is proportional to the number of iteration. The results obtained from these two fits show how the values follow a Gaussian distribution and are reported in picture 3.13, for the 64 experimental values taken into account in this analysis and for the 500 synthetic residues used in the Monte Carlo simulation. The second fit is better defined than the experimental value but

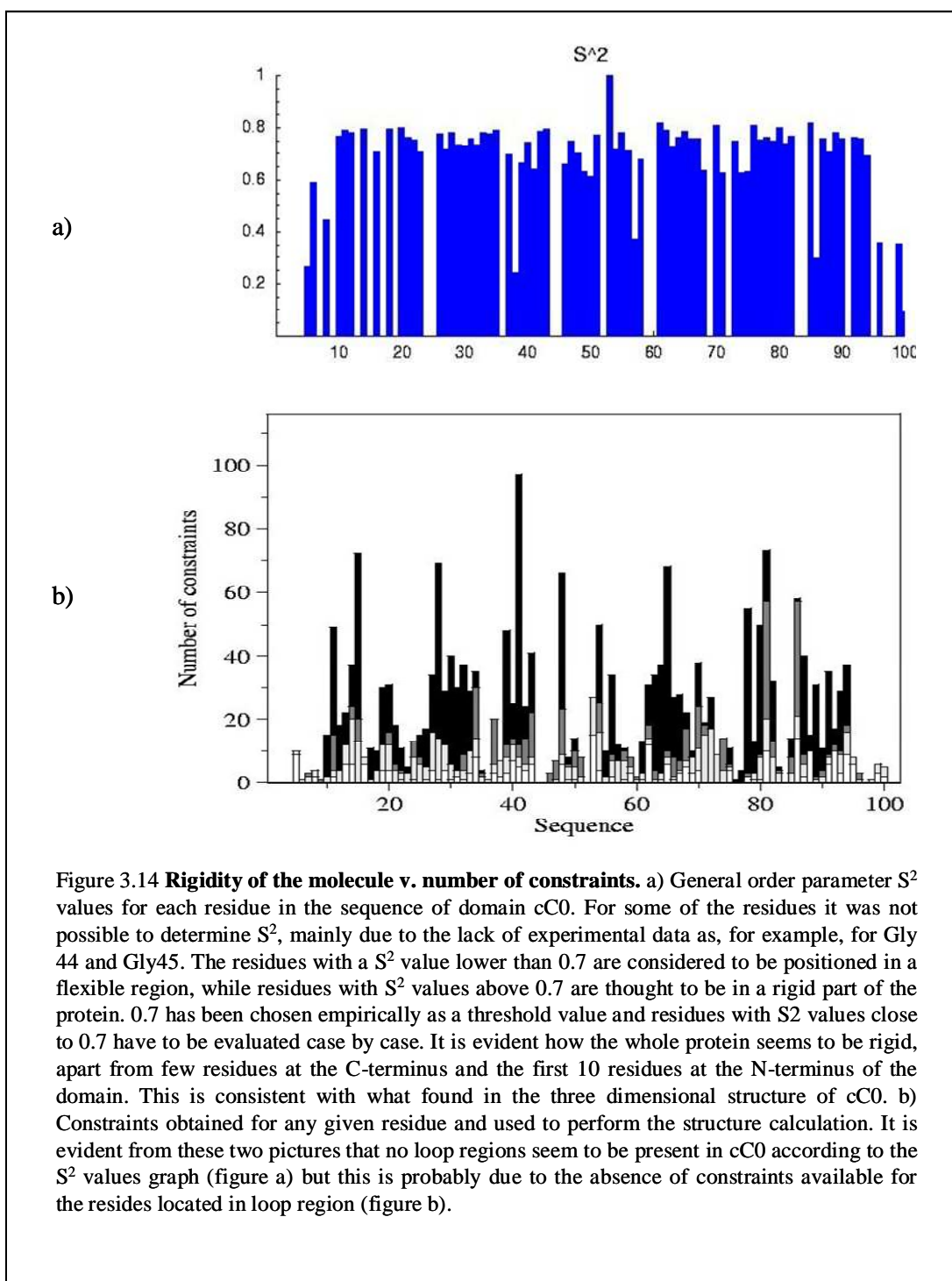
we can notice the good agreement between experimental and simulation results. The average value for  $\tau_c$  was determined to be  $5.81 \pm 0.16$  ns.



Once  $\tau_c$  has been determined, the five different models shown in table 2.8 were used in the numerical fit to the experimental  $R_1$ ,  $R_2$  and NOE values. The equation that fit better the experimental data was then used to calculate the appropriate variables necessary to describe the motion, such as  $S^2$ ,  $R_{ex}$ ,  $S^2_f$ ,  $\tau_i$ , etc.

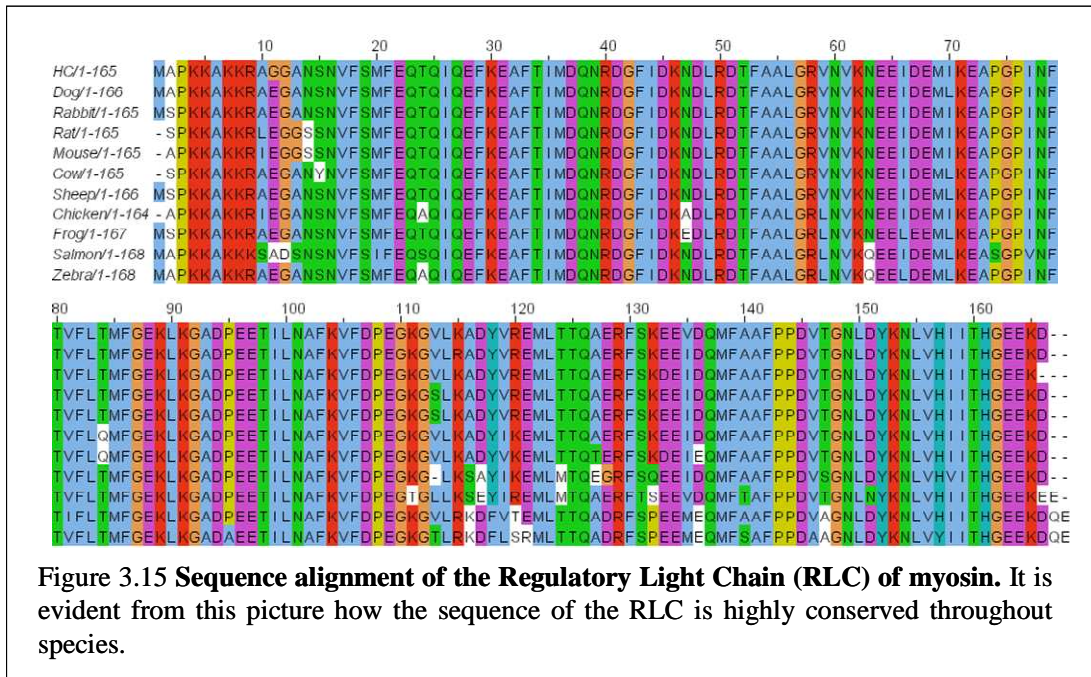
$S^2$  it is an important parameter as it gives an idea of the local dynamics of the protein analysed.  $S^2$ , in fact, can assume any value between 0, corresponding to maximal flexibility, and 1, corresponding with maximal rigidity.

From picture 3.14 a) it is clear how the protein is rigid, having almost all residues listed with a  $S^2$  value larger than 0.7, value taken arbitrarily as the threshold between flexibility and rigidity of the region of the protein where the residue in question is located. Only the N-terminus of the protein appear flexible, together with a few residues at the C-terminus of the domain, confirming what found in the structure derived by the calculation.



### *3.1.7 Studies of the interaction between cC0 and RLC*

Studies carried out by our collaborator Dr Elena Rostkova (King's Collage, London) based on Differential Scanning Calorimetry (DSC), showed that domain cC0 interacts with the miniHMM fraction of myosin, comprising of two myosin heads, two essential light chains, two regulatory light chains and S2 $\Delta$ , the first 125 residues of myosin S2 forming a coiled coil and, more precisely, with the Regulatory Light Chain (RLC). The RLC is positioned in the neck region of myosin and, together with the Essential Light Chain (ELC), stabilises the 8.5 nm long  $\alpha$ - helical fragment that forms it. The N-terminus of the RLC is wrapped around the myosin heavy chain (Rayment et al., 1993) in the region comprised between residues 808 and 842. The RLC seems to be of great importance for both myosin structure and function; in fact, selective removal of the RLC caused a change in the structure of the cardiac myosin molecule (Margossian and Slayter, 1987) and, upon removal of the RLC, myosin would lose its ordered structure (Levine et al., 1998). The regulatory light chain is a member of the superfamily of EF-hand  $\text{Ca}^{2+}$  binding protein, even though it has lost its ability to bind to  $\text{Ca}^{2+}$  in sites 2, 3 and 4 (Moncrief et al., 1990) and presents only one high affinity binding site at the N-terminus (Reinach et al., 1986), between residues 37 and 48 (Szczesna et al., 2001). The RLC shows also a phosphorylation site at residue Ser15. This domain results being highly conserved throughout species, as visible from the alignment shown below. Also the RLC is linked to HCM, presenting 8 missense mutations that cause the disease.



The first preliminary analysis on the interaction of domain cC0 and miniHMM and RLC was performed by our collaborator Dr Elena Roskova (King’s College, London) using the technique of differential scanning calorimetry (DSC). The results obtained with this analysis showed that the two protein interact with one another. To confirm these results and to take advantage of the structure of domain cC0, NMR spectroscopy was used to study this interaction, first with miniHMM and then with RLC.

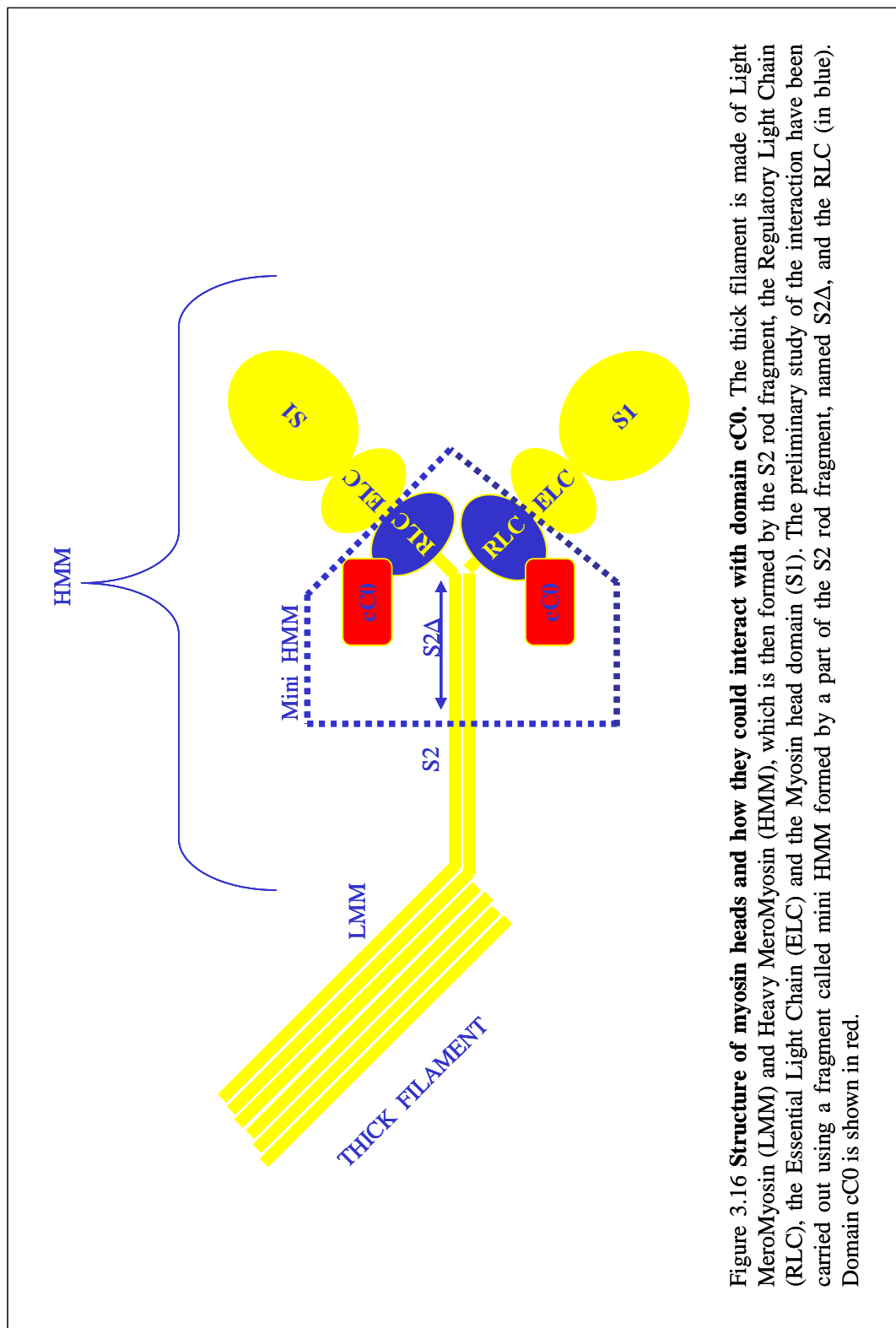


Figure 3.16 **Structure of myosin heads and how they could interact with domain cC0.** The thick filament is made of Light Meromyosin (LMM) and Heavy Meromyosin (HMM), which is then formed by the S2 rod fragment, the Regulatory Light Chain (RLC), the Essential Light Chain (ELC) and the Myosin head domain (S1). The preliminary study of the interaction have been carried out using a fragment called mini HMM formed by a part of the S2 rod fragment, named S2A, and the RLC (in blue). Domain cC0 is shown in red.

### 3.1.7.1 $^1\text{H}/^{15}\text{N}$ NMR spectroscopy titration between cC0 and miniHMM

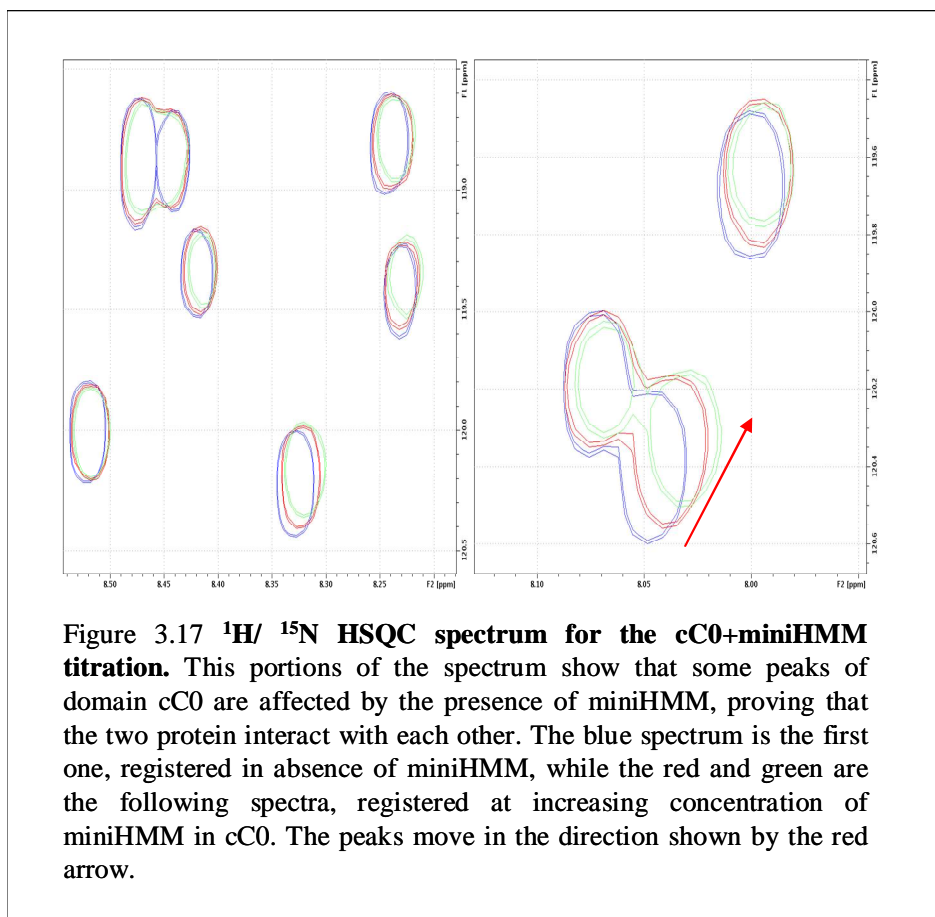
Domain cC0 is thought to interact with Myosin Regulatory Light Chain (RLC) located in the Heavy MeroMyosin (HMM), the fragment containing the Myosin heads. To prove that this interaction takes place, a preliminary titration was carried out using as a binding partner the so called mini HMM, which is formed by a fragment of the S2 rod, the so called S2 $\Delta$ , and the Regulatory Light Chain (RLC). The five steps of the titration are reported in table 3.3

Ratios	[cC0] $\mu\text{M}$	[miniHMM] $\mu\text{M}$
1:0	200	0
1:0.5	200	96
1:1	200	289
1:2.5	200	481
1:3.5	200	673

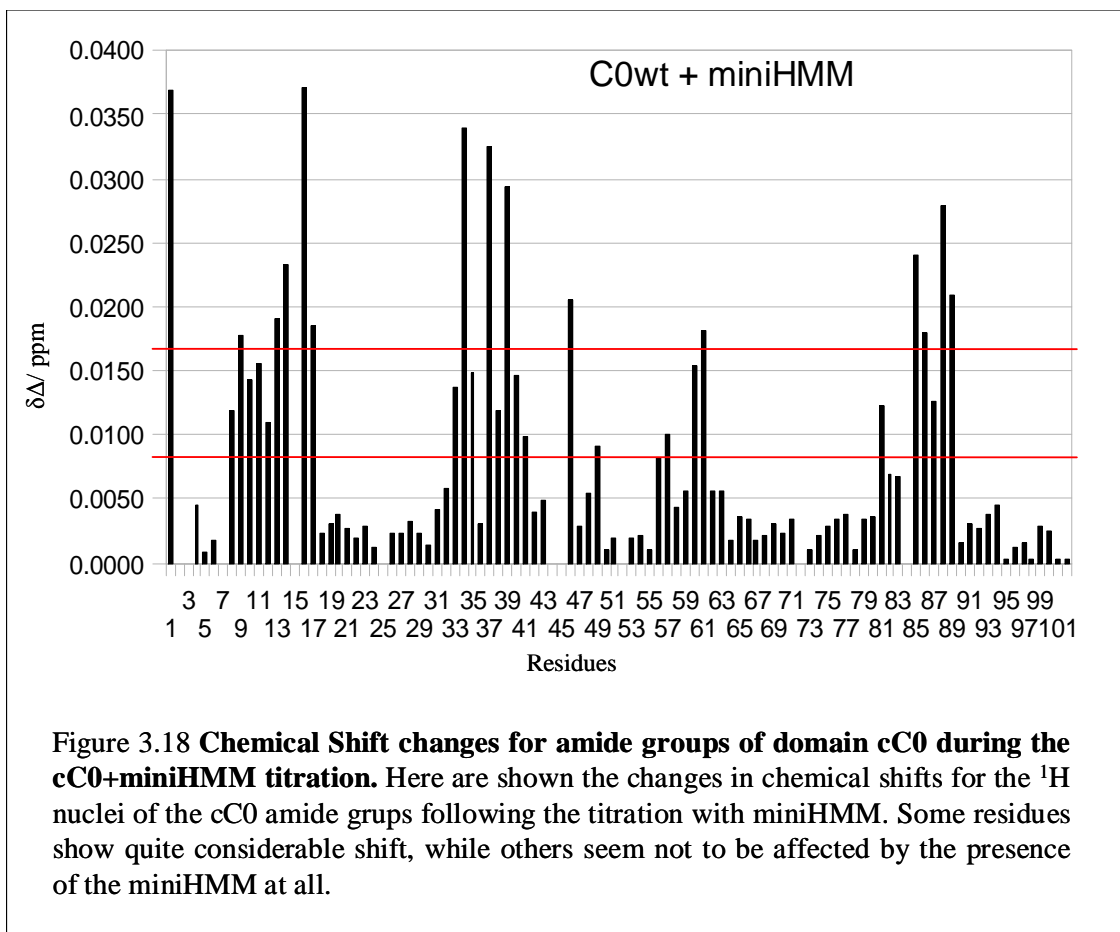
**Table 3.3: ratios and final concentrations of cC0 and the miniHMM fragment used in the titration.**

At the time of this experiment the assignment for domain cC0 was not available yet, so these changes in the spectrum were interpreted as a proof that the interaction was happening. Once the spectra for domain cC0 have been fully assigned, it was possible to repeat the titration, with both miniHMM and RLC, and to map the result on cC0 surface, so to understand where the two proteins interact with each other. The peaks in the green spectrum (Fig. 3.17) are less intense than the ones shown in the other preceding spectra, this is due to the large dimensions of miniHMM; at very high concentrations of miniHMM the spectrum of cC0 would completely disappear due to

the slow tumbling of a large molecule, such as the complex formed by cC0 and miniHMM, that leads to fast transverse relaxation ( $T_2$ ), causing broadening of the signals and ultimately disappearance of any signal.



The chemical shift perturbations are reported on the histogram (Fig. 3.18). The most affected residues resulted being F11, K14, R16, R34, V37, S46, G60, K86, V87, K88, F89, showing a  $\delta\Delta$  bigger than 0.017 ppm, depicted in the figure as the higher red horizontal line.



Most of the residues involved in this interaction are positively charged amino acids, mainly Lysines and Arginines, all exposed on the domain surface, as expected for charged residues.

### 3.1.7.2 $^1\text{H}/^{15}\text{N}$ NMR spectroscopy titration between cC0 and RLC

A titration was performed using a  $^{15}\text{N}$  labelled NMR sample of cC0 to which an increasing concentration of RLC was added.  $^1\text{H}/^{15}\text{N}$  HSQC spectra were recorded after every addition. The ratios used in this experiments are reported in the table following.

Ratios	[cC0] $\mu$ M	[RLC] $\mu$ M
1:0	50	0
1:1	50	50
1:2	50	100
1:4	50	200
1:6	50	300

**Table 3.4: ratios and final concentrations of cC0 and RLC used in the titration performer to study their interaction.**

The changes in the  $^1\text{H}/^{15}\text{N}$  HSQC spectrum have been monitored and are reported in figures 3.20- 3.23 For clarity only three points have been reported in the pictures, corresponding to the ratios 1:0, 1:1 and 1:6.

The histogram shows which residues were more affected by the addition of RLC to cC0; being the  $^1\text{H}/^{15}\text{N}$  HSQC spectrum fully assigned, it was possible to identify the residues that show the main shifts. As expected all of them are to be found on the surface of cC0 and most of them are charged residues, such as Lys and Arg.

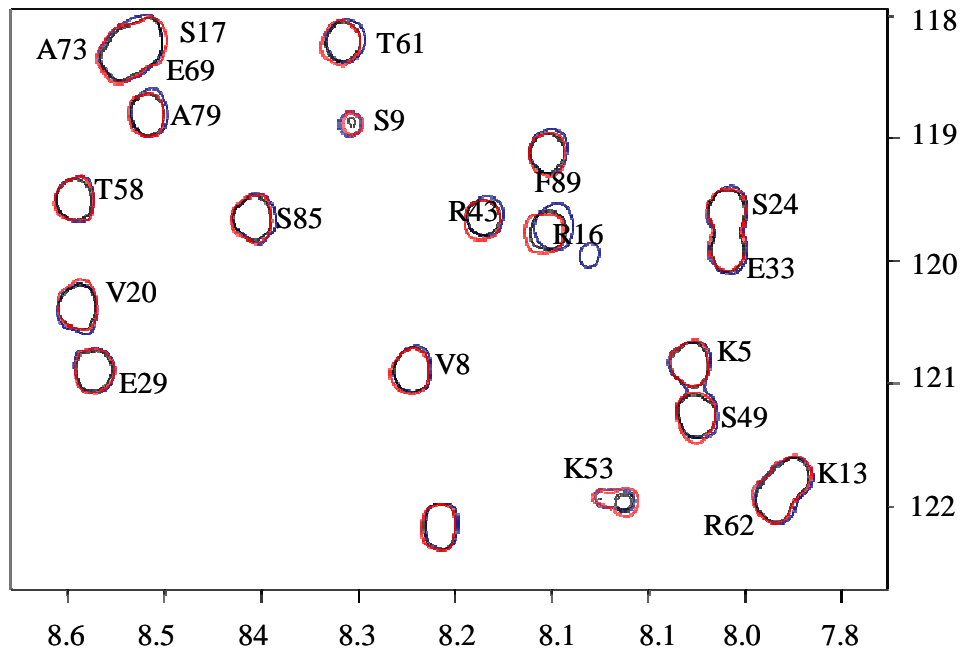


Figure 3.19  $^1\text{H}/^{15}\text{N}$  HSQC spectrum for the cC0+RLC titration. **Panel 1.** In the picture are shown some of the peaks of the  $^1\text{H}/^{15}\text{N}$  HSQC spectrum, one of which corresponds to the residue R16 that is the most affected by the addition of RLC to cC0. For clarity in the picture are shown only three of the five titration points registered during the experiment. (Ratios cC0:RLC Red 1:0; Blue 1:6)

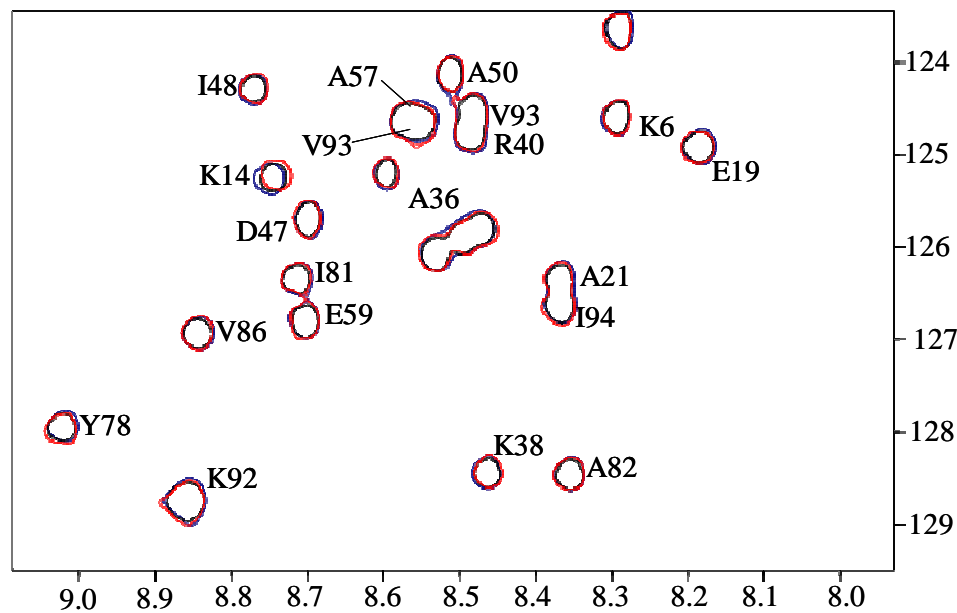


Figure 3.20  $^1\text{H}/^{15}\text{N}$  HSQC spectrum for the cC0+RLC titration. **Panel 2.** In the picture are shown some of the peaks of the  $^1\text{H}/^{15}\text{N}$  HSQC spectrum, one of which corresponds to the residue K14 one of the most affected peaks by the addition of RLC to cC0. For clarity in the picture are shown only three of the five titration points registered during the experiment.

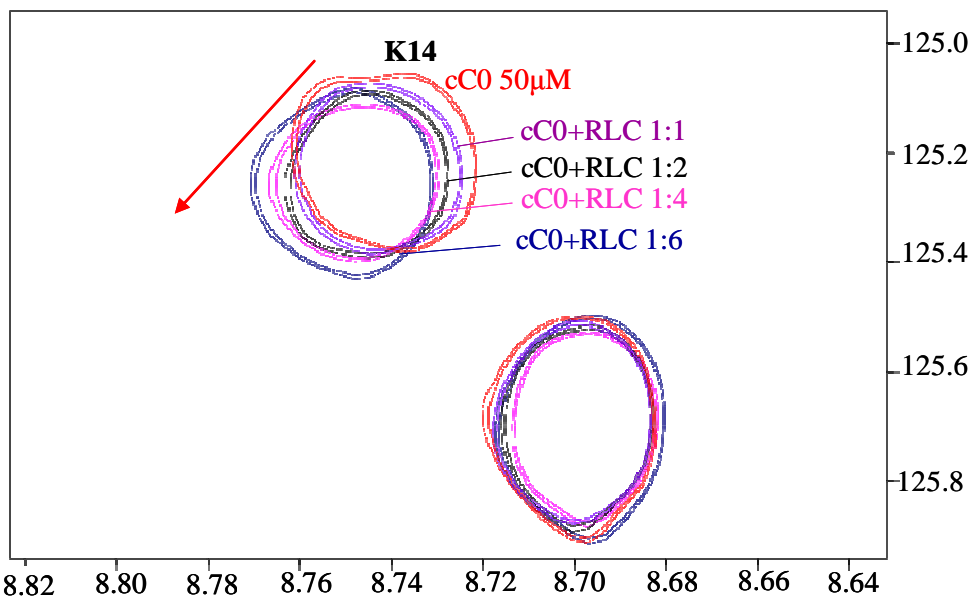


Figure 3.21 **Reside Lys14 during the cC0+RLC titration.** In the picture are shown the successive shifts of the K14 peak during the cC0+RLC titration, showing all five points registered during the experiment. It is clearly visible how the peak moves in the arrow direction, starting from the red spectrum, corresponding to cC0, to the blue spectrum, corresponding to a ratio of cC0 and RLC 1:6 respectively.

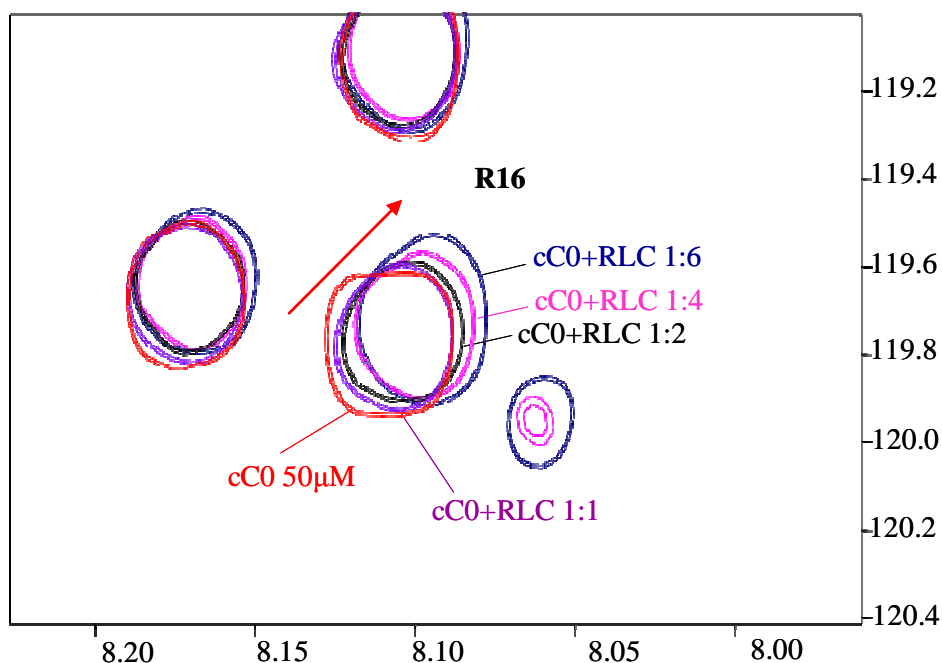
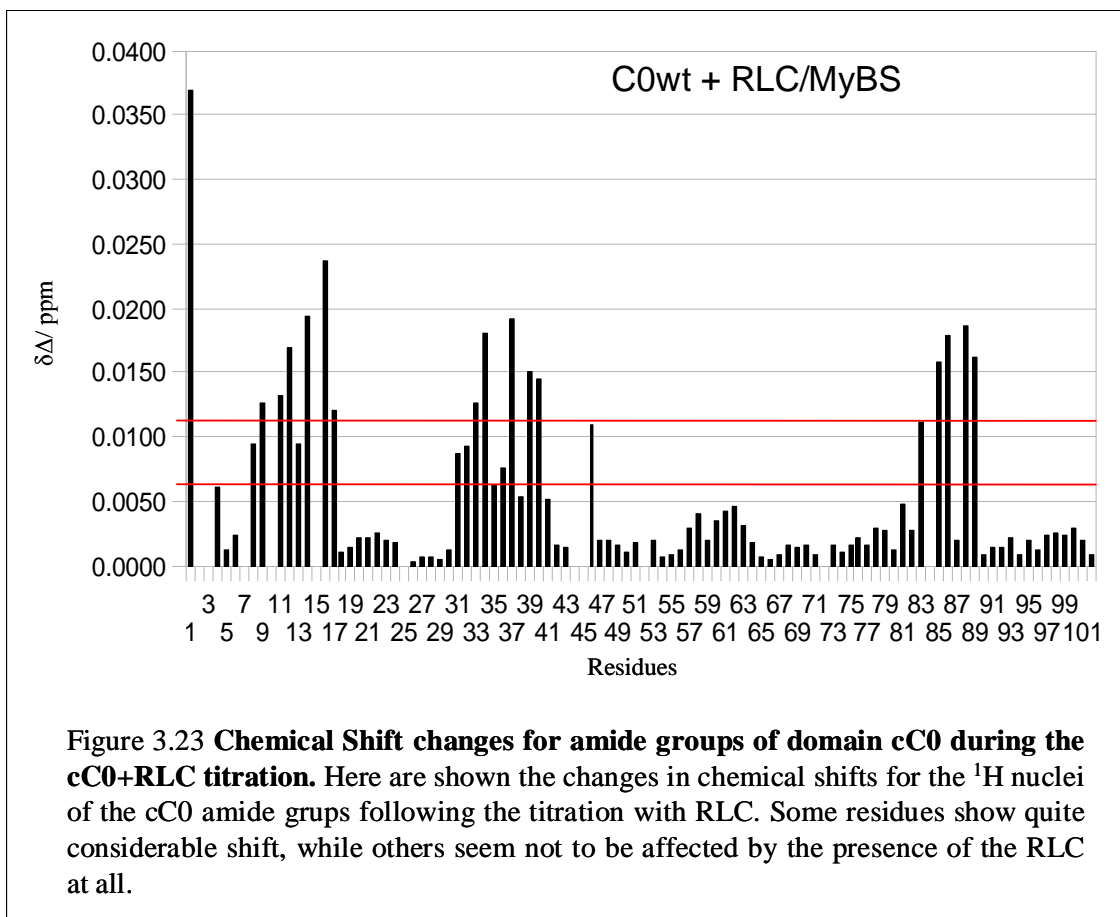
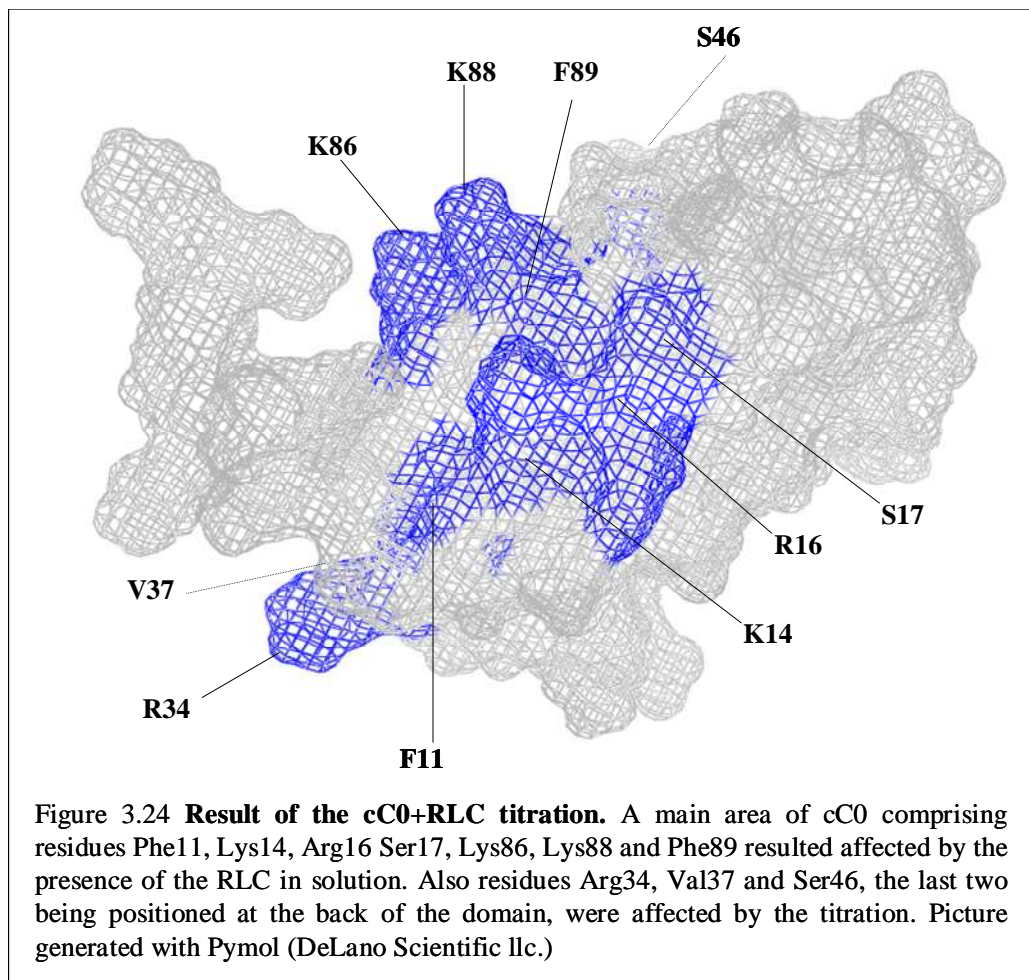


Figure 3.22 **Reside Arg16 during the cC0+RLC titration.** In the picture are shown the successive shifts of the R16 peak during the cC0+RLC titration, showing all five points registered during the experiment. It is clearly visible how the peak moves in the arrow direction, starting from the red spectrum, corresponding to cC0, to the blue spectrum, corresponding to a ratio of cC0 and RLC 1:6 respectively.



In Fig. 3.23 above are shown the peaks that moved the most in the  $^1\text{H}/^{15}\text{N}$  HSQC spectrum due to the addition of Ht<sub>T</sub>RLC, corresponding to the residues more affected by the interaction. Most of the residues involved in this interaction are positively charged amino acids, mainly Lysines and Arginines, all exposed on the domain surface, as expected for charged residues. Moreover, all the peaks in the spectrum appear broaden; this is a consequence of the formation of the complex between cC0 and the Ht<sub>T</sub>RLC, the peaks in the spectra registered at a high concentration of Ht<sub>T</sub>RLC behave like those in the spectrum of a molecule with a higher molecular weight, hence the broadening of the NMR signals.

It was possible to identify on the domains surface the residues that more resulted affected by the titration and are reported below.



### 3.1.8 Mutogenesis Studies

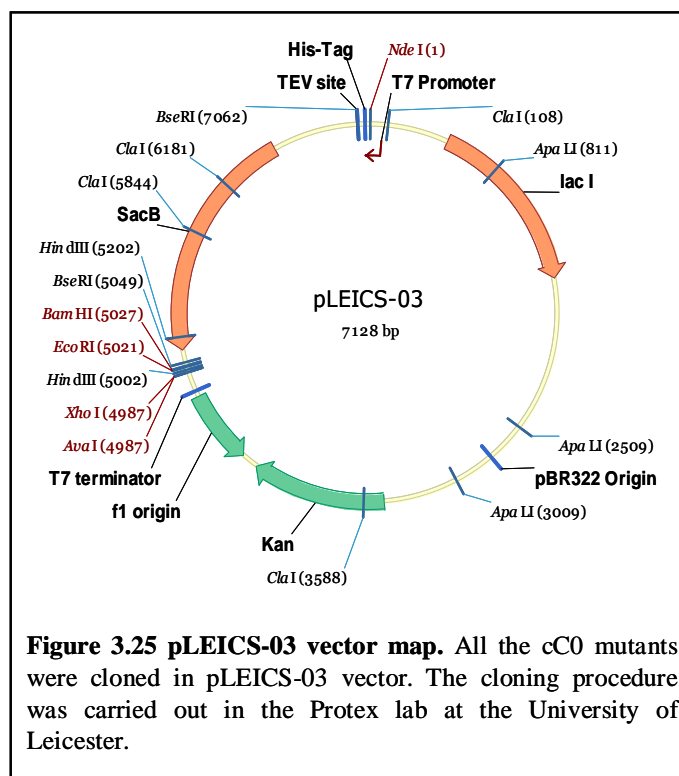
Only three HCM related mutation have been identified in domain cC0 (Table 1.2). G4R (Van Driest et al., 2004) is shown to have an early onset (around 20 years of age) while T59A (Niimura et al., 2002) has a more delayed onset and it appeared in individuals 56 years old. This last mutation is thought to be mild as many species present an Ala residue in this position instead of the Thr present in the human cardiac isoform, so no great disruption in either structure or function can be expected. The last of the cC0 mutations is R34W (Peng et al., 2005. direct submission at <http://genepath.med.harvard.edu/~seidman/cg3/>), involving one of the residues affected

by the interaction with RLC. No clinical information have been deposited or published so far regarding this mutation.

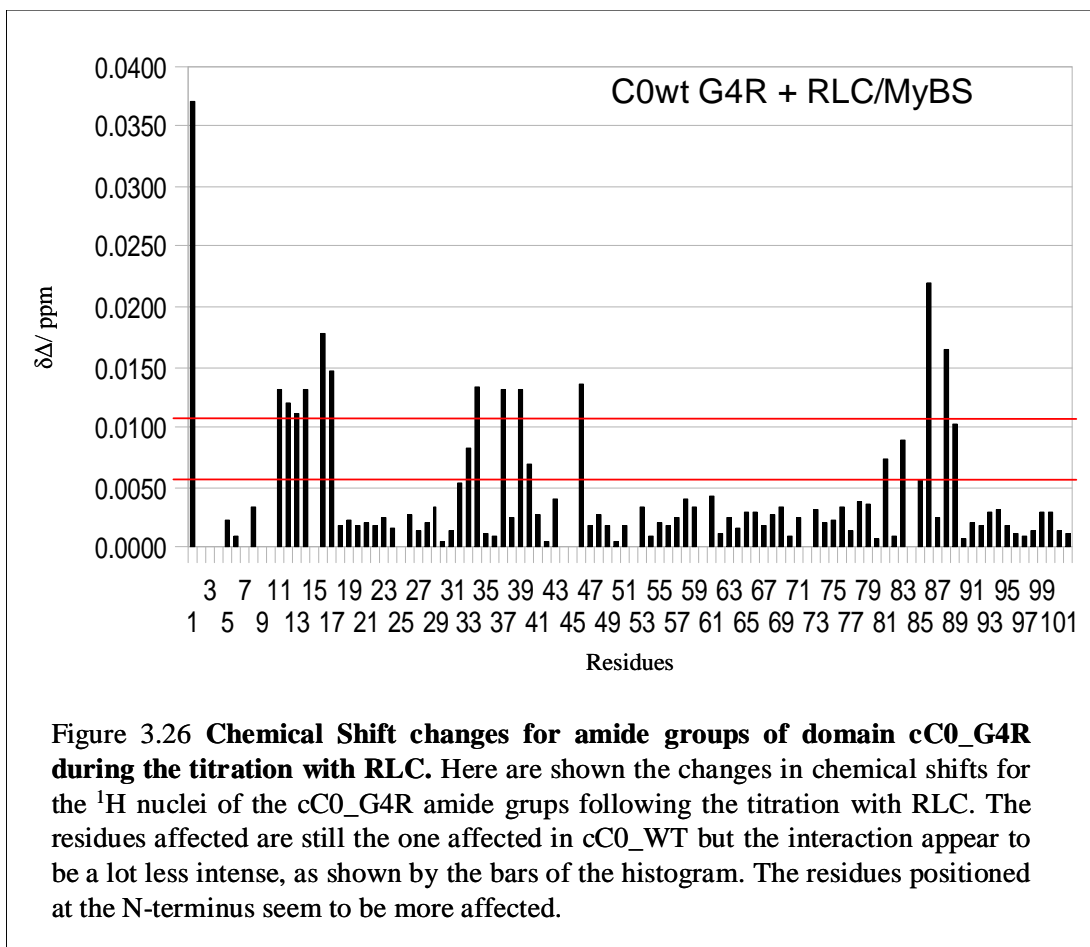
To determine the effect of these mutations on cC0 structure and function, four mutants were produced of the protein to study their interaction with RLC and to compare their behaviour with wildtype cC0 used in the previous interaction studies. The primers used are reortend in table 3.5.

	Primers for generating entry vector		
			T <sub>m</sub>
cC0_WT	F	5' -ACTTCCCAATCCATGCCTGAGCCGGGAAGAAGCCA-3'	70°C
	R	5' -TATCCACCTTTACTGTCAAAATTCCTCACGCGTGGA-3'	64°C
cC0_G4R	F	5' -ACTTCCCAATCCATGCCTGAGCCGGGAAGAAG-3'	68°C
	R	5' -TATCCACCTTTACTGTCAAAATTCCTCACGCGTGGA-3'	64°C
cC0_R34W	F	5' -GCCGAGACAGAGTGGGCAGGAGTG-3'	64°C
	R	5' - CACTCCTGCCACTCTGTCTCGGC-3'	64°C
cC0_A30P	F	5' -GTGTTCCGAGCCCCGAGACAGAGCGG-3'	64°C
	R	5' -CCGCTCTGTCTCGGGCTCGAACAC-3'	64°C
cC0_K86E	F	5' -GGCTCCTCCGAGGTCAAGTTCGAC-3'	63°C
	R	5' -GTCGAACTTGACCTCGGAGGAGCC-5'	63°C

**Table 3.5 Primers used to clone wildtype cC0 and the four mutants**

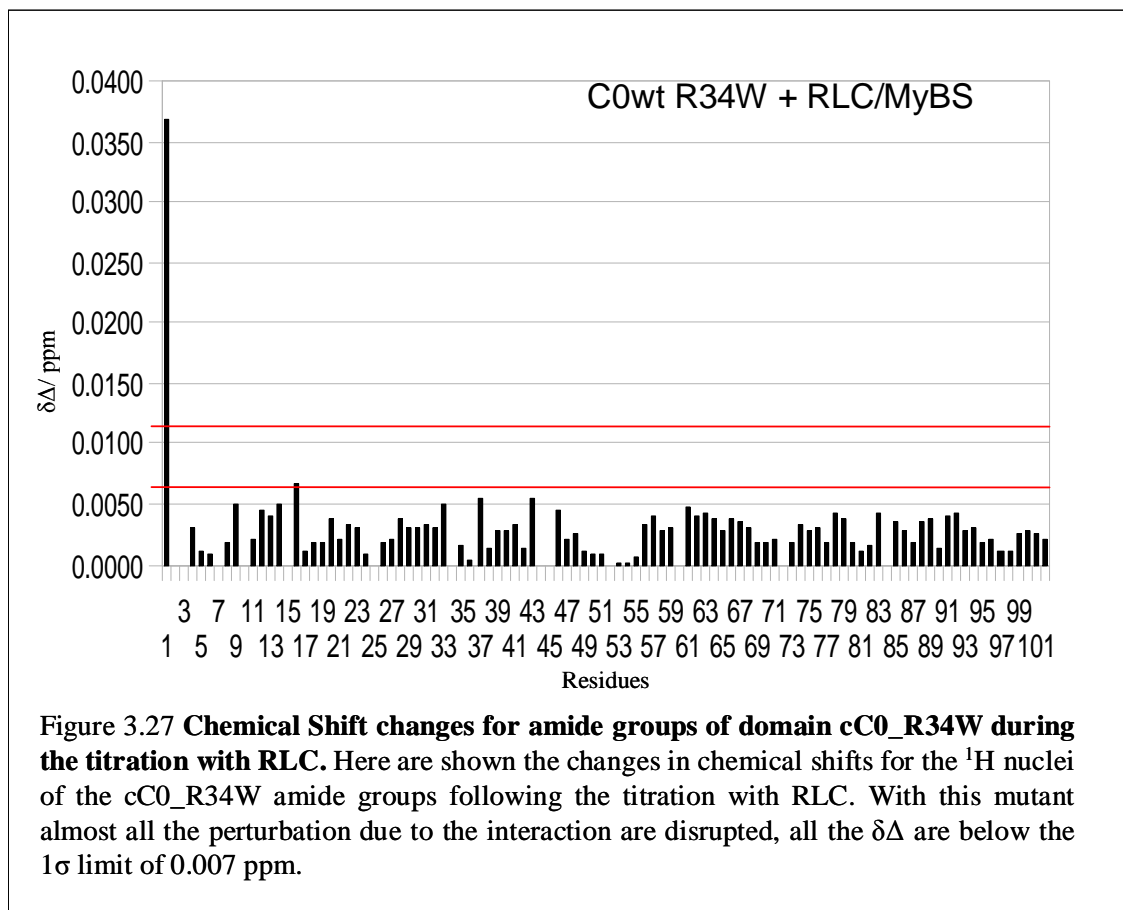


The first two mutants, cC0\_G4R and cC0\_R34W, are obvious choices as they are natural occurring mutations in human cardiac isoform; T58R was not chosen as in all other species analysed of cMyBPC the threonine residue is in fact substituted by an alanine, so the effect of this mutation is not expected to be extreme, a fact confirmed also by what concluded by clinical studies. The mutant cC0\_A30P was produced as an A30P missense mutation has been found in Maine Coon cats (Meurs et al., 2005). Finally, cC0\_K86E was cloned to confirm the hypothesis that the positive patch of which residue Lys86 is part, is involved in the interaction with the RLC as mutating the lysine residue to glutamic acid should have an impact on the interaction and possibly abolish it due to the inversion of charges. All mutants expressed well, apart from cC0\_G4R that went into inclusion bodies being probably insoluble. The lack of stability of this mutant is confirmed by the clinical observation reported for this mutation. The experiment was repeated for cC0\_G4R, cC0\_R34W and cC0\_K86E using 50  $\mu\text{M}$   $^{15}\text{N}$  labelled sample of the cC0 mutants and 200  $\mu\text{M}$  unlabelled samples RLC/ MyBS.

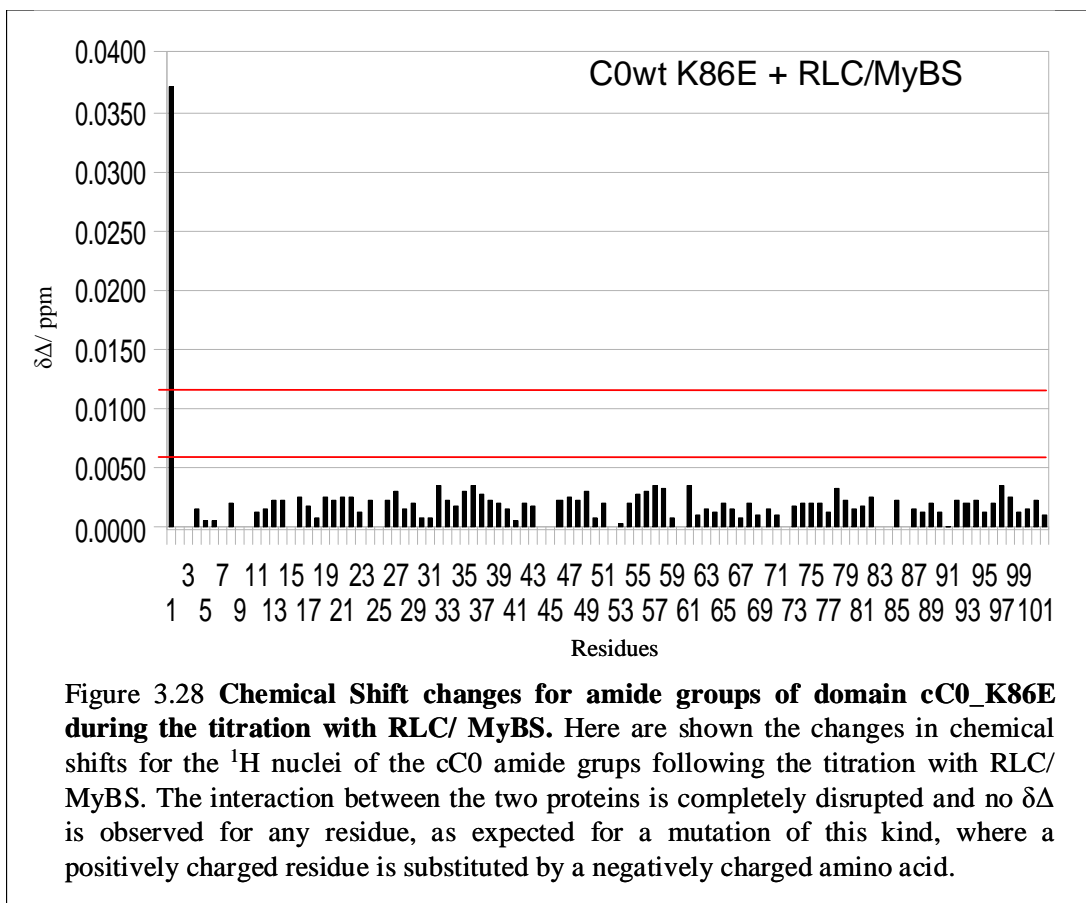


It is interesting to note how the mutation, despite reducing the strength of the interaction, does not disrupt the interaction completely and the same residues that are affected in cC0\_WT resulted being affected in the cC0\_G4R mutant.

Mutation cC0\_R34W affected even more the interaction with RLC that resulted being almost annulled by the substitution of Arg 34 with a Trp. This result could be hypothesised on the basis of the nature of the mutation, where a positively charged residue is substituted with an hydrophobic amino acid



The last experiment to be performed was between cC0\_K86E and RLC/ MyBS. In this case the interaction between the two protein is completely abolished and no residue seem to be affected by the presence of the binding partner.



The experiments with the mutants confirmed that the interaction between cC0 and RLC does in fact happen and that the residues perturbed are the one that take part in the interaction.

### 3.1.9 Actin Binding Assay

It has been suggested by different researchers that MyBPC might interact with actin, some think that the interaction would occur via a proline rich sequence that is located in the linker between cC0 and cC1 (Squire et al., 2003), which constitutes the N-terminus of the protein in non- cardiac isoforms, while others have pointed at domain cC0 as the binding partner of actin (Kulikovskaya et al., 2003). To understand better the

situation, an actin binding assay was performed, as described in the material and methods section.

The intent was to repeat this experiment for different groups of domains, cC0-2, cC1-2 and cC0 alone. The first preliminary experiment was performed with cC0, to understand if the protein would in fact interact with F-actin. A protein, MS1 (Arai et al., 2002), was used as a control as it has been shown to give a positive result at the actin binding assay.

The concentration of the three stock solutions used to perform this assay are:

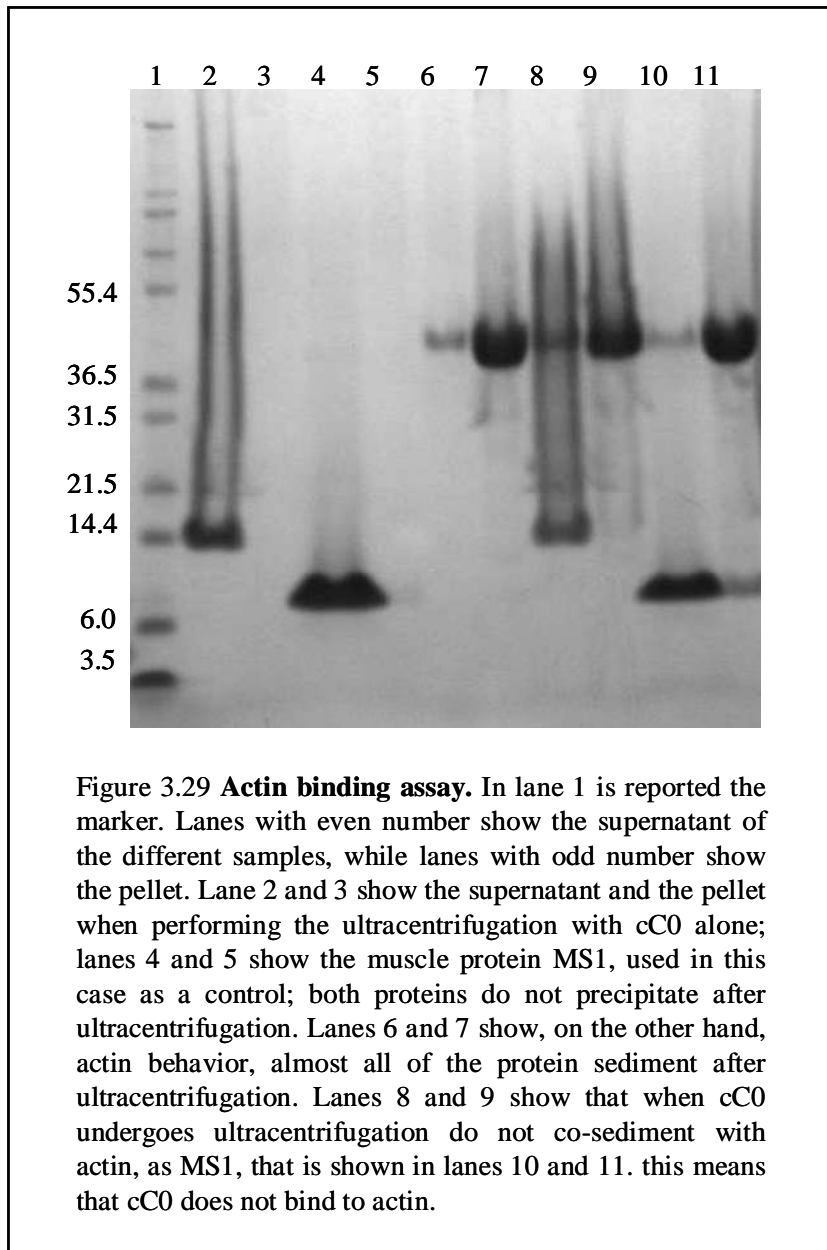
[Actin]= 314  $\mu$ M, [cC0]= 183  $\mu$ M and [MS1]= 373  $\mu$ M

This reaction was performed using a total volume of 1ml; the final concentrations of the three proteins is 50  $\mu$ M for actin and MS1, while it was a bit higher at 61  $\mu$ M for cC0.

	1	2	3	4	5
Actin	-	-	159 $\mu$ l	159 $\mu$ l	159 $\mu$ l
cC0	333 $\mu$ l	-	-	333 $\mu$ l	-
MS1	-	134 $\mu$ l	-	-	134 $\mu$ l
Buffer	667 $\mu$ l	866 $\mu$ l	841 $\mu$ l	508 $\mu$ l	707 $\mu$ l

**Table 2.7: sample composition of the solutions used in the Actin Binding cosedimentation assay**

After ultracentrifugation for 30 minutes at 4°C, an SDS-PAGE gel of the supernatant and the pellet was run, as described in the material and methods. The result show the behaviour of the three proteins on their own and then combined. From the SDS-PAGE picture is clear that both cC0 and MS1 do not tend to sediment during ultracentrifugation as they are not present in the pellet fraction, lanes 3 and 5 in the picture, while being present in lanes 2 and 4, corresponding to the supernatant fractions, they have a tendency for staying in solution.



Actin, on the other hand, sediments, as it is evident from lanes 6 and 7 that show that the major part of actin goes in the pellet and just a small fraction is present in the supernatant. When cC0 is combined with actin it does not shows the same behaviour of MS1, it is present only in the supernatant meaning that do not interact with actin as in this case the protein would co-sediment with actin and would be present in the pellet. From this result it was possible to conclude that cC0 does not bind to actin.

## 3.2 Discussion

### 3.2.1 Structural features of domain cC0

The structure of domain cC0 conforms to the IgI fold (Harpaz and Chothia, 1994) typical of the majority of MyBPC domains, being formed by a  $\beta$ -sandwich composed of two  $\beta$ -sheets, ABED and C'CFGA' respectively. Also the C' strand whose presence has caused controversy in the past (Mayans et al., 2001), is observed in this domain, as it is in the structures of domains cC1 (Ababou et al., 2008) and cC2 (Ababou et al., 2007), and seems to be a recurring feature in MyBPC domains. The hydrophobic core of the protein is well defined by the aromatic residues Trp41, which is highly conserved through species and is central to the domain stability, Tyr54 and Tyr78, the latter being also involved in the tyrosine corner (Hemmingsen et al., 1994), another characteristic feature of these domains, and Phe11, Phe28 and Phe89. Other hydrophobic residues positioned in the core of the protein and, as such considered of great importance for the protein to maintain its fold, are Ile48, Leu56, Leu65 and Leu91. Domain cC0 sequence appears to be well conserved between species, being unique to the cardiac isoform it was not possible to perform a comparison between isoforms, as usually done for the other domains studied so far. All the residues involved in the hydrophobic core of the protein appear to be well conserved, with Leu56 being the only one substitute by Ile in the chicken cardiac isoform.

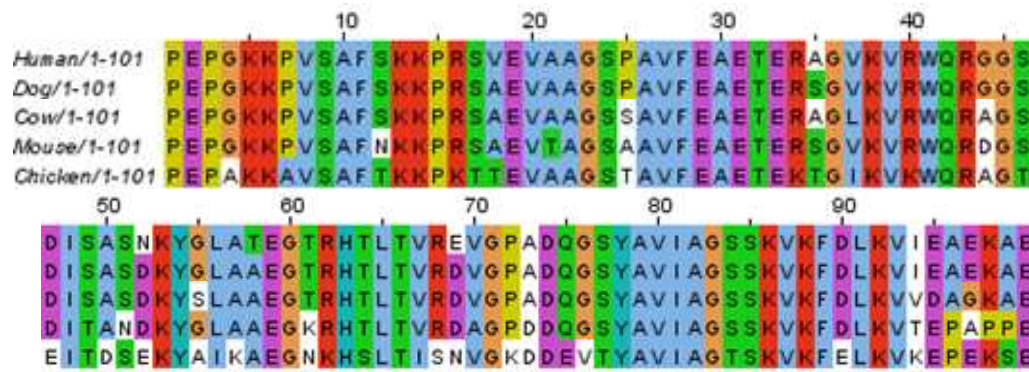
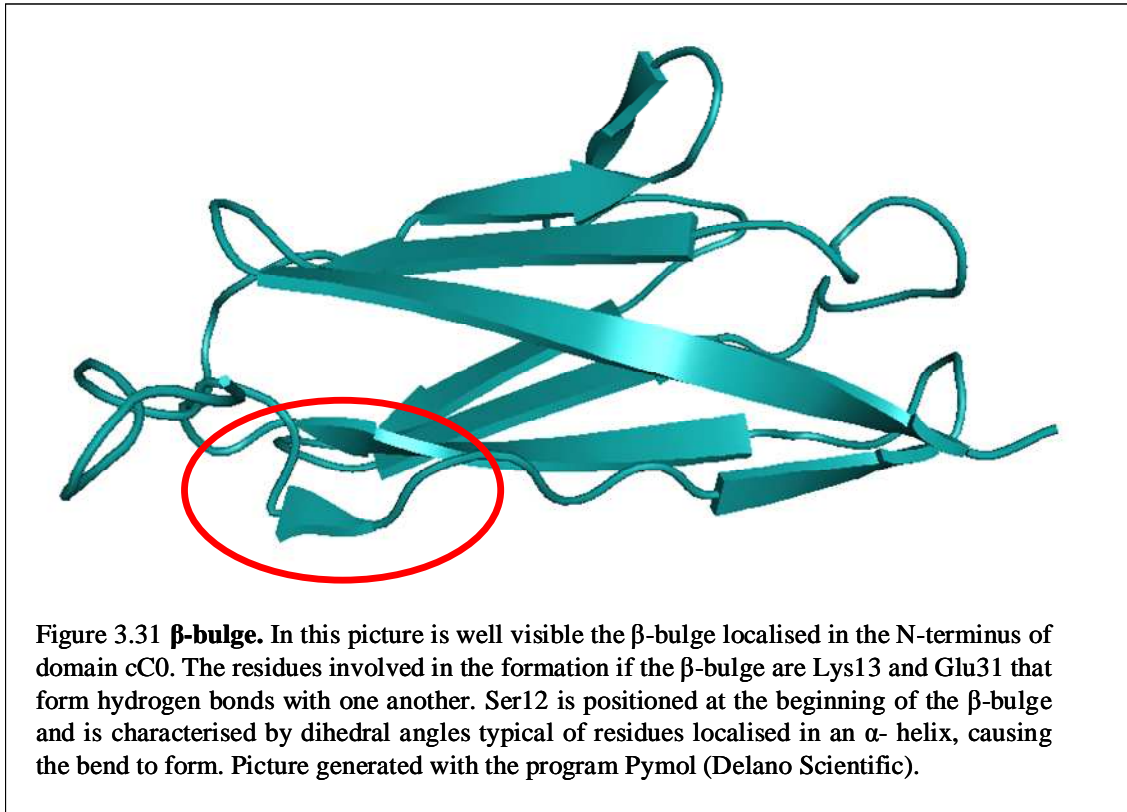


Figure 3.30 **Sequence alignment of domain cC0.** The domain appear to be well conserved through species. The residues localised in the hydrophobic core of the protein, Trp41, Tyr54, Tyr78, Phe11, Phe28, Phe89,Ile48, Leu56, Leu65 and Leu91, that are responsible for the three dimensional structure of the protein are clearly conserved as is Asp74 involved in the formation of the tyrosine corner. Picture generated with the program Jalview.

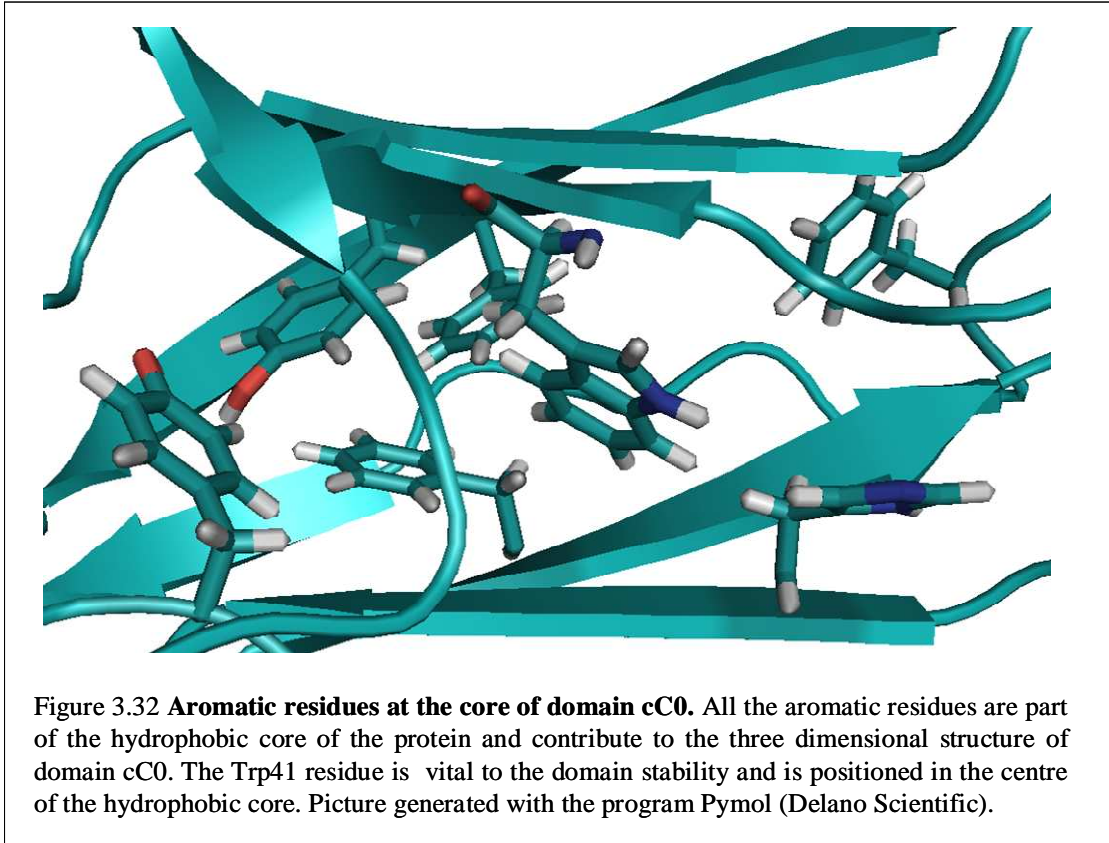
Strand A is composed of a very short  $\beta$ -sheet that does not form a proper strand antiparallel to the B strand as just one hydrogen bond can be formed between Lys13 and Glu31. The  $\beta$  bulge, a disruption of the regular hydrogen bonding of a  $\beta$ -sheet usually achieved by insertion of residues with helical dihedral angles (Richardson et al., 1978), seems to be a reoccurring feature of IgI domains and it is present in all other three MyBPC domains whose structure has being determined so far, being grossly enlarged in domain cC5 (Idowu et al., 2003). It appears that the  $\beta$  bulge is conserved in immunoglobulin domains as it helps dimerization and, as such, it is present in cMyBPC domains as an inherited feature with no apparent function as cMyBPC does not seem to dimerize. Domains cC0, cC1 and cC2 all show a phenylalanine residue at the N-terminus, in a poorly structured part of the protein, that is involved in the formation of the  $\beta$  bulge. Other human cMyBPC domains show the same kind of pattern, with an aromatic residue, either phenylalanine or tyrosine, positioned at the N-terminus, a fact that might suggest that more IgI domains of cMyBPC will present this feature in their structure. On the other hand, this is not true for domain cC5 that has a characteristically

enlarged  $\beta$  bulge. It is possible that the presence of an aromatic residue that anchors the N-terminus of the protein to its hydrophobic core is an important aspect of IgI domains structures.



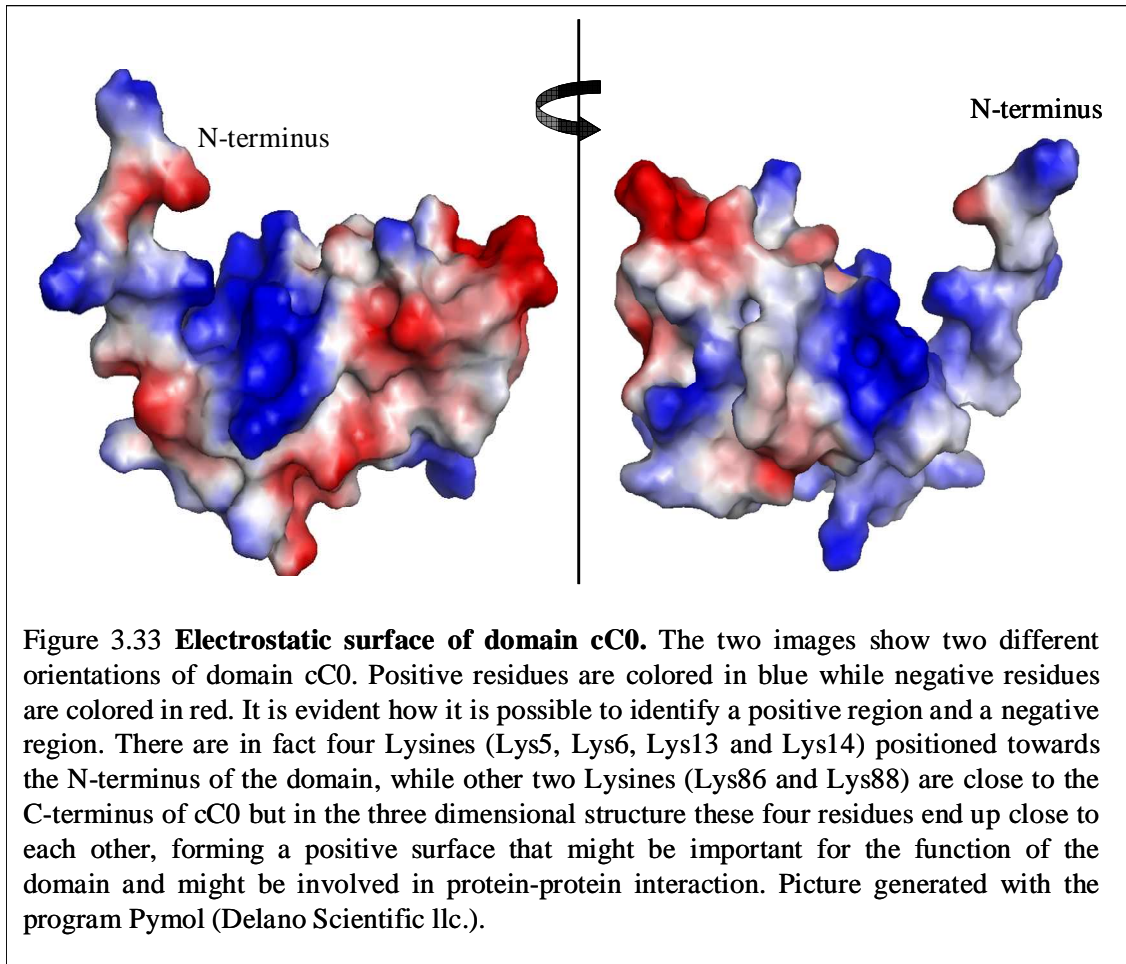
The tyrosine corner is also present in many IgI structures, being absent only in domain cC1 of cMyBPC, and, in domain cC0, is caused by the formation of an hydrogen bond between the  $-OH$  group positioned on the aromatic ring of Tyr78 and the carboxyl group on the sidechain of Asp 74. The distance between the two atoms involved resulted being  $3.84\text{\AA}$ , compatible with the formation of an hydrogen bond between the two. The Tyr corner (Hemmingsen et al., 1994) is a conformation in which a tyrosine near the beginning or the end of an antiparallel  $\beta$ -strand makes an hydrogen bond from its side-chain  $-OH$  group to the backbone NH and/or CO of residue  $Y - 4$  ( $\Delta 4$  Tyr corner).  $Y-2$  is almost always a glycine, which helps the backbone curve around the Tyr

ring, residue Y - 3 is usually a proline and Y - 5 is an hydrophobic residue, in this case it is an alanine, that packs next to the tyrosine ring.



The CD loop tends to be the longest loop in MyBPC IgI domains and usually accommodates additional elements of secondary structure, like C' strands, found in cC0 and cC2, or  $\alpha$  helical turns, as in domain cC1; the CD loop found in the central domain cC5 is even more peculiar as it is 40 residues long, compared to the 12-15 residues that form this loop in domains cC0, cC1 and cC2, and it contains the 28 amino acid insertion that makes the cardiac isoform of cC5 so unique. This loop is thought to play an important role in protein function, especially when it shows aromatic residues, as in cC1 and cC5, the latter also posses a Pro- rich region that could contribute to the domain function too (Idowu et al., 2003). The CD loop of domain cC1 comprises a tryptophan

residue (Trp196) that is affected by the interaction with the S2Δ fragment (Ababou et al., 2008). The CD loop of domain cC0 is probably not involved in a protein interaction as it does not show any of these features.



Apart from the short strand A positioned in the  $\beta$ -bulge, the N-terminus of cC0, which comprises residues 1-11, is highly unstructured; this is the only poorly defined part of the domain, as shown in figure 3.8 where a family of the first 20 structures is shown. This could be an important aspect linked to cC0 function as the N-terminus could be able to reach out to interact with another muscle protein component; this hypothesis is also supported by the presence of three proline residues, Pro1, Pro2 and Pro7, that might be involved in protein- protein interaction. This region also contains two of the five

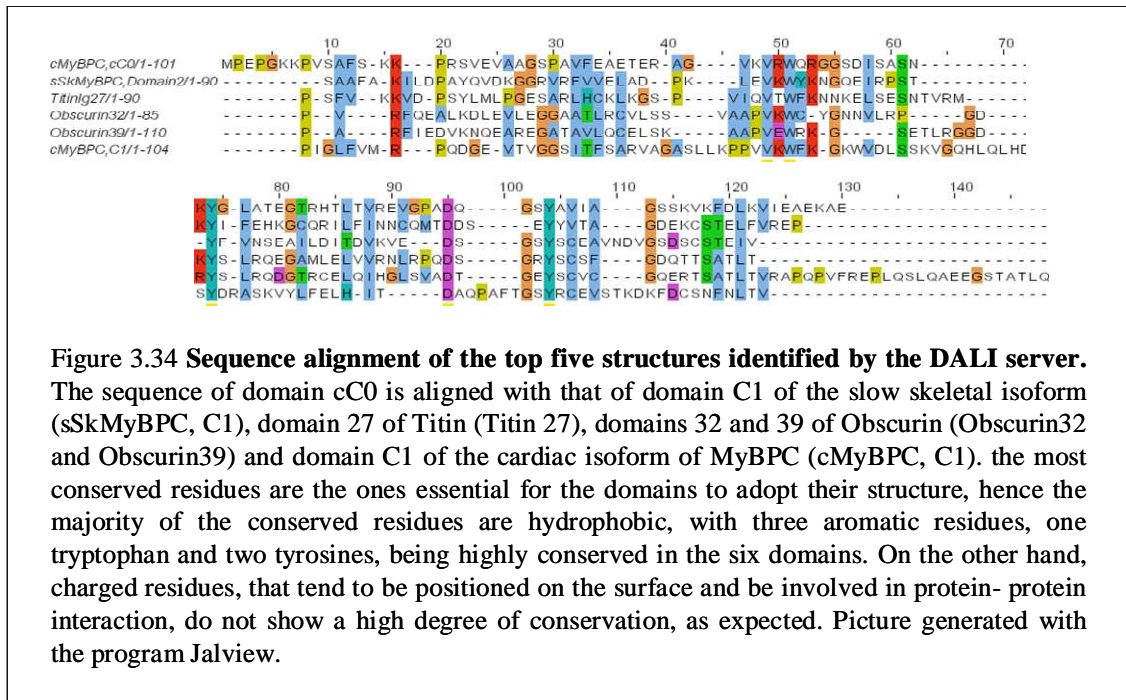
positively charged residues localised at the N-terminus of the protein, indicating a second possible way of interaction via charged amino acids.

The electrostatic surface for domain cC0 was determined using the program Pymol and is shown in picture 3.30: as expected on analyzing the sequence, domain cC0 shows an excess of positive charges, especially on the N-terminus side of the protein, as six Lysine residues, Lys5, Lys6, Lys13, Lys14, Lys86 and Lys88 are close in space in the structure. Another positively charged residue positioned in the vicinity is Arg16, which is located right at the end of the  $\beta$ -bulge. On the other hand the residues positioned at the C-terminus of the protein are predominantly negative, hence the red patch visible in the picture. Interestingly, two of the three HCM mutations found in this domain appear to involve charged residues, either mutating a charged residue to an uncharged one, as in Arg34Trp, or vice versa to mutate an uncharged residue to a charged one, as the case of Gly4Arg. Both these mutations could affect the binding of cC0 through electrostatic interaction, causing the onset of the disease.

A search using the DALI server (Holm and Park, 2000) was performed to identify the proteins with the most similar structure to cC0 present in the Protein Data Bank; the best fit are reported in the table below.

#	Protein	Pdb entry	z-score	RMSD	Sequence % identity
1	sSk MyBPC, domain C2	2yxm	14	1.9	27
2	Titin 27 <sup>th</sup> domain	1waa	14	1.9	28
3	Obscurin 32 <sup>nd</sup> domain	2yz8	13.3	1.8	26
4	Obscurin 35 <sup>th</sup> domain	2edt	13.1	2.2	25
5	Obscurin 39 <sup>th</sup> domain	2edl	12.7	3.9	25
6	cMyBPC, domain cC1	2v6h	12.7	1.9	27
7	sSk MyBPC, domain C3	1x44	12.4	2.8	21
8	sSk MyBPC, domain C1	2dav	12.1	2.3	20
9	sSk MyBPC, domain C4	2yuz	11.9	2.4	16

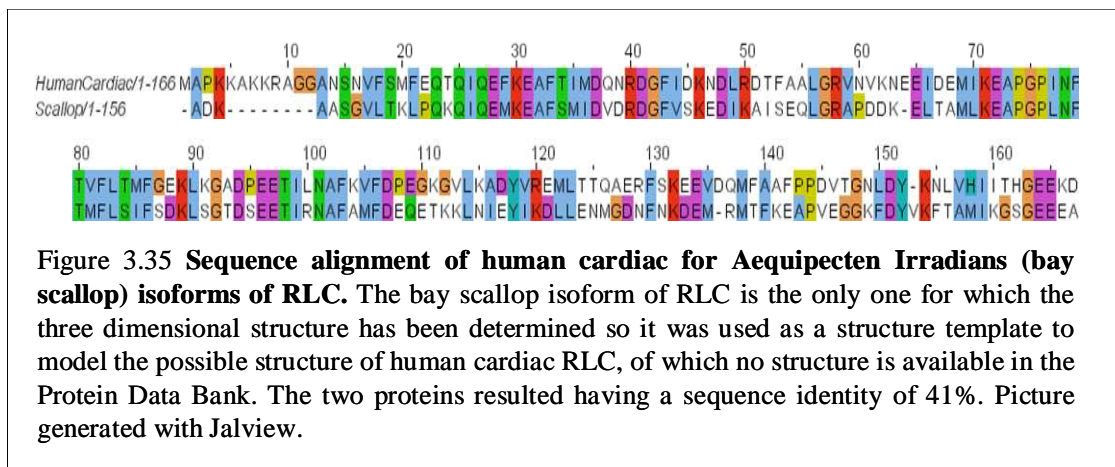
**Table 3.6: DALI results. Proteins with the most similar structure to domain cC0 within the Protein Data Bank.**



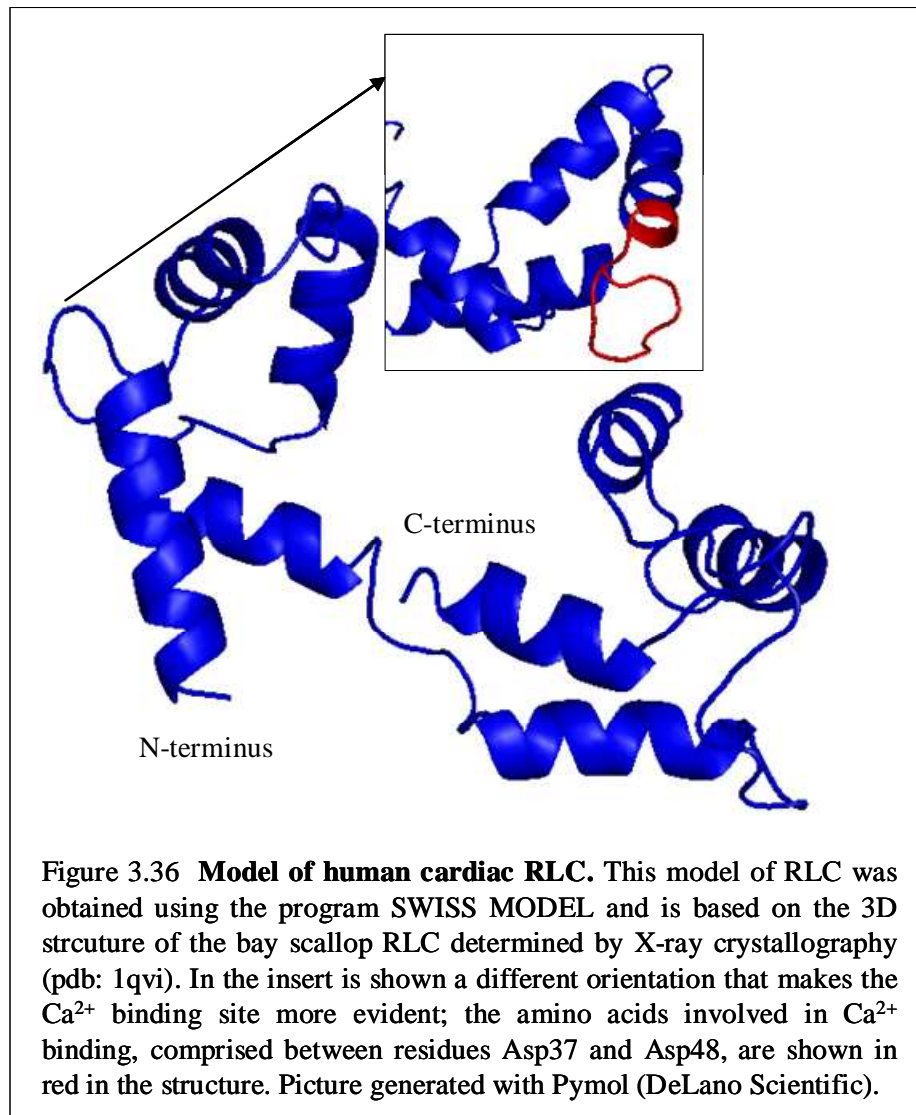
### 3.2.2 Characterization of the interaction between domain cC0 and the Regulatory Light Chain of Myosin

The preliminary results obtained via Differential Scanning Calorimetry showed that domain cC0 was interacting with the miniHMM fragment of Myosin, as well as domains cC1 and cC2 (data not shown); it has since been demonstrated that these two cMyBPC domains interact with the S2Δ fragment of myosin that is part of miniHMM, cC1 close to the junction between the myosin rod and the neck region of the myosin head (Ababou et al., 2008) and cC2 more towards the rod region of Light MeroMyosin (LMM) (Ababou et al., 2007) using both NMR spectroscopy and site directed mutagenesis investigation. Using DSC our collaborator at King's College was able to narrow down the binding partner of domain cC0, showing that the interaction occurred with the Regulatory Light Chain of myosin. These results were both confirmed using <sup>1</sup>H/<sup>15</sup>N HSQC NMR spectroscopy on <sup>15</sup>N labelled samples of domain cC0 with both

miniHMM and RLC. No structure of human cardiac RLC is at present available in the Protein Data Bank, however a model of the structure of the RLC was produced using the Swiss Model server (Arnold et al., 2006) based on the deposited structure obtained from bay scallop [*Aequipecten Irradians*] (Swiss Prot: P13543; PDB code: 1qvi) that resulted having a sequence identity of 41% with that of the human ventricular isoform used in this research (Swiss Prot: Q14908).

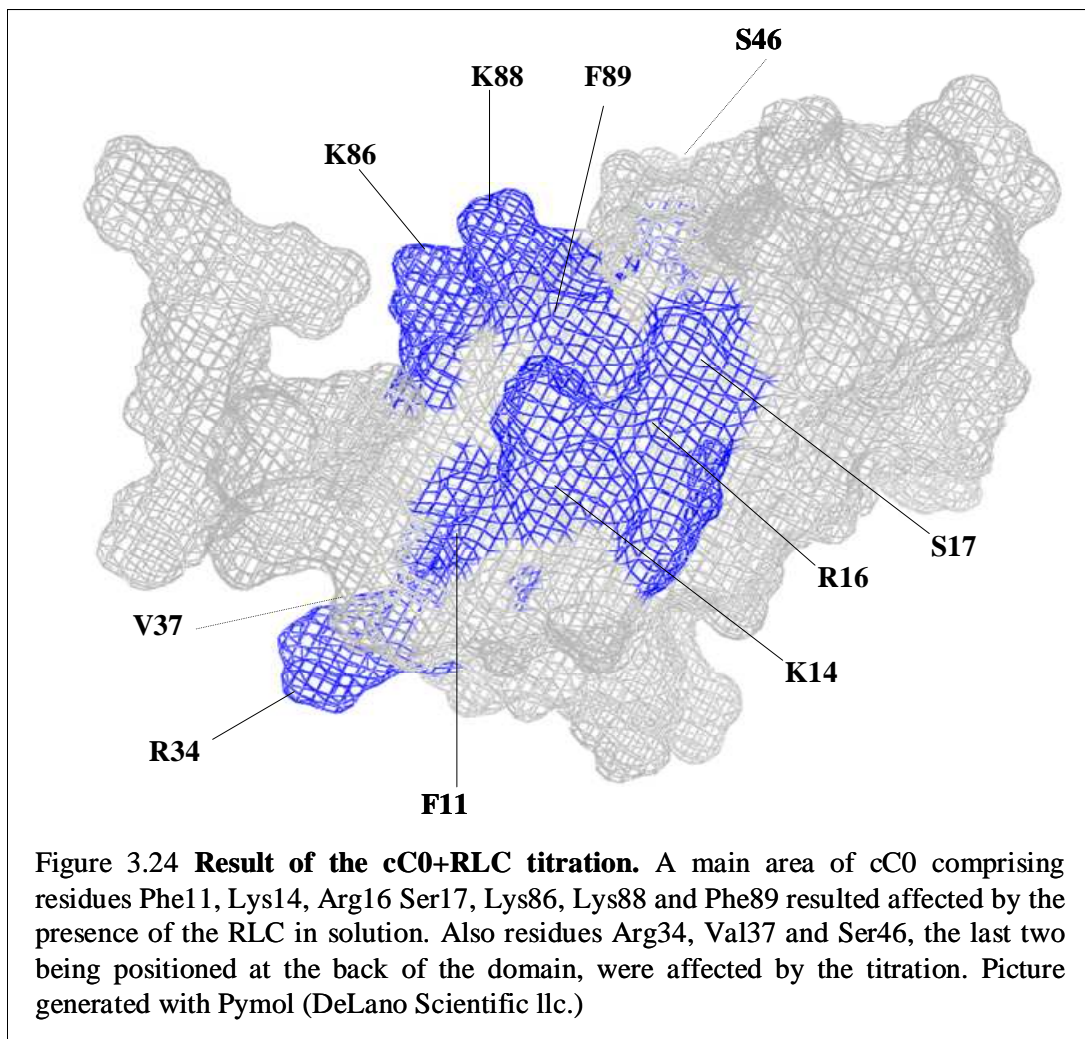


The model structure obtained in this way is reported in figure 3.31. The regulatory light chain is a member of the superfamily of EF-hand  $\text{Ca}^{2+}$  binding protein, even though it has lost its ability to bind to  $\text{Ca}^{2+}$  in sites 2, 3 and 4 (Moncrief et al., 1990) and presents only one high affinity binding site at the N-terminus (Reinach et al., 1986), between residues 37 and 48 (Szczena et al., 2001), shown in red in the insert of picture 3.33. It also has a phosphorylation site (S15) at the N-terminus of the protein not visible in the model as not defined in the pdb file deposited, being positioned in a poorly structured region not detected by x-ray crystallography.



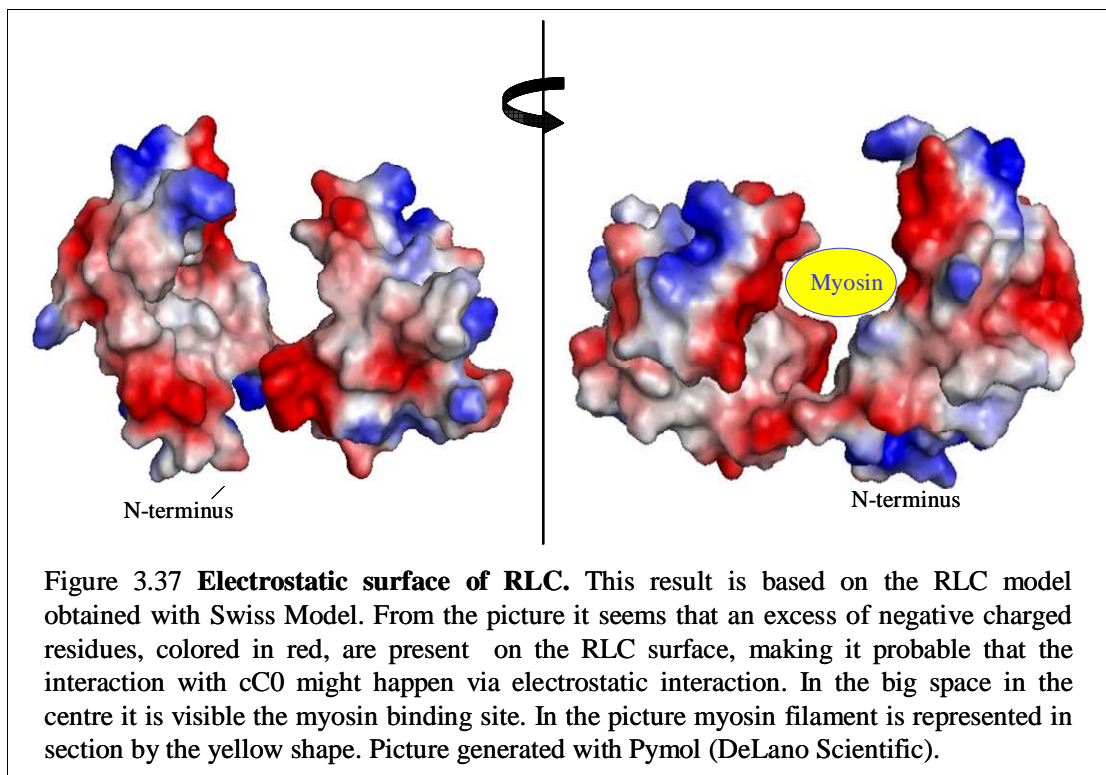
From the experimental results based on a titration of RLC in a sample of <sup>15</sup>N labelled cC0 followed by <sup>1</sup>H/<sup>15</sup>N HSQC NMR spectroscopy, it was possible to identify the residues involved in the interaction and map them on cC0 structure.

A region towards to N-terminus of the protein is clearly affected by the incremental additions of RLC, suggesting that these residues are involved in the interaction.



Within the residues most affected by the addition of RLC are Phe11, Lys14, Arg16, Ser17, Lys86, Lys88 and Phe89 that form a sort of interaction surface clearly visible in the above figure. Interestingly the two residues involved in the  $\beta$ -bulge, Ser12 and Lys13, are not affected by the presence of the RLC, even though they are positioned very close to the two residues that show the biggest shifts in the  $^1\text{H}/^{15}\text{N}$  HSQC spectra, Lys14 and Arg16. Also residue Arg34 that when mutated to Tryptophan causes HCM, seems to be affected by the presence of RLC, as confirmed by the mutagenesis studies carried out: Arg34, together with residues Val37 and Ser46, is positioned on the back surface of the domain. The two N-terminal lysine residues, Lys5 and Lys6, do not show any change in peak position during the titration, so it is unlikely that the mutation

Gly4Arg could cause HCM due to interference in the cC0-RLC interaction, as shown by the experiment carried out with the mutant cC0\_G4R that showed a total diminished interaction with the RLC. . Given the nature of the residues that resulted more affected by the titration, it is very likely that this interaction would happen via electrostatic interface between the two proteins, this hypothesis being based also on the observation that the RLC has an excess of negative charge, while cC0, on the contrary, posses more positive charged residues in its sequence, as visible in figure 3.32 where the electrostatic surfaces for the RLC model are shown, as obtained with the program Pymol.



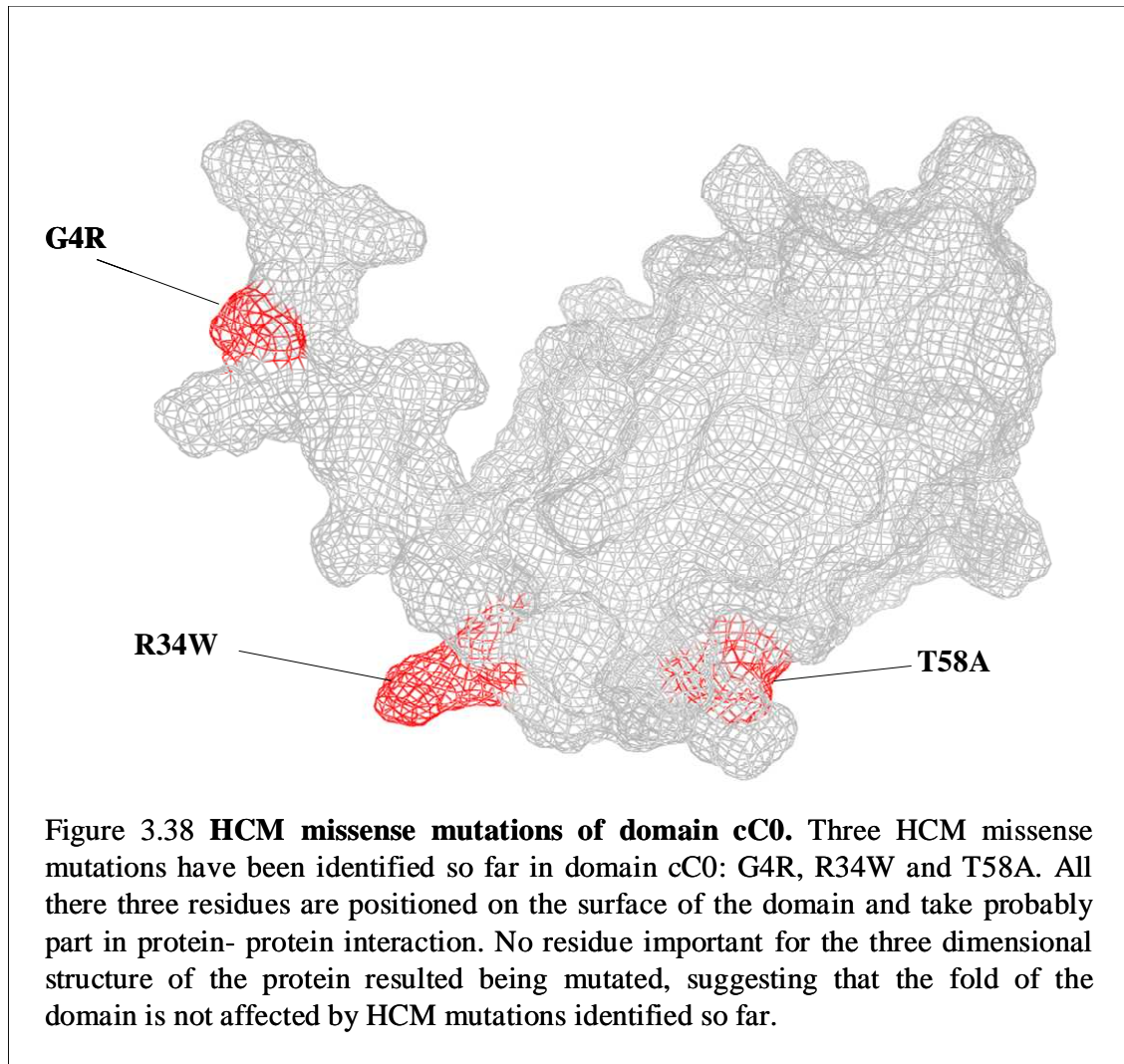
The big clef in the middle is occupied by the myosin molecule, shown in yellow in the figure. A possible binding site for domain cC0 is the external surface on the N-terminus lobe of the protein, characterised by the presence of a negative charged residues patch. However, no HCM mutations were found in this region to confirm this hypothesis.

### 3.2.3 Hypertrophic CardioMyopathy (HCM) missense mutations in domain cC0 of cMyBPC

As already mentioned, three HCM missense mutations have been identified in domain cC0: G4R (Van Driest et al., 2004), R34W (<http://genepath.med.harvard.edu/~seidman/cg3/>) and T58A (Niimura et al., 2002). G4R is reported in one single case in association with a second mutation, R502W found in domain cC3, with an age onset of  $20.7 \pm 11$  years and a left ventricular wall thickness (LVWT) of  $25.2 \pm 12$  mm; the phenotype resulted being quite severe as in all the combined mutations analysed in the reported study (Van Driest et al., 2004). Mutation T58A, on the other hand, showed a mild phenotype, causing HCM in elderly patients with an average age of onset of  $56 \pm 13.2$  years and a LVWT of  $22.7 \pm 5.5$  mm. For the third mutation no published report was found apart from the direct submission to the HCM mutation database so anything is at present known on the clinical effects of this mutation.

Mapping the mutation on cC0 three dimensional structure it was evident how all these three residues are localised on the surface of the protein (Figure 3.38), probably causing disease when mutated by interfering with protein- protein interaction; no hydrophobic residue central to the domains stability resulted being mutated suggesting that the fold of the domain is not affected by HCM mutations identified so far.

Arg34 is also one of the residues affected by the RLC titration, and it has been shown in the present work that the mutation R34W disrupts the electrostatic interaction taking place between the two binding partner; unfortunately, being absent any reference to clinical observation concerning this mutation, it is not possible to have a clear idea of the mutation severity, that one could be inclined to assume as severe, based on the nature of mutation itself.



The third mutation Thr58Ala was not studied through mutagenesis due to the mild phenotype shown by this mutation and also because of the fact that in the majority of species the cardiac isoform of cC0 presents an Ala in position 58 and not a Thr as in the human isoform. For this reason it is improbable that this mutation could cause a loss in stability of the domain or a diminished interaction with another sarcomeric protein.

#### 3.2.4 Model of the incorporation of cMyBPC N-terminus in the sarcomere

It has been shown (Ababou et al., 2007; Ababou et al., 2008) that domains cC1 and cC2 bind to the S2 $\Delta$  fragment of myosin, which comprises residues from 838 to 936, domain cC1 at the N-terminus of S2 $\Delta$ , towards the hinge region of myosin, and cC2 very close

to cC1 a bit toward the C-terminus of the fragment. The long linker between the two domains containing the three phosphorylation sites, is proposed as running parallel to the myosin heavy chain forming a sort of U shape, from domain cC1 to domain cC2. This places cC1 close to the hinge and the regulatory light chains. Domain cC0 has been shown to interact with the regulatory light chain and to do so through its N-terminal surface, on the other hand, domain cC1 is shown to interact with S2 $\Delta$  via its C-terminal surface, suggesting that these two domains could be positioned obliquely linking the myosin rod and the regulatory domain. It has been suggested that cC0 (Kulikovskaya et al., 2003), or more probably the linker between cC0 and cC1 (Squire et al., 2003), could interact with actin and this could happen stretching this part of MyBPC to reach for actin, possibly when the interaction between the N-terminus of MyBPC and the light chain is abolished.

It is clear how cMyBPC would be capable of regulating muscle contraction from this position, potentially adjusting the position of the S1 myosin head through its interaction with the regulatory light chain. It is probable that the phosphorylation of cMyBPC sites positioned in the linker does not cause dissociation of the N-terminus of the protein from myosin; the dissociation of the linker and domain cC2 from their position assumed in the un-phosphorylated form could be sufficient to allow the S1 myosin head to reach for actin causing muscle contraction.

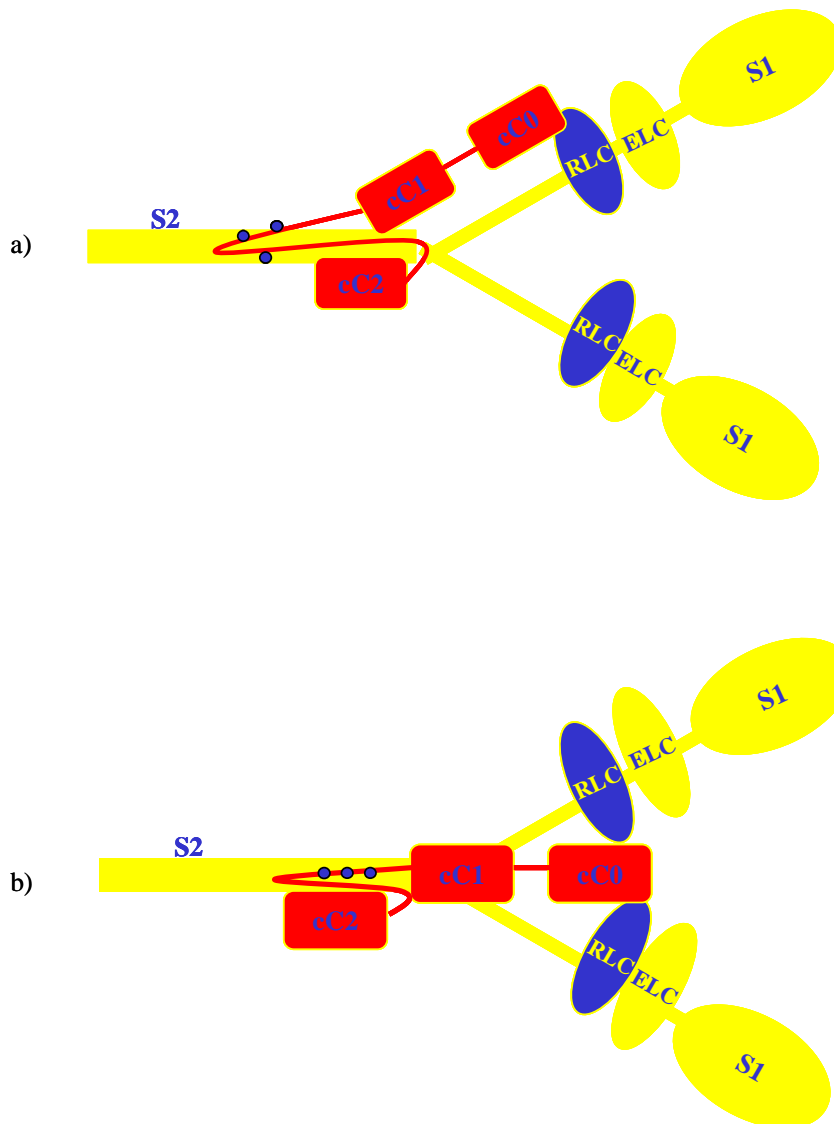
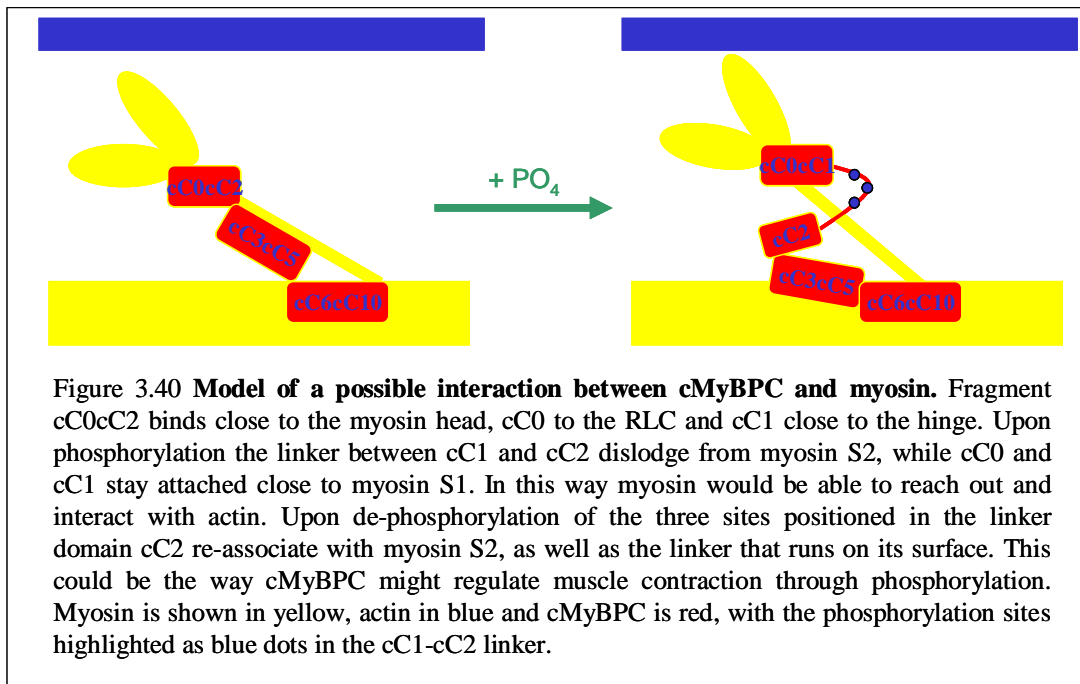


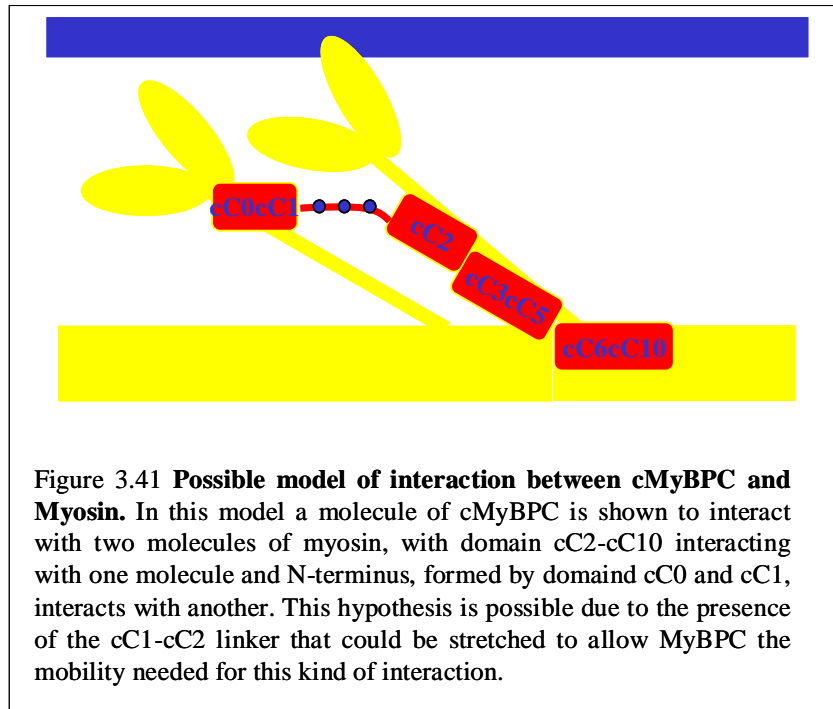
**Figure.3.39 Model of the interaction between the N-terminus of cMyBPC and Myosin.** a) Domain cC0 interacts through its N-terminus surface with the regulatory light chain of myosin; domain cC1 has been shown to interact through its C-terminus in the hinge region between S2 and S1 while domain cC2 interacts with S2 a bit far off the hinge region. The long linker between cC1 and cC2 that contains the three phosphorylation sites, runs parallel to S2. b) Based of the observation that the interaction between cC0 and the miniHMM is stronger than the interaction with RLC alone, it is possible to hypothesize that cC0 could interact with two molecules of RLC instead of one. This hypothesis is based on NMR and mutagenesis studies (Ababou et al., 2007; Ababou et al., 2008) and on the results obtained with the resent research.

It is possible that upon phosphorylation the linker and domain cC2 would dislodge from myosin, while the N-terminus could remain attached, influencing the myosin head position during cross bridge formation. This would also facilitate domain cC2 and the linker to re-attach to S2 after de-phosphorylation, making S1 to go back to its resting

position. In this model, the N-terminus of cMyBPC is always attached to the myosin head region whose freedom of movement is adjusted by phosphorylation of the cC1-cC2 linker. This could be a valid way for regulating actomyosin interaction and, hence, muscle contraction.



It is also possible that due to presence of the linker between cC1 and cC2, one molecule of cMyBPC could interact with more than one molecule of myosin, as shown in figure 3.36. while cC2 interacts with the C-terminal region of S2 $\Delta$ , the cC1-cC2 linker could be extended to allow cC1 and cC0 with S2 $\Delta$  and RLC of the neighbouring myosin molecule.



In conclusion it is possible that cMyBPC could have two different functions, a regulatory function localised in its N-terminus and mediated by the interactions that have been shown taking place between domains cC0 and the RLC and domain cC1 with S2 close to the hinge between the S1 and S2 domains of myosin; a structural function is probably achieved by the C-terminal domains that bind to LMM coiled-coil region of myosin.

### 3.2.5 *Conclusions*

NMR spectroscopy was used to determine the three dimensional structure of the cardiac specific domain cC0 of cMyBPC, a part of this protein that has been poorly investigated in the past and of which little was known. The structure determined as part of this research work has confirmed that domain cC0 is a member of the IgI class of proteins and it shows a well defines structure with many of the characteristic features of this type of molecules. Moreover, the data obtained during this research confirmed the hypothesised interaction between cC0 and the Regulatory Light Chain (RLC) of myosin, thus placing the N-terminus of the protein in proximity of the motor domain of myosin, as suggested by the studies carried out on domains cC1 and cC2 (Ababou et al., 2007; Ababou et al., 2008), and it was confirmed by the results of the mutagenesis studies. In conclusion, this research has offered new insight on how cMyBPC incorporate in the sarcomere and how it could contribute to the regulation of muscle contraction.

## Chapter 4

### Study of the interaction between domains cC5 and cC8 of cMyBPC

#### 4.1 Results

As discussed in the general introduction, it has been suggested that domains cC5 and cC8 of the cardiac isoform of MyBPC might interact with each other. This hypothesis was based on yeast two hybrid assay results (Moolman-Smook et al., 2002). One of the goals of my research was to confirm this result using NMR spectroscopy, taking advantage of the fact that the structure of domain cC5 has been determined few years ago (Idowu et al., 2003). It would have been possible, then, to map the cC5 surface involved in the interaction with cC8.

##### 4.1.1 cC5 protein expression and purification

Expression and purification of domain cC5 was easy to perform, for both labelled and unlabelled samples. The DNA sequence coding for cC5 has been cloned in vector pET-8C and then inoculated in *E. Coli* host cells BL21 STAR (DE3) (from Invitrogen). The domain was expressed in M9 medium, enriched with  $^{15}\text{N}$  to produce singularly labelled samples in order to perform a titration following the changes in  $^1\text{H}/^{15}\text{N}$  HSQC spectra, giving a yield around 10 mg/l. The protein was cloned such as it presents a hexahistidine tag at the N-terminus, to allow purification by Immobilized Metal ion affinity chromatography (IMAC), further purification was then achieved by size exclusion chromatography.

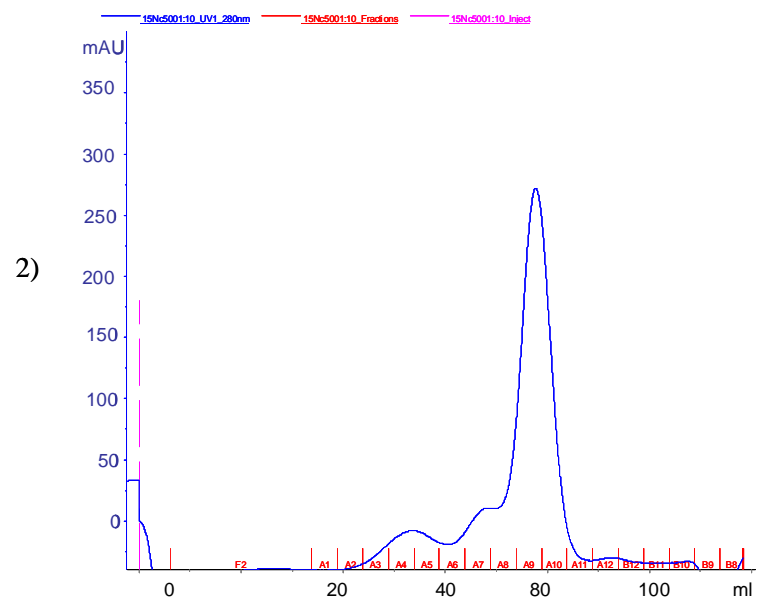
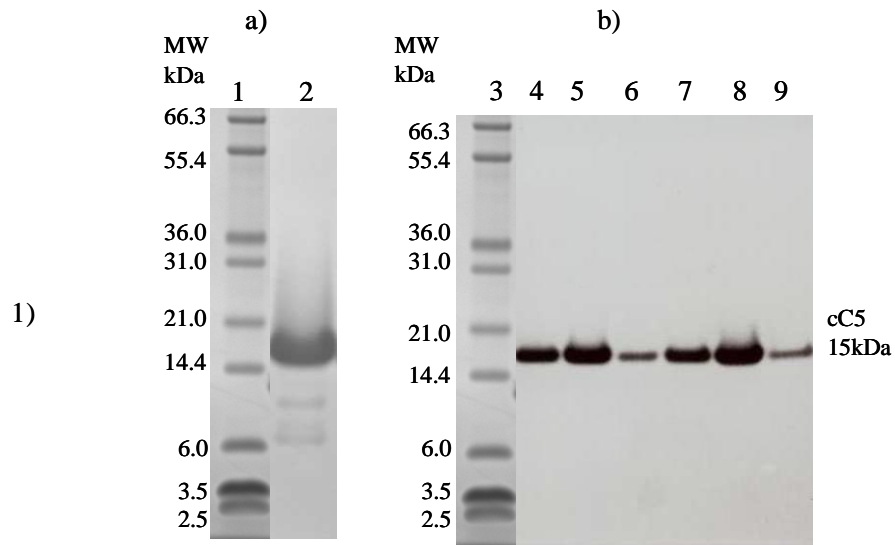


Figure 4.1 **Purification of cC5.** 1a, b) Purification of domain cC5 by Immobilized Metal ion Affinity Chromatography (IMAC) and size exclusion chromatography. In lane 1 and 3 of the SDS-PAGE gels is visible the marker, in lane 2 is cC5 obtained by Ni- column purification and in lanes 4-9 the gel filtration fractions A8, A9 and A10 for two different runs; 2) Chromatogram resulting from Size exclusion chromatography. cC0 is present in fractions A8, A9 and A10, and these fractions have been pooled together.

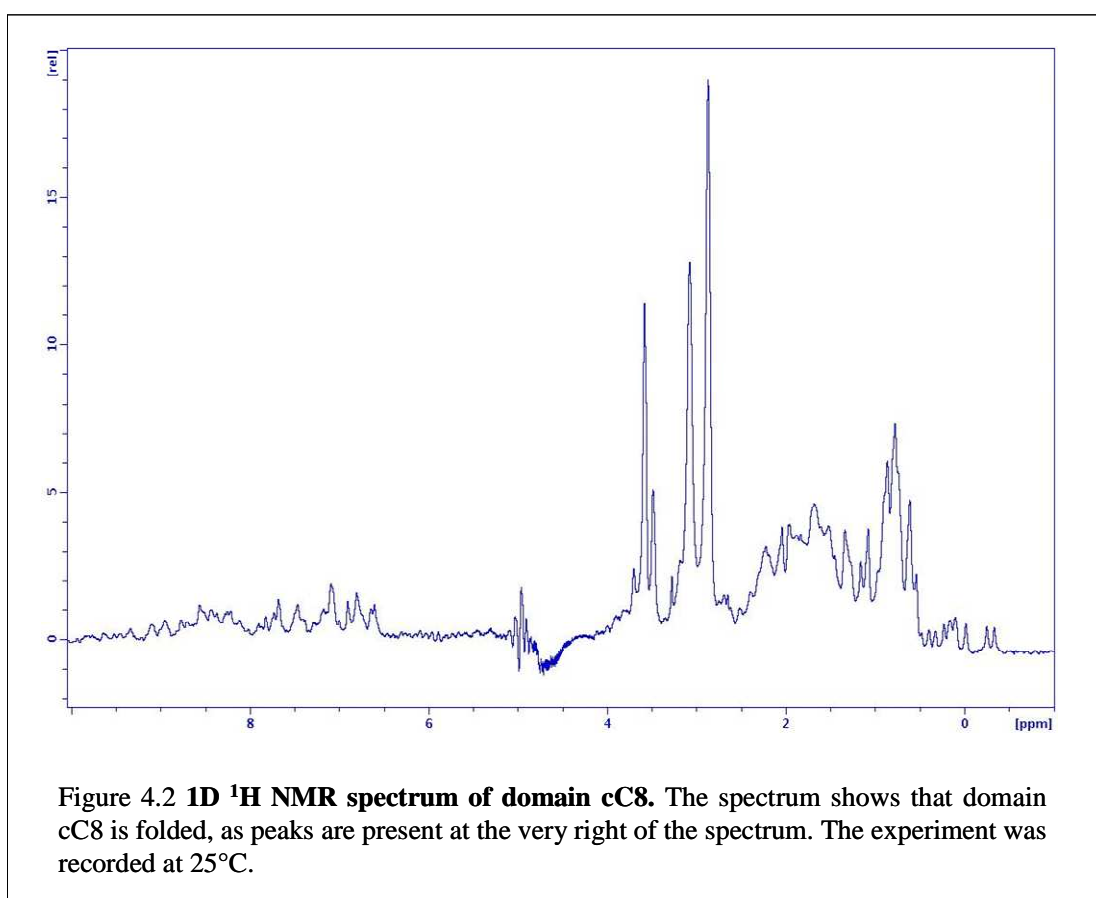
#### 4.1.2 *Expression of domain cC8*

Domain cC8 was cloned in pET-8C vector and inoculated in BL21 STAR (DE3) cells (from Invitrogen) but the expression proved difficult from the start. The protein synthesised was insoluble and tended to precipitate in inclusion bodies. A refolding procedure was then followed, using the two different protocols, a long method and a short one, as described in the material and methods (section 2.2.5).

#### 4.1.3 *Is domain cC8 properly folded?*

To confirm if a protein is folded, it is possible to perform a 1D  $^1\text{H}$  NMR experiment. The resulting spectrum for domain cC8 is of a higher order and it is not possible to interpret and assign it, but in some regions at the far end of the spectrum, specially just below zero, it is possible to identify peaks characteristic of folded proteins. Proton signals of organic compounds are usually positive, as the standard molecule TMS is arbitrarily placed at zero and is very unusual to have nuclei more shielded than the  $-\text{CH}_3$  groups attached to an atom of Silicon; in proteins, however, the  $^1\text{H}$  nuclei of residues buried in the hydrophobic core will be more shielded than the rest and will tend to be at negative chemical shifts if positioned near aromatic rings that interfere with their ring currents. This is due to the presence of  $\pi$  electrons in the aromatic rings. When there are electrons circulating, as in aromatic rings and in compounds with double or triple bonds, they will cause local magnetic fields that will reduce or increase the total magnetic field perceived by the nuclei, according to their position in space. The shielding region of aromatic rings is positioned above and underneath the ring, the so called plus region, while nuclei positioned on the ring plane will be de-shielded as the force line of the

magnetic field induced by the electronic currents will be added to the external magnetic field and so the total magnetic field will be stronger for these nuclei than for the rest. For this reason, nuclei positioned in the plus region of an aromatic ring, will give signals at low chemical shifts, while aromatic  $^1\text{H}$  nuclei are typically positioned between 6 and 8 ppm. If peaks at negative chemical shifts are present, it is reasonable to think that the protein is folded.



The amount of protein obtained after refolding was always quite small and it had a tendency to disappear during dialysis and concentration steps, suggesting that it might be misfolded, with some hydrophobic residue exposed on the surface. I have at this point, investigated the stability of domain cC8 after the refolding procedure.

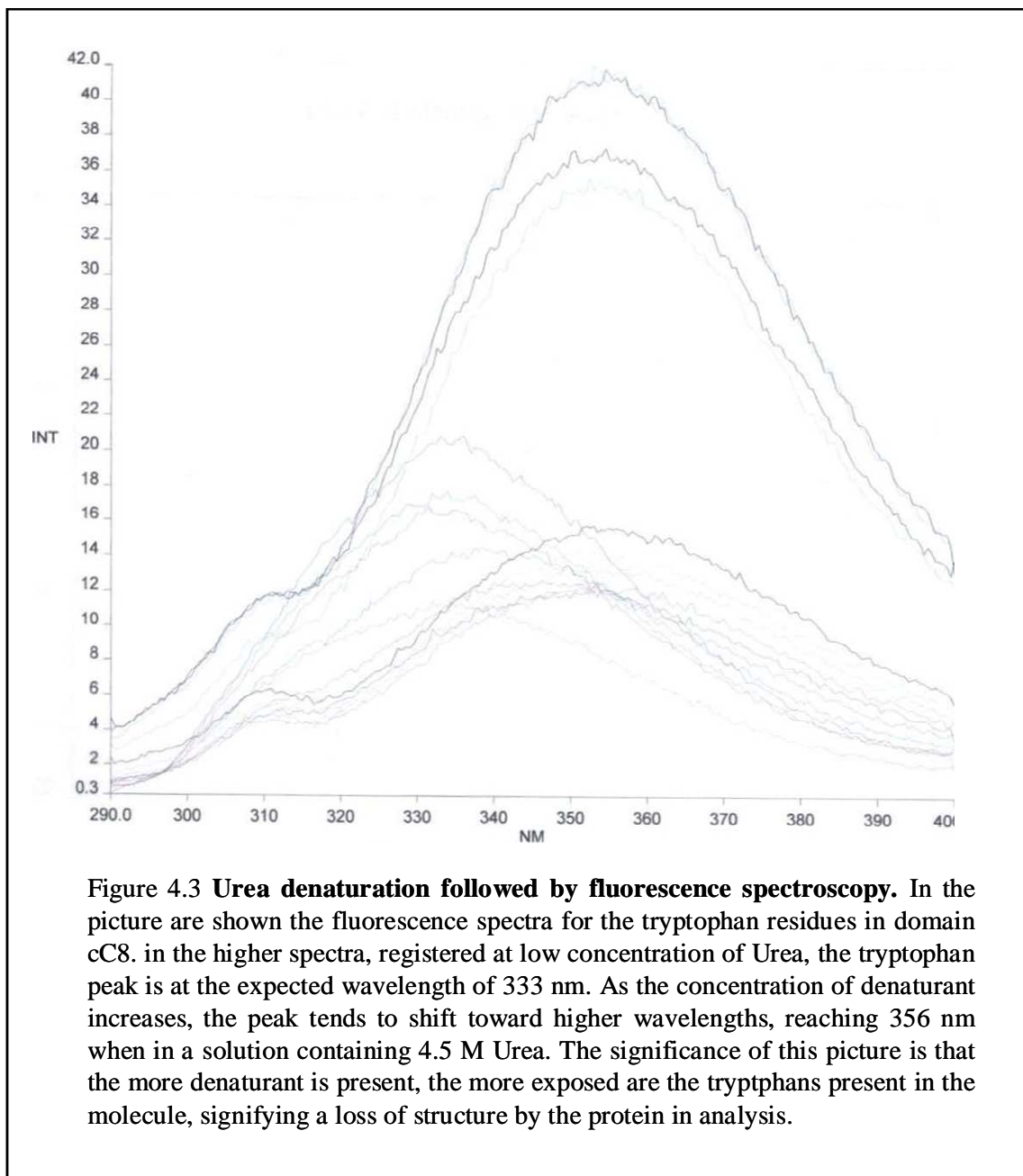
#### 4.1.3.1 Urea denaturation

To understand whether the protein was folded, a denaturation was performed, using different amount of urea, and followed by fluorescence spectroscopy. The main fluorophore in proteins is the indole side chain of the amino acid tryptophan, that gives a signal between 300 and 400 nm. In particular, when a tryptophan is buried in the hydrophobic core of a protein, it gives a characteristic signal around 330 nm, while in an unfolded protein its signal is localised around 350 nm. This difference in the fluorescence spectrum is usually sufficient to understand if a protein is folded or not, as tryptophans play an important role in stabilizing the core of the protein, giving many interactions with other amino acids, and are very rarely found on proteins surfaces being hydrophobic residues. The final concentration of cC8 used in this analysis was 2 $\mu$ M for each sample for 1 ml of total volume. All the steps of this experiment are reported in the table 4.1.

<b>[Urea] M</b>	<b>Wavelength (nm)</b>
0	333
0.5	333
1	333
1.5	335
2	340
2.5	347
3	352
3.5	352
4	352
4.5	356
5	356
5.5	356
6	355
6.5	354
7	353
7.2	352
7.6	351

**Table 4.1: Urea denaturation of domain cC8**

A fluorescence spectrum was recorded for each sample of the series reported in the table and the results were compared, as shown in picture 4.3.



The fluorescence spectra show the tryptophan residue in domain cC8. In the first spectra, registered at low concentration of urea, the tryptophan peak is at the expected wavelength of 333 nm. As the concentration of denaturant increases, the peak tends to shift toward higher wavelengths, reaching 356 nm when in a solution containing 4.5 M

urea and higher. This means that the more denaturant is present, the more exposed is the tryptophan residue present in the molecule, signifying a disruption of the hydrophobic core . This is compatible with a protein that is folded at the beginning of the procedure and loses its fold as the concentration of denaturant increases.

Using the program MATHEMATICA(Wolfram research) it was possible to fit the experimental data creating a diagram of the absorbance against urea concentration.

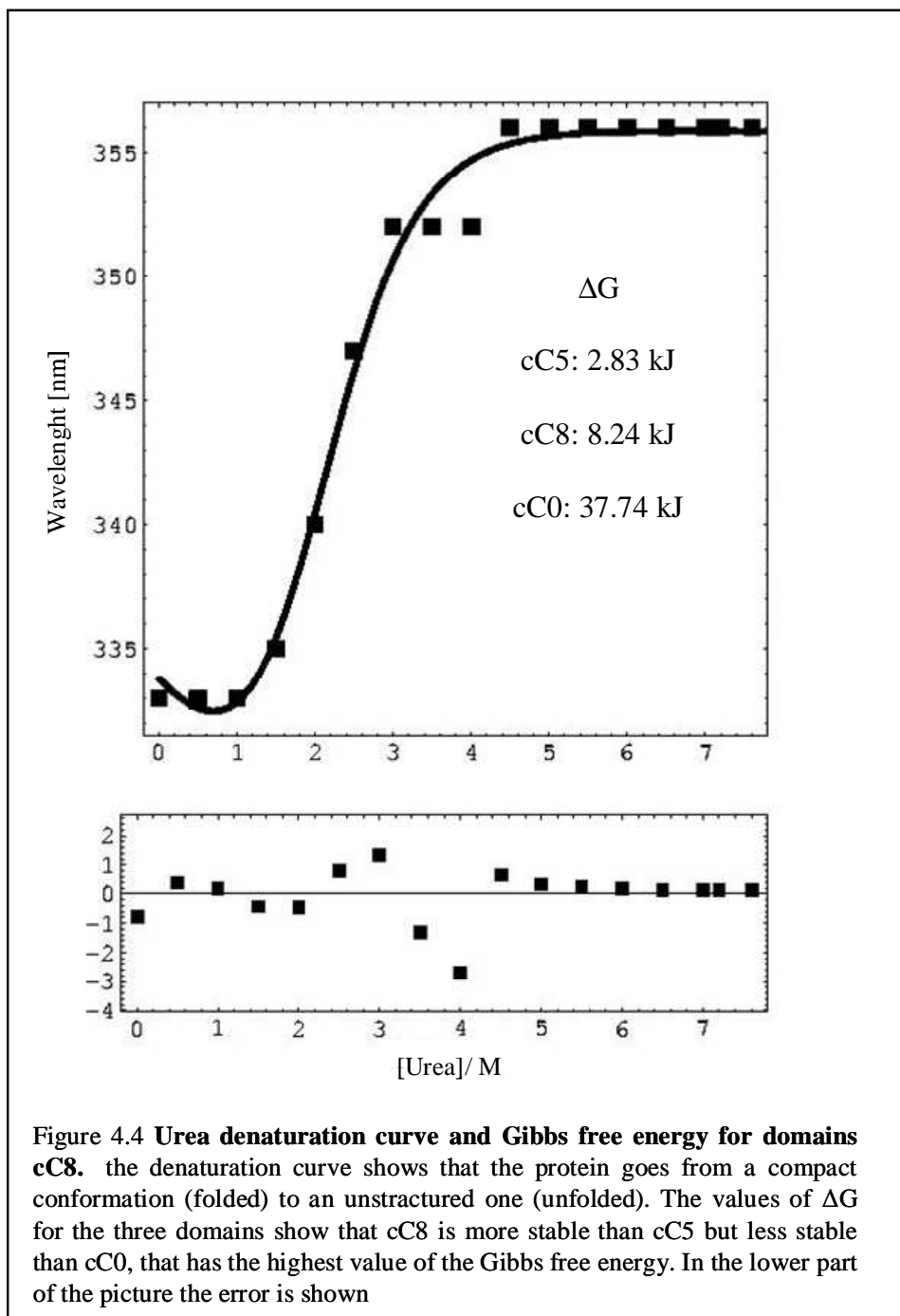


Figure 4.4 Urea denaturation curve and Gibbs free energy for domains cC8. the denaturation curve shows that the protein goes from a compact conformation (folded) to an unstructured one (unfolded). The values of  $\Delta G$  for the three domains show that cC8 is more stable than cC5 but less stable than cC0, that has the highest value of the Gibbs free energy. In the lower part of the picture the error is shown

The fitting was performed on the basis of the two- state equilibrium hypothesis and the equation used is the following:

$$F_f = \frac{(F + S_f X) + (U + S_u X) e^{-\left(\frac{\Delta G - S_u X}{RT}\right)}}{\left(1 + e^{-\left(\frac{\Delta G - S_u X}{RT}\right)}\right)}$$

Where  $F_f$  is the folded fraction,  $F$  is the signal for the folded fraction,  $U$  is the signal for the unfolded fraction,  $S$  represents the slope of the curve at either the folded or the unfolded state and  $X$  is the urea concentration.

The curve resulting from this analysis is similar to sigmoid, showing that the tryptophan residue contained in domain cC8 is buried in the hydrophobic core of the protein at low concentration of denaturant, as shown by the fluorescence absorbance of 333 nm, but tends to be exposed at increasing concentrations of urea, to reach a maximum at concentration of urea 4.5M. After this point the absorbance does not increase any further even at higher concentrations of urea, meaning that the domain has lost its structure and is fully denatured. With the program Mathematica it was also possible to calculate the Gibbs free energy, that resulted, for the process of denaturation of domain cC8, corresponding to 8.24 kJ. The Gibbs free energy ( $\Delta G$ ) is associated with the thermodynamic stability of a given molecule and tells us if a process is favoured or not. The same quantity has been previously calculated for other domains of c-MyBPC and so it was possible to compare the same value for different domains of the same protein, comparing in this way the stability of domain cC8 with the stability of known domains.

#### 4.1.3.2 1D <sup>1</sup>H NMR Melting curve

To study cC8 behaviour at different temperatures and to understand if the protein undergoes structural changes, a melting curve was performed, which consist in recording various 1D <sup>1</sup>H NMR spectra of domain cC8 at different temperatures. From the results, reported in picture 4.5, it is evident how the peak at -0.55 ppm in the spectrum recorded at 5°C, starts splitting in two at 15°C and how the two peaks grow more apart the higher the temperature rises. This signifies that something happens in the structure of domain cC8 which involves a residue buried in the hydrophobic core of the protein. This fact points towards an hypothesis that some major change takes place in the protein putting at risk its stability.

N°	Temperature (°C)
1	5
2	15
3	25
4	30
5	35
6	40
7	45
8	50
9	55
10	25

**Table 4.2: 1D NMR melting curve**

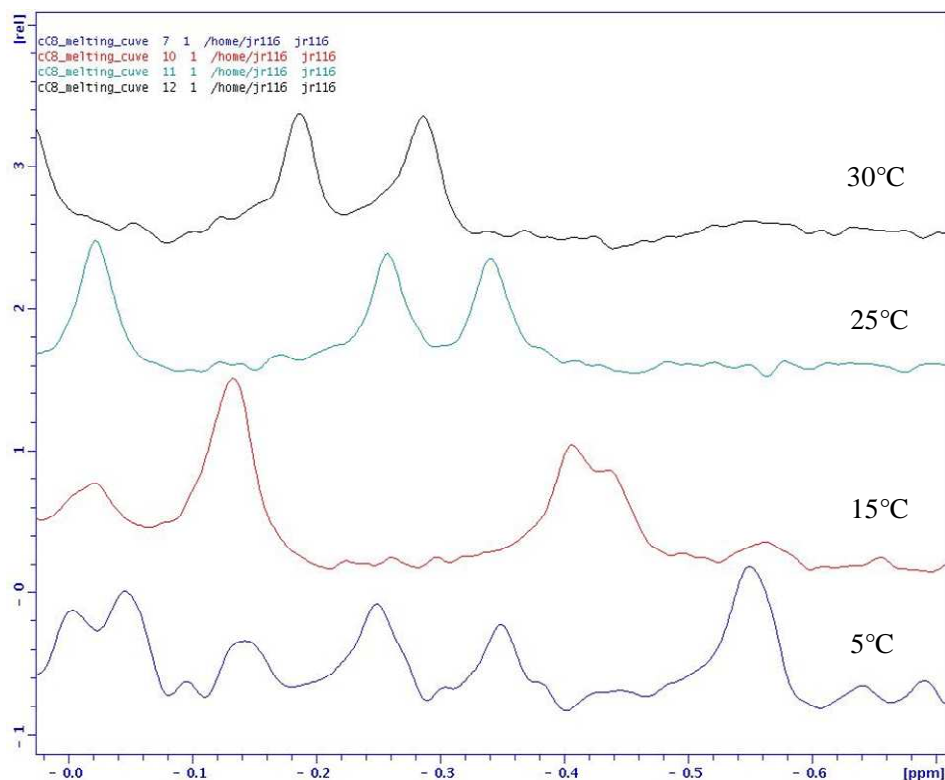


**Figure 4.5 Melting curve for domain cC8.** Four  $^1\text{H}$  1D NMR spectra have been acquired at four different temperatures. It is very evident that the peak at -0.55 ppm is a singlet at 5°C but starts splitting in two at 15°C. The two peaks move more apart the higher the temperature goes. This means that the protein is in two different conformations, at least some of its residues change chemical environment going from 5°C to higher temperatures. Moreover, this region at the very right of the spectrum, is where the signals of the internal residues, very shielded from the rest of the protein and so giving a signal at a high field. This means that the hydrophobic core of the protein is involved in this phenomenon.

From the results of both urea denaturation and melting curve, I concluded that cC8 produced by refolding of the insoluble synthesised protein has a fold but it is probably not the correct one. It is very likely that some of the hydrophobic residues of the sequence do not find a place in the hydrophobic core during the refolding and end up being exposed on the surface, causing the protein to stick to dialysis and concentrators membranes. The ideal solution to this problem would be to express domain cC8 as

soluble protein. This would avoid the refolding procedure, leading to the expression and purification of a protein properly folded.

#### 4.1.4 *cC8 expressed as a fusion protein*

The production of proteins by genetically engineered *E. Coli* is a well established technique, favoured by the fact that *E. Coli* has a relatively simple genetics, is well characterised and has a rapid growth rate. However, a possible disadvantage in expressing heterologous proteins in *E.Coli* is that these proteins could express as insoluble aggregated folding intermediates, known as inclusion bodies (Mitraki, 1989). A wide range of means have been exploited to increase the production of soluble protein, such as specific bacteria strains (Miroux and Walker, 1996; Prinz et al., 1997; Sauer and Nygaard, 1999), chaperone co-expression (de Marco and De Marco, 2004; de Marco et al., 2000), and modification of growth conditions. A further approach is to clone the gene of interest in vectors that offer the opportunity to fuse the target protein to a partner to increase its solubility (Kapust and Waugh, 1999; Makrides, 1996). Glutathione S-transferase (GST) (Nygren et al., 1994), maltose binding protein (MBP) (Pryor and Leiting, 1997) and thioredoxin (TrxA) (La Vallie, 2000) are the most popular fusion protein in use. In this research two fusion proteins have been produced, cloning the sequence coding for domain cC8 in two different vectors, pETM-20 to express cC8 as a fusion protein with TrxA, and pETM-60 to express a fusion protein with the *E.coli* protein NusA, that has been selected for its intrinsic solubility (De Marco et al., 2004) .

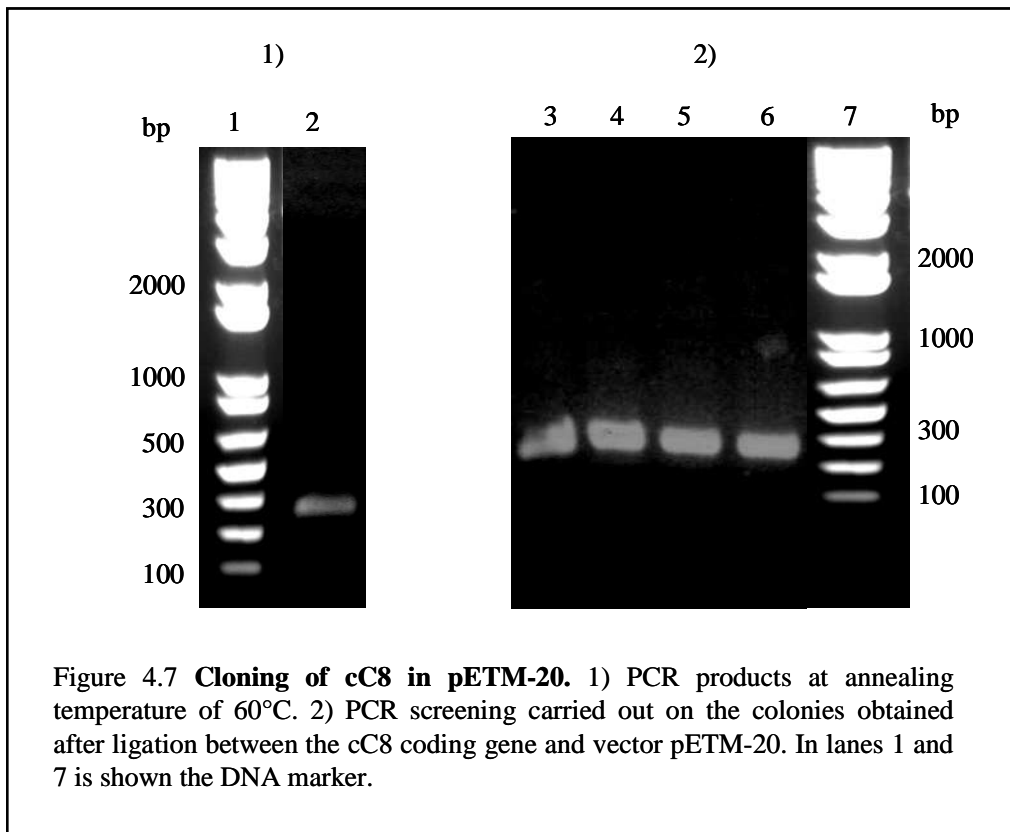
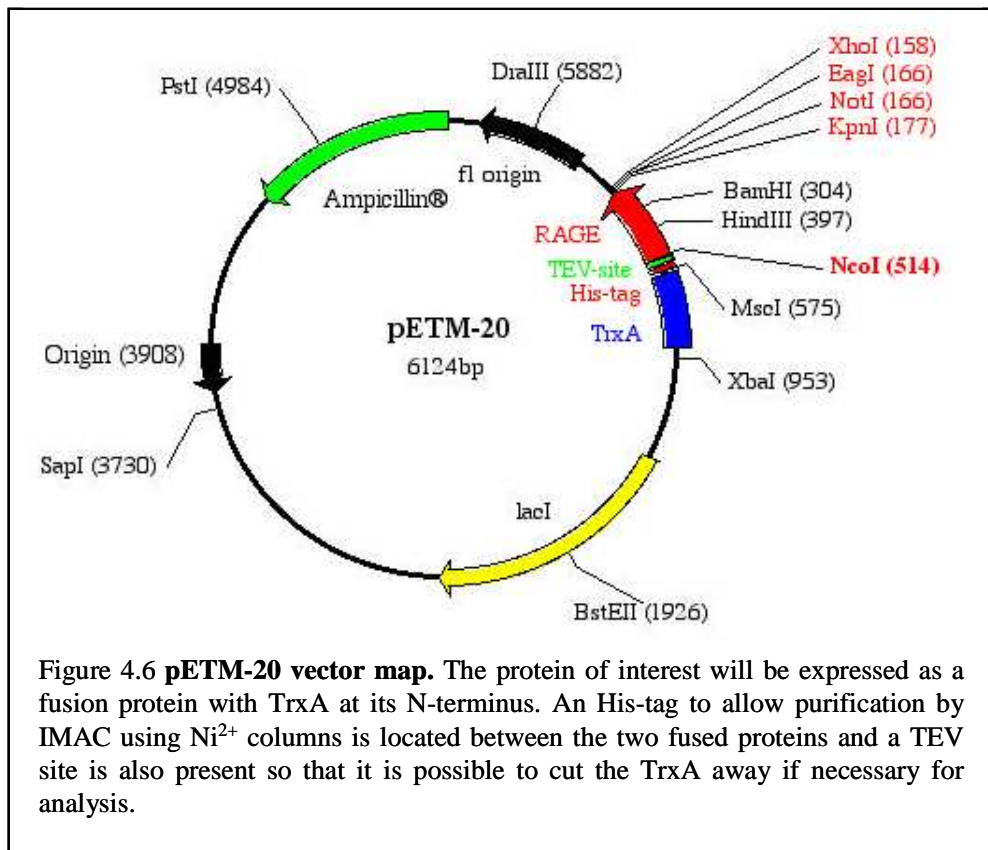
#### 4.1.4.1 Cloning of cC8 in pETM-20 and expression of TrxA\_cC8

Thioredoxin (TrxA) has several properties that make it well suited as a protein fusion partner, specially the fact that when it is expressed from plasmid vectors in *E.Coli*, it can accumulate to 40% of the total cellular protein content while remaining soluble. This extraordinary level of soluble expression suggest a very efficient translation. More importantly, this remarkable property is usually transferred to heterologous proteins fused with TrxA, especially when TrxA is positioned at the N-terminus of the protein of interest. The way TrxA works is probably as a covalently joined chaperone protein that keeps folding intermediates of linked heterologous proteins in solution long enough for them to adopt their correct final conformation (La Vallie, 2000). For this reason the cC8 gene was re-cloned in the pETM-20 vector so to express it as a fusion protein with TrxA.

The cloning procedure followed is the one described in the material and methods section.

Primers for generating entry vector			
			T <sub>m</sub>
cC8	Forward	5' -GCGCCCATGGCGCAACGGCCACGGCTTCAGC-3'	60°C
	Reverse	5' -GCGCGGATCCTACTTGTCAACAACCTGCAGCACC-3'	60°C

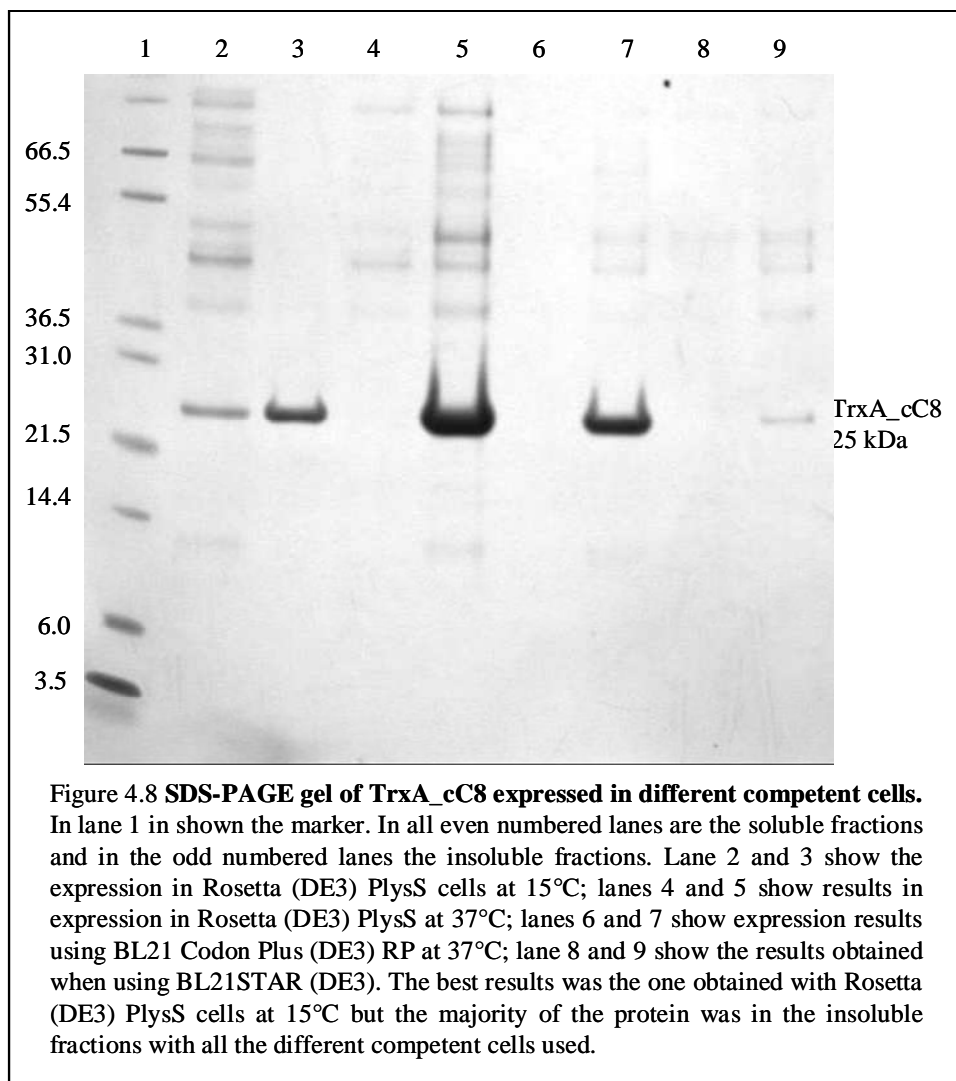
**Table 4.3: Primers used to lone cC8 in both vectors pETM-20 and pETM-60 vectors.**



Once the cloning procedure was completed, the new DNA construct was inoculated in different kind of competent cells to confront the efficiency of expression. The competent cells used in this analysis are the following.

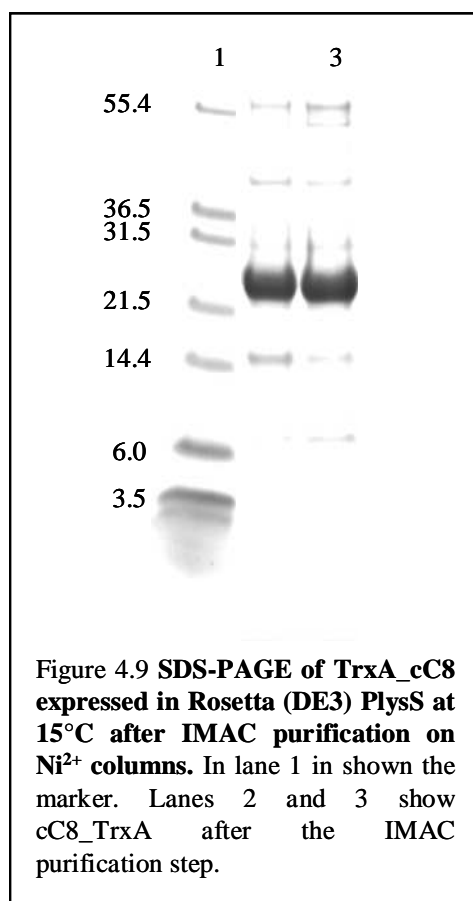
- BL21 STAR (DE3) (from Invitrogen)
- BL21 Codon Plus (DE3) RP (from Stratagene)
- Rosetta (DE3) PlysS (from Novagen)

The results obtained are shown in SDS-PAGE picture following.



According to the results obtained, it was decided to express the protein at 15°C with

Rosetta PlysS cells that gave the higher amount of soluble protein comparing to the other kind of competent cells used in this screening. It was possible to purify the synthesised fusion protein using IMAC on Ni<sup>2+</sup> columns and by size exclusion chromatography.



The fusion protein was purified with size exclusion chromatography and the three fractions containing it were pooled together. The protein was then concentrated, dialysed against NMR buffer and a titration with <sup>15</sup>N cC5 was performed. The final concentration of <sup>15</sup>N cC5 was a lot higher than the one of TrxA\_cC8 so it was possible to perform just three addition of TrxA\_cC8.

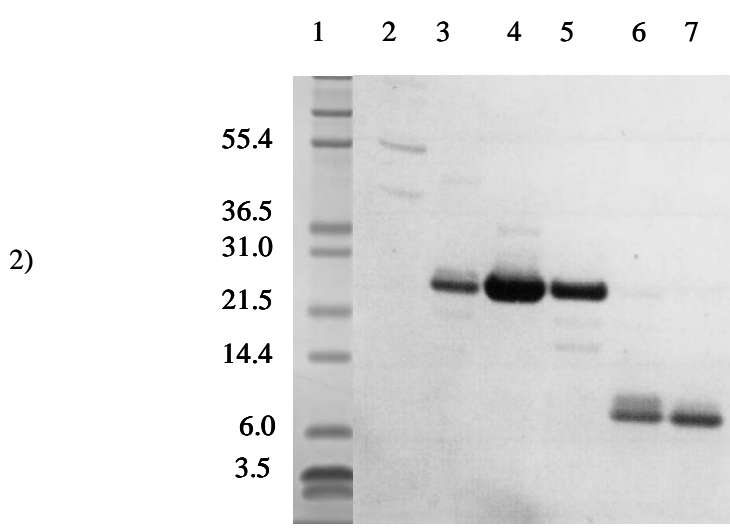
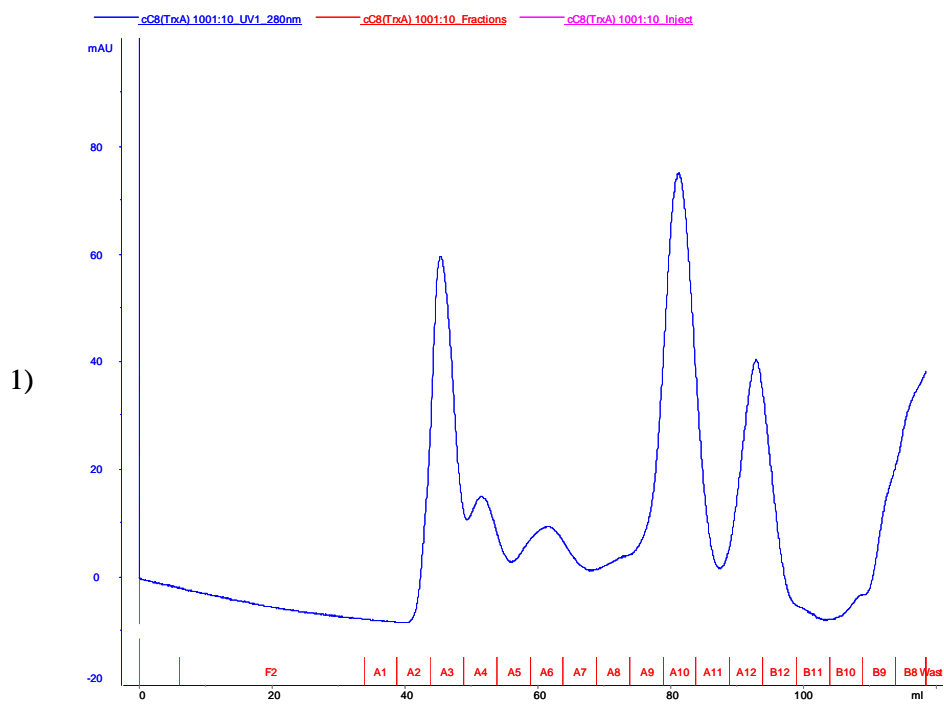
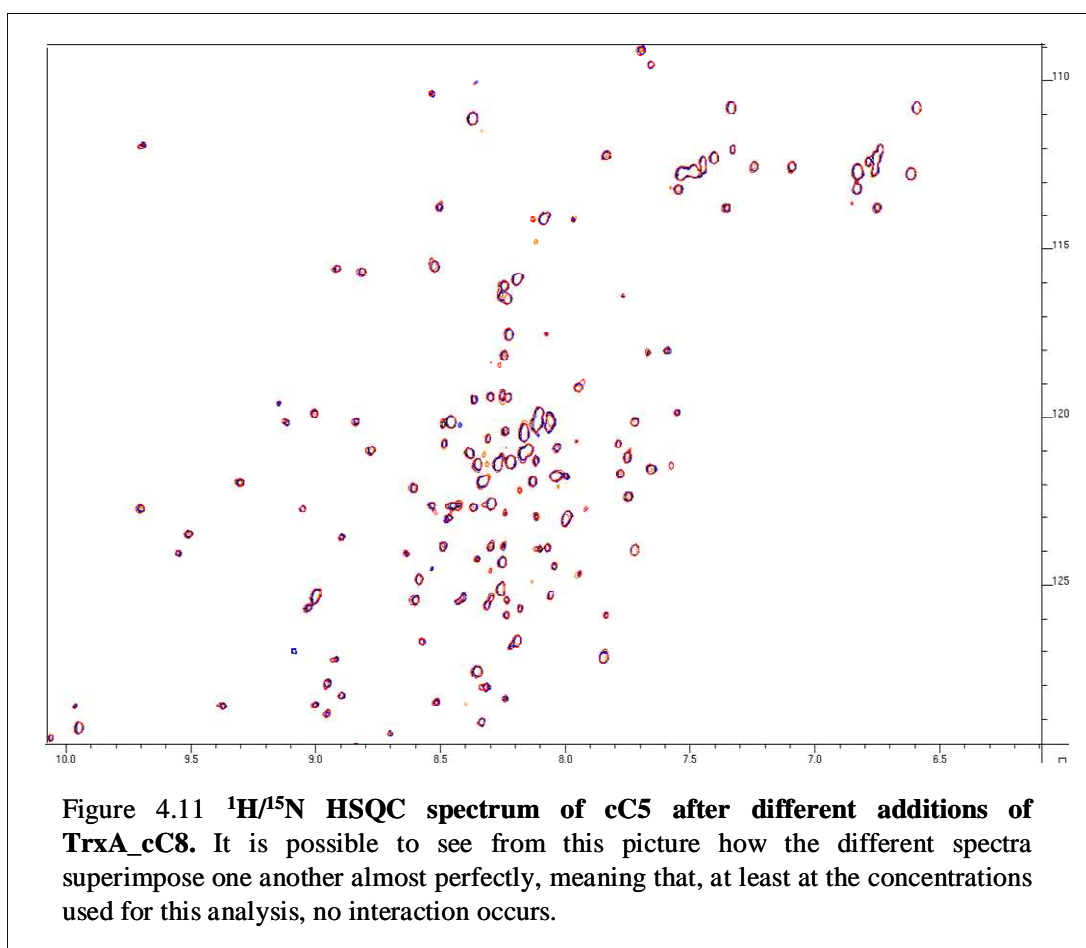


Figure 4.10 **Size exclusion chromatography purification step of TrxA\_cC8.** 1) size exclusion chromatography results for cC8\_TrxA. 2) SDS-PAGE gel of the fractions corresponding to the peaks shown in chromatogram. The fusion protein is present in fractions A9, A10 and A11, that correspond in the SDS-PAGE picture to lanes 3, 4 and 5.

Ratios	[cC5] $\mu\text{M}$	[TrxA_cC8] $\mu\text{M}$
1:0	100	0
1:0.5	100	50
1:1.5	100	150

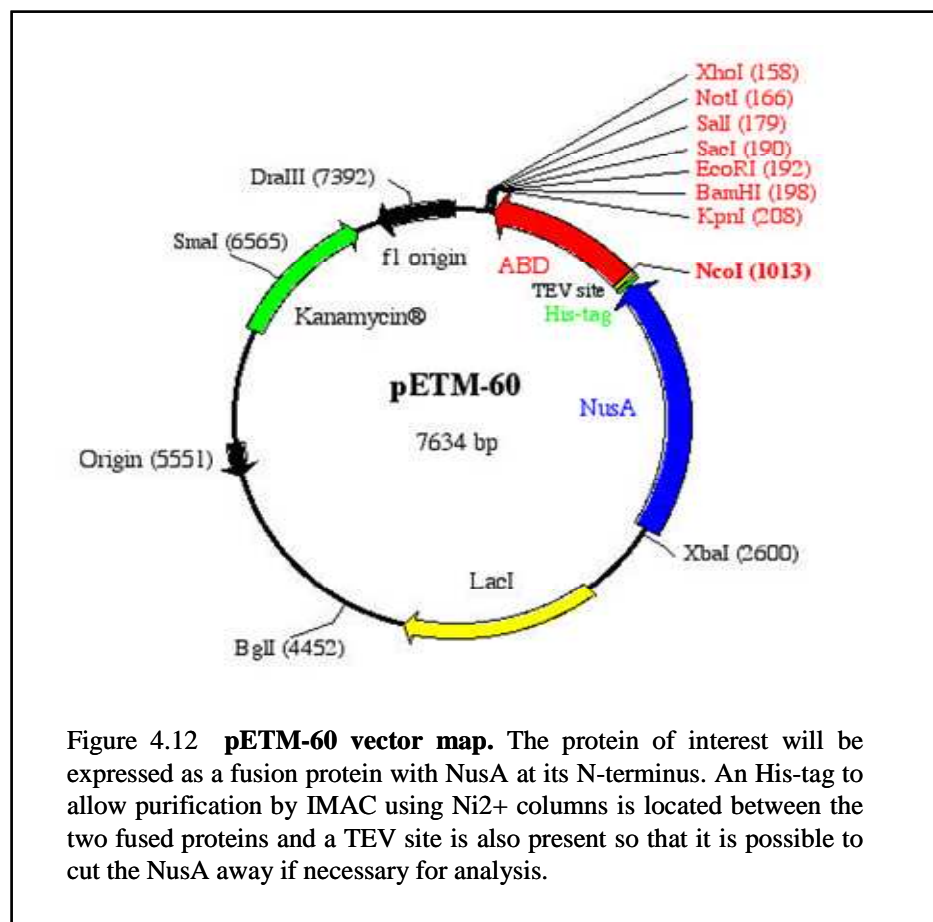
**Table 4.4: ratios and final concentrations of cC5 and cC8\_TrxA used in the titration performed to study their interaction.**

No positive results were obtained by this titration, it was not possible to detect any shift in the  $^1\text{H}/^{15}\text{N}$  HSQC spectrum peaks.



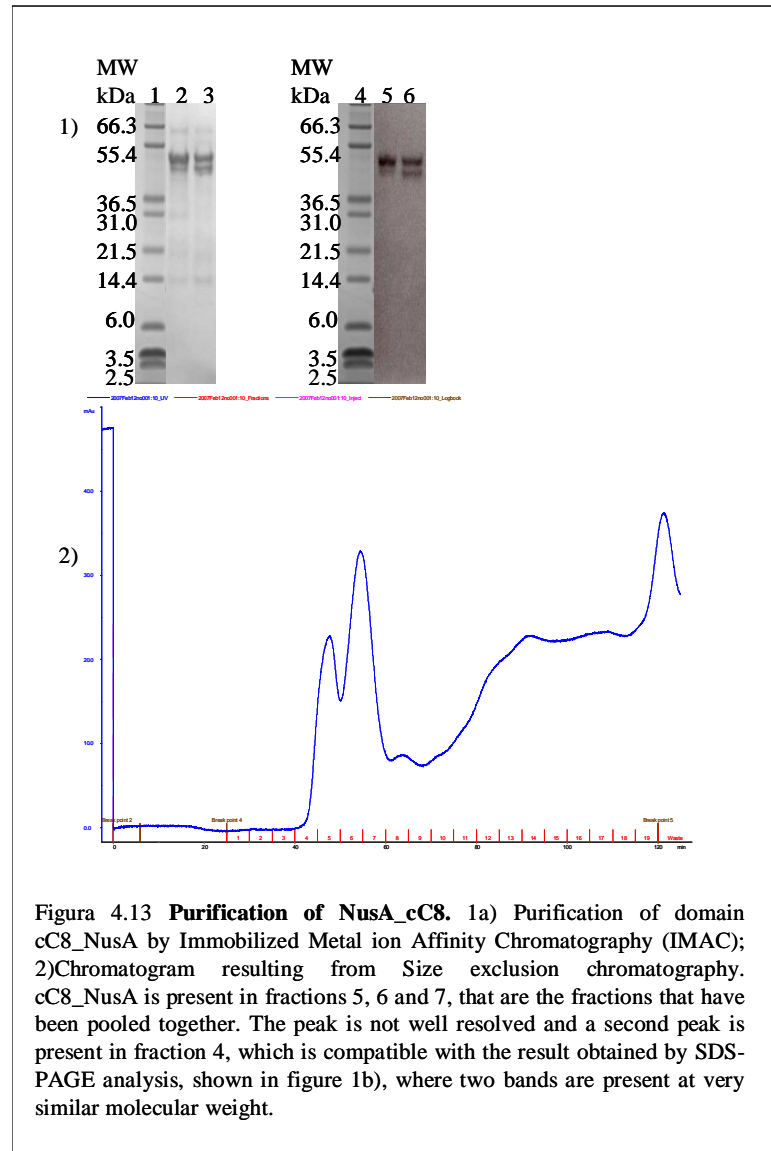
#### 4.1.4.2 Cloning of cC8 in pETM-60 vector and expression of NusA\_cC8

The same cC8 DNA fragment amplified by PCR and doubly digested with enzymes BamHI and NcoI, was ligated also with pETM-60 (De Marco et al., 2004) with the finality of expressing cC8 in a fusion protein with a second partner, *E.Coli* protein NusA. This protein was chosen as fusion partner on the basis of solubility screenings (Harrison, 2000), has a molecular weight of 55 kDa and has a role in termination of transcription; it is characterized by a solubility higher than 95% when over expressed and it has been proven to enhance the solubility of exogenous protein fused with it.



The same competent cells as the ones that gave the best result with the TrxA\_cC8construct were used, so expression was carried out with Rosetta (DE3) PlysS

cells (from Novagen). It was possible to purify the protein with both IMAC on Ni<sup>2+</sup> columns and by size exclusion chromatography, even though two unresolved peaks were present in the chromatogram.



A titration was performed to study the interaction between <sup>15</sup>N cC5 and NusA\_c8

Ratios	[cC5] $\mu$ M	[NusA_c8] $\mu$ M
1:0	100	0
1:0.5	100	50
1:1	100	100
1:1.5	100	150

**Table 4.5:** ratios and final concentrations of cC5 and NusA\_c8 used in the titration performed to study their interaction.

Some very small shifts were distinguishable, possibly due to small variations in pH or temperature, but not enough to reach a definitive conclusion about the occurrence of the interaction; the main problem with NusA\_cC8, as well as with TrxA\_cC8, is the impossibility to produce enough soluble protein to perform a titration going to the higher ratios that might be necessary for this interaction to be clearly detectable.

#### 4.1.5 *Expression in tRNA- supplemented host cells*

##### 4.1.5.1 *Expression of cC8 in BL21 Codon Plus (DE3) RP competent cells*

One of the most common problems encountered when over-expressing heterologous genes in *E.Coli*, is the failure of synthesis of the desired protein due to the presence of rare codons. This is caused by the redundancy of the genetic code; since the same amino acids can often be encoded for by more than one codon, different organisms use the possible coding triplets with varying frequency. Forced expression of heterologous genes containing codons rarely used by the host organism, can lead to a reduction of the corresponding tRNA pools and a stop in the translational process that will appear as a failure of producing the desired protein. This problem can be overcome co-expressing extra copies of the rare tRNA genes together with the protein of interest. For this purpose two pACYC-based vectors were created by Stratagene with copies of the codons that had the main effect when expressing heterologous proteins in *E. coli*. Four codons were implemented: *argU* (AGA/ AGG), *ileY* (AUA), *leuW* (CGA) and *proL* (CCC). Ideally all four codons would be present on the same vector but, since a functional incompatibility between *ileY* and *proL* was observed, two different vectors were made on the basis of their relative GC-richness. AGA (*argU*), AUA (*ileY*), CUA

(*leuW*) are more likely to be present in AT-rich organisms, while AGG (*argU*) and CCC (*proL*) are more frequently found in GC- rich organisms. These two vectors were introduced into the BL21- gold cells and the resulting cells go under the trade-name of BL21 Codon Plus (DE3) (from Straragene) and exist in two version, RIL and RP according to the rare codons present in their additional vector.

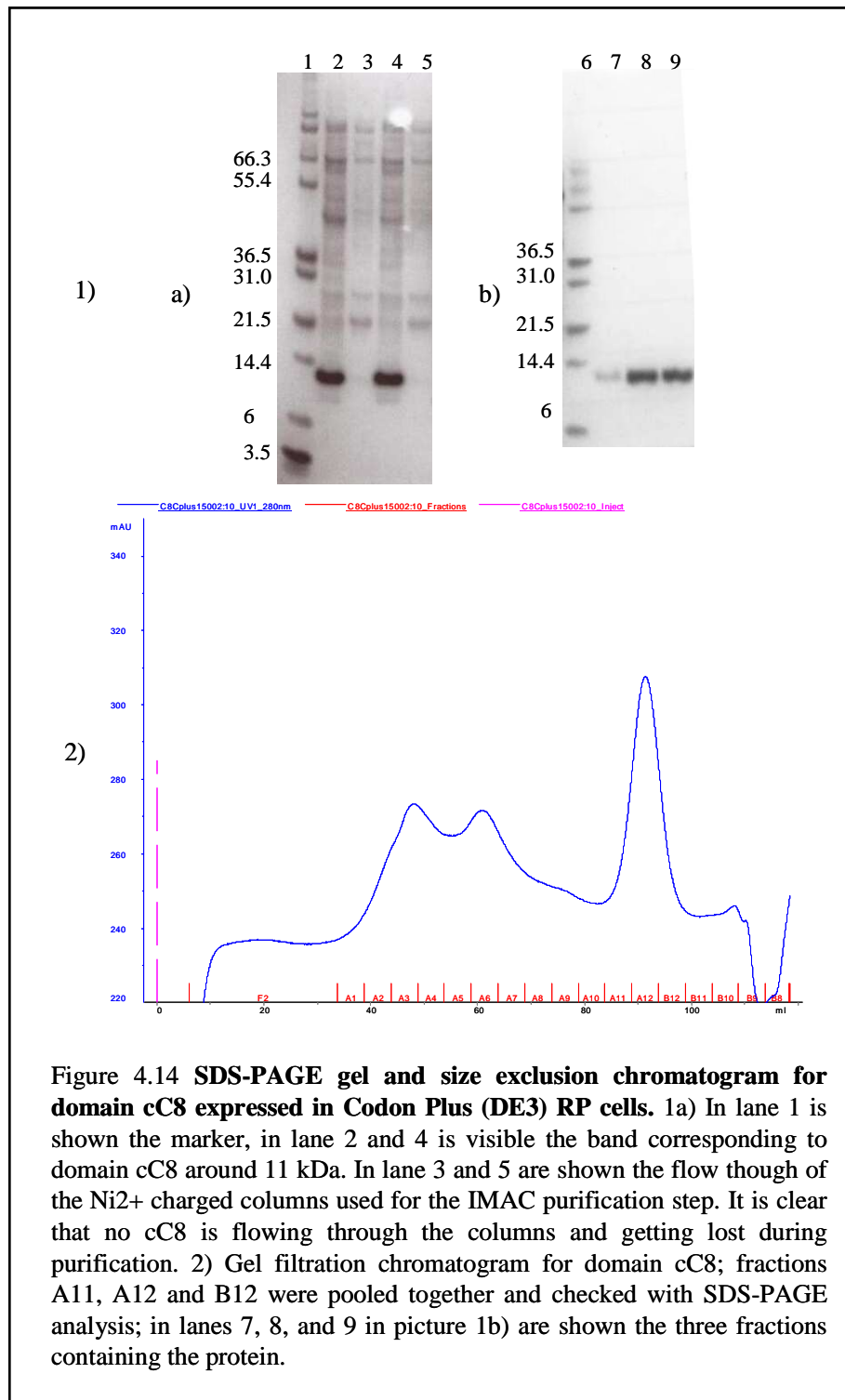
Since four rare codons are present in the DNA sequence coding for domain cC8, four CCC (*proL*) and one AGG (*argU*), it was decided to use the BL21 Codon Plus (DE3) RP.

**cC8 DNA coding sequence.**

```
atg cac cat cat cat cat cat tct tct ggt gag aat ctt tat ttt cag ggc gcc atg gcg caa cgg cca
cgg ctt cag ctg CCC AGG cac ctg cgc cag acc att cag aag aag gtc ggg gag cct gtg aac
ctt ctc atc cct ttc cag ggc aag CCC cgg cct cag gtg acc tgg acc aaa gag ggg cag CCC
ctg gca ggc gag gag gtg agc atc cgc aac agc CCC aca gac acc atc ctg ttc atc cgg gcc
gct cgc cgc gtg cat tca ggc act tac cag gtg acg gtg cgc att gag aac atg gag gac aag gcc
acg ctg gtg ctg cag gtt gtt gac aag tag
```

The expression was carried out at different temperatures, and the best results were obtained at 15°C expressing overnight, inducing with a solution of [IPTG]= 0.1 mM.

Using the BL21 Codon Plus (DE3) RP cells around 7 mg/l of soluble protein were obtained. The protein was purified by IMAC on Ni<sup>2+</sup> columns and with size exclusion chromatography.



#### 4.1.5.2 Expression of cC8 in Arctic Express RP cells

The best results obtained for domain cC8 have been obtained conducting the expression at low temperature. At standard temperature of 30-37°C the expressed heterologous protein can impair the cell's ability to properly process the recombinant protein, so low temperature expression is a common strategy to increase the recovery of soluble protein (Schein, 1989) that otherwise would precipitate. One problem that may arise from this approach is that *E. coli* chaperonins, that have a fundamental role in stabilizing unfolded and partially folded proteins keeping them in solution, lose activity at reduced temperatures. To overcome this obstacle, special competent cells have been engineered that co-express the cold-adapted chaperonins Cpn10 and Cpn60 from the *Oleispira Antarctica*; these chaperonins have 74% and 54% amino acid identity to the *E. coli* chaperonins GroEL and GroES respectively, and show high protein folding activities at temperatures between 4°C and 12°C. The cells used in this research are the Arctic Express RP (from Stratagene) that also contain extra copies of *argU* and *proL* genes necessary to overcome the rare codon presence in the heterologous gene. The expression was carried out at 13° overnight inducing with [IPTG]= 0.1 mM giving a yield of 186 mg/l. The protein was purified by IMAC on Ni<sup>2+</sup> columns and with size exclusion chromatography.

Confronting the two SDS-PAGE gels of cC8 expressed in Codon Plus RP and in Arctic RP, it does not seem to be a relevant difference in the amount of protein synthesised, I would conclude that using either of the two competent cells would give a good amount of recombinant protein.

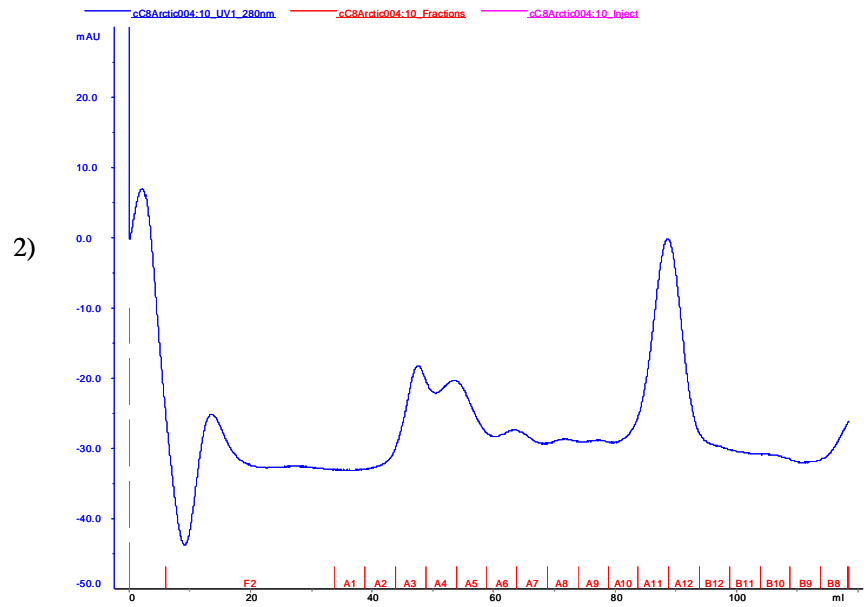
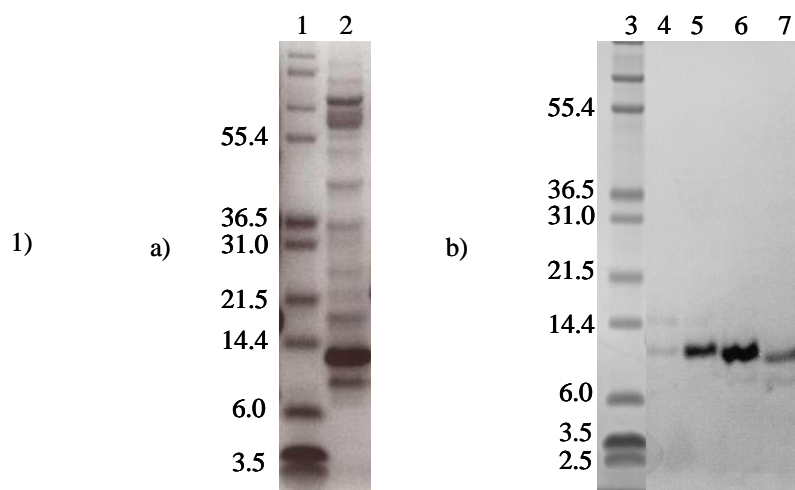


Figure 4.15 **Purification of cC8 expressed in Arctic Express RP cells.** 1) purification of domain cC8 by Immobilized Metal ion Affinity Chromatography (IMAC); 2) Chromatogram resulting from Size exclusion chromatography. cC8 is present in fractions A11, A12 and B12, and these fractions have been poured together. In lanes 4-7 picture 1b) are shown fractions A10, A11, A12 and B12 after SDS-PAGE analysis. Fractions A11, A12 and B12 have been pooled together.

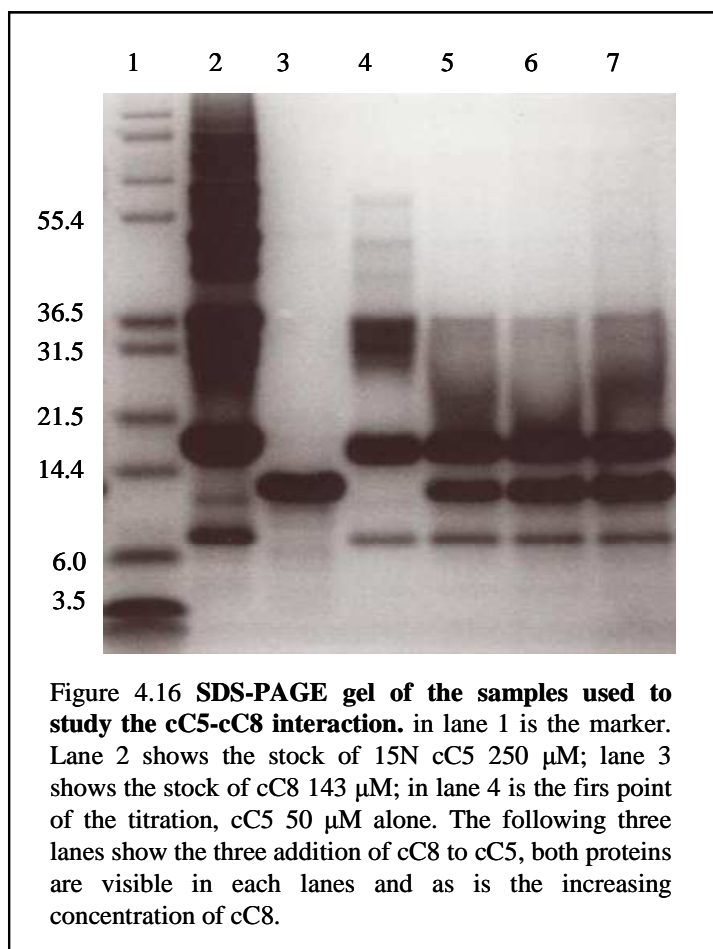
#### 4.1.6 Study of the interaction between domains cC5 and cC8

The interaction between domains cC5 and cC8 of cMyBPC was studied performing a titration of cC8 in a sample of  $^{15}\text{N}$  cC5, following the changes in chemical shift in an  $^1\text{H}/^{15}\text{N}$  HSQC spectrum.

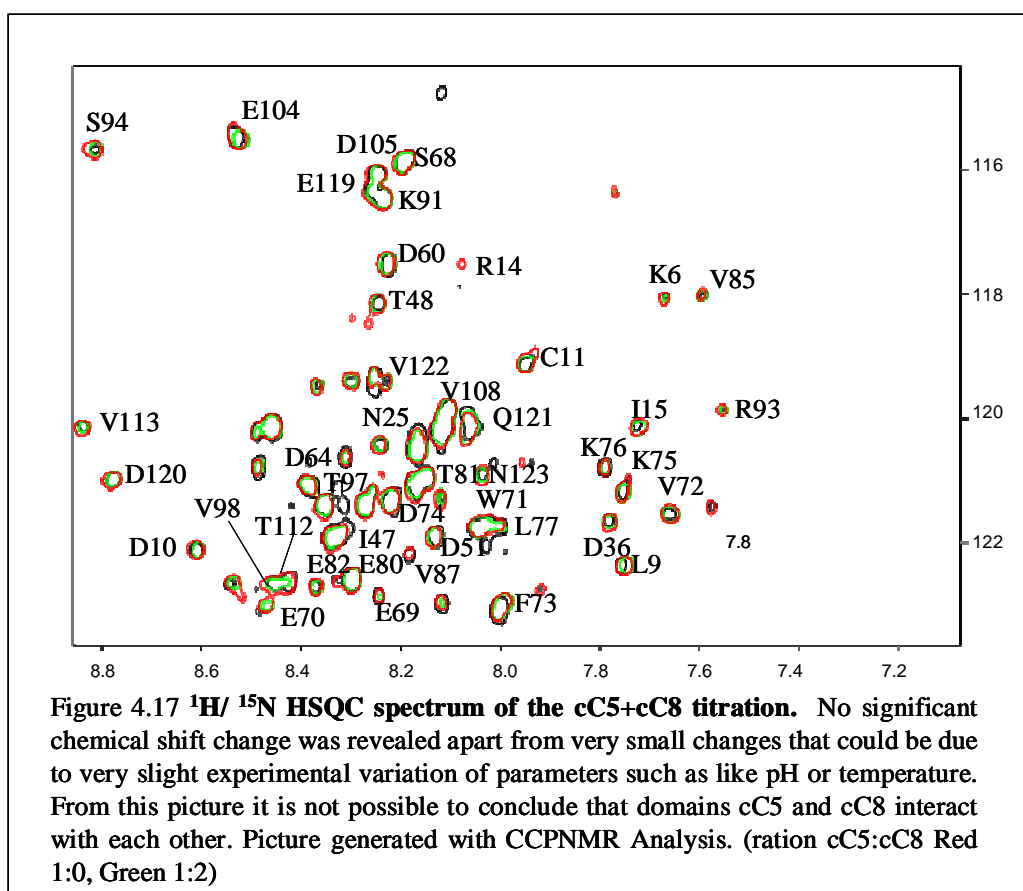
Once the problems regarding cC8 expression have been overcome, it was possible to synthesise enough protein to perform this study. Four points have been recorded, corresponding to three additions of cC8 to the  $^{15}\text{N}$  cC5 NMR sample.

Ratios	[cC5] $\mu\text{M}$	[cC8] $\mu\text{M}$
1:0	50	0
1:0.5	50	25
1:1	50	50
1:2	50	100

**Table 4.6: ratios and final concentration of C5 and cC8 used in the titration performed to study their interaction.**



Very small changes in chemical shifts were registered in the cC5  $^1\text{H}/^{15}\text{N}$  HSQC spectrum, meaning that the two proteins might interact even though not in a very strong way. These shifts could be also caused by small changes in the experimental conditions, such as pH or temperature, so this result is not sufficient to conclude that domain cC5 interacts with domain cC8.



#### 4.1.7 Cloning and protein expression of groups of domains cC5-7 and cC8-10

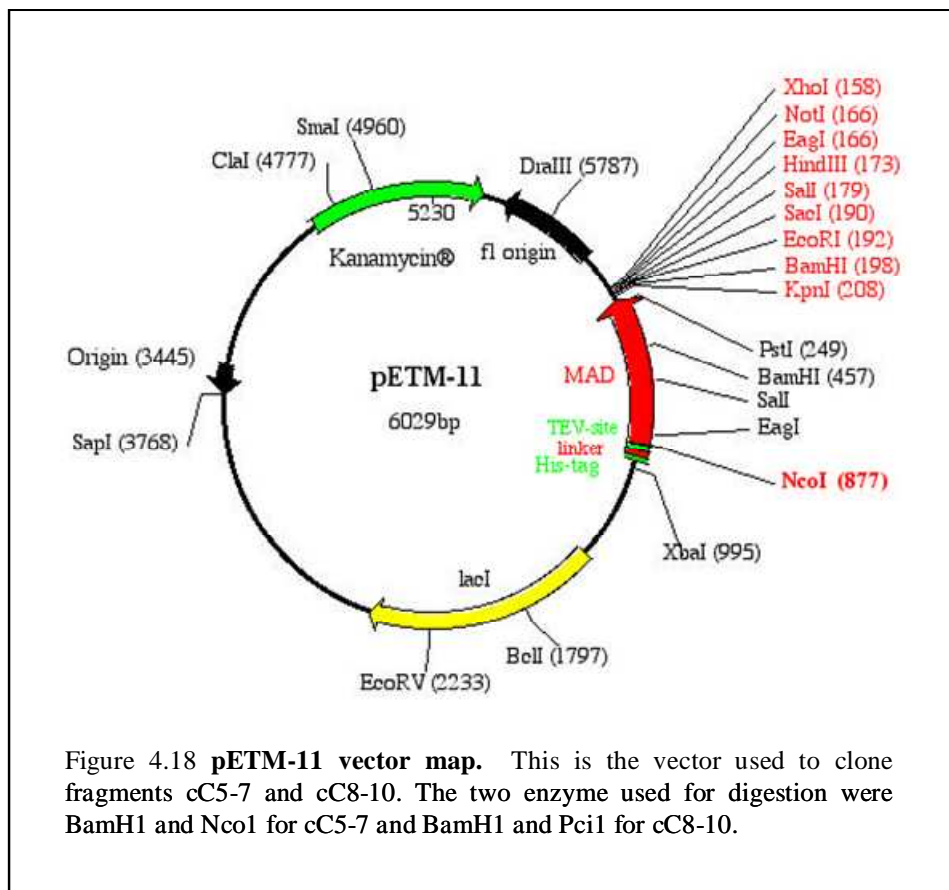
Given how small the observed shifts were in the  $^1\text{H}/^{15}\text{N}$  HSQC titration between cC5 and cC8, it was decided to clone two groups of domains as, according to the trimeric collar model (Moolman-Smook et al., 2002) domains cC5, cC6 and cC7 should interact with cC8, cC9 and cC10, respectively. So two bigger fragments of cMyBPC were

cloned, one comprising of domain cC5 to domain cC7 (fragment cC5-7) and the other comprising of domains cC8, cC9 and cC10 (fragment cC8-10).

The primers used for this procedure are reported in the following table. The new DNA fragments were cloned in vector pETM-11.

Primers for generating entry vector		T <sub>m</sub>	Expression vector
cC5 F	5' -GGCCGAGCCATGGCGCCCAAGATCCACCTGGAC -3'	55°C	
cC7 R	5' -GGATCCTTACACGGGCTCGGTGGTGGTCACGGG -3'	55°C	
cC8F	5' -GCCCGAGACATGTCCGCCACGGCTTCAGCTGCCC -3'	65°C	
cC10 R	5' -GGATCCTTACTGAGGCACTCGCACCTCCAGGCG -3'	65°C	

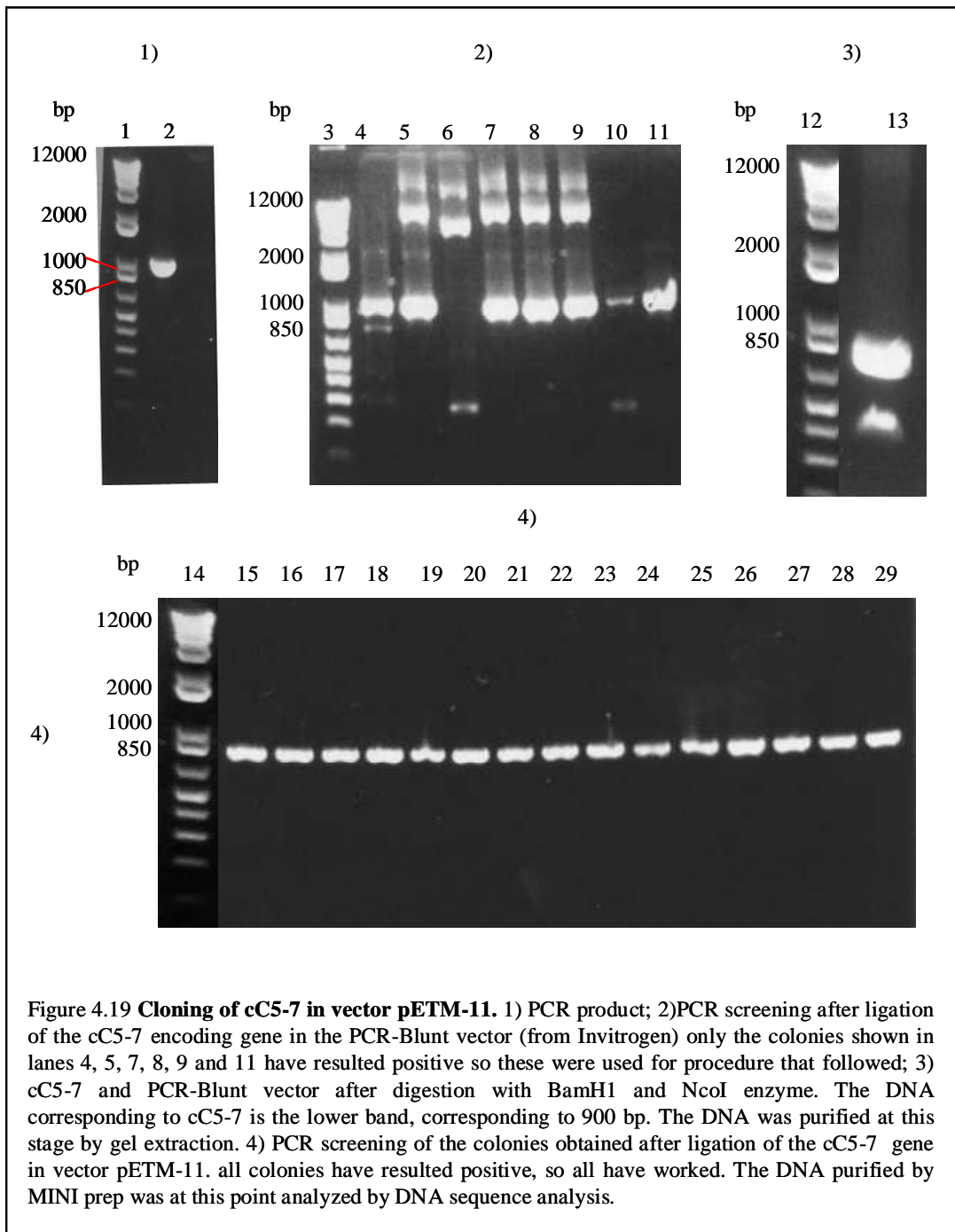
**Table 4.7: Primers used to clone cC5-7 and cC8-10 in pETM-11 vector.**

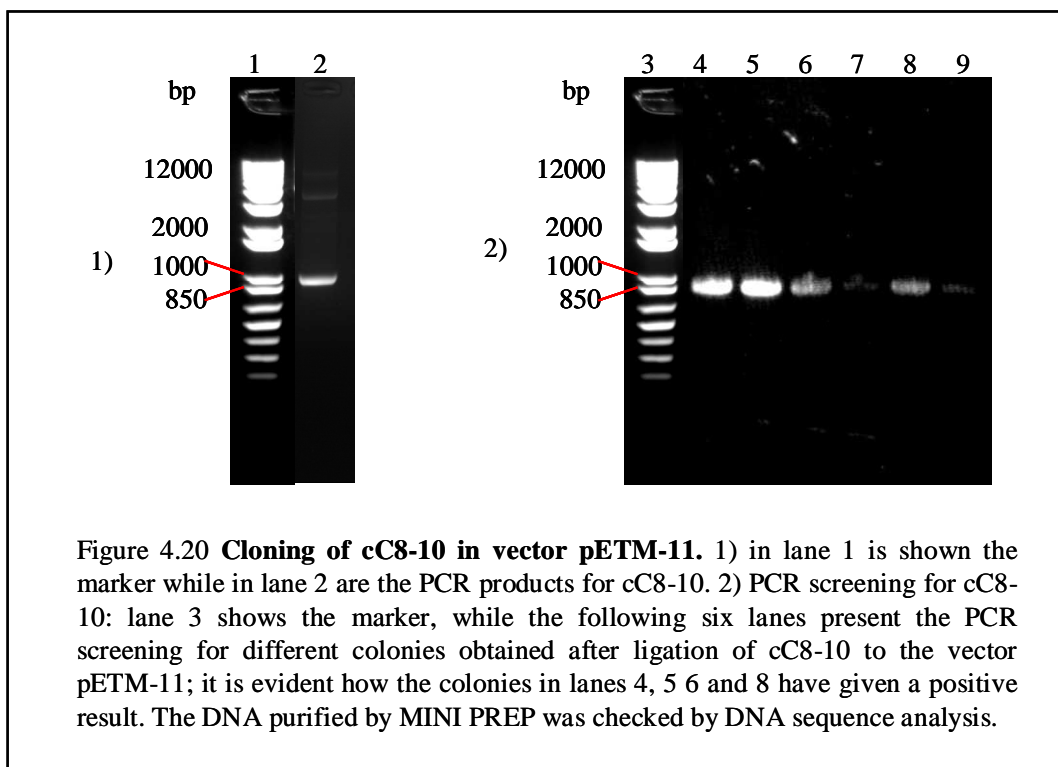


The procedure followed for the two cloning procedures is the same as the one described in the materials and methods section for the group of domains cC8-10; for cC5-7 it resulted difficult to perform the ligation directly after the double digestion, as this

procedure, repeated twice, failed to give any colony after transformation of TOP 10 cells. It was then decided to perform an extra step, ligating the digested cC5-7 encoding sequence in the pCR II Blunt TOPO vector (from Invitrogen). To do this the DNA fragment was allowed to react with pCR II Blunt TOPO vector (from Invitrogen). and then TOP 10 cells were transformed with this DNA construct. After purification by MINI PREP, the DNA was doubly digested with BamH1 and NcoI and then ligated to the doubly digested vector pETM-11 with ligase T4 (from Roche). This time the reaction worked and a few colonies were obtained after transformation of TOP 10 cells with this DNA construct. As shown by picture 4.20, the PCR screening of these colonies showed that all the colonies contained the right cC5-7 encoding gene, as confirmed by DNA sequencing.

While cC5-7 was doubly digested by restriction enzymes BamH1 and Nco1, before ligating it with the vector, cC8-10 was digested by BamH1 and Pci1 (from New England Bio Labs) due to the presence of a Nco1 cutting site in the sequence. Enzyme Pci1 creates sticky ends compatible to the ones created by Nco1 but the recognition sequence is different, being CCATGG for Nco1 and ACATGT for Pci1. The digestion of cC5-7 was carried out in Buffer B (from Roche), while the cC8-10 digestion was carried out in NEBuffer 2 (from Roche).



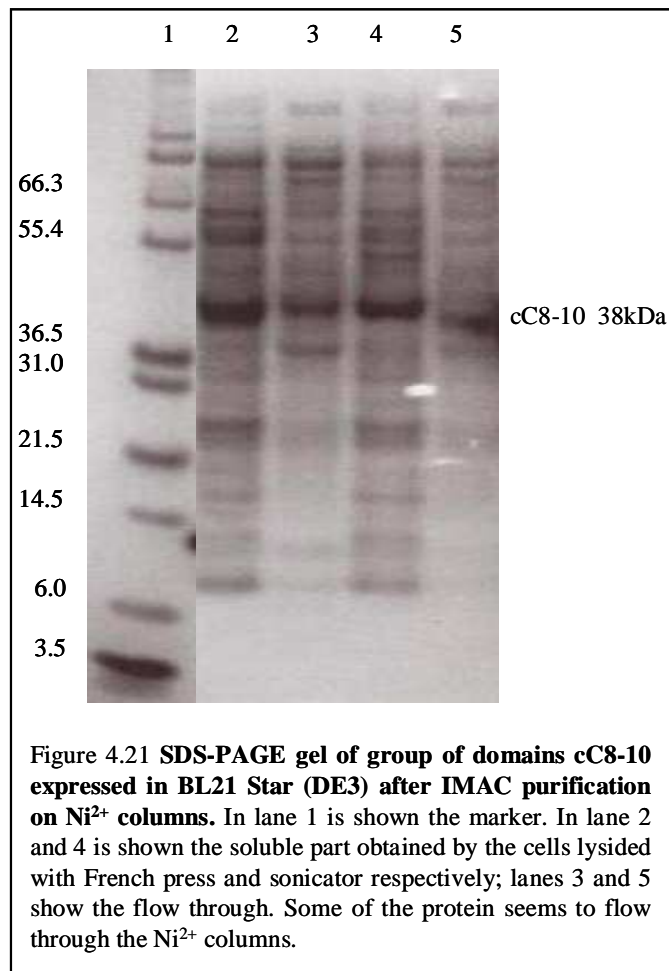


#### 4.1.7.1 Group of domains cC8-10

The DNA construct of cC8-10 in pETM-11 was inoculated in BL21 STAR (DE3) competent cells (from Invitrogen), expression was carried out at 15°C overnight and induced with [IPTG]= 0.75 mM.

From preliminary results it looked like cC8-10 expressed normally, as shown in figure 4.22. However, it was not possible to purify the protein using the size exclusion chromatography, no peak was present in the chromatogram, meaning that no protein was present in the sample or that part of the protein might be misfolded and stick to the gel filtration column. The strategies that worked best for domain cC8 were also used for the group of domains cC8-10, so the corresponding DNA construct was inoculated in BL21 Codon Plus (DE3) RP and Arctic Express RP but in both cases the amount of protein express would not improve. The lack of published work on these final domains

of cMyBPC suggest an intrinsic difficulty in the synthesis of this fragment of protein that could explain our lack of success.



#### 4.1.7.2 Group of domains cC5-7

Expression of cC5-7 was carried out at 15°C overnight, inducing expression with [IPTG]= 0.75 mM, giving a yield of 27 mg/l. It was possible to purify the synthesised protein with both IMAC on Ni<sup>2+</sup> columns and size exclusion chromatography.

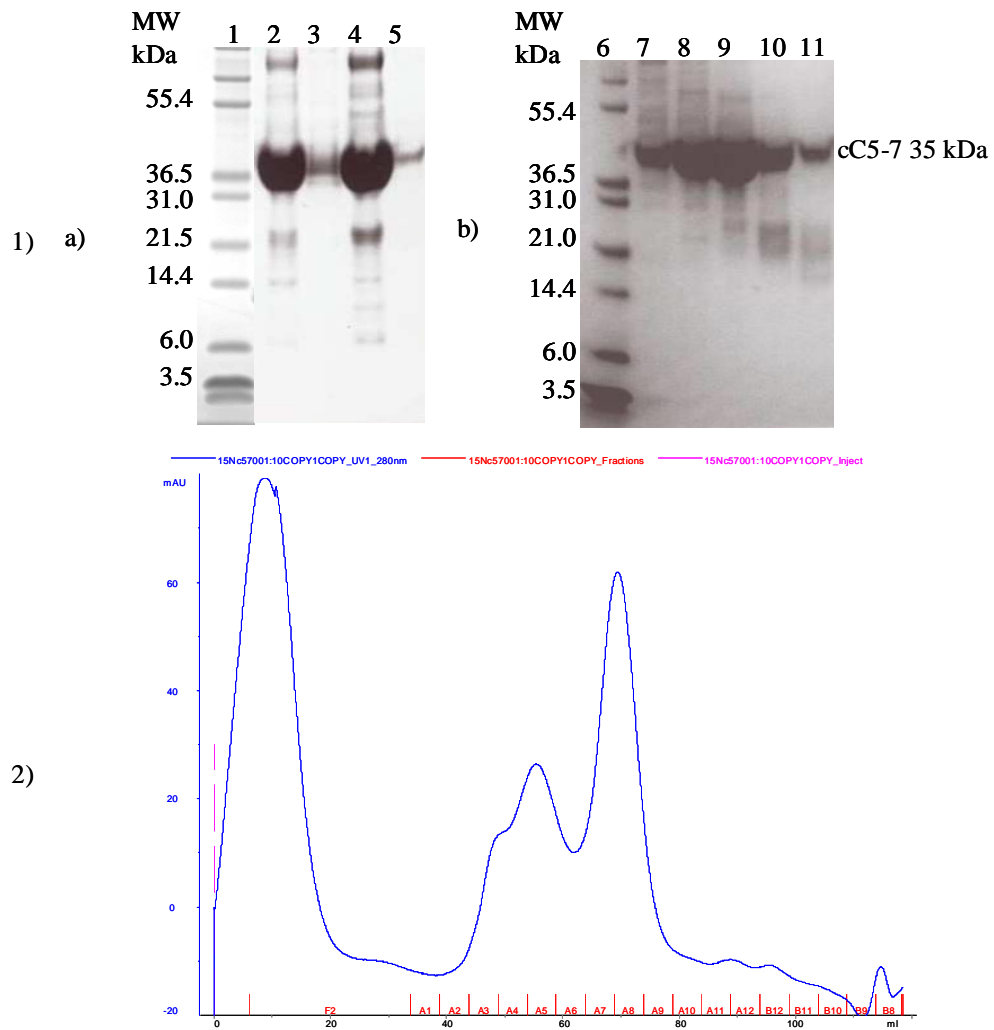
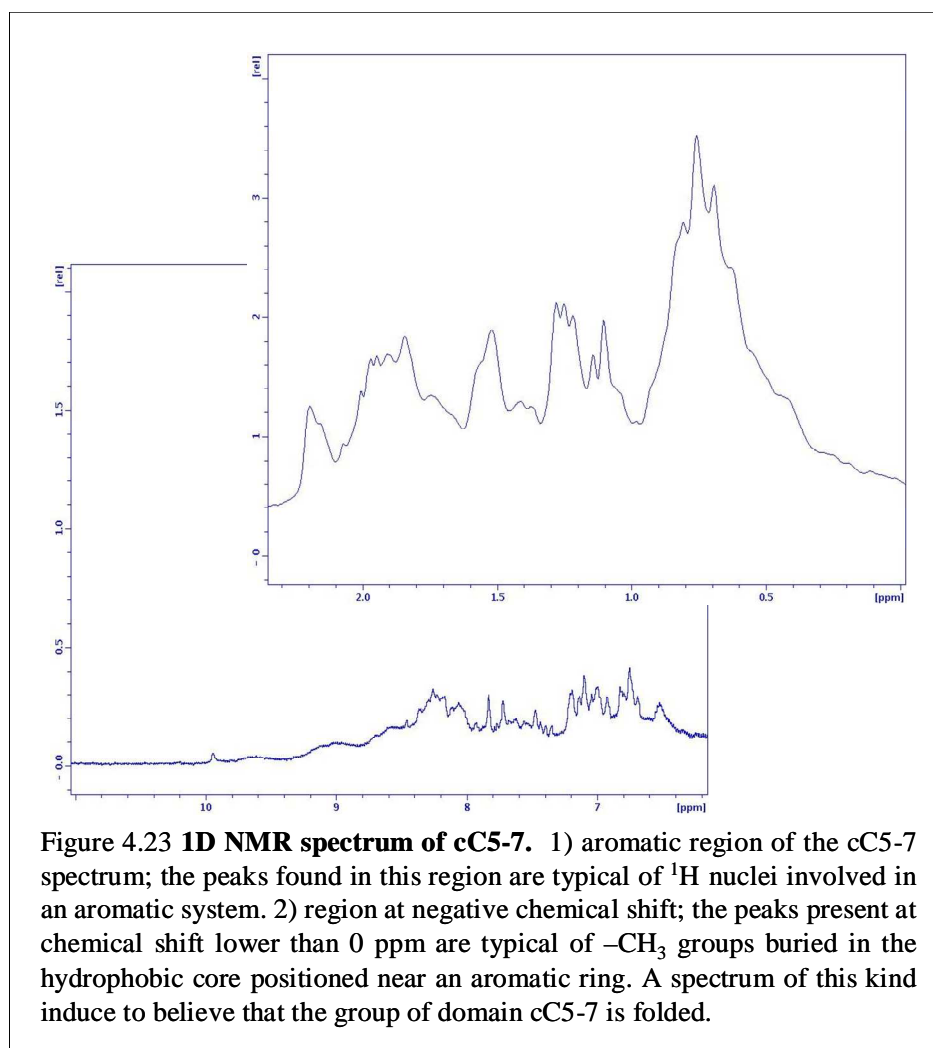


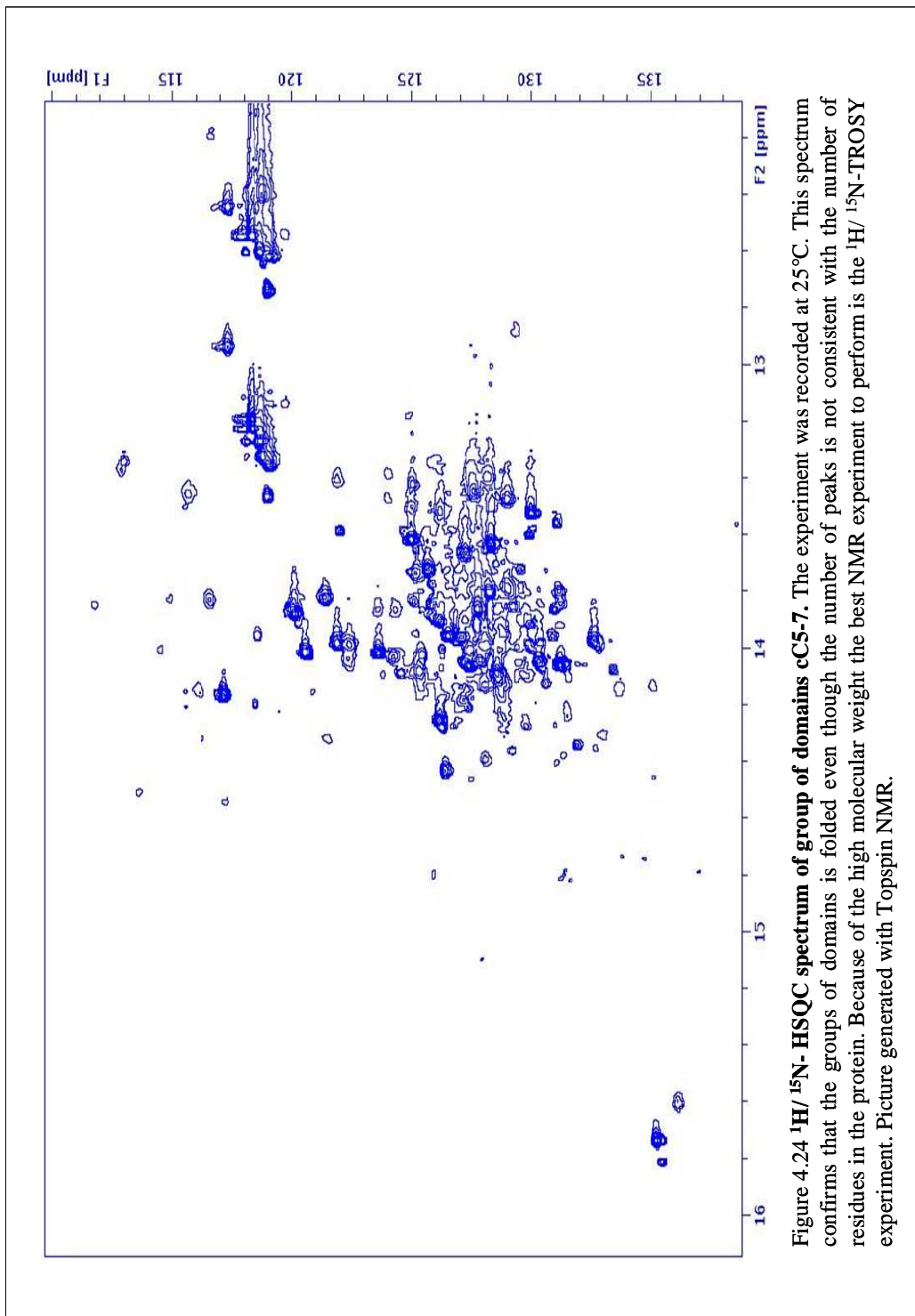
Figure 4.22 **SDS gel and size exclusion chromatogram for group of domains cC5-7 expressed in BL21Star (DE3) cells.** 1) In lane 1 is shown the marker, in lane 2 and 4 is visible the band corresponding to domain cC5-7 domains around 40 kDa. In lane 3 and 5 are shown the flowthrough of the Ni<sup>2+</sup> charged columns used for the IMAC purification step. It is clear that no cC5-7 is flowing through the columns and getting lost during purification. Lanes 2 and 3 show the result of purification after lysing the cells using the French press, while lanes 4 and 5 show the same after lysing the cells with a sonicator machine all after Ni column purification. 2) Gel filtration chromatogram for domains cC5-7; fractions A7 and A8 were pooled together on the basis of the chromatogram as the SDS-PAGE analysis gave very thick bands that made difficult to understand whether cC5-7 is also present in fraction A5 and A6.

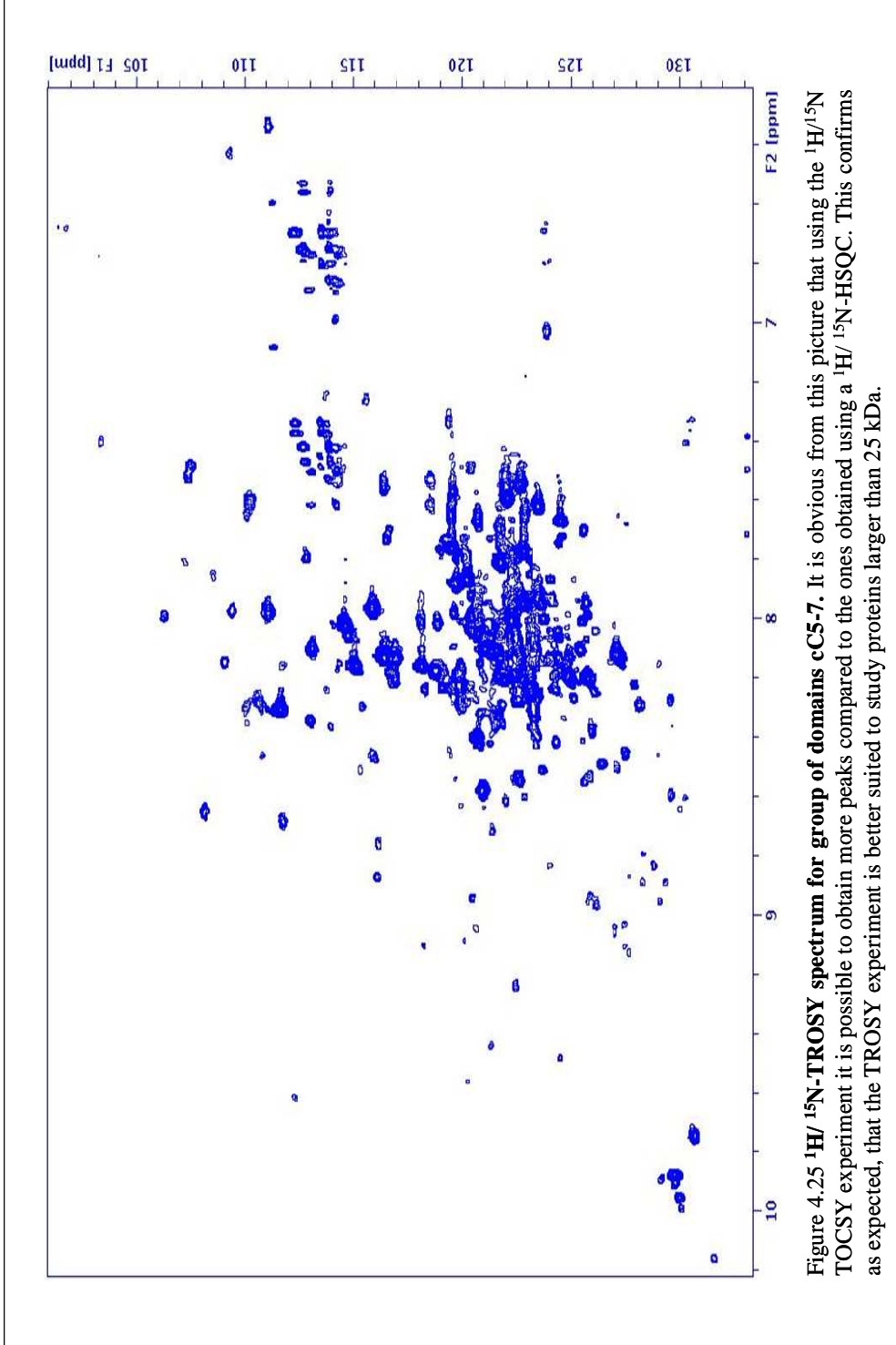
The protein was concentrated and dialysed against NMR buffer. An NMR sample was produced which concentration was 112 $\mu$ M and a 1D  $^1$ H NMR experiment was run to check whether the protein was folded, as suggested by its being soluble in aqueous solutions.



From the 1D  $^1$ H NMR spectrum it is possible to conclude that the protein is probably folded, due to the presence of peaks at negative chemical shifts, at the far right of the spectrum. However, to confirm this hypothesis, it was decided to perform a multidimensional experiment. The molecular weight of the group of domains cC5-7 is around 35 kDa; proteins larger than 25 kDa tend to give broader NMR signals, due to

their slower molecular tumbling rate compared to smaller molecules, causing fast transverse relaxation. A  $^1\text{H}/^{15}\text{N}$  HSQC of a protein this large would give broad signals and some of them will disappear completely, giving a spectrum with a number of peaks not corresponding to the number of residues in the protein. However, if we consider a  $^1\text{H}/^{15}\text{N}$  correlation experiment without  $^{15}\text{N}$  decoupling in both dimensions, every signal will be split in four signals separated by the N-H spin coupling constant in both dimensions  $F_1$  and  $F_2$ . It was noted that not all this four signals would broaden in big proteins spectra. Due to the interference of the cross-correlated dipole relaxation and chemical shift anisotropy relaxation one of them will stay sharp, one will be very broad and the remaining two will be intermediate. Based on these observation, a new experiment was proposed (Pervushin et al., 1997) which singles out the sharp resonance and detect it without decoupling. To this experiment was given the name TROSY (Transverse Relaxation Optimized Correlation Spectroscopy). If a 800MHz spectrometer is available, it is possible to perform experiments based on TROSY that would enable to solve the structure of a protein larger than 30 kDa. A TROSY experiment was performed for cC5-7, together with a  $^1\text{H}/^{15}\text{N}$  HSQC. It is evident that the TROSY spectrum shows a lot more peaks if compared with the  $^1\text{H}/^{15}\text{N}$  HSQC where mainly just the peak corresponding to the flexible linker of cC5 are shown (Idowu et al., 2003), this is a significant result that shows how this group of domains is rigid. In fact while for a flexible protein of around 30 kDa, such as the group of domains cC1-cC2, the  $^1\text{H}/^{15}\text{N}$  HSQC presents a number of peaks consistent with the number of residues present in the fragment, for a rigid protein of the same size much of the signal is lost due to the transverse relaxation so that many peaks will not be visible; performing a TROSY experiment, on the other hand, will give the opposite result, giving a good





spectrum for rigid proteins and a bad spectrum for a flexible one. So given the results obtained for the group of domains cC5-7, we can conclude that this fragment is rigid.

These results also confirm that the TROSY experiment is the best option when studying rigid proteins bigger than 25 kDa. It is not the finality of this research to determine the structure of the groups of domains cC5-7 but the quality of this TROSY spectrum shows that it would be possible to determine its three dimensional structure. Moreover, since we have shown that the group of domains cC5-7 is stable and expresses well in bacteria, it would be possible to study the interaction with its hypothetical binding partner cC8-10. Unfortunately it was not possible to perform a titration to study the interaction between the two due to the failure to express the group of domains cC8-10, as reported in the previous section. In conclusion it will be possible to investigate the interaction between this central domains of the protein and the C-terminal part of cMyBPC, once the technical problems concerning the latter will be overcome.

## *4.2 Discussion*

### *4.2.1 Problem of the solubility of domain cC8*

Domain cC8, together with the other C-terminal domains of cMyBPC, has shown a tendency in precipitating into inclusion bodies and limited solubility. Interestingly, the C-terminal domains are involved in sarcomere incorporation of cMyBPC, and this features are common to the other isoforms of the protein. The region comprise between cC7 and cC10 interacts with LMM, even though only domain cC10 seems to be indispensable for the binding to occur. To achieve maximal binding, on the other hand, the four C-terminal domains cC7-10 are necessary for cMyBPC to be properly

incorporated in the sarcomere (Welikson and Fischman, 2002). The cC8-10 region, also binds to titin (Furst et al., 1992; Koretz et al., 1993; Labeit et al., 1997; Soteriou et al., 1993), probably via domain cC9 and/ or cC10 (Freiburg and Gautel, 1996) interaction that resulted fundamental for the sarcomere to assume its proper structure. All these aspects point towards an important structural role of the C-terminus of cMyBPC that could also motivate the insoluble character of these domains when expressed on their own. It is in fact probable that the presence of the previous domains in the sequence could stabilise the most terminal domains, such as cC9 and cC10, and that the presence of other proteins with which the C-terminal domains of cMyBPC interact could play an important role in the expression of these final domains of the protein.

Another important aspect is the presence of rare codons in the DNA sequence coding for these domains, as seen for domain cC8 alone and, more importantly, for the group of domains cC8-10, that could cause a reduction of the tRNA pools of the host organism, *E. Coli* in this case, leading to a stop in the translational process, with the consequence failure in the synthesis of the desired protein. This is not the case for N-terminal domains, especially the other domain taken into account in this work, domain cC0, that has a total lack of *E. Coli* rare codons and consequently is very well expressed by these host cells.

In conclusion, it is possible that the insolubility problem of domain cC8 and even more so of the group of domains cC8-10, could be caused by the differences in codon preference between source and host organisms, and as such being a totally random phenomenon that does not present any reason lying in the intrinsic structure and protein synthesis in the real situation.

#### 4.2.2 *Stability of domain cC8*

We have seen in the result section regarding domain cC8 that the main problem encountered in working with this domain was the production of soluble protein. The domain, in fact, was synthesised when expressed at 37°C as insoluble and had a high tendency of precipitating in the so called inclusion bodies. In this situation it was decided to perform a refolding procedure in order to completely denature the protein and then allowing it to fold in its native structure removing the denaturant agent, urea 8M, in various steps in conditions of controlled temperature (4°C).

The protein obtained after the refolding procedure was tested in order to assess its thermodynamic stability, this was motivated by the behaviour of the protein that had a tendency to stick to surfaces, fact that suggested that cC8 could be misfolded, with some hydrophobic residue exposed on the surface and capable of interacting with membranes such as are present in concentrators and dialysis bags. To examine this aspect of domain cC8 various experiments were performed, as stated in the result section concerning this protein, comprising primarily in denaturation processes followed by the different means of fluorescence spectroscopy, in presence of a denaturant agent, and by <sup>1</sup>H 1D NMR spectroscopy performed on the same sample at different temperatures comprised between 5 and 55 °C.

##### 4.2.2.1 *Thermodynamic stability of domain cC8*

From the urea denaturation studied by fluorescence spectroscopy it was possible to conclude, by examination of the different spectra registered in the tryptophan region comprised between 300 and 400 nm, that in presence of growing concentrations of urea,

the tryptophan residue present in the protein, passed from a buried state, characterised by a fluorescence signal at 330 nm, to a situation where it was exposed on the surface, giving a peak at 350 nm, typical of this residue when it is not buried in the hydrophobic core of a protein. These results lead us to conclude that the protein is folded after the refolding procedure, at least the part where the tryptophan is located. Using the program Mathematica with the results obtained from this experiment, it was possible to calculate the *Gibbs free energy* ( $\Delta G$ ) and so to have a thermodynamic parameter to evaluate the stability of domain cC8.  $\Delta G$  is defined as

$$\Delta G = \Delta H - T\Delta S$$

for processes at constant pressure and volume, as it is our case.

$\Delta H$  is the energetic contribution, while  $\Delta S$  is the entropic contribution. An important role is played by the temperature of the system.

In general, a process is favoured if  $\Delta G < 0$ , the best situation being that of negative  $\Delta H$ , meaning that the system is at a minimum of energy, and positive  $\Delta S$ , so the system is in a situation of maximal entropy.

In the case of cC8, since we are considering the denaturation process, we obtain a positive  $\Delta G$ , in fact the value obtained for the protein in exam is 8.24 kJ; this is due to the fact that the denaturation of the protein is not a favoured process in normal conditions and it happens only in presence of a denaturant agent or at high temperatures.

In this case, the higher the  $\Delta G$ , the higher is the stability of the protein, as the process taken into account is the denaturation process.

The same value was determined for other domains of cMyBPC, like cC5 and cC0 (Idowu et al., 2003) and it was then possible to compare the value of this parameter for

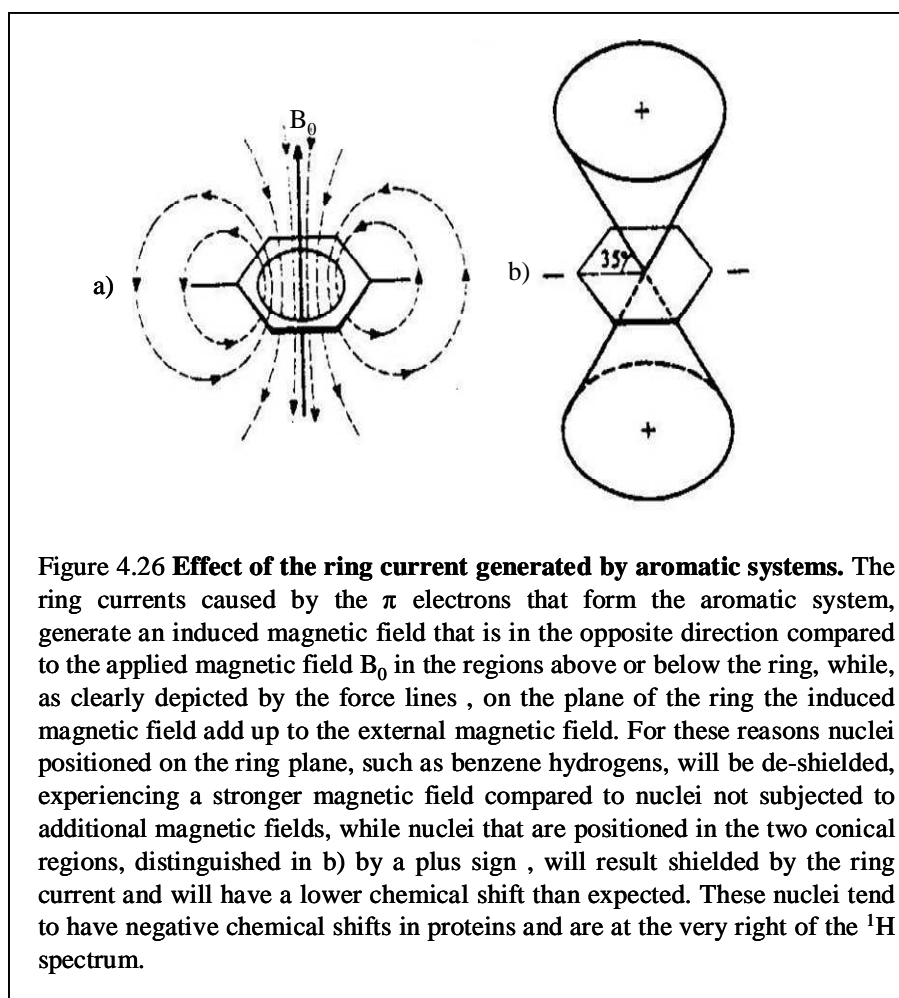
the three domains. The values of  $\Delta G$  obtained for these two domains are  $\Delta G_{cC5} = 2.83$  kJ and  $\Delta G_{cC0} = 37.74$  kJ. This means that between the three protein here considered, the most stable, being its denaturation process the less favourable, characterised by the higher value of  $\Delta G$ , is domain cC0; on the other hand cC5 resulted the less stable domain of the group. Interestingly, domain cC8 resulted having an intermediate stability. The stability of domain cC8 was also confirmed by an experimental procedure carried out by leaving samples of a solution of cC8 in different conditions such as different buffer composition (Gel filtration or NMR buffer) at different temperatures (room temperature, 4°C, -20°C and -80°C) for 30 days. After this period of time a SDS-PAGE analysis was performed that confirmed how the protein was stable in all the condition tested as present in every sample without precipitation.

From these analysis it was possible to conclude that domain cC8 is stable enough to be synthesised and purified in aqueous solution with the methodologies used in this research work.

#### *4.2.2.2 Stability of the hydrophobic core of the domain*

Once assessed the thermodynamic stability of the domain, it was necessary to understand whether the result of the refolding procedure was properly folded or not. To do this a 1D  $^1\text{H}$  NMR spectroscopy analysis was performed at different temperatures, bringing to the conclusion that the protein exists in two different conformations at low temperatures and at room temperature. A melting curve was performed, registering a 1D  $^1\text{H}$  NMR spectrum at different temperatures, between 5 and 55°C at 5°C intervals. The results, shown in picture 4.2, bring to the conclusion that the hydrophobic core of the protein undergoes conformational changes going from 5°C to 25°C. The peaks at the

very right of the spectrum, at negative chemical shifts, are characteristic of buried methyl groups that are shielded by the aromatic rings that with their ring current produce an inducted magnetic field that has an opposite direction to the external applied magnetic field, for this reason the nuclei are subjected to a weaker magnetic field and result shielded compared to the normal methyl groups that give signals around 1 ppm.



A peak positioned at -0.55 ppm was observed to split into two signals when the sample was warmed from 5°C to 25°C, meaning that in this temperature interval the hydrophobic core where the methyl group responsible of this signal is localised, undergoes some conformational changes. The hypothesis at this point was that the

refolded domain was not very stable as it existed in different conformations according to the temperature. However, the same experiment was performed on a sample of cC8 obtained using different strategies and not subjected to the refolding protocol as it was synthesised as soluble protein, but the results were consistent, bringing to the conclusion that the same phenomena happened in the soluble protein and are to be considered intrinsic structural features of the domain.

In conclusion it was not possible to detect a difference between samples obtained by refolding or by expression as soluble compound and, moreover, the refolded protein gave thermodynamic results compatible with those of a stable protein. Apart from the behaviour of domain cC8 obtained after refolding, that could bring us to the conclusion that the refolded protein presented some hydrophobic residue on the surface, there was no proof that could lead us to believe that the protein obtained after the refolding procedure was misfolded. In any case it was preferable to produce the protein as a soluble compound and this was achieved using different strategies.

#### *4.2.3 Interaction between domains cC5 and cC8 of cMyBPC*

The interaction between domain cC5 and domain cC8 of cMyBPC was suggested (Moolman-Smook et al., 2002) together with the hypothesis that a second interaction between domain cC7 and cC10 took place; these results lead the researchers to propose the trimeric collar model that took these interactions into account. In this model, also domains cC6 and cC9 are supposed to interact with one another.

As seen in the result section, soluble cC8 was obtained either as part of a fusion protein, with TrxA and NusA respectively, or by itself and the interaction was studied with cC8 obtained with both these methods. In none of the  $^1\text{H}/^{15}\text{N}$  HSQC titration experiments

performed on cC5 with different additions of cC8, was revealed a proof that the interaction took place. In the cases where a fusion protein was involved it is possible, even if not probable, that the protein fused with cC8 to increase its solubility, could prevent the two proteins from interacting. This could be caused by the sterical impediment that the fused partner could play. The best procedure would be to cut the fusion protein away with TEV protease, as a TEV cut site is present in both pETM-20 and pETM-60 vectors between the two fused proteins. This, however was not done in the first instance as it was not safe given the bad results obtained for domain cC8 alone and the risk of it precipitating appeared quite relevant. In the meantime, moreover, other strategies, were pursued and gave better results, so these analysis were not repeated on cC8 cut from the two fusion proteins.

Using tRNA supplemented competent cells, such as Codon Plus and Arctic Express cells (both from Stratagene) it was possible to produce soluble protein, easily purified, to perform  $^1\text{H}/^{15}\text{N}$  HSQC titration experiments on domain cC5, giving negative results. In this case, in contrast with the techniques used previously, it was obtained a good amount of domain cC8 that it was not present as part of a fusion protein, so these were the best conditions to determine whether the interaction took place or not. The fact that no positive result was detected induce to believe that the interaction between domain cC5 and cC8 of cMyBPC does not take place and so that the trimeric collar is not a probable model to describe how cMyBPC incorporate into the sarcomere. Moreover, from personal correspondence with Drs. Pugh and Atkinson, collaborators of Moolman. Smoock at the University of Western Cape in South Africa, we have learned that the same analysis on domains cC7 and cC10 was carried out, performing a titration followed by NMR spectroscopy on both labelled domains after the addition of a ratio 1:3 of the counterpart, in both cases without observing any shift of the peaks present in

the  $^1\text{H}/^{15}\text{N}$  HSQC spectrum (unpublished data). They have also encountered great difficulty in synthesising soluble cC8-10 that they intended to use to test its interaction with domain cC5, thus studying the system analysed by surface Plasmon resonance (Flashman et al., 2008; Moolman-Smook et al., 2002). Finally, the results obtained from the TROSY experiment performed on the group of domains cC5-7, have shown that this part of the protein is rigid, compared to the N-terminus that is flexible (Ababou et al., 2008); this makes it even harder to believe that the central and C-terminal fragments of cMyBPC could interact with one another to form a trimeric collar wrapped around the myosin filament. All these negative results cast a doubt on the veracity of the original yeast two hybrid assay and on the proposed trimeric collar model based on that result.

#### 4.2.4 Conclusions

Given the difficulties encountered in the attempt to synthesise soluble samples of domain cC8 of cMyBPC, the stability of the protein was studied using an array of different techniques. As a result of these studies it was shown that domain cC8 has a three dimensional fold and that it is thermodynamically stable. The problems faced in the synthesis of the protein are probably due to the codon content of its coding gene that create problems when trying to overexpress the protein in *E. Coli*, as using tRNA supplemented host cells gave a good protein yield. Once the solubility problems have been overcome, the possible interaction between domains cC5 and cC8 of cMyBPC was investigated, failing to give positive results. Moreover, the central part of the cMyBPC, formed by domains cC5, cC6 and cC7, has been shown to be rigid, and not flexible as it should be to be able to wrap around the thick filament. All these facts suggest that the

interaction between cC5 and cC8 might not take place and that the trimeric collar model is not a realistic hypothesis on how cMyBPC incorporate into the sarcomere.

## Chapter 5

### Conclusions

The first part of this research project focused on domain cC0 of cMyBPC; NMR was used to both determine the three dimensional structure of the cardiac specific domain cC0 and study its interaction with the Regulatory Light Chain of Myosin. The structure has been determined to high precision, showing all the features for an IgI domain, being formed, as expected, by two  $\beta$ -sheets that form a  $\beta$ -sandwich. An interesting characteristic of domain cC0 is that despite having a very well defined fold and a very compact structure, the first ten residues, containing proline residues together with patches of positively charged amino acids, are unstructured and could stretch from the domain to reach out for a still undefined binding partner. This most N-terminal fragment of cMyBPC, in fact has shown not to take part to the interaction with the RLC, suggesting that it might have a different function, specific to the cardiac isoform of MyBPC.

From the titration performed with domain cC0 and RLC it is evident how the two proteins interact via electrostatic surfaces, involving the majority of positively charged residues positioned on the N-terminal side of the domain but crucially not two lysines that are part of the unstructured region that precedes the A' strand. From the interaction studies carried out with both miniHMM and RLC is evident how domain cC0 interacts with this region of the thick filament, confirming the hypothesised (Ababou et al., 2008) mechanism by which cMyBPC could regulate cardiac contraction. It is important to note that both cC0 and two of the three phosphorylation sites present in the cC1-cC2 linker, are specific for the cardiac isoform, suggesting a direct role of cMyBPC in the continuous and rhythmic myocardial contraction. On the basis of what obtained from

interaction studies between cC1 and the S2Δ fragment of myosin, that is very close to the RLC, it has been hypothesised that the N-terminus of cMyBPC would play an important role in cardiac contraction, keeping the myosin heads in place to be ready to interact with actin; upon phosphorylation of the cC1-cC2 linker the myosin heads are free to move away from the thick filament to interact with actin, probably keeping the N-terminus of cMyBPC attached through domains cC0 and cC1, being then facilitated to go back to its resting position when the interaction with actin ceases and cMyBPC returns to its unphosphorylated form. It is also possible that not all the myosin molecules present in a sarcomere do interact with actin in normal conditions, the ones interacting with cMyBPC being impaired to do so; they could work as reinforcement when needed, allowing the heart to beat faster and increase its output upon cMyBPC phosphorylation.

The results obtained in this research work confirm this prominent role of cMyBPC in cardiac contraction, via cC0 interaction with the Regulatory Light Chain.

As for the second part of this project, focusing on domain cC8 and its possible interaction with domain cC5, it was not possible to conclude, from the results obtained, that the two domains interact with each other. Different experiments have been performed without a positive result obtained in this respect. From the results presented in this work and other data, not shown here and unpublished, obtained by other groups on the hypothesised interaction between domains cC7 and cC10, it is not possible to assume as valid the trimeric collar proposed by Moolman- Smook (Moolman-Smook et al., 2002) that was essentially based on the findings that the two couple of domains taken in exam gave a positive result when tested for interaction with a yeast two hybrid assay analysis.

Between the two models proposed for the incorporation of cMyBPC in the sarcomere is, as a consequence, more reliable the one proposed by Squire (Squire et al., 2003) where cMyBPC is arranged parallel to the myosin filament and the groups of domains cC5-7 and cC8-10 do not interact with each other. This is also confirmed by structural studies carried on the thick filament that showed as the trimeric geometry proposed by Moolman- Smoock and co-workers, would be too tight and so not allowed. In fact, the diameter of the thick filament around which cMyBPC should wrap, is 13-15 nm (Squire et al., 1998), resulting in 41-47 nm circumference, while the cMyBPC ring is supposed to be formed by three sets of three IgI domains, that have a diameter of 3.4 -3.9 nm (Improta et al., 1996; Pfuhl et al., 1995), giving a circumference of the collar around 35 nm, too short to be able to wrap around the thick filament efficiently.

In conclusion, even though not positive and conclusive results can be shown regarding the structure and the function of domain cC8, the results obtained by these studies are relevant for what concern the sarcomeric structure and the role that cMyBPC have in it. It remains to understand the function of domain cC8 and in this matter would be interesting to solve the structure of the domain, now that it has been shown that the protein can be produced in good quantity as a soluble compound. Moreover it will be important to identify its binding partner to understand whether this domain has a role other than structural in the protein.

Finally, now that domain cC8 has been shown not to be the binding partner of the central domain of cMyBPC, it would be of vital importance to identify the protein that interacts with it as to unveil the function of domain cC5 and, especially, of its cardiac specific insertion that makes it so unique.

## Appendices

### A.1 Culture media and Buffers

#### Luria Bertani culture medium

Per litre:

Yeast 5 g  
Tryptone 10 g  
NaCl 10 g

Make up to volume with deionised H<sub>2</sub>O and autoclave. When cool, add the desired antibiotics.

#### M9 medium modified according to Chen

This medium allows the introduction of selective nitrogen and carbon isotopes into expressed proteins and was prepared as follows:

Place 50ml 20X salts solution in a flask and make up to volume (1L) and autoclave. When cool, add the followings:

MgSO <sub>4</sub> 1M	2ml	
CaCl <sub>2</sub> 0.1M	100 µl	
Glucose	6g	dissolved in 50 ml of H <sub>2</sub> O
NH <sub>4</sub> Cl	1g	
Vitamins	1ml	
Micronutrients	1ml.	

#### 20X salts solution (per 1L)

Na <sub>2</sub> HPO <sub>4</sub>	120g
KH <sub>2</sub> PO <sub>4</sub>	60g
NaCl	10g

#### Micronutrients

NaMoO <sub>4</sub>	0.73 mg
H <sub>3</sub> BO <sub>3</sub>	24.7 mg
CoCl <sub>2</sub>	7.1 mg
CuSO <sub>4</sub>	2.5 mg
MnCl <sub>2</sub>	15.8 mg
ZnSO <sub>4</sub>	2.9 mg

### Vitamins

Choline Chloride	0.4 g
Folic Acid	0.5 g

### FF6 Wash Buffer

PO <sub>4</sub>	20 mM
NaCl	500 mM
Imidazole	10 mM
βME	2.5 mM
NaN <sub>3</sub>	0.02%

pH = 7.5-8.0

### FF6 Elution Buffer

PO <sub>4</sub>	20 mM
NaCl	500 mM
Imidazole	500 mM
βME	2.5 mM
NaN <sub>3</sub>	0.02%

pH = 7.5-8.0

### Gel Filtration Buffer

PO <sub>4</sub>	40 mM
NaCl	250 mM
DTT	2mM

pH = 7.0

### NMR Buffer

PO <sub>4</sub>	40 mM
NaCl	50 mM
DTT	2mM

pH = 7.0

SOC medium

Per litre:

Yeast	5 g
Tryptone	10 g
NaCl	10 mM
KCl	2.5 mM
MgCl <sub>2</sub>	10 mM
MgSO <sub>4</sub>	10 mM
Glucose	20 mM

TBS buffer

Tris.HCl	50 mM
NaCl	150 mM
BME	2.5 mM

pH 7.5.

## A.2 Sequence Specific Assignment for domain cC0

	Chemical Shift			Chemical Shift	
3 PRO	CA	63.375		HD2	3.561
	CB	31.835		HD3	3.731
	CG	27.043		HG2	1.916
	HA	4.235		HG3	1.913
	HB2	2.196			
	HB3	1.852			
	HD2	3.731			
	HD3	3.608			
	HG2	1.931			
	HG3	1.931			
4 GLY	CA	45.043			
	H	8.439			
	HA2	3.854			
	HA3	3.819			
	N	108.904			
5 LYS	CA	55.709			
	CB	33.081			
	CD	28.328			
	CE	41.719			
	CG	25.020			
	H	7.974			
	HA	4.265			
	HB2	1.638			
	HB3	1.724			
	HD2	1.613			
	HD3	1.613			
	HE2	2.900			
	HE3	2.900			
	HG2	1.280			
HG3	1.327				
N	120.616				
6 LYS	CA	54.105			
	CB	32.381			
	H	8.291			
	HA	4.505			
	HB2	1.651			
	HB3	1.662			
N	124.267				
7 PRO	CA	62.738			
	CB	31.942			
	CD	50.178			
	CG	27.191			
	HA	4.371			
	HB2	1.793			
	HB3	2.178			
8 VAL	CA	61.883			
	CB	32.743			
	CG1	20.005			
	CG2	20.005			
	H	8.244			
	HA	4.012			
	HB	1.956			
	HG11	0,588194			
	HG12	0,588194			
	HG13	0,588194			
9 SER	HG21	0,58125			
	HG22	0,58125			
	HG23	0,58125			
	N	120.593			
	CA	57.429			
	CB	63.804			
	H	8.296			
HA	4.315				
10 ALA	HB2	3.682			
	HB3	3.874			
	N	118.557			
	CA	53.042			
	CB	19.919			
	H	8.214			
	HA	4.069			
11 PHE	HB1	0,658333			
	HB2	0,658333			
	HB3	0,658333			
	N	125.277			
	CA	57.727			
	CB	39.854			
	CD1	131.338			
CD2	131.338				
CE1	130.933				
CE2	130.933				
H	8.238				
HA	4.816				
HB2	2.608				
HB3	2.827				
HD1	6.982				
HD2	6.982				

	HE1	6.675	16 ARG	CA	53.951
	HE2	6.675		CB	32.456
	HZ	6.608		CD	43.269
	N	114.771		CG	27.018
				H	8.118
12 SER	CA	58.641		HA	4.592
	CB	63.274		HB2	1.966
	H	8.809		HB3	1.966
	HA	4.395		HD2	3.189
	HB2	3.510		HD3	3.189
	HB3	3.747		HG2	1.697
	N	119.399		HG3	1.697
				N	119.622
13 LYS	CA	56.362	17 SER	CA	59.888
	CB	35.664		CB	63.405
	H	7.884		H	8.511
	HA	4.575		HA	5.281
	HB2	1.654		HB2	4.304
	HB3	1.653		HB3	4.238
	HD2	1.489		N	117.935
	HD3	1.543			
	HE2	2.843	18 VAL	CA	60.004
	HE3	2.843		CB	36.675
	HG2	1.249		CG1	21.498
	HG3	1.358		CG2	21.498
	N	121.565		H	8.389
				HA	4.660
14 LYS	CA	53.374		HB	1.942
	CB	32.741		HG11	0,542361
	CD	29.184		HG12	0,542361
	CG	25.400		HG13	0,542361
	H	8.744		HG21	0,546528
	HA	4.313		HG22	0,546528
	HB2	1.578		HG23	0,546528
	HB3	1.578		N	117.416
	HD2	1.619			
	HD3	1.671	19 GLU	CA	54.138
	HG2	1.029		CB	31.658
	HG3	1.368		H	8.190
	N	125.096		HA	5.351
				HB2	1.790
15 PRO	CA	62.248		HB3	1.710
	CB	31.343		HG2	1.923
	CD	49.521		HG3	1.978
	CG	27.823		N	124.652
	HA	4.693			
	HB2	1.584	20 VAL	CA	59.013
	HB3	0,578472		CB	36.048
	HD2	3.086		CG1	21.605
	HD3	2.915		CG2	20.411
	HG2	1.458		H	8.616
	HG3	1.446		HA	4.491

	HB	1.846		26 ALA	CA	49.972
	HG11	0,453472			CB	22.877
	HG12	0,453472			H	8.688
	HG13	0,453472			HA	4.396
	HG21	0,517361			HB1	0,670833
	HG22	0,517361			HB2	0,670833
	HG23	0,517361			HB3	0,670833
	N	120.245			N	123.024
21 ALA	CA	51.307		27 VAL	CA	60.899
	CB	18.726			CB	33.331
	H	8.375			CG1	20.663
	HA	4.364			H	7.751
	HB1	1.275			HA	4.522
	HB2	1.275			HB	1.525
	HB3	1.275			HG11	0,384028
	N	126.173			HG12	0,384028
					HG13	0,384028
22 ALA	CA	53.104			HG21	0,455556
	CB	17.631			HG22	0,455556
	H	8.287			HG23	0,455556
	HA	3.899			N	121.938
	HB1	1.284		28 PHE	CA	56.051
	HB2	1.284			CB	42.218
	HB3	1.284			CD1	133.446
	N	123.045			CD2	133.446
					CE1	132.118
23 GLY	CA	44.741			CE2	132.118
	H	9.862			H	9.196
	HA2	3.255			HA	4.561
	HA3	4.371			HB2	2.356
	N	112.047			HB3	2.354
					HD1	6.719
24 SER	CA	57.787			HD2	6.719
	CB	63.296			HE1	6.992
	H	7.944			HE2	6.992
	HA	4.750			HZ	6.781
	HB2	3.874			N	126.818
	HB3	3.932				
	N	119.405		29 GLU	CA	54.508
					CB	33.692
25 PRO	CA	61.743			H	8.583
	CB	31.751			HA	5.405
	CD	49.384			HB2	1.811
	CG	26.460			HB3	1.744
	HA	5.142			HG2	1.933
	HB2	2.010			HG3	2.002
	HB3	1.433			N	120.733
	HD2	3.651				
	HD3	3.743		30 ALA	CA	49.421
	HG2	1.949			CB	23.523
	HG3	1.958			H	9.484

	HA	4.691	35 ALA	CA	51.762
	HB1	1.169		H	8.614
	HB2	1.169		HA	4.050
	HB3	1.169		HB1	1.247
	N	124.341		HB2	1.247
31 GLU	CA	54.301		HB3	1.247
	CB	33.336		N	125.041
	CG	36.469	36 GLY	CA	45.703
	H	9.001		H	8.647
	HA	6.016		HA2	3.634
	HB2	1.955		HA3	3.960
	HB3	1.779		N	108.031
	HG2	2.114	37 VAL	CA	61.469
	HG3	2.162		CB	32.942
	N	120.169		CG1	21.112
32 THR	CA	59.738		CG2	21.112
	CB	69.791		H	7.077
	CG2	22.123		HA	3.869
	H	9.330		HB	1.750
	HA	4.842		HG11	0,447917
	HB	4.515		HG12	0,447917
	HG21	0,477083		HG13	0,447917
	HG22	0,477083		HG21	0,508333
	HG23	0,477083		HG22	0,508333
	N	115.538		HG23	0,508333
33 GLU	CA	58.563		N	119.457
	CB	29.836	38 LYS	CA	55.873
	CG	35.634		CB	30.881
	H	7.950		CD	26.795
	HA	3.944		CG	26.885
	HB2	1.911		H	8.467
	HB3	1.839		HA	4.267
	HG2	2.019		HB2	1.755
	HG3	2.143		HB3	1.656
	N	119.723		HD2	3.085
34 ARG	CA	53.485		HD3	3.085
	CB	32.411		HG2	1.502
	CD	42.823		HG3	1.502
	CG	26.552		N	128.214
	H	7.791	39 VAL	CA	60.114
	HA	4.490		CB	33.719
	HB2	1.743		CG1	20.059
	HB3	1.511		CG2	20.375
	HD2	3.134		H	7.993
	HD3	3.134		HA	4.537
	HG2	1.488		HB	1.126
	HG3	1.486		HG11	-0.059
	N	113.251		HG12	-0.059
				HG13	-0.059

	HG21	-0.072	CG	26.530	
	HG22	-0.072	H	8.209	
	HG23	-0.072	HA	4.039	
	N	123.133	HB2	1.515	
40 ARG	CA	54.098	HB3	1.325	
	CB	33.701	HD2	2.471	
	CD	43.962	HD3	2.742	
	CG	26.219	HG2	0,593056	
	H	8.507	HG3	1.032	
	HA	4.503	N	119.579	
	HB2	1.689	46 SER	CA	56.766
	HB3	1.401		CB	64.815
	HD2	2.923		H	7.513
	HD3	3.162		HA	4.674
	HG2	1.357		HB2	3.771
	HG3	1.524		HB3	3.631
	N	124.492		N	114.927
41 TRP	CA	55.134	47 ASP	CA	55.177
	CB	31.370		CB	40.385
	CE3	121.341		H	8.698
	CH2	123.826		HA	4.830
	CZ2	114.432		HB2	2.522
	H	9.083		HB3	2.522
	HA	5.311		N	125.553
	HB2	2.829	48 ILE	CA	61.218
	HB3	3.113		CB	39.345
	HD1	7.214		CD1	13.311
	HE1	10.427		CG1	27.943
	HE3	7.464		CG2	17.465
	HH2	6.488		H	8.781
	HZ2	7.013		HA	3.879
	HZ3	6.434		HB	1.326
	N	123.367		HD11	0,270139
	NE1	129.996		HD12	0,270139
42 GLN	CA	54.445		HD13	0,270139
	CB	34.775		HG12	0,286806
	CG	33.383		HG13	0,294444
	H	9.532		HG21	0,1125
	HA	5.159		HG22	0,1125
	HB2	1.606		HG23	0,1125
	HB3	1.443		N	124.032
	HE21	7.520	49 SER	CA	56.256
	HE22	7.520		CB	65.243
	HG2	1.776		H	7.963
	HG3	2.011		HA	4.681
	N	118.692		HB2	3.840
43 ARG	CA	54.790		HB3	3.813
	CB	32.202		N	121.077
	CD	42.579			

50 ALA	CA	53.052	55 GLY	CA	44.332	
	CB	18.821		H	9.666	
	H	8.516		HA2	4.653	
	HA	4.302		HA3	3.343	
	HB1	1.496		N	110.691	
	HB2	1.496		56 LEU	CA	54.213
	HB3	1.496			CB	45.206
N	123.977	CD1	25.698			
51 SER	CA	56.946	CD2		25.698	
	CB	65.759	CG		27.947	
	H	9.564	H		8.542	
	HA	4.797	HA		5.138	
	HB2	4.118	HB2	1.609		
	HB3	4.245	HB3	1.609		
	N	117.545	HD11	0,478472		
52 ASN	CA	55.930	HD12	0,574306		
	CB	37.045	HD13	0,574306		
	HB2	1.603	HD21	0,58125		
53 LYS	CA	53.699	HD22	0,565278		
	CB	33.687	HD23	0,58125		
	CD	26.920	HG	1.372		
	CE	42.339	57 ALA	CA	51.318	
	CG	23.075		CB	22.564	
	H	8.053		H	8.594	
	HA	3.995		HA	4.790	
	HB2	1.049		HB1	1.296	
	HB3	1.364		HB2	1.296	
	HD2	1.307		HB3	1.296	
	HD3	1.541	N	124.534		
	HE2	2.413	58 THR	CA	62.034	
	HE3	2.776		CB	72.197	
	HG2	0,507639		CG2	21.244	
HG3	0.014	H		8.602		
N	121.638	HA		4.862		
54 TYR	CA	55.016		HB	3.824	
	CB	40.147		HG21	1.078	
	CD1	134.261	HG22	1.078		
	CD2	134.261	HG23	1.078		
	CE1	118.090	59 GLU	CA	54.955	
	CE2	118.090		CB	31.121	
	H	6.779		CG	35.799	
	HA	5.484		H	8.883	
	HB2	2.414		HA	4.378	
	HB3	2.893		HB2	1.872	
	HD1	7.116		HB3	1.775	
	HD2	7.116	HG2	2.025		
	HE1	6.832				
	HE2	6.832				
N	114.754					

	HG3	2.031		HG22	1.002
	N	128.594		HG23	1.002
				N	117.400
60 GLY	CA	47.127	65 LEU	CA	52.783
	H	9.045		CB	41.350
	HA2	4.081		CD1	23.288
	HA3	3.529		CD2	25.721
	N	117.047		CG	27.621
61 THR	CA	61.659		H	8.456
	CB	68.477		HA	4.642
	CG2	21.961		HB2	-1.049
	H	8.332		HB3	0,184028
	HA	4.129		HD11	0,268056
	HB	4.973		HD12	0,268056
	HG21	0,626389		HD13	0,268056
	HG22	0,626389		HD21	0,315278
	HG23	0,626389		HD22	0,315278
	N	118.086		HD23	0,315278
				HG	1.036
				N	129.806
62 ARG	CA	56.040	66 THR	CA	61.072
	CB	31.775		CB	70.346
	CD	43.198		CG2	20.199
	CG	27.651		H	9.381
	H	7.906		HA	4.975
	HA	4.754		HB	3.668
	HB2	1.757		HG21	0,613889
	HB3	1.860		HG22	0,613889
	HD2	3.083		HG23	0,613889
	HD3	3.083		N	123.110
	HG2	1.381	67 VAL	CA	61.300
	HG3	1.505		CB	31.636
	N	121.911		CG1	21.786
63 HIS	CA	55.066		CG2	19.338
	CB	33.860		H	9.493
	CE1	139.890		HA	4.317
	H	9.212		HB	2.034
	HA	5.364		HG11	0,593056
	HB2	2.971		HG12	0,593056
	HB3	3.572		HG13	0,593056
	HD2	6.870		HG21	0,593056
	HE1	7.786		HG22	0,593056
	N	127.111		HG23	0,593056
64 THR	CA	60.691		N	128.451
	CB	71.788	68 ARG	CA	57.379
	CG2	21.532		CB	30.481
	H	9.261		CD	42.878
	HA	5.510		CG	29.809
	HB	3.763		H	8.500
	HG21	1.002			

	HA	3.839	73 ALA	CA	53.826
	HB2	1.637		CB	18.152
	HB3	1.586		H	8.558
	HD2	3.004		HA	4.186
	HD3	3.004		HB1	1.352
	HG2	1.295		HB2	1.352
	HG3	1.412		HB3	1.352
	N	124.308		N	118.164
69 GLU	CA	55.733	74 ASP	CA	55.178
	CB	28.793		CB	42.280
	CG	36.565		H	8.381
	H	8.545		HA	4.586
	HA	3.147		HB2	2.638
	HB2	1.854		HB3	2.859
	HB3	1.626		N	113.856
	HG2	2.036	75 GLN	CA	56.682
	HG3	2.036		CB	30.337
	N	118.177		CG	36.612
70 VAL	CA	63.848		H	7.409
	CB	31.885		HA	4.252
	CG1	23.112		HB2	2.007
	CG2	23.209		HB3	1.889
	H	7.771		HG2	2.144
	HA	3.810		HG3	2.191
	HB	2.044		N	119.456
	HG11	0,540972	76 GLY	CA	44.149
	HG12	0,540972		H	8.984
	HG13	0,540972		HA2	4.610
	HG21	0,605556		HA3	3.863
	HG22	0,605556		N	112.000
	HG23	0,605556	77 SER	CA	58.199
	N	117.579		CB	64.099
71 GLY	CA	43.915		H	8.106
	H	9.389		HA	5.009
	HA2	4.470		HB2	3.609
	HA3	3.895		HB3	3.583
	N	114.169		N	114.587
72 PRO	CA	65.800	78 TYR	CA	56.450
	CB	31.553		CB	43.805
	CD	49.371		CD1	133.581
	CG	27.502		CD2	133.581
	HA	4.038		CE1	117.163
	HB2	2.325		CE2	117.163
	HB3	1.900		H	9.056
	HD2	3.404		HA	4.530
	HD3	3.726		HB2	2.121
	HG2	1.908		HB3	1.199
	HG3	2.095		HD1	6.836

		HD2	6.836		HB3	0,345833
		HE1	6.590		N	128.273
		HE2	6.590			
		N	127.751	83 GLY	CA	46.917
					H	8.841
79 ALA		CA	50.806		HA2	3.815
		CB	23.130		HA3	3.509
		H	8.558		N	113.065
		HA	5.233			
		HB1	1.027	85 SER	CA	58.485
		HB2	1.027		CB	64.397
		HB3	1.027		H	8.423
		N	118.647		HA	4.659
					HB2	3.951
80 VAL		CA	58.760		HB3	3.956
		CB	35.087		N	119.428
		CG1	20.518			
		CG2	19.044	86 LYS	CA	54.822
		H	8.717		CB	35.340
		HA	4.905		CD	29.225
		HB	1.464		CE	41.340
		HG11	-0.604		CG	24.861
		HG12	-0.604		H	8.490
		HG13	-0.604		HA	5.243
		HG21	0,092361		HB2	1.631
		HG22	0,092361		HB3	1.507
		HG23	0,092361		HD2	1.431
		N	118.846		HD3	1.431
					HE2	2.592
81 ILE		CA	59.751		HE3	2.592
		CB	42.030		HG2	0,654861
		CD1	13.667		HG3	1.040
		CG1	27.852		N	125.678
		CG2	17.484			
		H	8.739	87 VAL	CA	60.870
		HA	5.012		CB	34.228
		HB	1.342		CG1	21.238
		HD11	0,358333		CG2	21.404
		HD12	0,358333		H	8.863
		HD13	0,358333		HA	4.300
		HG12	1.140		HB	1.633
		HG13	0,471528		HG11	0,583333
		HG21	0,446528		HG12	0,583333
		HG22	0,446528		HG13	0,583333
		HG23	0,446528		HG21	0,396528
		N	126.232		HG22	0,396528
					HG23	0,396528
82 ALA		CA	50.839		N	126.631
		CB	21.160			
		H	8.388	88 LYS	CA	55.124
		HA	4.449		CB	34.479
		HB1	0,345833		CD	29.073
		HB2	0,345833		CG	24.829

	H	8.475		CB	35.261
	HA	5.065		CD	28.775
	HB2	1.756		CE	41.729
	HB3	1.615		CG	25.087
	HD2	1.527		H	8.892
	HD3	1.527		HA	4.733
	HE2	2.784		HB2	1.799
	HE3	2.784		HB3	1.706
	HG2	1.245		HD2	1.617
	HG3	1.354		HD3	1.617
	N	125.592		HE2	2.882
				HE3	2.882
89 PHE	CA	56.311		HG2	1.287
	CB	39.383		HG3	1.407
	CD1	133.287		N	128.486
	CD2	133.287			
	H	8.152	93 VAL	CA	60.568
	HA	4.601		CB	33.024
	HB2	2.657		CG1	21.362
	HB3	2.886		CG2	21.362
	HD1	6.387		H	8.563
	HD2	6.387		HA	4.818
	HE1	5.811		HB	1.712
	HE2	5.811		HG11	0,41875
	HZ	6.748		HG12	0,41875
	N	119.005		HG13	0,41875
				HG21	0,41875
90 ASP	CA	53.532		HG22	0,41875
	CB	45.151		HG23	0,41875
	H	9.006		N	124.459
	HA	5.565			
	HB2	2.464	94 ILE	CA	60.238
	HB3	2.464		CB	39.279
	N	118.742		CD1	12.635
				CG1	26.893
91 LEU	CA	54.171		CG2	17.256
	CB	45.625		H	8.395
	CD2	24.928		HA	4.162
	CG	28.631		HB	1.617
	H	8.733		HD11	0,458333
	HA	5.137		HD12	0,458333
	HB2	1.358		HD13	0,458333
	HB3	2.245		HG12	0,583333
	HD11	0,480556		HG13	1.181
	HD12	0,480556		HG21	0,532639
	HD13	0,480556		HG22	0,532639
	HD21	0,577083		HG23	0,532639
	HD22	0,577083		N	126.433
	HD23	0,577083			
	HG	1.358	95 GLU	CA	56.738
	N	121.344		CB	30.590
				H	8.707
92 LYS	CA	54.910		HA	4.317

HB2	1.979
HB3	1.979
HG2	2.245
HG3	2.245
N	126.596

### A.3 Sequence alignment for cMyBPC

```

cHuman/1-1273      1 MPEPGKKPVSAF SKKPRSAEVAAGSSAVFEAETERAGVKVRWQRGGSDISASNKYG 56
cCow/1-1269        1 MPEPGKKPVSAF SKKPRSAEVAAGSSAVFEAETERAGLKVVRWQRAGSDISASDKYS 56
cMouse/1-1270      1 MPEPGKKPVSAF NKKPRSAEVTAGSAAVFEAETERSGMVVRWQRDSDITANDKYG 56
cChicken/1-1271    1 -PEPAKKAVSFAFTKKPKTTEVAAGSTAVFEAETEKTIKVKWQRAGTEITDSEKYA 55
Hum_fok1-1142      1 M..... 1
Mouse_fok1-1136    1 .....
Chick_fok1-1131    1 .....
Hum_sol1-1141      1 M.....

cHuman/1-1273      57 LATEGTRHTLTVREVGPADQGSYAVIAGSSKVKFDLKVIEA...EKAEPMLAP-AP 108
cCow/1-1269        57 LAATEGTRHTLTVRDVGPADQGSYAVIAGSSKVKFDLKVVDAG...KAEPVSAAPA-P 108
cMouse/1-1270      57 LAAEGRKHTLTVRDASDDQGSYAVIAGSSKVKFDLKVTEPAPPEKAESEVAPGAP 112
cChicken/1-1271    56 IKAEGNKHSLTISNVGKDDDEVTYAVIAGTSKVKFELKVKEPE...KSEPVAPAEAS 108
Hum_fok1-1142      2 .....
Mouse_fok1-1136    2 .....
Chick_fok1-1131    2 .....
Hum_sol1-1141      2 .....PEPTK 6

cHuman/1-1273      109 -APAEATG-APG-EAPAPAAELGESAPSPKG-SSSAALNGPTPGAFDDPIGLFVM 159
cCow/1-1269        109 -APTEAPG-APG-EAPTSAPVEEAG-APSPREESSAAPEGPPSA-PGDP IGLFVM 157
cMouse/1-1270      113 EEVP--APATELEESVSSFE-0---SVSVTDDGSAAEHQ-GA...PDDPIGLFLM 157
cChicken/1-1271    109 PAPAASELPAPPVE-SNQNF--EV--PPAE-...TQPEE...FVDP IGLFVT 148
Hum_fok1-1142      4 AKPAAKKAPKKGKDAKGAPEAPPEAPAEAPKEAPPEEQSPTAEPT...GVFLK 56
Mouse_fok1-1136    2 PEAKPAAKKASKGDAPKEAPAKOTPEEPPKEAPPEEQSPTAEPT...GIFLK 52
Chick_fok1-1131    1 --PEPSKAAPKKEAKKKEEKKEEKKEAPPQEHKDEAPDDVHPRETDPPEGLFLS 53
Hum_sol1-1141      7 KEENEVPAPAPPEEPESKEKEAGTTPAKDWTLVETPPGEEQAKQNANSQLSILFIE 62

cHuman/1-1273      160 RPQDGEVTVGGSITFSARVAGASLLKPPVVKWFKGKWVDLSSKVGQHLQLHDSYDR 215
cCow/1-1269        158 RPQDGEVTVGGTITFSARVAGASLLKPPVVKWFKGKWVDLSSKVGQHLQLHDSYDR 213
cMouse/1-1270      158 RPQDGEVTVGGSIVFSARVAGASLLKPPVVKWFKGKWVDLSSKVGQHLQLHDSYDR 213
cChicken/1-1271    149 RPQDGEVTVGGNITFTAVAGESLLKPPSVKWFKGMWDLASKVGHKHLQLHDSYDR 204
Hum_fok1-1142      57 KPDSVSVETGKDAVVVAHVNGKELPKPTIKWFKGKWLELGSKSGARFIFKESHNS 112
Mouse_fok1-1136    53 KPDSVSVETGKDAVILAKVNGKELPKGKPTIKWFKGKWLELGSKSGARFIFKESHNS 109
Chick_fok1-1131    54 KPDSVSVETGKDAVIVSARVAGAAALCAPAVKWFKGMWELGDKS-ARCRLRHSVDD 108
Hum_sol1-1141      63 KPQGGTVKVGEDITFIKVKKAEDLLKPTIKWFKGKWMDLASKAGKHLQLKETFER 118

cHuman/1-1273      216 ASKVYLFELHI TDAQPAFTGYSRCEVSTKDNFDCSNFNLTVHEAMGTGDL DLS-A 270
cCow/1-1269        214 TSKVYLFELRIMDAQTFAGGYRCEVSTKDNFDCSNFNLTVHEAVGPGDVLRS-T 208
cMouse/1-1270      214 ASKVYLFELHI TDAQTSAGGYRCEVSTKDNFDCSNFNLTVHEALGSGDLDLRS-A 208
cChicken/1-1271    205 NNKVYTFEMEI IEANMTFAGGYRCEVSTKDNFDCSNFNLIVNEAPVSGEMDIRA-A 259
Hum_fok1-1142      113 ANVYTVLHIGKVVLDGRGYRLEVKAKDTDCSGFNIDV-EAPRQDASQSL-E 166
Mouse_fok1-1136    109 TNVYTVLHIGKVVLDGRGDYFLEIKAKDVCDCSFNVDV-EAPRQDSQSL-E 162
Chick_fok1-1131    109 DK-VHTFELTIKVMAGDRGDYFCEVTAKEKDCSFSIDV-EARR-SSEGNVL-Q 180
Hum_sol1-1141      119 HSKVYTFEMQIIKAKDNFAGNYRCEVTVKDNFDCSCEDELVHE-STGTTNIDIRS 173

cHuman/1-1273      271 FRRTSLAGGRRISDSHEDTGLDFSSLLKKSSSFRTPRDSKLEAPAEEDVWEILR 328
cCow/1-1269        269 FRRTSLAGGRRISDSHEDAGTDFSSLLRKSRLRT-P--RLEAPAEEDVWEILR 320
cMouse/1-1270      269 FRRTSLAGARRTSDSHEDAGTDFSSLLKKRDSFRRD--SKLEAPAEEDVWEILR 322
cChicken/1-1271    260 FRRTSLAGGRRMTSAFLSTEGLEESGELNFSALLKRRDSFLRTANRGDGKSDSOP 315
Hum_fok1-1142      167 SFRTSEKKS DTA-GELDFSGLLKKREVVEEKKKKKKDDDDLGIPPE--IWELLK 219
Mouse_fok1-1136    163 SFKRSGDGKSEDA-GELDFSGLLKKREVVEEKKKKK- DDDDLGIPPE--IWELLK 214
Chick_fok1-1131    161 AFRTGEGKDDTA-GELDFSGLLKKREVQVEEKKKKKDEDDEQF--PPE--IWELLK 211
Hum_sol1-1141      174 AFKRSGEGQED-A-GELDFSGLLKRREVMKQEEEPQVDV-----WELLKN 216

cHuman/1-1273      327 QA-----PPSEYERIAFQYGVITDLRGM LKRLKGMRRDEKKSSTAFQKKLEPAY 373
cCow/1-1269        321 QA-----PPSEYERIAFQHGVTDLRGM LKRLKGIHRDEKKSSTAFQKKLQPAY 367
cMouse/1-1270      323 QA-----PPSEYERIAFQHGVEACHRPLKRLKGMHQDEKKSSTAFQKKLEPAY 369
cChicken/1-1271    316 DVDVWEILRKAPPSEYERIAFQYGVITDLRGM LKRLKRIKKEEKSSTAFLLKLDPAY 371
Hum_fok1-1142      220 GA-----KKSEYERIAFQYGVITDLRGM LKRLKKAHVVEKKSAAFTKKLDPAY 266
Mouse_fok1-1136    215 GA-----KKSEYERIAFQYGVITDLRGM LKRLKKAHVVEKKSAAFTKKLDPAY 261
Chick_fok1-1131    212 GV-----TKKSEYERIAFQYGVITDLRGM LKRLKRVHVEPKKSEAFIRKLDPAY 259
Hum_sol1-1141      217 A-----KPSYERIAFQYGVITDLRGM LKRLKRMREEKKSAAFAKILDPAY 262

cHuman/1-1273      374 QVSKGHKIRLTVLADHDAEVKWLKNGQEIQMSG-RYIFESIGAKRRLTISQCSLA 428
cCow/1-1269        368 QVSKGHKIRLMLVELADPAEVKWLKNGQEIQMSGSKYIFESIGAKRRLTISQCSLA 423
cMouse/1-1270      370 QVSKGHKIRLTVLADPAEVKWLKNGQEIQMSGSKYIFESVGAKRRLTISQCSLA 425
cChicken/1-1271    372 QVDHGQKIRLMLVEVAPDADVWVWLKNGQEIQVSGSKYIFEAIGNKRLTINHCSLA 427
Hum_fok1-1142      267 QVDRGNKIRLMLVEISDPDLTLKWFKNGQEIKPS-SKYVVENVGKRLTINKCTLA 321
Mouse_fok1-1136    262 QVDRGNKIRLVVEISDPDLPLKWFKNGQEIKPS-SKYVVENVGKRLTINKCTLA 316
Chick_fok1-1131    260 QVDHGKIRLVLVELSDPDLPLKWFKNGQLKPS-TKYVVENVGKRLTINKCTLA 314
Hum_sol1-1141      263 QVDKGGRVFVVELADPKLEVWVWVNGQEI RPS-TKYIFEHKGQRILFINNCOMT 317

```

*cHuman/1-1273* 429 DDAAAYOCVVGGEEKCS TELFVKPPVLI TRPLEDQLVMVGORVEFECEVSEEGAQVK 484  
*cCow/1-1269* 424 DDAAAYOCVVGGEEKCS TELFVKPPVLI TRPLEDQLVMVGORVEFECEVSEEGAQVK 479  
*cMouse/1-1270* 426 DDAAAYOCVVGGEEKCS TELFVKPPVLI TRPLEDQLVMVGORVEFECEVSEEGAQVK 481  
*cChicken/1-1271* 428 DDAAAYOCVVAAEKS TELFVKPPVLI TRPLEDQVMVGERVEFECEVSEEGATVK 483  
*Hum\_fok1-1142* 322 DDAAAYEVAVKDEKCF TELFVKPPVLI VTPLEDQVQVFGDRVEMAVEVSEEGAQVM 377  
*Mouse\_fok1-1136* 317 DDAAAYEVAVQDEKCF TELFVKPPVLI VTPLEDQVQVFGDRVEMAVEVSEEGAQVM 372  
*Chick\_fok1-1131* 315 DDAAAYECRVNDEKCF TELFVKPPVLI VTRPLEDQVQVFGDRVLEAEVSEEGAQVM 370  
*Hum\_sol1-1141* 318 DDSEYVVTAGDEKCS TELFVREPPIMVTQLLEDTTAYCGERVELECEVSEEDANVN 373

*cHuman/1-1273* 485 WLKDGVELTREETF KYRFK - - KDGDRHLLIINEAMLEDAGHYALCTSGGQALAEI 538  
*cCow/1-1269* 480 WLKDGVELTREETF KYRFK - - KDGDKHLLIINEATLEDAGHYALRTSGGQALAEI 533  
*cMouse/1-1270* 482 WLKDGVELTREETF KYRFK - - KDGKRLHLLIINEATLEDAGHYAVRTSGGSLAEI 535  
*cChicken/1-1271* 484 WEKDGVELTREETF KYRFK - - KDGKKQYLLIINESTKEDSGHYTKTNGGVSVAEI 537  
*Hum\_fok1-1142* 378 WMKDGVELTREDSF KARYRFKDKGKRHLIFSDVVQEDRGRYQVITNGGCCEAEI 433  
*Mouse\_fok1-1136* 373 WMKDGVEMTREDSY KARYRFKDKGKRHLIYSDVAQEDGGRYQVITNGGCCEAEI 428  
*Chick\_fok1-1131* 371 WLKDGVDVTRDD - - AFKYRFKDKGKRHLIINEAELSDSAHYKIMTNGGSEAEI 424  
*Hum\_sol1-1141* 374 WFKNGEELIPGPKSR YRIRV - - EGKHLILIEGATKADAAEYSVMTGGSSAKLS 427

*cHuman/1-1273* 539 VQENKLELVYQSIADLMVGAKDQAVFKCEVSDENVRGVWLKNGKELVPDSRIKVSII 594  
*cCow/1-1269* 534 VQENKLELVYQSIADLVGSKDQAVFKCEVSDENVRGVWLKNGKELVPDSRIKVSII 589  
*cMouse/1-1270* 538 VQENKLELVYQSIADLAVGAKDQAVFKCEVSDENVRGVWLKNGKELVPDSRIKVSII 591  
*cChicken/1-1271* 538 VQENKLELVYQSIADLVKARDQAVFKCEVSDENVRGVWLKNGKELVPDSRIKVSII 593  
*Hum\_fok1-1142* 434 VEEKQLEVLQDIADLVKASEDQAVFKCEVSDKVTGKWYKNGVEVRPSKRITISHV 489  
*Mouse\_fok1-1136* 429 VEEKQLEVLQDIADLVKAAEDQAVFKCEVSDKVTGKWYKNGVEVRPSKRITISHV 484  
*Chick\_fok1-1131* 425 VEEKQLEVLQDIADLVKASEDQAVFKCEVSDKVTGRWFRNGVEVRPSKRITISHV 480  
*Hum\_sol1-1141* 428 VDLNPLKILTLTLDIVNLGKEICLKCEISENI - PGKWTKNGLPVQESDLKVVHK 482

*cHuman/1-1273* 595 GRVHKLTI DDVTPADEADYSFVPEGFAC - NLSAKLHFMEVKIDFVPRQEPPIHLD 649  
*cCow/1-1269* 590 GRVHKLTI DDVTPADEADYSFVPEGFAC - NLSAKLHFMEVKIDFVPRQEPPIHLD 644  
*cMouse/1-1270* 592 GRVHKLTI DDVTPADEADYSFVPEGFAC - NLSAKLHFMEVKIDFVPRQEPPIHLD 648  
*cChicken/1-1271* 594 GRVHKLTI DDVTPADEADYSFVPEGFAC - NLSAKLQFLEVKIDFVPRQEPPIHLD 648  
*Hum\_fok1-1142* 490 GRFHKLVI DDVTPDEEDYTFVDPGYALGSLAKLNFLIKVEYVPKQEPPIHLD 545  
*Mouse\_fok1-1136* 485 GRFHKLVI DDVTPDEEDYTFVDPGYAL - SLAKLNFLIKVEYVPKQEPPIHLD 539  
*Chick\_fok1-1131* 481 GRFHKLVI DDVTPDEEDYTFVDPGYAL - SLAKLNFLIKVEYVPKQEPPIHLD 535  
*Hum\_sol1-1141* 483 GRVHKLVIADALTEDEEDYVFAPDQAVNV - TLPAKVHVID - - - - - PPKIILD 527

*cHuman/1-1273* 650 CPGRI PDIIVVVA - GNKLRLDVPI SGDPAPTIVWQKAITQGNKAPARPAPDAPEE 704  
*cCow/1-1269* 645 CPGV PDIIVVVA - GNKLRLDVPI SGDPAPTIVWQKAITKGNKVPAGPAPDASEE 699  
*cMouse/1-1270* 647 CPGST PDIIVVVT - GNKLRLDVPI SGDPAPTIVWQKVTQGNKASAGPAPDAPEE 701  
*cChicken/1-1271* 649 CLGSPDIIVVVA - GNKLRLDVPI SGDPAPTIVWQKVNKKG - ELVHQSNEDSLTPS 702  
*Hum\_fok1-1142* 546 CSGKTS ENAIVVVAGNKLRLDVSITGEPPTVATWLR - - - - - GDEVFTTTEGRTRIEK 597  
*Mouse\_fok1-1136* 540 CSGKTS DNSIVVVAGNKLRLDVAITGEPPTATWLR - - - - - GDEVFTATEGRTRIEQ 591  
*Chick\_fok1-1131* 536 CSGAAENTIVVVAGNKLRLDVPISGEPAPTIVWKR - - - - - GDQLFTATEGRVHIDS 587  
*Hum\_sol1-1141* 528 - - GLDADNTIVVIAGNKLRLIPIISGEPKAMWS - - - - - GDKAIMEGSGRIRTES 577

*cHuman/1-1273* 705 GDSDEWVFDKLLCETEGRRVRETTKDRSIFTVEGA EKEDEGVTVTVKKNPVGEDQ 760  
*cCow/1-1269* 700 GAGDEWVFDKLLCETEGRRVRETTKDRSIFTVEGA EREDEGVTVTVKKNPVGEDQ 755  
*cMouse/1-1270* 702 GADDEWVFDKLLCETEGRRVRETTKDRSIFTVEGA EKEDEGVTVTVKKNPVGEDQ 757  
*cChicken/1-1271* 703 ENSSDLSTDKLLFESGRRVREKHEDHCVFIIEGA EKEDEGVTVTVKKNPVGEDK 758  
*Hum\_fok1-1142* 598 RVDCCS FVIESAQREDEGR - - - - - YTIKVTNPVGEDV 629  
*Mouse\_fok1-1136* 592 RVDCCS FVIESAERSDEGR - - - - - YTIKVTNPVGEDV 623  
*Chick\_fok1-1131* 588 QADLSSFVIESAERSDEGR - - - - - YCITVTNPVGEDS 619  
*Hum\_sol1-1141* 578 YPDSSTLV IDIAERDSSGV - - - - - YHINLKN EAGEAH 609

*cHuman/1-1273* 761 VNLTVKVIDVDPDAPAAPKISN VGEDSCTVQWEPAYDGGQPVLGYILERKKKKS YR 816  
*cCow/1-1269* 758 VNLTVKVIDVDPDAPAAPEISKVGEDSCTVQWEPAYDGGQPVLGYILERKKKKS YR 811  
*cMouse/1-1270* 758 VNLTVKVIDVDPDAPAAPKISN VGEDSCTVQWEPAYDGGQPVLGYILERKKKKS YR 813  
*cChicken/1-1271* 759 ADITV KVIDVDPDPEAPKISNIGEDYCTVQWPPYDGGQPVLGYILERKKKKS YR 814  
*Hum\_fok1-1142* 630 ASIFLRVVDVDPDPEAVRITSVGEDWAILVWEP PPMYDGGKPVGYLVERKKKKSQR 685  
*Mouse\_fok1-1136* 624 ASIFLRVVDVDPDPEAVRITSVGEDWAILVWEP PPKYDGGKPVGYLVERKKKKSQR 679  
*Chick\_fok1-1131* 620 ATLHYRVVDVDPDPEAVRITSVGEDWAVLSWEAPPFDGGMPITGYLVERKKKKSQR 675  
*Hum\_sol1-1141* 610 ASIKV KVIDVDPDPPVARTVTEVGDWECIMNWEPPAYDGGSPILGYIFERKKKKSQR 685

*cHuman/1-1273* 817 WMR LNF DL IQEL SHEARRMI EG VVYEMRVYAVNAIGMSR PPSASQPFMP I GPPSEP 872  
*cCow/1-1269* 812 WMR LNF D LLRELSHEARRMI EG VVYEMRVYAVNAVMSR PPSASQPFMP I GPPSEP 867  
*cMouse/1-1270* 814 WMR LNF D LLRELSHEARRMI EG VVYEMRVYAVNAVMSR PPSASQPFMP I GPPSEP 869  
*cChicken/1-1271* 815 WMR LNF D LLKELTYEARRMI EG VVYEMRIYAVNSIGMSR PPSASQPFMP I APPSEP 870  
*Hum\_fok1-1142* 686 WMK LNF E VFTT TTYESTNMI EG ILYEMRVFAVNAIGVSPSMNTKPFMP IAPTSEP 741  
*Mouse\_fok1-1136* 680 WMK LNF E VFTT TTYESTNMI EG VLYEMRVFAVNAIGVSPSMNTKPFMP IAPTSEP 735  
*Chick\_fok1-1131* 676 WMK LNF E VFPD TTYESTNMI EG VYEMRVFAVNAIGVSPSLNTKPFMP IAPTSEP 731  
*Hum\_sol1-1141* 666 WMR LNF D LCKETTFEPKMI EG VAYEVRFVAVNAIGISNPSMP RPFVPLAVTSP 721

*cHuman/1-1273* 873 T H L A V E D V S D T T V S L K W R P P E R V G A G G L D G Y S V E Y C P E G C S E . . . . . 914  
*cCow/1-1269* 868 T H L A V E D I S D T T V S L K W R P P E R A G A G G L D G Y S V E Y R R E G S G S A . . . . . 910  
*cMouse/1-1270* 870 T H L A V E D V S D T T V S L K W R P P E R V G A G G L D G Y S V E Y C O E G C S E . . . . . 911  
*cChicken/1-1271* 871 T H F T V E D V S D T T V A L K W R P P E R I G A G G L D G Y I V E Y C K D G S A E . . . . . 912  
*Hum\_fsk/1-1142* 742 L H L I V E D V T D T T T T L K W R P P N R I G A G G I D G Y L V E Y C L E G S E E . . . . . 783  
*Mouse\_fsk/1-1136* 738 O H L T V E D V T D T T T T L K W R P P D R I G A G G I D G Y L V E Y C L E G S E E . . . . . 777  
*Chick\_fsk/1-1131* 732 T H V V L E D V T D T T A T I K W R P P E R I G A G G V D G Y L V E W C R E G S N E . . . . . 773  
*Hum\_sol/1-1141* 722 T L L T V D S V T D T T V T M R W R P P D H I G A A G L D G Y V L E Y C F E G S T S A K Q S D E N G E A A Y D L 777

*cHuman/1-1273* 915 . . . . W V A A L Q G L T E H T S I L V K D L P T G A R L L F R V R A H N M A G P G A P V T T T E F V T V Q E I 966  
*cCow/1-1269* 911 . . . . W V S A L P G L I E R T S L L V K D L P T G A R V L F R V R A H N L A G A G P P V T T K E P V T V Q E L 962  
*cMouse/1-1270* 912 . . . . W T P A L O G L T E R R S M L V K D L P T G A R L L F R V R A H N V A G P G G P I V T K E P V T V Q E I 963  
*cChicken/1-1271* 913 . . . . W T P A L P G L T E R T S A L I K D L V T G D K L Y F R V A I N L A G E S G A A I K E P V T V Q E I 964  
*Hum\_fsk/1-1142* 784 . . . . W V P A N T E P V E R C G F T V K N L P T G A R I L F R V V G V N I A G R T E P A T L A Q P V T I R E I 835  
*Mouse\_fsk/1-1136* 778 . . . . W V P A N K E P V E R C G F T V K D L P T G A R I L F R V V G V N I A G R S E P A T L L Q P V T I R E I 829  
*Chick\_fsk/1-1131* 774 . . . . W V A A N T E L V E R C G L T A G L P T G A R L L F R V I S V N M A G K S P P A T M A Q P V T I R E I 825  
*Hum\_sol/1-1141* 778 P A E D W I V A N K D L I D T K E T I T G L P T D A K I F V R V K A V N A A G A S E R K Y S Q P I L V K E I 833

*cHuman/1-1273* 967 L Q R P R L Q L P R H L R Q T I Q K K V G E P V N L L I P F G K P R P Q V T W T K E G Q P L A G E E V S I R N 1022  
*cCow/1-1269* 963 L Q R P R L Q L P R H L R Q T I Q K K V G E P V N L L I P F G K P R P Q V T W T K E G Q P L A G E E V S I R N 1018  
*cMouse/1-1270* 964 L Q R P R L Q L P R H L R Q T I Q K K V G E P V N L L I P F G K P R P Q V T W T K E G Q P L A G E E V S I R N 1019  
*cChicken/1-1271* 965 M Q R P K I C V P R H L R Q T L V K K V G E T I N I M I P F G K P R P K I S W M K D G Q T L D S K D V G I R N 1020  
*Hum\_fsk/1-1142* 836 A E P P K I R L P R H L R Q T Y I R K V G E Q L N L V V P F G K P R P Q V V W T K - G G A - P L D T S R V H V 889  
*Mouse\_fsk/1-1136* 830 V E G P K I R L P R H L R Q T Y I R K V G E A L N L V I P F G K P R P Q V V W T K - G G A - P L D T S R V N V 893  
*Chick\_fsk/1-1131* 826 V E R P K I R L P R H L R Q T Y I R R V G E Q V N L V I P F G K P R P Q V T W S R E G G A L P A E . . . V Q T 878  
*Hum\_sol/1-1141* 834 I E P P K I R I P R H L K Q T Y I R R V G E A V N L V I P F G K P R P E L T W K D G A E I D K N Q I N I . . 887

*cHuman/1-1273* 1023 S P T D T I L F I R A A . . . . R R V H S G T Y Q V T V R I E N M E D K A T L V L Q V V D K P S P P D L R V 1073  
*cCow/1-1269* 1019 S P T D T I L F I R A A . . . . H R A H S G T Y Q V T L R V E D M E K A Q L V L Q V V D K P S P P D I Q V 1069  
*cMouse/1-1270* 1020 S P T D T I L F I R A A . . . . R T H S G T Y Q V T V R I E N M E D K A T L I L Q I V D K P S P P D I R I 1070  
*cChicken/1-1271* 1021 S S T D T I L F I R K A E L . . . . H H S G A Y E V T L Q I E N M T D T V A I T I Q I I D K P G P P N I K L 1071  
*Hum\_fsk/1-1142* 890 R T S D F D T V F F V R - - - Q A A R S D S G E Y E L S V Q I E N M K D T A T I R I R V V E K A G P R I N V M V 942  
*Mouse\_fsk/1-1136* 884 R T S D - - - F D T V F F V R Q A A R S D S G E Y E L S V Q I E N M K D T A T I R I R V V E K A G P A E N V M V 936  
*Chick\_fsk/1-1131* 879 R T S D - - - V D S V F F I R S A A R P L S G N Y E M R V R I D M E D C A T L R L R V V E R P G P P A V R V 931  
*Hum\_sol/1-1141* 888 R N S E T D T I L F I R - - - K A E R S H S G K Y D L Q V N V D K F V E T A S I D I Q I I D R P G P P Q I V K I 940

*cHuman/1-1273* 1074 T D A W G L N V A L E W K P P Q D V G N T E L W G Y T V Q K A D K K T M E W F T V L E H Y R R T H C V V P E L I 1129  
*cCow/1-1269* 1070 A E A W G F N V A L E W K P P Q D G N T E L W G Y T V Q K A D K K T M E W F T V L E H Y R R T H C V V S E L I 1125  
*cMouse/1-1270* 1071 V E T W G F N V A L E W K P P Q D G N T E I W G Y T V Q K A D K K T M E W F T V L E H Y R R T H C V V S E L I 1126  
*cChicken/1-1271* 1072 A D V W G F N V A L E W T P Q D D G N A Q I L G Y T V Q K A D K K T M E W Y V Y D H Y R R T N C V V S D L I 1127  
*Hum\_fsk/1-1142* 943 K E V W G T N A L V E W Q A P K D D G N S E I M G Y F V Q K A D K K T M E W F N V Y E R N R H T S C T V S D L I 998  
*Mouse\_fsk/1-1136* 937 K E V W G T N A L V E W Q P P K D D G N S E I T G Y F V Q K A D K K T M E W F N V Y E H N R H T S C T V S D L I 992  
*Chick\_fsk/1-1131* 932 M E V W G S N A L L Q W E P P K D D G N A E I S G Y T V Q K A D T R T M E W F T V L E H S R P T R C T V S E L V 987  
*Hum\_sol/1-1141* 941 E D V W G E N V A L T W T P P K D D G N A A I T G Y T I Q K A D K K S M E W F T V I E H Y H R T S A T I T E L V 996

*cHuman/1-1273* 1130 I G N G Y Y F R V F S Q N M V G F S D R A A T T H E P V F I P R P G I T Y E P P N Y K A L D F S E A P S F T Q P 1185  
*cCow/1-1269* 1126 I G N S Y Y F R V F S H N T V G P S D T A A T T H E P V L I P R P G I T Y E L P K Y K A L D F S E A P S F T R P 1181  
*cMouse/1-1270* 1127 I G N G Y Y F R V F S H N M V G S S D K A A A T T H E P V F I P R P G I T Y E P P K Y K A L D F S E A P S F T Q P 1182  
*cChicken/1-1271* 1128 M G N E Y F R V F S E N L C G L S E T A A T T N P A Y I Q H T G T T Y K P P S Y K E H D F S E P K F T H P 1183  
*Hum\_fsk/1-1142* 999 V G N E Y Y F R V Y T E N I C G L S D S P G V S N T A R I L N T G I T F N P F E Y K E H D F R M A P K F L T P 1054  
*Mouse\_fsk/1-1136* 993 V G N E Y Y F R I F S E N I C G L S D S P G V S N T A R I L N T G I T L P L E Y K E H D F R T A P K F L T P 1048  
*Chick\_fsk/1-1131* 988 M G N E Y Y F R V Y S E N V C G T S Q E P A T S H N T A R I A E G L T L K M V P Y K E R D L R A A P O F L T P 1043  
*Hum\_sol/1-1141* 997 I G N E Y Y F R V F S E N M C G L S E D A T M T H E S A V I A R D G K I Y N P V Y E D F D F S E A R M F T Q P 1052

*cHuman/1-1273* 1186 L V N R S V I A G Y T A M L C C A V R G S P K P I S W F K N G L D L - G E D A R F R M F S K O G V L T L E I R 1240  
*cCow/1-1269* 1182 L V N R S V I A G Y N T T L C C A V R G S P K P I S W F K N G L D L - G K D A R F R M F S K O G V L T L E I R 1236  
*cMouse/1-1270* 1183 L A N R S I I A G Y N A I L C C A V R G S P K P I S W F K N G L D L - G E D A R F R M F C K O G V L T L E I R 1237  
*cChicken/1-1271* 1184 L V N R S V I A G Y N T T L S C A V R G I P K P I F W Y K N K V D L S G - D A K Y R M F S K O G V L T L E I R 1238  
*Hum\_fsk/1-1142* 1055 L I D R V V V A G Y S A A L N C A V R G H P K P K V V W M K N K M E I - R E D P K F L I T N Y O G V L T L N I R 1109  
*Mouse\_fsk/1-1136* 1040 L M D R V V V A G Y T A A L N C A V R G H P K P K V V W M K N K M E I - H E D P K F L I T N Y O G I L T L N I R 1103  
*Chick\_fsk/1-1131* 1044 L V D R S V V A G Y T V T L N C A V R G H P K P V T W L K N S V E I - G A D P K F L R H G L G V L S L L I R 1098  
*Hum\_sol/1-1141* 1053 L V N T Y A I A G Y N A T L N C S V R G N P K P I T W M K N K V A I - V D D P R Y R M F S N G G V C L E I R 1107

*cHuman/1-1273* 1241 K P C P F D G G I V C R A T L Q G E A R C E R L E V R V - P Q 1273  
*cCow/1-1269* 1237 K P C P F D G G I Y A C R A T N L E G E A Q C E C R L E V R V - P Q 1269  
*cMouse/1-1270* 1238 K P C P Y D G G V V C R A T N L Q G E A Q C E C R L E V R V - P Q 1270  
*cChicken/1-1271* 1239 K P T P L D G G F Y T C K A V N E R G E A I E C R L D V R V - P Q 1271  
*Hum\_fsk/1-1142* 1110 R P S P F D A G T Y T C R A V N L E G E A L E A E C K L D V R V - P Q 1142  
*Mouse\_fsk/1-1136* 1104 R P S P F D A G T Y S C R A F N E L G E A L A E C K L D V R V - P Q 1136  
*Chick\_fsk/1-1131* 1099 R P G P F D G G T Y G C R A V N E M G E A T T E C R L D V R V - P Q 1131  
*Hum\_sol/1-1141* 1108 K P S P Y D G G T Y C K A V N D L G T V E I E C K L E V R V I A Q 1141

## References

- Ababou, A., M. Gautel, and M. Pfuhl. 2007. Dissecting the N-terminal myosin binding site of human cardiac myosin-binding protein C. Structure and myosin binding of domain C2. *J Biol Chem.* 282:9204-15.
- Ababou, A., E. Rostkova, S. Mistry, C. Le Masurier, M. Gautel, and M. Pfuhl. 2008. Myosin binding protein C positioned to play a key role in regulation of muscle contraction: structure and interactions of domain C1. *J Mol Biol.* 384:615-30.
- Alyonycheva, T.N., T. Mikawa, F.C. Reinach, and D.A. Fischman. 1997. Isoform-specific interaction of the myosin-binding proteins (MyBPs) with skeletal and cardiac myosin is a property of the C-terminal immunoglobulin domain. *J Biol Chem.* 272:20866-72.
- Anan, R., H. Shono, and C. Tei. 2000. Novel cardiac beta-myosin heavy chain gene missense mutations (R869C and R870C) that cause familial hypertrophic cardiomyopathy. *Hum Mutat.* 15:584.
- Arai, A., J.A. Spencer, and E.N. Olson. 2002. STARS, a striated muscle activator of Rho signaling and serum response factor-dependent transcription. *J Biol Chem.* 277:24453-9.
- Arnold, K., L. Bordoli, J. Kopp, and T. Schwede. 2006. The SWISS-MODEL workspace: a web-based environment for protein structure homology modelling. *Bioinformatics.* 22:195-201.
- Barbato, G., M. Ikura, L.E. Kay, R.W. Pastor, and A. Bax. 1992. Backbone dynamics of calmodulin studied by <sup>15</sup>N relaxation using inverse detected two-dimensional NMR spectroscopy: the central helix is flexible. *Biochemistry.* 31:5269-78.
- Bax, A., Clore, G.M., Gronenberg, A. M. 1990. H-1-H1 correlation via isotopic mixing of C-13 magnetization, a new 3-dimensional approach for assigning H-1 and C-13 spectra of C-13 enriched proteins. *J Magn Reson.* 88:425- 431.
- Bennett, P.M., D.O. Furst, and M. Gautel. 1999. The C-protein (myosin binding protein C) family: regulators of contraction and sarcomere formation? *Rev Physiol Biochem Pharmacol.* 138:203-34.
- Bodenhausen, G.R., DJ. 1980. Natural abundance N-15 NMR by enhanced heteronuclear spectroscopy. *Chem. Phys. Lett.* 69:185-189.
- Bonne, G., L. Carrier, J. Bercovici, C. Cruaud, P. Richard, B. Hainque, M. Gautel, S. Labeit, M. James, J. Beckmann, J. Weissenbach, H.P. Vosberg, M. Fiszman, M. Komajda, and K. Schwartz. 1995. Cardiac myosin binding protein-C gene splice acceptor site mutation is associated with familial hypertrophic cardiomyopathy. *Nat Genet.* 11:438-40.
- Bonne, G., L. Carrier, P. Richard, B. Hainque, and K. Schwartz. 1998. Familial hypertrophic cardiomyopathy: from mutations to functional defects. *Circ Res.* 83:580-93.
- Branden, C.I., Tooze J. 1999. Introduction to Protein Structure. Garland Publisher.
- Brooks, C.L., M. Karplus, and B.M. Petit. 1988. Proteins: a Theoretical Prospective of Dynamics, Structure and Thermodynamics. Wiley, New York.
- Charron, P., O. Dubourg, M. Desnos, M. Bennaceur, L. Carrier, A.C. Camproux, R. Isnard, A. Hagege, J.M. Langlard, G. Bonne, P. Richard, B. Hainque, J.B. Bouhour, K. Schwartz, and M. Komajda. 1998. Clinical features and prognostic implications of familial hypertrophic cardiomyopathy related to the cardiac myosin-binding protein C gene. *Circulation.* 97:2230-6.

- Clore, G.M., A. Szabo, A. Bax, L.E. Kay, P.C. Driscoll, and A.M. Gronenborn. 1990. Deviation from the single two-parameter model-free approach to the interpretation of nitrogen-15 nuclear magnetic relaxation of proteins. *J Am Chem Soc.* 112:4989- 4991.
- Cornilescu, G., F. Delaglio, and A. Bax. 1999. Protein backbone angle restraints from searching a database for chemical shift and sequence homology. *J Biomol NMR.* 13:289-302.
- Crilley, J.G., E.A. Boehm, E. Blair, B. Rajagopalan, A.M. Blamire, P. Styles, W.J. McKenna, I. Ostman-Smith, K. Clarke, and H. Watkins. 2003. Hypertrophic cardiomyopathy due to sarcomeric gene mutations is characterized by impaired energy metabolism irrespective of the degree of hypertrophy. *J Am Coll Cardiol.* 41:1776-82.
- Daehmlow, S. 2002. Novel mutations in sarcomeric protein genes in dilated cardiomyopathy. *Biochem Biophys Res Commun.* 298:116-120.
- Davis, J.S. 1988. Interaction of C-protein with pH 8.0 synthetic thick filaments prepared from the myosin of vertebrate skeletal muscle. *J Muscle Res Cell Motil.* 9:174-83.
- de Marco, A., and V. De Marco. 2004. Bacteria co-transformed with recombinant proteins and chaperones cloned in independent plasmids are suitable for expression tuning. *J Biotechnol.* 109:45-52.
- de Marco, A., S. Volrath, T. Bruyere, M. Law, and R. Fonne-Pfister. 2000. Recombinant maize protoporphyrinogen IX oxidase expressed in *Escherichia coli* forms complexes with GroEL and DnaK chaperones. *Protein Expr Purif.* 20:81-6.
- De Marco, V., G. Stier, S. Blandin, and A. de Marco. 2004. The solubility and stability of recombinant proteins are increased by their fusion to NusA. *Biochem Biophys Res Commun.* 322:766-71.
- de Pereda, J. 1999. Crystal structure of a tandem pair of fibronectin type III domains from the cytoplasmic tail of integrin alpha6beta4. 18:1468\_1479.
- Decker, R.S., M.L. Decker, I. Kulikovskaya, S. Nakamura, D.C. Lee, K. Harris, F.J. Klocke, and S. Winegrad. 2005. Myosin-binding protein C phosphorylation, myofibril structure, and contractile function during low-flow ischemia. *Circulation.* 111:906-12.
- Dominguez, R., Y. Freyzon, K.M. Trybus, and C. Cohen. 1998. Crystal structure of a vertebrate smooth muscle myosin motor domain and its complex with the essential light chain: visualization of the pre-power stroke state. *Cell.* 94:559-71.
- Eliezer, D., E. Kutluay, R. Bussell, Jr., and G. Browne. 2001. Conformational properties of alpha-synuclein in its free and lipid-associated states. *J Mol Biol.* 307:1061-73.
- Flashman, E., L. Korkie, H. Watkins, C. Redwood, and J.C. Moolman-Smook. 2008. Support for a trimeric collar of myosin binding protein C in cardiac and fast skeletal muscle, but not in slow skeletal muscle. *FEBS Lett.* 582:434-8.
- Flashman, E., C. Redwood, J. Moolman-Smook, and H. Watkins. 2004. Cardiac myosin binding protein C: its role in physiology and disease. *Circ Res.* 94:1279-89.
- Flavigny, J., M. Souchet, P. Sebillon, I. Berrebi-Bertrand, B. Hainque, A. Mallet, A. Bril, K. Schwartz, and L. Carrier. 1999. COOH-terminal truncated cardiac myosin-binding protein C mutants resulting from familial hypertrophic cardiomyopathy mutations exhibit altered expression and/or incorporation in fetal rat cardiomyocytes. *J Mol Biol.* 294:443-56.

- Freiburg, A., and M. Gautel. 1996. A molecular map of the interactions between titin and myosin-binding protein C. Implications for sarcomeric assembly in familial hypertrophic cardiomyopathy. *Eur J Biochem.* 235:317-23.
- Furst, D.O., R. Nave, M. Osborn, and K. Weber. 1989. Repetitive titin epitopes with a 42 nm spacing coincide in relative position with known A band striations also identified by major myosin-associated proteins. An immunoelectron-microscopical study on myofibrils. *J Cell Sci.* 94 (Pt 1):119-25.
- Furst, D.O., U. Vinkemeier, and K. Weber. 1992. Mammalian skeletal muscle C-protein: purification from bovine muscle, binding to titin and the characterization of a full-length human cDNA. *J Cell Sci.* 102 (Pt 4):769-78.
- Garvey, J.L., E.G. Kranias, and R.J. Solaro. 1988. Phosphorylation of C-protein, troponin I and phospholamban in isolated rabbit hearts. *Biochem J.* 249:709-14.
- Gautel, M., O. Zuffardi, A. Freiburg, and S. Labeit. 1995. Phosphorylation switches specific for the cardiac isoform of myosin binding protein-C: a modulator of cardiac contraction? *Embo J.* 14:1952-60.
- Geisterfer-Lowrance, A.A., M. Christe, D.A. Conner, J.S. Ingwall, F.J. Schoen, C.E. Seidman, and J.G. Seidman. 1996. A mouse model of familial hypertrophic cardiomyopathy. *Science.* 272:731-4.
- Geisterfer-Lowrance, A.A., S. Kass, G. Tanigawa, H.P. Vosberg, W. McKenna, C.E. Seidman, and J.G. Seidman. 1990. A molecular basis for familial hypertrophic cardiomyopathy: a beta cardiac myosin heavy chain gene missense mutation. *Cell.* 62:999-1006.
- Gilbert, R., J.A. Cohen, S. Pardo, A. Basu, and D.A. Fischman. 1999. Identification of the A-band localization domain of myosin binding proteins C and H (MyBP-C, MyBP-H) in skeletal muscle. *J Cell Sci.* 112 (Pt 1):69-79.
- Gilbert, R., M.G. Kelly, T. Mikawa, and D.A. Fischman. 1996. The carboxyl terminus of myosin binding protein C (MyBP-C, C-protein) specifies incorporation into the A-band of striated muscle. *J Cell Sci.* 109 (Pt 1):101-11.
- Goll, C.M., A. Pastore, and M. Nilges. 1998. The three-dimensional structure of a type I module from titin: a prototype of intracellular fibronectin type III domains. *Structure.* 6:1291-302.
- Gordon, A.M., E. Homsher, and M. Regnier. 2000. Regulation of contraction in striated muscle. *Physiol Rev.* 80:853-924.
- Govada, L., L. Carpenter, P.C. da Fonseca, J.R. Helliwell, P. Rizkallah, E. Flashman, N.E. Chayen, C. Redwood, and J.M. Squire. 2008. Crystal structure of the C1 domain of cardiac myosin binding protein-C: implications for hypertrophic cardiomyopathy. *J Mol Biol.* 378:387-97.
- Gregorio, C.C., H. Granzier, H. Sorimachi, and S. Labeit. 1999. Muscle assembly: a titanic achievement? *Curr Opin Cell Biol.* 11:18-25.
- Gregorio, C.C., K. Trombitas, T. Centner, B. Kolmerer, G. Stier, K. Kunke, K. Suzuki, F. Obermayr, B. Herrmann, H. Granzier, H. Sorimachi, and S. Labeit. 1998. The NH2 terminus of titin spans the Z-disc: its interaction with a novel 19-kD ligand (T-cap) is required for sarcomeric integrity. *J Cell Biol.* 143:1013-27.
- Gruen, M., and M. Gautel. 1999. Mutations in beta-myosin S2 that cause familial hypertrophic cardiomyopathy (FHC) abolish the interaction with the regulatory domain of myosin-binding protein-C. *J Mol Biol.* 286:933-49.
- Gruen, M., H. Prinz, and M. Gautel. 1999. cAPK-phosphorylation controls the interaction of the regulatory domain of cardiac myosin binding protein C with myosin-S2 in an on-off fashion. *FEBS Lett.* 453:254-9.

- Grzesiek, S., and A. Bax. 1993. Amino acid type determination in the sequential assignment procedure of uniformly  $^{13}\text{C}/^{15}\text{N}$ -enriched proteins. *J Biomol NMR*. 3:185-204.
- Grzesiek, S., H. Dobeli, R. Gentz, G. Garotta, A.M. Labhardt, and A. Bax. 1992.  $^1\text{H}$ ,  $^{13}\text{C}$ , and  $^{15}\text{N}$  NMR backbone assignments and secondary structure of human interferon-gamma. *Biochemistry*. 31:8180-90.
- Güntert, P. 2003. Automated NMR protein structure calculation. *Progress in nuclear magnetic resonance spectroscopy*. 43:105-125.
- Güntert, P., C. Mumenthaler, and K. Wüthrich. 1997. Torsion angle dynamics for NMR structure calculation with the new program DYANA. *J Mol Biol*. 273:283-98.
- Guyton, H. 2005. Textbook of Medical Physiology. Saunders (W.B.) Co Ltd.
- Hanson, J., and H.E. Huxley. 1957. Quantitative studies on the structure of cross-striated myofibrils. II. Investigations by biochemical techniques. *Biochim Biophys Acta*. 23:250-60.
- Harpaz, Y., and C. Chothia. 1994. Many of the immunoglobulin superfamily domains in cell adhesion molecules and surface receptors belong to a new structural set which is close to that containing variable domains. *J Mol Biol*. 238:528-39.
- Harris, S.P., C.R. Bartley, T.A. Hacker, K.S. McDonald, P.S. Douglas, M.L. Greaser, P.A. Powers, and R.L. Moss. 2002. Hypertrophic cardiomyopathy in cardiac myosin binding protein-C knockout mice. *Circ Res*. 90:594-601.
- Harrison, R.G. 2000. Expression of soluble heterologous proteins via fusion with NusA protein. *inNovation (newsletter of Novagen)*.
- Hartzell, H.C., and W.S. Sale. 1985. Structure of C protein purified from cardiac muscle. *J Cell Biol*. 100:208-15.
- Hartzell, H.C., and L. Titus. 1982. Effects of cholinergic and adrenergic agonists on phosphorylation of a 165,000-dalton myofibrillar protein in intact cardiac muscle. *J Biol Chem*. 257:2111-20.
- Hemmingsen, J.M., K.M. Gernert, J.S. Richardson, and D.C. Richardson. 1994. The tyrosine corner: a feature of most Greek key beta-barrel proteins. *Protein Sci*. 3:1927-37.
- Herrmann, T., P. Güntert, and K. Wüthrich. 2002. Protein NMR structure determination with automated NOE assignment using the new software CANDID and the torsion angle dynamics algorithm DYANA. *J Mol Biol*. 319:209-27.
- Herron, T.J., E. Rostkova, G. Kunst, R. Chaturvedi, M. Gautel, and J.C. Kentish. 2006. Activation of myocardial contraction by the N-terminal domains of myosin binding protein-C. *Circ Res*. 98:1290-8.
- Holm, L., and J. Park. 2000. DaliLite workbench for protein structure comparison. *Bioinformatics*. 16:566-7.
- Hooft, R.W., C. Sander, and G. Vriend. 1997. Objectively judging the quality of a protein structure from a Ramachandran plot. *Comput Appl Biosci*. 13:425-30.
- Horowitz, R. 1999. The physiological role of titin in striated muscle. *Rev Physiol Biochem Pharmacol*. 138:57-96.
- Horowitz, R., G. Luo, J.Q. Zhang, and A.H. Herrera. 1996. Nebulin and nebulin-related proteins in striated muscle. *Adv Biophys*. 33:143-50.
- Houser, S.R., V. Piacentino, 3rd, and J. Weisser. 2000. Abnormalities of calcium cycling in the hypertrophied and failing heart. *J Mol Cell Cardiol*. 32:1595-607.
- Huxley, A.F., and R. Niedergerke. 1954. Structural changes in muscle during contraction; interference microscopy of living muscle fibres. *Nature*. 173:971-3.
- Huxley, H., and J. Hanson. 1954. Changes in the cross-striations of muscle during contraction and stretch and their structural interpretation. *Nature*. 173:973-6.

- Huxley, H.E. 1957. The double array of filaments in cross-striated muscle. *J Biophys Biochem Cytol.* 3:631-48.
- Huxley, H.E. 1963. Electron Microscope Studies On The Structure Of Natural And Synthetic Protein Filaments From Striated Muscle. *J Mol Biol.* 7:281-308.
- Huxley, H.E. 1969. The mechanism of muscular contraction. *Science.* 164:1356-65.
- Huxley, H.E., and W. Brown. 1967. The low-angle x-ray diagram of vertebrate striated muscle and its behaviour during contraction and rigor. *J Mol Biol.* 30:383-434.
- Huxley, H.E., and J. Hanson. 1957. Quantitative studies on the structure of cross-striated myofibrils. I. Investigations by interference microscopy. *Biochim Biophys Acta.* 23:229-49.
- Idowu, S.M., M. Gautel, S.J. Perkins, and M. Pfuhl. 2003. Structure, stability and dynamics of the central domain of cardiac myosin binding protein C (MyBP-C): implications for multidomain assembly and causes for cardiomyopathy. *J Mol Biol.* 329:745-61.
- Ikura, M., L.E. Kay, and A. Bax. 1990. A novel approach for sequential assignment of <sup>1</sup>H, <sup>13</sup>C, and <sup>15</sup>N spectra of proteins: heteronuclear triple-resonance three-dimensional NMR spectroscopy. Application to calmodulin. *Biochemistry.* 29:4659-67.
- Improta, S., A.S. Politou, and A. Pastore. 1996. Immunoglobulin-like modules from titin I-band: extensible components of muscle elasticity. *Structure.* 4:323-37.
- Jaaskelainen, P., J. Kuusisto, R. Miettinen, P. Karkkainen, S. Karkkainen, S. Heikkinen, P. Peltola, J. Pihlajamaki, I. Vauhkonen, and M. Laakso. 2002. Mutations in the cardiac myosin-binding protein C gene are the predominant cause of familial hypertrophic cardiomyopathy in eastern Finland. *J Mol Med.* 80:412-22.
- Jardezky, O. 1996. Protein dynamics and conformational transitions in allosteric proteins. *Prog Biophys Mol Biol.* 65:171-219.
- Jeffries, C.M., A.E. Whitten, S.P. Harris, and J. Trehwella. 2008. Small-angle X-ray scattering reveals the N-terminal domain organization of cardiac myosin binding protein C. *J Mol Biol.* 377:1186-99.
- Kabsch, W., and J. Vandekerckhove. 1992. Structure and function of actin. *Annu Rev Biophys Biomol Struct.* 21:49-76.
- Kapust, R.B., and D.S. Waugh. 1999. Escherichia coli maltose-binding protein is uncommonly effective at promoting the solubility of polypeptides to which it is fused. *Protein Sci.* 8:1668-74.
- Kirkpatrick, S., C.D. Gelatt, Jr., and M.P. Vecchi. 1983. Optimization by Simulated Annealing. *Science.* 220:671-680.
- Koretz, J.F. 1979a. Effects of C-protein on synthetic myosin filament structure. *Biophys J.* 27:433-446.
- Koretz, J.F. 1979b. Effects of C-protein on synthetic myosin filament structure. *Biophys J.* 27:433-46.
- Koretz, J.F., T.C. Irving, and K. Wang. 1993. Filamentous aggregates of native titin and binding of C-protein and AMP-deaminase. *Arch Biochem Biophys.* 304:305-9.
- Kulikovskaya, I., G. McClellan, J. Flavigny, L. Carrier, and S. Winegrad. 2003. Effect of MyBP-C binding to actin on contractility in heart muscle. *J Gen Physiol.* 122:761-74.
- Kunst, G., K.R. Kress, M. Gruen, D. Uttenweiler, M. Gautel, and R.H. Fink. 2000. Myosin binding protein C, a phosphorylation-dependent force regulator in muscle that controls the attachment of myosin heads by its interaction with myosin S2. *Circ Res.* 86:51-8.

- La Vallie, E.R. 2000. Thioredoxin as a fusion partner for soluble recombinant protein production in *Escherichia coli*. *Methods Enzymology*.
- Labeit, S., M. Gautel, A. Lakey, and J. Trinick. 1992. Towards a molecular understanding of titin. *Embo J.* 11:1711-6.
- Labeit, S., and B. Kolmerer. 1995. Titins: giant proteins in charge of muscle ultrastructure and elasticity. *Science.* 270:293-6.
- Labeit, S., B. Kolmerer, and W.A. Linke. 1997. The giant protein titin. Emerging roles in physiology and pathophysiology. *Circ Res.* 80:290-4.
- Lankford, E.B., N.D. Epstein, L. Fananapazir, and H.L. Sweeney. 1995. Abnormal contractile properties of muscle fibers expressing beta-myosin heavy chain gene mutations in patients with hypertrophic cardiomyopathy. *J Clin Invest.* 95:1409-14.
- Laskowski, R.A., J.A. Rullmann, M.W. MacArthur, R. Kaptein, and J.M. Thornton. 1996. AQUA and PROCHECK-NMR: programs for checking the quality of protein structures solved by NMR. *J Biomol NMR.* 8:477-86.
- LaVallie, E.R., E.A. DiBlasio, S. Kovacic, K.L. Grant, P.F. Schendel, and J.M. McCoy. 1993. A thioredoxin gene fusion expression system that circumvents inclusion body formation in the *E. coli* cytoplasm. *Biotechnology (N Y).* 11:187-93.
- Lekanne Deprez, R.H., J.J. Muurling-Vlietman, J. Hrudá, M.J. Baars, L.C. Wijnaendts, I. Stolte-Dijkstra, M. Alders, and J.M. van Hagen. 2006. Two cases of severe neonatal hypertrophic cardiomyopathy caused by compound heterozygous mutations in the MYBPC3 gene. *J Med Genet.* 43:829-32.
- Levine, R., A. Weisberg, I. Kulikovskaya, G. McClellan, and S. Winegrad. 2001. Multiple structures of thick filaments in resting cardiac muscle and their influence on cross-bridge interactions. *Biophys J.* 81:1070-82.
- Levine, R.J., Z. Yang, N.D. Epstein, L. Fananapazir, J.T. Stull, and H.L. Sweeney. 1998. Structural and functional responses of mammalian thick filaments to alterations in myosin regulatory light chains. *J Struct Biol.* 122:149-61.
- Lipari, G., and A. Szabo. 1982a. Model-free approach to the interpretation of nuclear magnetic resonance relaxation in macromolecules. 1. Theory and range of validity. *J Am Chem Soc.* 104:4546-4559.
- Lipari, G., and A. Szabo. 1982b. Model-free approach to the interpretation of nuclear magnetic resonance relaxation in macromolecules. 2. Analysis of experimental results. *J Am Chem Soc.* 104:4559-4570.
- Lowey, S., H.S. Slayter, A.G. Weeds, and H. Baker. 1969. Substructure of the myosin molecule. I. Subfragments of myosin by enzymic degradation. *J Mol Biol.* 42:1-29.
- Main, A.L., T.S. Harvey, M. Baron, J. Boyd, and I.D. Campbell. 1992. The three-dimensional structure of the tenth type III module of fibronectin: an insight into RGD-mediated interactions. *Cell.* 71:671-8.
- Makrides, S.C. 1996. Strategies for achieving high-level expression of genes in *Escherichia coli*. *Microbiol Rev.* 60:512-38.
- Margossian, S.S., and H.S. Slayter. 1987. Electron microscopy of cardiac myosin: its shape and properties as determined by the regulatory light chain. *J Muscle Res Cell Motil.* 8:437-47.
- Marian, A.J., Y. Wu, D.S. Lim, M. McCluggage, K. Youker, Q.T. Yu, R. Brugada, F. DeMayo, M. Quinones, and R. Roberts. 1999. A transgenic rabbit model for human hypertrophic cardiomyopathy. *J Clin Invest.* 104:1683-92.
- Marion, D., P.C. Driscoll, L.E. Kay, P.T. Wingfield, A. Bax, A.M. Gronenborn, and G.M. Clore. 1989 a. Overcoming the overlap problem in the assignment of 1H

- NMR spectra of larger proteins by use of three-dimensional heteronuclear  $^1\text{H}$ - $^{15}\text{N}$  Hartmann-Hahn-multiple quantum coherence and nuclear Overhauser-multiple quantum coherence spectroscopy: application to interleukin 1 beta. *Biochemistry*. 28:6150-6.
- Marion, D., Kay, L.E., Sparks, S.W., Torchia, D.A., Bax, A. 1989 b. 3-Dimensional heteronuclear NMR of  $^{15}\text{N}$  labeled proteins. *J Am Chem Soc*. 111:1515-1517.
- Maron, B.J. 1996. Triggers for sudden cardiac death in the athlete. *Cardiol Clin*. 14:195-210.
- Maron, B.J. 2002. Hypertrophic cardiomyopathy: a systematic review. *Jama*. 287:1308-20.
- Maron, B.J., H. Niimura, S.A. Casey, M.K. Soper, G.B. Wright, J.G. Seidman, and C.E. Seidman. 2001. Development of left ventricular hypertrophy in adults in hypertrophic cardiomyopathy caused by cardiac myosin-binding protein C gene mutations. *J Am Coll Cardiol*. 38:315-21.
- Maruyama, K. 1999. Comparative aspects of muscle elastic proteins. *Rev Physiol Biochem Pharmacol*. 138:1-18.
- Matsubara, I. 1974. Light and x-ray diffraction studies on chick skeletal muscle under controlled physiological conditions. *J Physiol*. 238:473-86.
- Matsubara, I., and B.M. Millman. 1974. X-ray diffraction patterns from mammalian heart muscle. *J Mol Biol*. 82:527-36.
- Mayans, O., J. Wuerges, S. Canela, M. Gautel, and M. Wilmanns. 2001. Structural evidence for a possible role of reversible disulphide bridge formation in the elasticity of the muscle protein titin. *Structure*. 9:331-40.
- McCammon, J.A., and S. Harvey. 1987. Dynamics of Proteins and Nuclei Acids. Cambridge University Press.
- McClellan, G., I. Kulikovskaya, and S. Winegrad. 2001. Changes in cardiac contractility related to calcium-mediated changes in phosphorylation of myosin-binding protein C. *Biophys J*. 81:1083-92.
- McConnell, B.K., K.A. Jones, D. Fatkin, L.H. Arroyo, R.T. Lee, O. Aristizabal, D.H. Turnbull, D. Georgakopoulos, D. Kass, M. Bond, H. Niimura, F.J. Schoen, D. Conner, D.A. Fischman, C.E. Seidman, and J.G. Seidman. 1999. Dilated cardiomyopathy in homozygous myosin-binding protein-C mutant mice. *J Clin Invest*. 104:1771.
- McLachlan, A.D., and J. Karn. 1982. Periodic charge distributions in the myosin rod amino acid sequence match cross-bridge spacings in muscle. *Nature*. 299:226-31.
- Meurs, K.M., X. Sanchez, R.M. David, N.E. Bowles, J.A. Towbin, P.J. Reiser, J.A. Kittleson, M.J. Munro, K. Dryburgh, K.A. Macdonald, and M.D. Kittleson. 2005. A cardiac myosin binding protein C mutation in the Maine Coon cat with familial hypertrophic cardiomyopathy. *Hum Mol Genet*. 14:3587-93.
- Miroux, B., and J.E. Walker. 1996. Over-production of proteins in Escherichia coli: mutant hosts that allow synthesis of some membrane proteins and globular proteins at high levels. *J Mol Biol*. 260:289-98.
- Mitraki, A.K., J. 1989. Protein folding intermediates and inclusion body formation. *Bio/Technology*.
- Miyamoto, C.A., D.A. Fischman, and F.C. Reinach. 1999. The interface between MyBP-C and myosin: site-directed mutagenesis of the CX myosin-binding domain of MyBP-C. *J Muscle Res Cell Motil*. 20:703-15.

- Moncrief, N.D., R.H. Kretsinger, and M. Goodman. 1990. Evolution of EF-hand calcium-modulated proteins. I. Relationships based on amino acid sequences. *J Mol Evol.* 30:522-62.
- Moolman-Smook, J., E. Flashman, W. de Lange, Z. Li, V. Corfield, C. Redwood, and H. Watkins. 2002. Identification of novel interactions between domains of Myosin binding protein-C that are modulated by hypertrophic cardiomyopathy missense mutations. *Circ Res.* 91:704-11.
- Moolman-Smook, J.C., B. Mayosi, P. Brink, and V.A. Corfield. 1998. Identification of a new missense mutation in MyBP-C associated with hypertrophic cardiomyopathy. *J Med Genet.* 35:253-4.
- Moos, C., C.M. Mason, J.M. Besterman, I.N. Feng, and J.H. Dubin. 1978. The binding of skeletal muscle C-protein to F-actin, and its relation to the interaction of actin with myosin subfragment-1. *J Mol Biol.* 124:571-86.
- Moos, C., G. Offer, R. Starr, and P. Bennett. 1975. Interaction of C-protein with myosin, myosin rod and light meromyosin. *J Mol Biol.* 97:1-9.
- Morner, S., P. Richard, E. Kazzam, U. Hellman, B. Hainque, K. Schwartz, and A. Waldenstrom. 2003. Identification of the genotypes causing hypertrophic cardiomyopathy in northern Sweden. *J Mol Cell Cardiol.* 35:841-9.
- Mornet, D., R.U. Bertrand, P. Pantel, E. Audemard, and R. Kassab. 1981. Proteolytic approach to structure and function of actin recognition site in myosin heads. *Biochemistry.* 20:2110-20.
- Mornet, D., P. Pantel, E. Audemard, and R. Kassab. 1979. The limited tryptic cleavage of chymotryptic S-1: an approach to the characterization of the actin site in myosin heads. *Biochem Biophys Res Commun.* 89:925-32.
- Nanni, L., M. Pieroni, C. Chimenti, B. Simionati, R. Zimbello, A. Maseri, A. Frustaci, and G. Lanfranchi. 2003. Hypertrophic cardiomyopathy: two homozygous cases with "typical" hypertrophic cardiomyopathy and three new mutations in cases with progression to dilated cardiomyopathy. *Biochem Biophys Res Commun.* 309:391-8.
- Niimura, H., L.L. Bachinski, S. Sangwatanaroj, H. Watkins, A.E. Chudley, W. McKenna, A. Kristinsson, R. Roberts, M. Sole, B.J. Maron, J.G. Seidman, and C.E. Seidman. 1998. Mutations in the gene for cardiac myosin-binding protein C and late-onset familial hypertrophic cardiomyopathy. *N Engl J Med.* 338:1248-57.
- Niimura, H., K.K. Patton, W.J. McKenna, J. Soultis, B.J. Maron, J.G. Seidman, and C.E. Seidman. 2002. Sarcomere protein gene mutations in hypertrophic cardiomyopathy of the elderly. *Circulation.* 105:446-51.
- Nygren, P.A., S. Stahl, and M. Uhlen. 1994. Engineering proteins to facilitate bioprocessing. *Trends Biotechnol.* 12:184-8.
- Offer, G., C. Moos, and R. Starr. 1973. A new protein of the thick filaments of vertebrate skeletal myofibrils. Extractions, purification and characterization. *J Mol Biol.* 74:653-76.
- Okagaki, T., F.E. Weber, D.A. Fischman, K.T. Vaughan, T. Mikawa, and F.C. Reinach. 1993. The major myosin-binding domain of skeletal muscle MyBP-C (C protein) resides in the COOH-terminal, immunoglobulin C2 motif. *J Cell Biol.* 123:619-26.
- Olsson, M.C., B.M. Palmer, B.L. Stauffer, L.A. Leinwand, and R.L. Moore. 2004. Morphological and functional alterations in ventricular myocytes from male transgenic mice with hypertrophic cardiomyopathy. *Circ Res.* 94:201-7.

- Palmer, A.G., 3rd. 1997. Probing molecular motion by NMR. *Curr Opin Struct Biol.* 7:732-7.
- Perry, S.V. 1998. Troponin T: genetics, properties and function. *J Muscle Res Cell Motil.* 19:575-602.
- Perry, S.V. 2001. Vertebrate tropomyosin: distribution, properties and function. *J Muscle Res Cell Motil.* 22:5-49.
- Pervushin, K., R. Riek, G. Wider, and K. Wuthrich. 1997. Attenuated T2 relaxation by mutual cancellation of dipole-dipole coupling and chemical shift anisotropy indicates an avenue to NMR structures of very large biological macromolecules in solution. *Proc Natl Acad Sci U S A.* 94:12366-71.
- Pfuhl, M., M. Gautel, A.S. Politou, C. Joseph, and A. Pastore. 1995. Secondary structure determination by NMR spectroscopy of an immunoglobulin-like domain from the giant muscle protein titin. *J Biomol NMR.* 6:48-58.
- Pollard, T.D. 1990. Actin. *Curr Opin Cell Biol.* 2:33-40.
- Port, J.D., and M.R. Bristow. 2001. Altered beta-adrenergic receptor gene regulation and signaling in chronic heart failure. *J Mol Cell Cardiol.* 33:887-905.
- Prinz, W.A., F. Aslund, A. Holmgren, and J. Beckwith. 1997. The role of the thioredoxin and glutaredoxin pathways in reducing protein disulfide bonds in the Escherichia coli cytoplasm. *J Biol Chem.* 272:15661-7.
- Pryor, K.D., and B. Leitig. 1997. High-level expression of soluble protein in Escherichia coli using a His6-tag and maltose-binding-protein double-affinity fusion system. *Protein Expr Purif.* 10:309-19.
- Ramachandran, G.N., C. Ramakrishnan, and V. Sasisekharan. 1963. Stereochemistry of polypeptide chain configurations. *J Mol Biol.* 7:95-9.
- Rayment, I., W.R. Rypniewski, K. Schmidt-Base, R. Smith, D.R. Tomchick, M.M. Benning, D.A. Winkelmann, G. Wesenberg, and H.M. Holden. 1993. Three-dimensional structure of myosin subfragment-1: a molecular motor. *Science.* 261:50-8.
- Razumova, M.V., J.F. Shaffer, A.Y. Tu, G.V. Flint, M. Regnier, and S.P. Harris. 2006. Effects of the N-terminal domains of myosin binding protein-C in an in vitro motility assay: Evidence for long-lived cross-bridges. *J Biol Chem.* 281:35846-54.
- Reinach, F.C., K. Nagai, and J. Kendrick-Jones. 1986. Site-directed mutagenesis of the regulatory light-chain Ca<sup>2+</sup>/Mg<sup>2+</sup> binding site and its role in hybrid myosins. *Nature.* 322:80-3.
- Rhee, D.S., J.W. 1994. The premyofibril: evidence for its role in myofibrillogenesis. *Cell Motil Cytoskeleton.* 28:1-24.
- Richard, P.C. 2003a. "Hypertrophic Cardiomyopathy: Distribution of Disease Genes, Spectrum of Mutations, and Implications for a Molecular Diagnosis Strategy." *Circulation.* 107:2227-2232.
- Richard, P.C., P. 2003b. Hypertrophic Cardiomyopathy: Distribution of Disease Genes, Spectrum of Mutations, and Implications for a Molecular Diagnosis Strategy. *Circulation.* 107:2227-2232.
- Richardson, J.S., E.D. Getzoff, and D.C. Richardson. 1978. The beta bulge: a common small unit of nonrepetitive protein structure. *Proc Natl Acad Sci U S A.* 75:2574-8.
- Richardson, P., W. McKenna, M. Bristow, B. Maisch, B. Mautner, J. O'Connell, E. Olsen, G. Thiene, J. Goodwin, I. Gyarfás, I. Martin, and P. Nordet. 1996. Report of the 1995 World Health Organization/International Society and Federation of

- Cardiology Task Force on the Definition and Classification of cardiomyopathies. *Circulation*. 93:841-2.
- Rottbauer, W., M. Gautel, J. Zehelein, S. Labeit, W.M. Franz, C. Fischer, B. Vollrath, G. Mall, R. Dietz, W. Kubler, and H.A. Katus. 1997. Novel splice donor site mutation in the cardiac myosin-binding protein-C gene in familial hypertrophic cardiomyopathy. Characterization Of cardiac transcript and protein. *J Clin Invest*. 100:475-82.
- Sadayappan, S., J. Gulick, H. Osinska, L.A. Martin, H.S. Hahn, G.W. Dorn, 2nd, R. Klevitsky, C.E. Seidman, J.G. Seidman, and J. Robbins. 2005. Cardiac myosin-binding protein-C phosphorylation and cardiac function. *Circ Res*. 97:1156-63.
- Sauer, J., and P. Nygaard. 1999. Expression of the Methanobacterium thermoautotrophicum hpt gene, encoding hypoxanthine (Guanine) phosphoribosyltransferase, in Escherichia coli. *J Bacteriol*. 181:1958-62.
- Schein, C. 1989. Production of soluble protein in bacteria. *Bio/Technology*:1141- 1149.
- Schlender, K.K., and L.J. Bean. 1991. Phosphorylation of chicken cardiac C-protein by calcium/calmodulin-dependent protein kinase II. *J Biol Chem*. 266:2811-7.
- Schlender, K.K., M.G. Hegazy, and T.J. Thysseril. 1987. Dephosphorylation of cardiac myofibril C-protein by protein phosphatase 1 and protein phosphatase 2A. *Biochim Biophys Acta*. 928:312-9.
- Schultheiss, T.L., Z.X. 1990. Differential distribution of subset of myofibrillar proteins in cardiac, nonstrated and strated myofibrils. *J Cell Biol*. 110:1159-1172.
- Seidman, J.G., and C. Seidman. 2001. The genetic basis for cardiomyopathy: from mutation identification to mechanistic paradigms. *Cell*. 104:557-67.
- Sharma, A., J.A. Askari, M.J. Humphries, E.Y. Jones, and D.I. Stuart. 1999. Crystal structure of a heparin- and integrin-binding segment of human fibronectin. *Embo J*. 18:1468-79.
- Sheterline, P., J. Clayton, and J. Sparrow. 1995. Actin. *Protein Profile*. 2:1-103.
- Solaro, R.J., and H.M. Rarick. 1998. Troponin and tropomyosin: proteins that switch on and tune in the activity of cardiac myofilaments. *Circ Res*. 83:471-80.
- Soteriou, A., M. Gamage, and J. Trinick. 1993. A survey of interactions made by the giant protein titin. *J Cell Sci*. 104 (Pt 1):119-23.
- Spirito, P., C.E. Seidman, W.J. McKenna, and B.J. Maron. 1997. The management of hypertrophic cardiomyopathy. *N Engl J Med*. 336:775-85.
- Squire, J., M. Cantino, M. Chew, R. Denny, J. Harford, L. Hudson, and P. Luther. 1998. Myosin rod-packing schemes in vertebrate muscle thick filaments. *J Struct Biol*. 122:128-38.
- Squire, J.M., P.K. Luther, and C. Knupp. 2003. Structural evidence for the interaction of C-protein (MyBP-C) with actin and sequence identification of a possible actin-binding domain. *J Mol Biol*. 331:713-24.
- Starr, R., and G. Offer. 1978. The interaction of C-protein with heavy meromyosin and subfragment-2. *Biochem J*. 171:813-6.
- Swan, R.C., and D.A. Fischman. 1986. Electron microscopy of C-protein molecules from chicken skeletal muscle. *J Muscle Res Cell Motil*. 7:160-6.
- Szczesna, D., D. Ghosh, Q. Li, A.V. Gomes, G. Guzman, C. Arana, G. Zhi, J.T. Stull, and J.D. Potter. 2001. Familial hypertrophic cardiomyopathy mutations in the regulatory light chains of myosin affect their structure, Ca<sup>2+</sup> binding, and phosphorylation. *J Biol Chem*. 276:7086-92.
- Tardiff, J.C., S.M. Factor, B.D. Tompkins, T.E. Hewett, B.M. Palmer, R.L. Moore, S. Schwartz, J. Robbins, and L.A. Leinwand. 1998. A truncated cardiac troponin T

- molecule in transgenic mice suggests multiple cellular mechanisms for familial hypertrophic cardiomyopathy. *J Clin Invest.* 101:2800-11.
- Thompson, J.D., T.J. Gibson, F. Plewniak, F. Jeanmougin, and D.G. Higgins. 1997. The CLUSTAL\_X windows interface: flexible strategies for multiple sequence alignment aided by quality analysis tools. *Nucleic Acids Res.* 25:4876-82.
- Timson, D.J., and I.P. Trayer. 1997. The role of the proline-rich region in A1-type myosin essential light chains: implications for information transmission in the actomyosin complex. *FEBS Lett.* 400:31-6.
- Trinick, J. 1996. Titin as a scaffold and spring. Cytoskeleton. *Curr Biol.* 6:258-60.
- van der Velden, J., Z. Papp, R. Zaremba, N.M. Boontje, J.W. de Jong, V.J. Owen, P.B. Burton, P. Goldmann, K. Jaquet, and G.J. Stienen. 2003. Increased Ca<sup>2+</sup>-sensitivity of the contractile apparatus in end-stage human heart failure results from altered phosphorylation of contractile proteins. *Cardiovasc Res.* 57:37-47.
- Van Driest, S.L., V.C. Vasile, S.R. Ommen, M.L. Will, A.J. Tajik, B.J. Gersh, and M.J. Ackerman. 2004. Myosin binding protein C mutations and compound heterozygosity in hypertrophic cardiomyopathy. *J Am Coll Cardiol.* 44:1903-10.
- Vibert, P., and C. Cohen. 1988. Domains, motions and regulation in the myosin head. *J Muscle Res Cell Motil.* 9:296-305.
- Wagner, G., S. Hyberts, and J.W. Peng. 1993. Study of protein dynamics by NMR. Macmillan, London. 220-257 pp.
- Wang, K., and J. Wright. 1988. Architecture of the sarcomere matrix of skeletal muscle: immunoelectron microscopic evidence that suggests a set of parallel inextensible nebulin filaments anchored at the Z line. *J Cell Biol.* 107:2199-212.
- Watkins, H., D. Conner, L. Thierfelder, J.A. Jarcho, C. MacRae, W.J. McKenna, B.J. Maron, J.G. Seidman, and C.E. Seidman. 1995a. Mutations in the cardiac myosin binding protein-C gene on chromosome 11 cause familial hypertrophic cardiomyopathy. *Nat Genet.* 11:434-7.
- Watkins, H., W.J. McKenna, L. Thierfelder, H.J. Suk, R. Anan, A. O'Donoghue, P. Spirito, A. Matsumori, C.S. Moravec, J.G. Seidman, and et al. 1995b. Mutations in the genes for cardiac troponin T and alpha-tropomyosin in hypertrophic cardiomyopathy. *N Engl J Med.* 332:1058-64.
- Watkins, H., A. Rosenzweig, D.S. Hwang, T. Levi, W. McKenna, C.E. Seidman, and J.G. Seidman. 1992. Characteristics and prognostic implications of myosin missense mutations in familial hypertrophic cardiomyopathy. *N Engl J Med.* 326:1108-14.
- Weisberg, A., and S. Winegrad. 1996. Alteration of myosin cross bridges by phosphorylation of myosin-binding protein C in cardiac muscle. *Proc Natl Acad Sci U S A.* 93:8999-9003.
- Weisberg, A., and S. Winegrad. 1998. Relation between crossbridge structure and actomyosin ATPase activity in rat heart. *Circ Res.* 83:60-72.
- Welikson, R.E., and D.A. Fischman. 2002. The C-terminal IgI domains of myosin-binding proteins C and H (MyBP-C and MyBP-H) are both necessary and sufficient for the intracellular crosslinking of sarcomeric myosin in transfected non-muscle cells. *J Cell Sci.* 115:3517-26.
- Whiting, A., J. Wardale, and J. Trinick. 1989. Does titin regulate the length of muscle thick filaments? *J Mol Biol.* 205:263-8.
- Winegrad, S. 1999. Cardiac myosin binding protein C. *Circ Res.* 84:1117-26.
- Winegrad, S. 2000. Myosin binding protein C, a potential regulator of cardiac contractility. *Circ Res.* 86:6-7.

- Witt, C.C., B. Gerull, M.J. Davies, T. Centner, W.A. Linke, and L. Thierfelder. 2001. Hypercontractile properties of cardiac muscle fibers in a knock-in mouse model of cardiac myosin-binding protein-C. *J Biol Chem.* 276:5353-9.
- Wittekind, M.M., L. 1993. HNCACB, a high-sensitivity 3D NMR experiment to correlate amide- proton and nitrogen resonances with the alpha- carbon and beta- carbon resonances in proteins. *J Magn Reson.* 101:201- 205.
- Yamamoto, K. 1986. The binding of skeletal muscle C-protein to regulated actin. *FEBS Lett.* 208:123-7.
- Yamamoto, K., and C. Moos. 1983. The C-proteins of rabbit red, white, and cardiac muscles. *J Biol Chem.* 258:8395-401.
- Yang, Q., A. Sanbe, H. Osinska, T.E. Hewett, R. Klevitsky, and J. Robbins. 1998. A mouse model of myosin binding protein C human familial hypertrophic cardiomyopathy. *J Clin Invest.* 102:1292-300.
- Yang, Q., A. Sanbe, H. Osinska, T.E. Hewett, R. Klevitsky, and J. Robbins. 1999. In vivo modeling of myosin binding protein C familial hypertrophic cardiomyopathy. *Circ Res.* 85:841-7.
- Yu, B., J.A. French, L. Carrier, R.W. Jeremy, D.R. McTaggart, M.R. Nicholson, B. Hambly, C. Semsarian, D.R. Richmond, K. Schwartz, and R.J. Trent. 1998. Molecular pathology of familial hypertrophic cardiomyopathy caused by mutations in the cardiac myosin binding protein C gene. *J Med Genet.* 35:205-10.
- Zot, A.S., and J.D. Potter. 1987. Structural aspects of troponin-tropomyosin regulation of skeletal muscle contraction. *Annu Rev Biophys Biophys Chem.* 16:535-59.